

A Unified Representation of Gas-Phase Element Depletions in the Interstellar Medium ¹

Edward B. Jenkins

*Princeton University Observatory
Princeton, NJ 08544-1001*

ebj@astro.princeton.edu

ABSTRACT

A study of gas-phase element abundances reported in the literature for 17 different elements sampled over 243 sight lines in the local part of our Galaxy reveals that the depletions into solid form (dust grains) are extremely well characterized by trends that employ only three kinds of parameters. One is an index that describes the overall level of depletion applicable to the gas in any particular sight line, and the other two represent linear coefficients that describe how to derive each element's depletion from this sight-line parameter. The information from this study reveals the relative proportions of different elements that are incorporated into dust at different stages of grain growth. An extremely simple scheme is proposed for deriving the dust contents and metallicities of absorption-line systems that are seen in the spectra of distant quasars or the optical afterglows of gamma-ray bursts. Contrary to presently accepted thinking, the elements sulfur and krypton appear to show measurable changes in their depletions as the general levels of depletions of other elements increase, although more data are needed to ascertain whether or not these findings truly compelling. Nitrogen appears to show no such increase. The incorporation of oxygen into solid form in the densest gas regions far exceeds the amounts that can take the form of silicates or metallic oxides; this conclusion is based on differential measurements of depletion and thus is unaffected by uncertainties in the solar abundance reference scale.

Subject headings: ISM: abundances ISM: atoms – ultraviolet: ISM

¹Based in large part on published observations from (1) the NASA/ESA *Hubble Space Telescope* obtained at the Space Telescope Science Institute, which is operated by the Association of Universities for Research in Astronomy, Inc., under NASA contract NAS 5-26555 (2) the *Far Ultraviolet Spectroscopic Explorer (FUSE)* mission operated by Johns Hopkins University, supported by NASA contract NAS5-32985 and (3) The *Copernicus* satellite, supported by NASA grant NAGW-77 to Princeton University.

1. Introduction

1.1. Brief History

For atomic species in the neutral interstellar medium (ISM), nearly all of the transitions out of the ground electronic state of the preferred ionization stages for H I regions occur in the ultraviolet part of the electromagnetic spectrum. While the elements Be and Ti have such transitions at visible wavelengths (Dunham 1939; Spitzer & Field 1955; Habing 1969), only those from singly-ionized titanium are strong enough to yield detectable absorption features in the spectra of background stars, leaving this element as the only one that has been successfully surveyed from ground-based observatories to derive the atomic abundances in the ISM (Wallerstein & Goldsmith 1974; Stokes 1978; Wallerstein & Gilroy 1992; Welsh et al. 1997; Prochaska, Tripp, & Howk 2005; Ellison, Prochaska, & Lopez 2007). Attempts even with powerful telescopes of the present era have failed to show measurable amounts of Be II in the ISM (Boesgaard 1985; Hébrard et al. 1997). Useful kinematic information could be derived from the strong visible absorption features from atomic species in stages below the preferred ones, e.g., Na I and Ca II (Merrill et al. 1937; Adams 1949; Münch 1957; Münch & Zirin 1961), but quantitative abundances were difficult to obtain owing to uncertainties in our knowledge of the physical conditions and atomic physics parameters that govern the ionization balances (Strömgren 1948; Herbig 1968).

In large part, for investigations of the abundances of gas-phase atomic constituents in the ISM of our Galaxy, it is essential that this research be conducted by observatories above the Earth’s atmosphere.² The earliest observations of UV stellar spectra at moderate resolution were carried out using small photographic spectrographs on sounding rockets, but the spectra were only good enough to sense the presence of interstellar features (Morton & Spitzer 1966; Morton, Jenkins, & Bohlin 1968), without permitting derivations any column densities except for that of atomic hydrogen based on $L\alpha$ absorption (Jenkins 1970, 1971). The first satellite to provide stellar spectra was the second *Orbiting Astronomical Observatory* (*OAO-2*) that was launched in 1968, but once again only $L\alpha$ absorption features provided any useful information on the ISM (Savage & Jenkins 1972; Jenkins & Savage 1974).

The era of investigations of UV interstellar absorption features from heavy elements began in earnest with a series of observations with the far-UV spectrometer (Rogerson et al. 1973a) aboard the *Copernicus* satellite, a facility that provided stellar spectra of high precision over a decade that started 37 years ago (Jenkins et al. 1973; Morton et al. 1973; Rogerson et al. 1973b; Spitzer et al. 1973); see an early review of highlights by Spitzer & Jenkins (1975). Among the principal findings that emerged from these studies was that, to varying degrees, the abundances of heavy elements in atomic form relative to that of hydrogen were below the solar abundance ratios, which are presumed to approximate the true total element abundances for the ISM in our part of the

²An exception was the *BUSS* balloon-borne payload which could observe over limited wavelength intervals in the near-UV (de Boer et al. 1986).

Galaxy. The differences in these two abundances were taken to represent the loss of atoms into solid form within dust grains, a picture that was reinforced by the approximate trend in the strengths of depletions relative to measures of chemical affinity, such as condensation temperatures in a chemical equilibrium of an extended stellar atmosphere (Field 1974) or atomic sticking probabilities that can govern how rapidly different elements are incorporated into the grains as they grow in the ISM (or, conversely, how easily they are returned to the gas phase by sputtering).

The *International Ultraviolet Explorer* (*IUE*) extended our reach to stars that were fainter than those observable with *Copernicus* and allowed a far greater number of features and stars to be observed [e.g., Van Steenberg & Shull (1988)], but the accuracies of the line measurements were not as good as those that were obtained previously with *Copernicus*. Later, several new instrumental developments brought about considerable progress in the study of atomic absorption lines. First, after the launch of the *Hubble Space Telescope* (*HST*) in 1992, we experienced substantial improvements in wavelength resolution and the ability to observe faint stars, which in turn broadened our knowledge of depletion trends over more elements and sightlines (Savage & Sembach 1996a). This facility, in conjunction with the *Far Ultraviolet Spectroscopic Explorer* (*FUSE*) satellite that came later, also increased our coverage to systems outside our galaxy, such as the Small and Large Magellanic Clouds (Roth & Blades 1997; Welty et al. 1997, 2001; Mallouris 2003; Sofia et al. 2006), NGC 1705 (Sahu & Blades 1997), I Zw18 (Aloisi et al. 2003), NGC 625 (Cannon et al. 2005) and SBS1543+593 (Bowen et al. 2005). Second, large aperture telescopes on the ground with high resolution echelle spectrographs extended our reach to gas systems in front of bright quasars at high redshift, where the UV transitions could be viewed at visible wavelengths. In recent years, new opportunities have arisen to view gases within or in front of the host galaxies of gamma ray bursts (GRBs), whose optical afterglows are often bright enough to permit observations to be performed at high wavelength resolution. With the study of these new systems came a higher level of complexity, since the results could be influenced by not only dust depletion but also intrinsic abundance differences of these objects, many of which are less chemically evolved than our Galaxy (Pettini et al. 1994, 1997, 1999, 2002; Lu et al. 1996; Prochaska & Wolfe 2002; Pettini 2003; Khare et al. 2004; Prochaska 2004; Kulkarni et al. 2005; Wolfe, Gawiser, & Prochaska 2005; Péroux et al. 2006a,b, 2008; Vladilo et al. 2006; Prochaska et al. 2007; Vladilo, J. 2008; Calura et al. 2009). One of the aims of the present paper is to give some guidance on how these two effects can be separated from each other (§10.4).

1.2. General Findings on Depletions

Aside from the differences in depletions from one element to the next, it has been noted that the overall strengths of depletions of many elements collectively show large changes over different lines of sight. Attempts to understand these variations have been moderately successful, but not without some ambiguity. For instance, Savage & Bohlin (1979), Harris, et al. (1984), Jenkins et al. (1986) Jenkins (1987) and Crinklaw et al. (1994) showed that the depletion strengths correlated

well with the average density of hydrogen along each sight line. This measure is admittedly a crude indication of local conditions, since one cannot distinguish a uniform density over a long extent from strongly clumped, denser material with a low filling factor. Nevertheless Spitzer (1985) created a simple model for explaining the observations in terms of random mixtures of three different kinds of clouds with different densities and depletion strengths. A slightly different tactic was adopted by Savage & Sembach (1996a), who summarized element depletions in terms of averages of warm (presumably low density) gas and cool (denser) gas, with some recognition of the differences between gas in the disk of the Galaxy and gas in the lower part of the halo. In their study that compared column densities of Si III and Al III, Howk & Savage (1999) showed that even fully ionized regions exhibited depletions onto dust grains.

Other ways of characterizing depletions for different lines of sight included simply comparing them to the hydrogen column density, i.e., not divided by the length of the sight line to obtain an average density (Wakker & Mathis 2000) or, alternatively, comparing them to the fraction of hydrogen atoms that are in molecular form (Cardelli 1994; Snow, Rachford, & Figoski 2002; Jensen, Rachford, & Snow 2005; Jensen, & Snow 2007a,b). The former of the two methods is one that is useful for lines of sight that extend out far from the Galactic plane, where the effective length is of order of the scale height times the cosecant of the Galactic latitude. The latter represents an attempt to obtain a more accurate index for sight-line conditions, but it has the drawback of not factoring in variables other than local density that govern the molecular fraction, such as the strength of dissociating radiation field, the self shielding of the H₂ transitions, or the finite amount of time needed to reach an equilibrium state.

All of the above comparisons with external sight-line variables were carried out for each element independently, with the recognition that the characters of the trends would differ from one case to the next but ultimately could be compared with each other. A shortcoming of this approach is that the individual investigations are weakened by two factors that are difficult to control: (1) errors in the individual measurements (for both the depletions of single elements and the external variables) and (2) a lack of fidelity between the external variables and whatever real depletion processes that they are supposed to represent.

1.3. New Approach

The approach of the present study is to concentrate on how the depletions of different elements are found to relate to each other, irrespective of any external factors, but with the recognition that the severity of the depletions generally differ in a systematic way from one location to another and from one element to the next. Our objective is to build a framework that describes the depletions in terms of a set of simple parameters that form an abstract model that can be used later to investigate some important issues on the formation and destruction of dust grains. The general protocol is developed in §2.2 based on an exposition of some empirical findings about element depletions; we demonstrate this by using two comparisons for three different elements that were chosen to give

the most instructive examples. On the basis of these findings, assuming they apply generally, one can develop an equation with a few free parameters that offers an acceptable fit to the observations (§3) and then use a comprehensive survey of depletions gathered from measurements that have already been published (§4) to derive the best solutions for the parameter values (§5). In §6 we explore how these parameters offer insights on the elemental compositions of dust grains and how the mix in the buildup of these grains changes as the overall severity of depletions increase. Here, we supply the basic information that can be used to build upon the earlier interpretations by Spitzer & Fitzpatrick (1993), Fitzpatrick & Spitzer (1994), Sofia, Cardelli & Savage (1994), Sembach & Savage (1996), Mathis (1996) and Draine (2004) on some plausible mixtures of grain compounds that are consistent with the amounts of missing gas atoms.

The conclusions presented here on the highly predictable patterns of element depletions open the way for investigations of intrinsic abundances in Damped Lyman Alpha (DLA) and other gas systems that are seen in absorption in the spectra of distant QSOs or the optical afterglows of gamma-ray bursts (GRBs). A straightforward method of compensating for the loss of material into dust grains in such systems is presented in §10.4, based on a simple least-squares fit to a linear equation (§7), which then allows the total elemental abundances to be derived from the measured gas-phase column densities. This approach is also useful for the determinations of depletions in our Galaxy for which measures of hydrogen are not available, such as surveys of matter in front of white dwarf stars that are at distances up to about 100 pc from the Sun (§8).

2. Concept

The depletion of an element X in the ISM is defined in terms of (a logarithm of) its reduction factor below the expected abundance relative to that of hydrogen if all of the atoms were in the gas phase,

$$[X_{\text{gas}}/\text{H}] = \log\{N(X)/N(\text{H})\} - \log(X/\text{H})_{\odot} , \quad (1)$$

which is based on the assumption that solar abundances $(X/\text{H})_{\odot}$ are good reference values that truly reflect the underlying total abundances. In this formula, $N(X)$ is the column density of element X and $N(\text{H})$ represents the column density of hydrogen in both atomic and molecular form, i.e., $N(\text{H I}) + 2N(\text{H}_2)$. The missing atoms of element X are presumed to be locked up in solids within dust grains or large molecules that are difficult to identify spectroscopically, with fractional amounts (again relative to H) given by

$$(X_{\text{dust}}/\text{H}) = (X/\text{H})_{\odot}(1 - 10^{[X_{\text{gas}}/\text{H}]}) . \quad (2)$$

2.1. Reference Abundances

One issue that has bedeviled investigators of interstellar depletions has been the mutually inconsistent results from reasonable sources of information on the “cosmic reference abundances,”

which, as stated above, are taken here to be $(X/H)_{\odot}$. Viewpoints on these abundance scales have changed through the years due either to different opinions on how they should be linked to the abundances in different types of stars (or H II regions) or, alternatively, to actual changes in some of the measurement outcomes themselves (Mathis 1996; Savage & Sembach 1996a; Snow & Witt 1996; Sofia & Meyer 2001; Li 2005). The most dramatic revisions in the recent past (and some of the most important ones for the ISM) have been for the solar abundances of the elements C, N and O relative to H, where the values have decreased by about -0.2 dex from previously accepted scales (Grevesse & Sauval 1998), but which still exhibit disquieting fluctuations from one determination to the next (Holweger 2001; Allende Prieto, Lambert, & Asplund 2002; Asplund et al. 2004, 2005; Socas-Navarro & Norton 2007; Allende Prieto 2008; Centeno & Socas-Navarro 2008; Meléndez & Asplund 2008; Caffau et al. 2009). These newer abundances now seem to be in accord with recent studies of B-star abundances (Daflon et al. 2003; Nieva & Przybilla 2008a,b) but are inconsistent with the results from helioseismological studies of the sound speed and depth of the convection zone inside the Sun (Bahcall et al. 2005a,b; Antia & Basu 2005, 2006), which favor the earlier abundances when the opacities are computed (Badnell et al. 2005).

For the study of interstellar depletions presented here, we adopt the abundances compiled by Lodders (2003) for the proto-Sun, which she estimates to have been higher by 0.07 dex than the current abundances in the solar photosphere (due to the fact that some gravitational settling may have occurred, thus depleting the photospheric abundances by this amount). These abundances will be adopted to represent our view of the expected atomic densities relative to that of hydrogen when there are no dust grains or molecules present. However, they are somewhat higher than the abundances of nearby B-type stars determined by Przybilla, Nieva & Butler (2008), suggesting that the 0.07 dex upward corrections may be too large.

One unique aspect of the study here will be the development of a way to learn about the depletion of atoms onto dust grains that does not depend on the correctness of the reference abundances. This approach, which looks at differential changes in element atomic gas abundances instead of absolute depletions, will be presented in §6.

2.2. Underlying Strategy

To gain an understanding of how depletions behave under different conditions, it is helpful to compare the trends for pairs of elements over different lines of sight. This comparison will lay the groundwork for the analysis that will be developed in later sections of this paper. Figure 1 shows two such comparisons, using depletions extracted from the data discussed in §4. The depletions of Mg and P shown in the upper panel of the figure for a collection of individual sight lines exhibit an approximately linear relationship with respect to each other, with a slope slightly steeper than unity and with an intercept at the axis representing zero P depletion being about 0.5 dex below the zero axis for the Mg depletion. This displacement of the zero point indicates that Mg shows a small amount of depletion when P is undepleted, but this conclusion is dependent on the accuracy

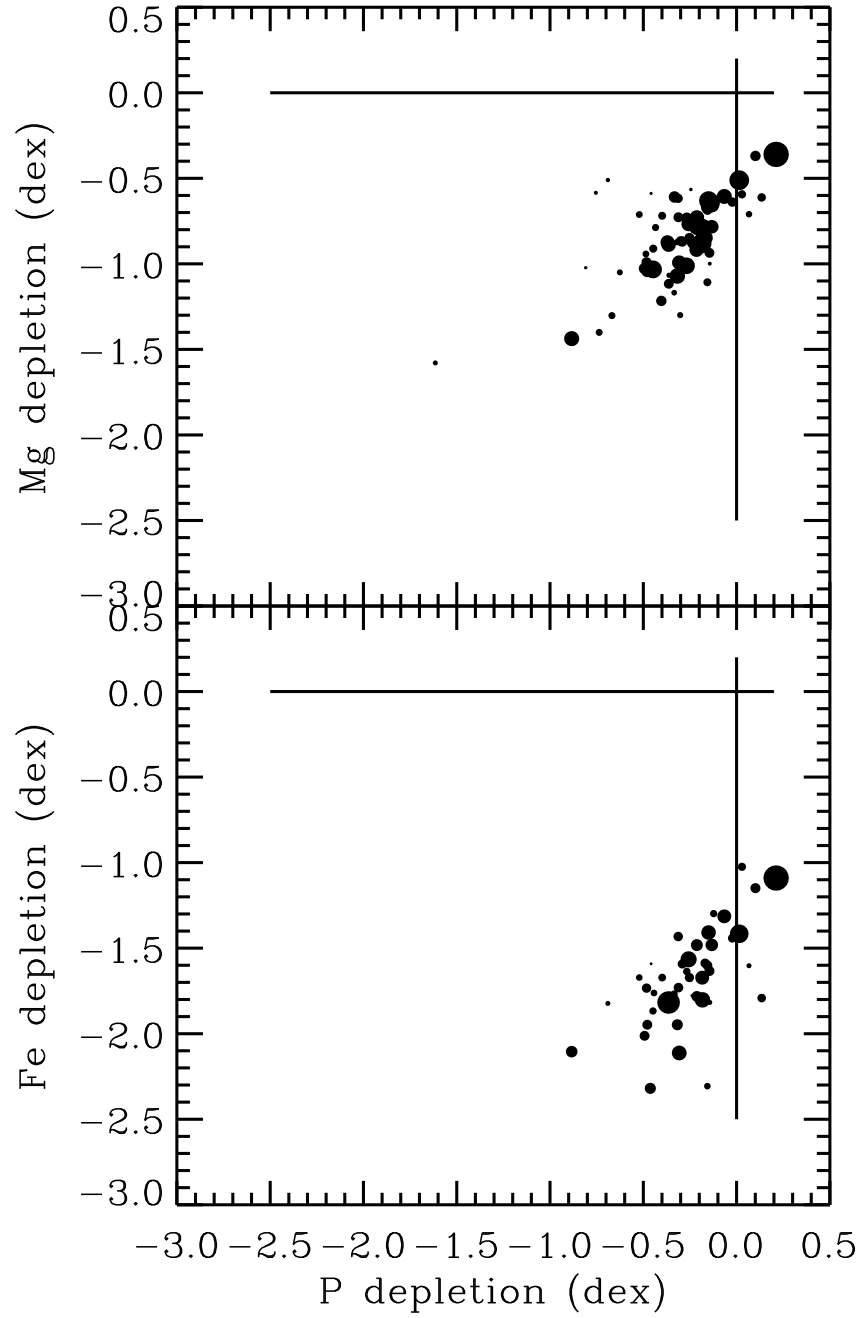


Fig. 1.— Interstellar atomic depletion factors $[\text{Mg}_{\text{gas}}/\text{H}]$ (*top panel*) and $[\text{Fe}_{\text{gas}}/\text{H}]$ (*bottom panel*) vs. $[\text{P}_{\text{gas}}/\text{H}]$. Measurements with small errors are depicted with disks that have large diameters, while those with large errors are more point-like.

of both the respective solar abundances of these two elements and the f -values of the transitions used to measure their interstellar abundances, together with the applicability of the assumption that solar abundances are a correct standard to apply to elements in the ISM.³ While this may be so, the slope of the line has no sensitivity to these uncertainties; it depends only on the correctness of the derived column densities. The lower panel of the figure shows that the same behavior is seen when the depletions of Fe and P are compared; it is important to note that the slope and intercept of a best fit to these points are larger in magnitude than for Mg and P. A diagram similar to these two has been presented earlier by Fitzpatrick (1996) for the elements Fe and Si vs. S (see his Fig. 2), and the qualitative features are fundamentally similar.

By extension from these two examples, one can anticipate that there could be a linear relationship between all depletions; that is, in the hyperspace whose axes represent the strengths of depletions of all the different elements, an acceptable fit to the data for different sight lines will approximately conform to a single straight line. An alternative to this representation is to describe the depletion of each element in terms of a linear relationship against a generalized depletion parameter that is common to all elements through some linear relations, but which can change from one line of sight to the next. This approach will be adopted for this paper.

3. Definitions⁴ and Derivations of Parameters

The line-of-sight depletion strength factor, which we denote as F_* , represents how far the depletion processes have progressed collectively for all elements for any given case, i.e., a larger F_* implies a stronger depletion for all elements. Aside from a few exceptions discussed in §4.3, we are generally not able to sense true local depletions for different regions along any sight line, but only the results in the form of a single value for each element that represents a composite view of such depletions taken from samples seen in projection. We examine the consequences of this kind of blend in a later section (§7.2), where an example with kinematically distinct parcels of gas with different depletions is analyzed as a single unit.

The slope of a best-fit line for the observed depletions $[X_{\text{gas}}/\text{H}]_{\text{obs}}$ for any given element X against F_* may be called A_X , and this parameter represents the propensity of that element to increase (the absolute value of) its particular depletion level as F_* becomes larger. For even the smallest observed values of F_* , most elements still show some depletion, as we learned from Fig. 1.

³The fact that some measurements of the abundances of P seem to be above the solar value demonstrates that depletion measurements are subject to these three types of systematic errors. However, the f -value adopted for the strongest P line, a line that is most influential in measuring the abundance of P for sightlines with low column densities, has recently been re-examined by Federman et al. (2007), and their new measurements show that the earlier value of the line strength is essentially correct.

⁴Throughout this paper, symbols with asterisk subscripts pertain to different sight lines (mnemonic aid: think of “*” representing a target star), and X subscripts denote different elements.

We denote this level of depletion as $[X_{\text{gas}}/\text{H}]_0$.

While the nature of F_* has been defined, its numerical scale has not. That is, the values of A_X and $[X_{\text{gas}}/\text{H}]_0$ are dependent on this scale, which is arbitrary. We assign a value of 0 for F_* to be that which corresponds to a sight line with the lowest collective depletions observed in our sample. At the opposite extreme, we define $F_* = 1.0$ to conform approximately to the strength of depletions for the low velocity component ($v_{\odot} = -15 \text{ km s}^{-1}$) seen toward the star ζ Oph (HD149757), for which the best studied and most detailed information is available for the depletions of many different elements (Savage, Cardelli, & Sofia 1992). The sight line toward this star has been generally regarded as a prototype of the strong depletions that are seen in the cold, neutral medium (Savage & Sembach 1996a).

3.1. Determinations of F_*

Now that we have defined two fiducial values of F_* , we can state that a best fit of the experimental data to differing values of this depletion parameter is given by the simple linear relation

$$[X_{\text{gas}}/\text{H}]_{\text{fit}} = [X_{\text{gas}}/\text{H}]_0 + A_X F_* , \quad (3)$$

subject to the normalization conditions for F_* stated earlier. Unfortunately, the observations of depletions that are needed to define the parameters $[X_{\text{gas}}/\text{H}]_0$, A_X and F_* are sparse. All elements have only a partial coverage of the sight lines, and many sight lines have only a few column density determinations. For this reason, coupled with the fact that each quantity is linked to the adopted values for the others, solutions for the values of F_* for each of the sight lines had to be derived using a series of iterations, described in the next paragraph, for converging upon successively more accurate values of this quantity based on a set of provisional values A'_X of the fundamental parameters A_X (which will be derived more accurately in a later calculation). The values for A'_X are continually adjusted to make them more realistically follow the element depletions during the iteration cycles that improve upon the F_* solution set. We must also employ provisional values for the zero-point offsets $[X_{\text{gas}}/\text{H}]_0$, which we denote as $[X_{\text{gas}}/\text{H}]'_0$. New values of $[X_{\text{gas}}/\text{H}]'_0$ are not derived in successive iteration steps because the accuracy of this parameter is not critical in defining F_* . The convergence of these iterations was monitored and found to be quite rapid and not dependent on the initial values input to the first iteration (except for small, uniform increases or decreases in all of the A'_X values from one trial case to the next, which are compensated by uniform changes in the opposite sense for the F_* set).

The calculations begin with an evaluation of a weighted average of the available observed depletions $[X_{\text{gas}}/\text{H}]_{\text{obs}}$ for a given line of sight, after they have had their respective zero-point depletions subtracted and have been normalized to the values of A'_X ,

$$F_* = \frac{\sum_X \{W_X ([X_{\text{gas}}/\text{H}]_{\text{obs}} - [X_{\text{gas}}/\text{H}]'_0) / A'_X\}}{\sum_X W_X} , \quad (4)$$

where the weight factors W_X are set equal to the inverse squares of the combined uncertainties of the other terms in the sum, i.e.,

$$W_X = \left(\sigma\{([X_{\text{gas}}/\text{H}]_{\text{obs}} - [X_{\text{gas}}/\text{H}]'_0)/A'_X\} \right)^{-2} \quad (5)$$

($W_X = 0$ if the observation is unavailable for element X .) For the initial evaluation of Eq. 4, values of A'_X were set to the depletions of elements measured toward ζ Oph (-15 km s^{-1} velocity component) less the respective values of $[X_{\text{gas}}/\text{H}]'_0$, thus insuring that the scale for F_* is approximately consistent with the definition stated earlier. The uncertainties in our derived values for F_* are given simply by the relation

$$\sigma(F_*) = \left(\sum_X W_X \right)^{-\frac{1}{2}}. \quad (6)$$

The weights W_X in Eq. 4 guarantee that depletion measurements with large relative errors have a weak influence in the outcome. These weights make use of error estimates for the quotients of the two terms that appear in Eq. 5, $[X_{\text{gas}}/\text{H}]_{\text{obs}} - [X_{\text{gas}}/\text{H}]'_0$ and A'_X . A conventional approach to evaluating these errors is to add in quadrature the relative errors of the two terms, yielding the relative error of the quotient. However, this scheme breaks down when the error of the denominator $\sigma(A'_X)$ is not very much less than the denominator's value A'_X . Appendix A shows how one may compute errors in the quotients when the errors of the two terms are moderately large.

At the point that an initial solution set for F_* is obtained, revised values for A'_X can be evaluated from a counterpart to Eq. 4 with summations \sum_* over applicable lines of sight,

$$A'_X = \frac{\sum_* \{W_* ([X_{\text{gas}}/\text{H}]_{\text{obs}} - [X_{\text{gas}}/\text{H}]'_0)/F_*\}}{\sum_* W_*}, \quad (7)$$

which, as with Eq. 6, has an uncertainty

$$\sigma(A'_X) = \left(\sum_* W_* \right)^{-\frac{1}{2}} \quad (8)$$

for

$$W_* = \left(\sigma\{([X_{\text{gas}}/\text{H}]_{\text{obs}} - [X_{\text{gas}}/\text{H}]'_0)/F_*\} \right)^{-2}. \quad (9)$$

Again, the scheme for deriving the errors of quotients is invoked to evaluate the error term that appears within the weight factor in Eq. 9. Once we have defined the improved values for A'_X and their associated errors using Eqs. 7-9, we start over by repeating the evaluations of F_* . We cycle through Eqs. 4 and 7 until the values of F_* and A'_X stabilize.

3.2. Determinations of A_X , B_X and z_X

Now that values of F_* and their associated uncertainties for all lines of sight have been established, we can improve upon the earlier representations of element depletions that made use of the

provisional parameters $[X_{\text{gas}}/\text{H}]'_0$ and A'_X . We accomplish this by using a more direct (noniterative) approach for determining new parameters that describe how the gas-phase abundances of element X should be depleted for different values of F_* . An improved linear form

$$[X_{\text{gas}}/\text{H}]_{\text{fit}} = B_X + A_X(F_* - z_X) \quad (10)$$

is a modification of Eq. 3, where the zero-point reference in F_* is displaced to an intermediate value z_X , which is unique to element X (instead of being at F_* equal to 0), and the depletion at this point is called B_X . For each element we can solve for values of the two coefficients A_X and B_X through the evaluation of a least-squares fit [using the routine `FITEXY` described by Press et al. (2007)] that properly accounts for differing errors in both the dependent and independent measurement variables that are being fitted, $[X_{\text{gas}}/\text{H}]_{\text{obs}}$ and F_* . The reason for replacing $[X_{\text{gas}}/\text{H}]_0$ (i.e., the expected depletion for $F_* = 0$) in the earlier equation with $B_X - A_X z_X$ is that for a choice

$$z_X = \frac{\sum_* W_* F_*}{\sum_* W_*}, \quad (11)$$

where in this case

$$W_* = \{[\sigma([X_{\text{gas}}/\text{H}]_{\text{obs}})]^2 + [\sigma(F_*)A'_X]^2\}^{-1}, \quad (12)$$

there is a near zero covariance between the formal fitting errors for the solutions of B_X and A_X . This independence for the uncertainties in the derived parameters makes them easier to state and comprehend, and it allows the errors in quantities that arise from linear combinations of A_X and B_X to be calculated in a straightforward fashion (see Eqs. 14 and 16 below). The W_* factors derived in Eq. 12 account for errors in the individual observations which can be compounded by the effect of the uncertainties in F_* (which become worse if A'_X is large).

In practical circumstances, one must add in quadrature an uncertainty in the reference solar abundance $\sigma(X/\text{H})_{\odot}$ to the formal error $\sigma(B_X)$ that arises from the least-squares fit. This is done in the listing of B_X values for different elements (Table 4 that appears in §5) because the contents of this table are of general practical use, but deviations in the fit for each element shown much later in Tables 7 to 23 of Appendix B do not include the $\sigma(X/\text{H})_{\odot}$ term so that one can judge better how well individual observations fit the general trend irrespective of any overall systematic errors in the solar abundances. Some of the column density measurements were not included in the least-squares fitting; these cases are discussed in §4.2. Results for the fit parameters and their errors will be presented in §5.

While the formulation given in Eq. 10 allows us to use parameters that have more straightforward errors, it is nevertheless still useful to know what the values of $[X_{\text{gas}}/\text{H}]_{\text{fit}}$ are for two fiducial values of F_* , one representing the smallest depletions ($F_* = 0$) and the other representing heavy depletions ($F_* = 1$). These two quantities are evaluated from the simple relations,

$$[X_{\text{gas}}/\text{H}]_0 = B_X - A_X z_X, \quad (13)$$

with an error

$$\sigma([X_{\text{gas}}/\text{H}]_0) = \sqrt{\sigma(B_X)^2 + [z_X \sigma(A_X)]^2}, \quad (14)$$

and

$$[X_{\text{gas}}/\text{H}]_1 = B_X + A_X(1 - z_X) , \quad (15)$$

with an error

$$\sigma([X_{\text{gas}}/\text{H}]_1) = \sqrt{\sigma(B_X)^2 + [(1 - z_X)\sigma(A_X)]^2} \quad (16)$$

4. Accumulation and Processing of Data from the Literature

The depletion study can draw upon a substantial and diverse accumulation of atomic column density measurements that have been published in the astronomical literature over several decades. One challenge in making use of these results is the creation of a good balance between two extremes in selecting the data: one being a strong discrimination in favor of the best quality results at the expense of obtaining a broad coverage of elements and sight lines, as opposed to the alternative of accepting nearly everything, good and bad, in an effort to lessen the perturbing effects of natural variations and to obtain a fuller representation of conditions in the ISM. By necessity, any reasonable compromise between these extremes will still entail the use of a very inhomogeneous mixture of data from different investigations that had different measurement methodologies and error estimation techniques.

To some extent, differences in data quality can be recognized in a proper fashion by using the stated uncertainties to govern the weighting of the terms used in the parameter estimations, as described earlier in §§ 3.1 and 3.2. A weakness of this approach is that different authors employ different standards for estimating errors, which is an effect that may partly undermine the validity of the weighting process. It would be a monumental task to attempt to scrutinize each investigator's means of estimating errors and then adjust them according to some uniform standard. Some papers did not state any errors in the column densities. For these situations, conservative estimates were made for these works, and they are noted in the notes section of Table 1. This section also states some special considerations that applied to our treatment of the investigation in question.

Elements covered in the present study include carbon, nitrogen, magnesium, silicon, phosphorus, sulfur, chlorine, titanium, chromium, manganese, iron, nickel, copper, zinc, germanium, and krypton. Argon was initially included in the compilation process, but there were too few reliable measurements taken to produce meaningful results, so this element was not considered further. Moreover, the apparent abundance of Ar, as traced by its neutral form, is strongly susceptible to being altered in partially ionized regions (Sofia & Jenkins 1998).

4.1. Special Treatment of Uncertainties Listed in one Survey

The results shown by Jenkins, Savage & Spitzer (1986) (hereafter JSS86) were processed in a special manner. These investigators quoted limits for the column densities at the 2σ level of

significance, which had to be replaced by reasonable estimates for the 1σ results to be consistent with the limits expressed by other investigators. For lower limits based on the strengths of weak lines that had a strong random noise contribution, JSS86 found it appropriate to quote formal results that were negative in situations where a chance positive intensity fluctuation created a negative equivalent width. This tactic was carried out to allow anyone to overcome an upward bias in any general average that would arise from blindly setting these lower limits to zero. The following rules were adopted for converting the 2σ lower limits to approximate representations of the 1σ values: if the lower limit was positive, the logarithm of the adopted new value would be a mean of the stated lower limit for $\log N$ and the logarithm of the best value, on the presumption that most of the time the relative likelihoods are symmetric in the logarithms. By contrast, for very weak detections these likelihoods are governed by nearly linear processes, so that if the stated lower limit was negative (and the best value was stated as a positive number), the mean would be evaluated in terms of the linear representations of these values and would then be converted into logarithmic form. If, after evaluating this average, the linear form was still negative, then the logarithm of the lower limit was set to a very low (out of range) number so that subsequent processing would recognize the best value as really an upper limit, even at the 1σ level.

For upper limits, the new limit was simply an average of the logarithms of the stated best and upper limits, except when the best value was stated as a negative (logarithmic) number and a linear average was used instead. As an exception, when JSS86 stated that the upper limit corresponded to a situation where the weakest line had a central optical depth greater than 2 (designated by an asterisk in their tables), the old upper limit based on the 2σ level of confidence was retained as a hedge against possible errors arising from such saturations. Finally, in the interest of following guideline nr. 2 stated in §4.2 below, any of the best values that had special notations (or a negative number) given in the tables of JSS86 were not considered for any of the values of generalized element depletions, but positive values were retained for expositions in tables and figures.

4.2. Criteria for Rejection

In recognition of the fact that error estimates in various works have their shortcomings, we invoke some quality control measures by implementing a few simple rules to bypass observations that may be of questionable validity. Moreover, in some cases, we must also reject investigations that include data that for good reasons probably misrepresent the trends that are under study here.

The following censorship rules were adopted for the selection and use of data incorporated in the current study:

1. Data on atomic column densities from observations using the *International Ultraviolet Explorer (IUE)* were not accepted, except for measurements of $N(\text{H I})$ from the $\text{L}\alpha$ absorption feature. The limitations of wavelength resolution and the maximum achievable S/N of this fa-

cility decrease the likelihood that, with the usual small velocity dispersions found in the ISM⁵, proper corrections for saturation can be made for absorption features that have large enough equivalent widths to be measured accurately. Moreover, Massa et al. (1998) concluded that the *IUE* NEWSIPS reductions had serious photometric inconsistencies. The *BUSS* balloon-borne payload (de Boer et al. 1986) recorded spectra of quality similar to those of *IUE*, and thus they likewise were not included in the current study.

2. There has been a persistent problem with investigators being overconfident about the reliability of column density measurements based exclusively on the equivalent widths of features on or very near the flat portion of the curve of growth. For this reason, grounds for rejecting individual element abundances along any of the sight lines included determinations that did not have at least one absorption line that was clearly on the linear portion of the curve of growth, or alternatively at least 2 lines that were either on or not far above the linear part. For instance, a low resolution observation of a doublet with a 2:1 strength ratio was deemed to be acceptable only if the ratio of the two equivalent widths was greater than 1.5.⁶ However, mildly saturated single lines were accepted if the curve of growth was established by multiple lines of other species that were expected to behave in a similar fashion.⁷ Deviations in the standards of leniency in accepting such results varied from one study to the next, driven by perceptions on how well the velocity structures were determined from the other species. Cases based on saturated lines that were measured using the apparent optical depth method (Savage & Sembach 1991; Jenkins 1996) for lines recorded with sufficiently high resolution were deemed to be acceptable as long as the apparent central optical depths were not too large. The application of this rule may have not been fully rigorous in all cases, since for some investigations it was difficult to determine if saturation effects created problems. In some cases, results from saturated lines were reported as lower limits for the column density; these values are recorded as such and appear in Tables 7 to 23 and Figs 5–8, but they are not included in the analyses of depletions. Once in a while, very saturated lines could yield column densities through the measurement of weak damping wings, and these cases were accepted.

⁵Exceptions to this are the lines of highly ionized species such as Al III, Si IV and C IV (Savage, Meade, & Sembach 2001), which have large enough b -values to permit reliable determinations of column densities. These species are not relevant to the present study however.

⁶Even though we are aware of the fact that a typical line of sight exhibits many separate velocity components, each with different column densities and velocity dispersions, a standard curve of growth analysis of the complete features that make up such an ensemble still yields an answer for the aggregate column density that is remarkably close to the correct answer, provided the features are not badly saturated. An analysis by Jenkins (1986) indicates that our adopted lower cutoff for the doublet ratio is a very conservative choice.

⁷As shown originally by Routly & Spitzer (1952), highly depleted species (Ca II) have more broadly distributed velocities than less depleted ones (Na I). Hence using one element as a velocity surrogate for another when multiple components are considered collectively must be done with caution. See also Jenkins (2009).

3. If any particular line of sight shows $\log N(\text{H}) < 19.5$, there is a reasonable possibility that a nonnegligible fraction of the atoms of any element is in a stage (or stages) of ionization above the preferred one (i.e., the lowest level with an ionization potential greater than 13.6 eV), because the gas is not well shielded from ionizing photons that have energies well above that of the Lyman limit of hydrogen; see a discussion of this topic by Jenkins (2004). Aside from this possibility, there is also a chance that contributions from fully ionized gas could contribute to the column density of an ion in its expected preferred stage for an H I region. If $N(\text{H I})$ is small, the relative level of contamination from one or more H II regions (including the one surrounding the target star) could be large. Such regions, of course, do not make any contribution to the $\text{L}\alpha$ absorption that is used to measure $N(\text{H I})$. While it is true that in principle one can estimate the probable contamination from partially or fully ionized regions by comparing the amounts of more highly ionized forms of some elements to their singly-ionized stages (Cardelli, Sembach, & Savage 1995; Sembach & Savage 1996; Howk & Savage 1999; Howk & Sembach 1999; Prochaska et al. 2002; Howk, Sembach, & Savage 2003), a uniform application of any corrections for ionization is not feasible in a generalized study such as this one, where varying degrees of coverage of various ions emerge from diverse sources in the literature. Aside from ionization corrections, for low column density cases there is also a possibility that material very close to the star, in the form of either a shell or disk, could have its own resonance absorption features (Snow, Peters, & Mathieu 1979; Oegerle & Polidan 1984) that could distort the results for the ISM. The imposition of a single column density threshold for all cases may seem like a blunt instrument, given the large variations of conditions encountered in this survey. Indeed, we argue later (§8) that the criterion $\log N(\text{H}) > 19.5$ is probably too conservative for short sight lines ($d \lesssim 100$ pc). While this may be so, there is evidence that over much longer sight lines that could hold multiple absorbing clouds a higher threshold for $N(\text{H})$ may be more appropriate. For instance, Howk, Sembach & Savage (2006) show an example where small systematic abundance shifts caused by ionization along an extended line of sight can arise even for $N(\text{H I}) = 10^{20} \text{cm}^{-2}$. While lines of sight that had $\log N(\text{H}) < 19.5$ were not used for determining the parameters A'_X , A_X , B_X and z_X , their values of F_* were still evaluated so that the results could be shown in the figures and be tabulated. The reader is advised to consider these results with some caution however. Figure 2 shows the distribution of total hydrogen column densities $N(\text{H})$ covered in this study.
4. Stars for which only one or two elements were observed were not included in the analysis, since they were of little or no value in constraining the comparisons of depletions for different elements. Nevertheless, as with stars that had $\log N(\text{H}) < 19.5$, their F_* values were computed and entries appear in the tables and figures.
5. Any absorbing systems well outside the disk of our Galaxy are excluded (e.g., those in either of the Magellanic Clouds or the Magellanic Stream), since their intrinsic element abundances are not known. Stars in the lower halo of the Galaxy are included, but the analysis is restricted

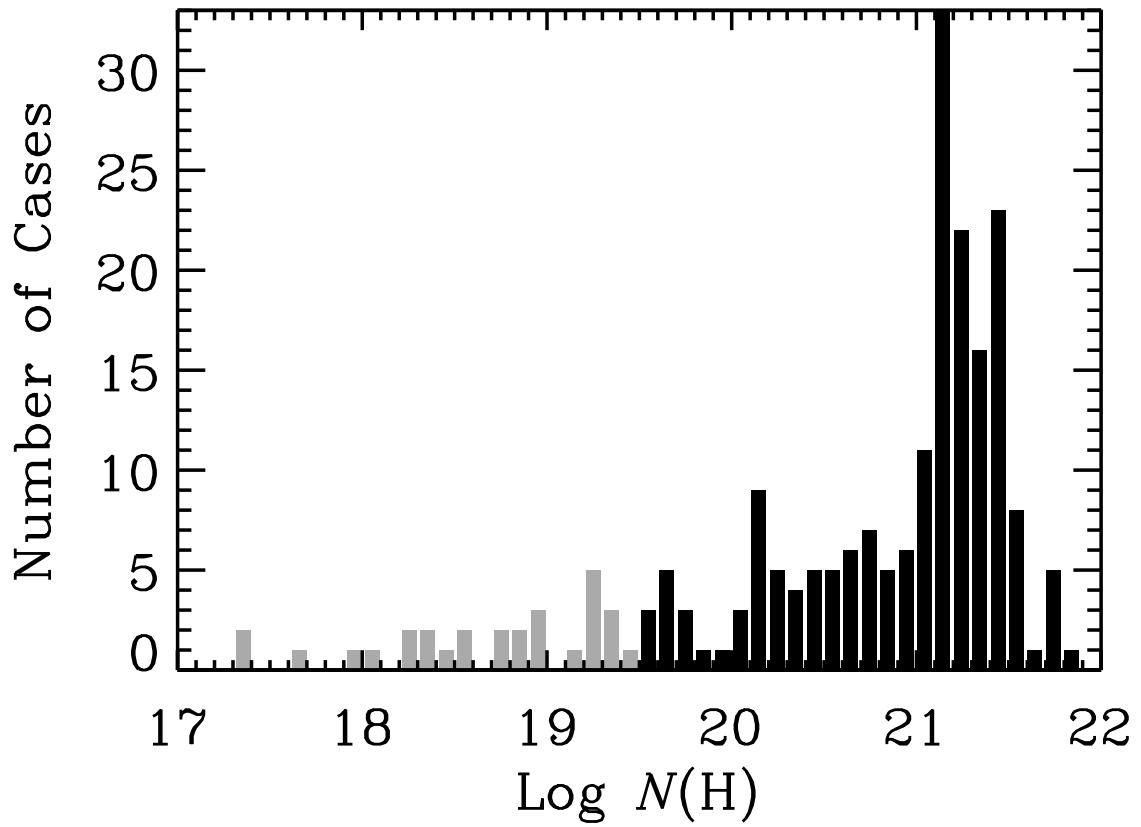


Fig. 2.— The distribution of total hydrogen column densities (atomic and molecular) for the sightlines studied in this survey. The gray bars represent cases below the cutoff $N(\text{H}) = 10^{19.5} \text{cm}^{-2}$ established for defining the best-fit element parameters.

to gas at low and intermediate velocities. Infalling gas at high velocities (Wakker 2001) is not included in this study, since the kinematics of this material point to an origin outside the Galactic disk, and the intrinsic abundances of the heavy elements are low (Wakker et al. 1999; Murphy et al. 2000; Gibson et al. 2001; Richter et al. 2001; Collins, Shull, & Giroux 2003; Tripp et al. 2003).

6. Gas that is explicitly identified to be in shocks at extraordinarily high velocity are not included. (Such clouds generally have $\log N(\text{H I}) < 19.5$ anyway, as indicated by their abundances of S II). Grains are usually destroyed in such gas (Jenkins, Silk, & Wallerstein 1976), and photons generated in the shock front (Shull & McKee 1979) can raise the ionization level of the post-shock material (Jenkins et al. 1998).
7. A diverse set of observations has revealed that the intrinsic abundances of the elements show a gradient with galactocentric distance R_{GC} that ranges from about -0.03 to -0.10 dex kpc^{-1} (Shaver et al. 1983; Afferbach, Churchwell, & Werner 1997; Gummershach et al. 1998; Deharveng et al. 2000; Martins & Viegas 2000; Rolleston et al. 2000; Giveon et al. 2002; Martín-Hernández et al. 2002; Luck, Kovtyukh, & Andrievsky 2006). To limit the influence of these changes on our results, we do not consider stars outside the range $7 < R_{\text{GC}} < 10$ kpc (projected onto the plane of the Galaxy) for the determinations of A_X , B_X and z_X , however they are plotted in Figs. 5–8 and appear in Tables 5 and 7–23. (Later, in §10.3, we show that an abundance gradient does not seem to be evident within the entire collection of sight lines studied here.)

Figure 3 summarizes the distributions of distances and heights above or below the Galactic plane for all of the sight lines covered in this study. The absence of stars with distances much below 0.1 kpc arises from the fact that the survey was almost completely restricted to data recorded for O- and B-type stars. A good coverage of distances below this limit has been provided by surveys of limited selections of elements toward late-type stars (Redfield & Linsky 2004a) and white dwarf stars (Friedman et al. 2002; Kruk et al. 2002; Lehner et al. 2003; Oliveira et al. 2003). A special discussion of interstellar depletions toward the white dwarf stars will appear in §8.

4.3. Other Considerations

Comparisons of element column densities are made with respect to $N(\text{H I})$ derived from $\text{L}\alpha$ absorptions and $N(\text{H}_2)$ derived from Lyman band absorptions. Hence these measurements apply to gas at all velocities. Thus, even for investigations that revealed separate column densities of heavy elements over different radial velocity ranges, the results had to be combined over all velocities. However, there are five special lines of sight where this consolidation of the column densities over all velocities was not applied. First, Spitzer & Fitzpatrick (1993) and Fitzpatrick & Spitzer (1997) analyzed exceptionally good observations of the stars HD 93521 and HD 215733 taken with the highest resolution mode of the GHRS instrument on *HST*, and they went to great

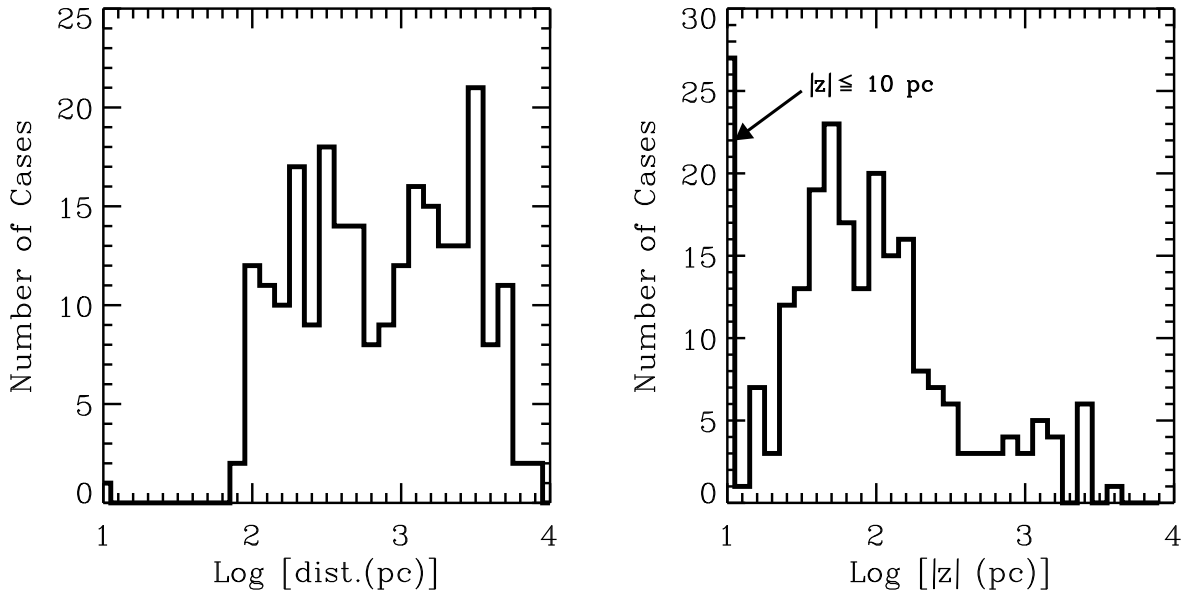


Fig. 3.— The distributions of distances to the target stars considered in this survey (*left-hand panel*), and their separations away from the Galactic plane (*right-hand panel*).

effort to decompose their profiles into separate velocity components. A principal motivation for studying the separate components of these stars for the present study is to gain information on the depletions of sulfur, which is a difficult element to study because the features are usually strongly saturated. These two stars are at large distances from the Galactic plane ($z = 1.56$ and -1.65 pc, respectively), and the sulfur profiles were sufficiently spread out in velocity that their saturation was not a problem when observed at a good velocity resolution. Also, since there is not much H I behind these stars, we can in principle rely on 21-cm observations to indicate the amount of hydrogen at each velocity (while this is true, there is a better method to find $N(\text{H})$ that will be outlined later in §7). Second, for the line of sight toward γ^2 Vel, Fitzpatrick & Spitzer (1994) showed that a significant fraction of all of the gas is fully ionized, and they could identify which velocity components were ionized and which were neutral. (This star has a foreground neutral hydrogen column density just barely above the adopted threshold of $10^{19.5} \text{cm}^{-2}$). Thus, for this star, only column densities associated with H I regions were included. Other stars [e.g. λ Sco (York 1983) and 23 Ori (Welty et al. 1999) had components that were identified with H II regions, but their contributions were small compared to those from the neutral gas components. Finally, the star ζ Oph had specific velocity components identified separately because the highly depleted one at -15 km s^{-1} serves as a standard for establishing the scale of $F_* [N(\text{H})$ for the other component is small enough to neglect – see the discussion in §7.2], and α CMa had small enough H column densities that the $\text{L}\alpha$ absorption could be decomposed into two principal components by Hébrard et al (1999).

4.4. Renormalization to Recent f -values

Many of the earlier determinations of atomic column densities were reported using transition f -values that have since been revised. The current analysis now includes adjustments to compensate for the differences between the old and new values. In many situations we must acknowledge that this is an inexact process since the column densities in the earlier studies were determined from several transitions, not all of which may have been revised (or had different changes).

When multiple lines were measured, the task of making the proper correction was made easier when the investigator indicated which line was the primary source of information for determining a column density. However, most authors did not provide such guidance. Usually, one can count on the weakest lines being the ones that constrain the column density outcome, while strong ones only define the velocity dispersion parameter b . However, these weakest lines sometimes had to be overlooked if the relative errors in the equivalent widths were large.

When two or more lines with different f -value corrections were considered to be about equally influential in the column density determination, their logarithmic corrections were averaged together. This can be a potentially hazardous approach, as illustrated by the following example. The weaker of the two P II lines analyzed by JSS86 has now had its f -value revised downwards by 0.127 dex, while the stronger line has remained virtually unchanged. As a result, any new determination of the curve of growth would make the new b value lower, the inferred saturation of both lines would increase, and $N(\text{P II})$ would need to be revised in an upward direction by more than 0.127 dex. However, this will happen only if indeed the weak line is perceived to be saturated, and it is deemed to be well enough measured to be useful (i.e., it is not dominated by noise). If the strong line dominates in the determination of $N(\text{P II})$ because its errors are so much smaller than those of the weak line and a χ^2 minimization is used (as was the case with JSS86), the column density should remain unchanged. In the particular case of P II in the study by JSS86, the overall distortion of the P II b values is probably small, since there seems to be no systematic offset from the b values measured for Fe II toward the same stars (see their Fig. 1).

All column density adjustments were made on the basis of correcting to the f -values published in a compilation by Morton (2003). While there have been some newer determinations for a few species that have appeared in the literature since 2003, we retain Morton’s values in the interest in having a single standard list that could be consulted in the future. The only new result that was accepted was an f -value for the Ni II transition at 1317 Å reported by Jenkins & Tripp (2006), for which no line strength was listed by Morton. A summary of the f -value correction factors for different investigations, presented in logarithmic form, is shown in Table 1. These numbers represent the amounts by which the originally reported values of $\log N$ were increased for this study.

Table 1—Continued

Code ^a (1)	Reference (2)	Correction Factors (dex)																	Notes (20)
		C (3)	N (4)	O (5)	Mg (6)	Si (7)	P (8)	S (9)	Cl (10)	Ti (11)	Cr (12)	Mn (13)	Fe (14)	Ni (15)	Cu (16)	Zn (17)	Ge (18)	Kr (19)	
CSS95	Cardelli, Sembach, & Savage 1995	0.251	0.001	0.008	...	-0.045	0.017	
DG98	Dupin & Gry 1998	-0.017	...	0.006	-0.013	-0.048	
DS94	Diplas & Savage 1994	5
EPL07	Ellison, Prochaska, & Lopez 2007	0	6
FM90	Fitzpatrick & Massa 1990	7
FS94	Fitzpatrick & Spitzer 1994	-0.369	-0.017	0.127	0.006	-0.011	-0.048	8, 9
FS97	Fitzpatrick & Spitzer 1997	-0.403	-0.017	...	0.006	0.02	-0.018	-0.007	0.007	21
H++03	Hoopes et al. 2003	...	-0.078	10
H++03	Hoopes et al. 2003	...	-0.063	0.002	11
H++93	Hobbs et al. 1993	0.16	...	-0.147	0.021	12
H++99	Hébrard et al. 1999	...	0.007	0.008	-0.001	-0.067	-0.028	
HSF99	Howk, Savage, & Fabian 1999	...	-0.027	0.008	-0.02	0.021	0.132	0.002	0.008	-0.141	0	0	0.16	0.017	
HYO82	Hobbs, York, & Oegerle 1982	0.147	
J++99	Jenkins et al. 1999	...	0.064	
JGD00	Jenkins, Gry, & Dupin 2000	...	-0.027	0.006	
JJ91	Joseph & Jenkins 1991	-0.437	...	0.127	-0.222	-0.036	13
JRS05	Jensen, Rachford, & Snow 2005	0	
JRS07	Jensen, Rachford, & Snow 2007	...	0	
JS07a	Jensen, & Snow 2007a	0.142	

Table 1—Continued

Code ^a (1)	Reference (2)	Correction Factors (dex)																	Notes (20)
		C (3)	N (4)	O (5)	Mg (6)	Si (7)	P (8)	S (9)	Cl (10)	Ti (11)	Cr (12)	Mn (13)	Fe (14)	Ni (15)	Cu (16)	Zn (17)	Ge (18)	Kr (19)	
JS07b	Jensen, & Snow 2007b	0
JSS86	Jenkins, Sav- age, & Spitzer 1986	-0.437	...	0.127	...	0.028	-0.222	0.008	0.114	0.243	14
JSS86	Jenkins, Sav- age, & Spitzer 1986	-0.369	...	-0.009	...	0.028	-0.222	-0.009	15
JSS86	Jenkins, Sav- age, & Spitzer 1986	-0.369	...	0.059	...	0.028	-0.222	0.008	16
JSS86	Jenkins, Sav- age, & Spitzer 1986	-0.369	...	0.059	...	0.028	-0.222	0.008	17
JW96	Jenkins & Wallerstein 1996	0.004	0.27	0.005	...	-0.002	...	-0.022	-0.137	0.404	18
JY78	Jura & York 1978	0.126	...	0.025	19
KAMM03	Knauth et al. 2003	...	-0.063	0	20
KML06	Knauth, Meyer, & Lauroesch 2006	...	0
L++95	Linsky et al. 1995	0	-0.028
L++03	Lehner et al. 2003	0.017	...	-0.01	0	0.021
LHW08	Lallement, Hébrard, & Welsh 2008	0
LKF05	Lebouteiller, Kuassivi, & Ferlet 2005	0	0
LP95	Lipman & Pet- tini 1995	-0.022
LVY79	Laurent, Vidal- Madjar, & York 1979	21
LYBM78	Lugger et al. 1978	...	-0.014
M++07	Miller et al. 2007	0	0	22

Table 1—Continued

Code ^a (1)	Reference (2)	Correction Factors (dex)																Note (20)	
		C (3)	N (4)	O (5)	Mg (6)	Si (7)	P (8)	S (9)	Cl (10)	Ti (11)	Cr (12)	Mn (13)	Fe (14)	Ni (15)	Cu (16)	Zn (17)	Ge (18)		Kr (19)
M78	Morton 1978	0.159	0.251	0.134	−0.006	0.025	...	0.407	−0.199	0.034	0.202	0.242	−0.086	23
MCS97	Meyer, Cardelli, & Sofia 1997	...	−0.063
MD76	Morton & Din- enstein 1976	2
MJC98	Meyer, Jura, & Cardelli 1998	0.032
MJHC94	Meyer et al. 1994	0.033
MY82	Martin & York 1982	...	−0.015	−0.006	24
O++03	Oliveira et al. 2003	0	...	0	0	−0.045
OH06	Oliveira & Hébrard 2006	...	0	0	0	...	0	...	0	0
PTH05	Prochaska, Tripp, & Howk 2005	0
R++00	Ryu et al. 2000	2
R++01	Rachford et al. 2001	2
R++02	Rachford, et al. 2002
RB95	Roth & Blades 1995	0.008	0.015	25
S++03	Sonnentrucker et al. 2003	...	−0.063
S++07	Sheffer et al. 2007	2
S++08a	Shull, private communication	2
S++08b	Sheffer et al. 2008	2, 26
S++96	Snow et al. 1996	0.084	...	0.032	−0.399	0	0.386	−0.045	...	0.032	...	0.327	27
S76	Snow 1976	0.5	−0.3	0.045	0.121	0.312	28
S77	Snow 1977	0.159	...	0.5	...	−0.025	−0.3	0.18	...	0.312	28
S78	Stokes 1978	−0.046
S98	Sarlin 1998	2
SB79	Savage & Bohlin 1979	−0.018

Table 1—Continued

Code ^a (1)	Reference (2)	Correction Factors (dex)																	Notes (20)
		C (3)	N (4)	O (5)	Mg (6)	Si (7)	P (8)	S (9)	Cl (10)	Ti (11)	Cr (12)	Mn (13)	Fe (14)	Ni (15)	Cu (16)	Zn (17)	Ge (18)	Kr (19)	
SY77	Shull & York 1977	0.5	0.057	
VF02	Vidal-Madjar & Ferlet 2002	
W++97	Welsh et al. 1997	-0.023	35
W++99	Welty et al. 1999	0	-0.068	0.002	0	0	0.266	-0.023	0.011	-0.14	0	-0.003	0.16	0.011	0	0	36
WG92	Wallerstein & Gilroy 1992	-0.106	26
WRLS02	Wood et al. 2002	0	0.007	-0.013	...	0.234	...	-0.01	
Y++83	York et al. 1983	...	0.122	37
Y++83	York et al. 1983	...	-0.014	38
Y++83	York et al. 1983	...	0.211	39

Table 1—Continued

Code ^a	Reference	Correction Factors (dex)																	Notes	
		C	N	O	Mg	Si	P	S	Cl	Ti	Cr	Mn	Fe	Ni	Cu	Zn	Ge	Kr		
(1)	(2)	(3)	(4)	(5)	(6)	(7)	(8)	(9)	(10)	(11)	(12)	(13)	(14)	(15)	(16)	(17)	(18)	(19)	(20)	
Y76	York 1976	40
Y83	York 1983	...	-0.016	-0.025	...	0.458	-0.016	-0.006	0.025	0.052
YK79	York & Kinahan 1979	...	-0.027	-0.036	...	0.456	-0.009	-0.006	0.026	...	0.218	-0.228	-0.012	-0.43	0.312	-0.086
YR76	York & Rogerson 1976	41

^aThese codes appear in columns (14) and (18) of Table 2 and column (6) of Tables 7 through 23. The codes L++03 and O++03 do not appear in these tables because they apply only to the white dwarf target stars in the Local Bubble, which are discussed separately in §8.

Note. — (1) Used only for obtaining column densities of H I and H₂; (2) Used only for obtaining column densities of H₂; (3) Adopted weak line results for C, O, and Mg instead of damping wings for strong lines; (4) Adopted Si II from 1808 even though partly saturated; correction was done with care and $\tau_0 = 2.1$; (5) Used only for obtaining column densities for H I; (6) No f -values listed or referenced. Assume the same as PTH05. Ti II toward γ^2 Vel all in the H I component; (7) H I only; no errors given, but from their Fig. 1 errors seem to be about 30%; (8) Used only components identified as coming from H I gas (comps 5,6,7) Comp 2 often blended with H II region comp 3, but it's weak; (9) Error limits for the combination of components simply added together instead of being combined in quadrature; (10) Applies to HD 191877: N I f -values listed in their Table 6 do not agree with those listed by Morton (1991) although they claimed to have used them. Assumed that Morton (1991) values were indeed used; (11) Applies HD 195965; (12) Kr I and Ge II: Preference was given to the strongest line or in best part of the spectrum; tabulated errors were 2σ , so errors were halved; (13) Fe II f -values given; JSS86 f -value used for Mg, P, and Mn (Joseph, private communication); no column density errors stated, so we assume ± 0.20 dex except for Fe II, where the errors were assumed to be ± 0.10 dex (14) Applies to their class 1 stars; (15) Applies to their class 2 stars; (16) Applies to their class 3 stars; (17) Applies to their class 4 stars; (18) Column density errors not stated explicitly; we assign -0.05 and $+0.10$ dex except for Si and S where the positive error was increased to 0.20 dex; (19) Column density error bars increased from 0.1 to 0.2 and 0.2 to 0.3, since their determinations often disagree with later, better ones when there were duplications; (20) Used the 1159.8 and 1160.9Å lines; no f -values stated but they say that they are consistent with those used by MCJS97; (21) Column density errors not listed. Assigned errors of -0.10 dex and $+0.20$ dex; (22) Mostly used f -values from Morton (2003), but found deviations for two lines. We assume other lines defined Fe; (23) Column density entries without errors were assigned an error of ± 0.2 dex. (24) There are some significant disagreements with the N I measurements by Vidal-Madjar et al. (1982); (25) No column density errors stated. We assume they are ± 0.05 dex; (26) No column density errors stated. We assume they are ± 0.10 dex; (27) No col. dens. errors stated, but their Fig. 10 suggests that errors are about 0.3 dex for all elements. For C, O & Mn, we used W_λ errors of very weak lines. We reject the strong C II line fitted to a Ca II curve of growth. (28) Selected measurements of unsaturated or lightly saturated lines much better than those of Bohlin et al (1983), so these values replace those of JSS86. (29) Lower error bars for velocity component nr. 7 reduced by 20% to account for possible contamination by component 7A; (30) f -value corrections apply to an average of the 5 weakest lines that had only a moderate dispersion of strengths; (31) They claim to have used the same f -values as those listed in Table 2 of Savage & Sembach (1996a), otherwise we assume they used Morton (1991); (32) f -value corrections apply to HD 18100; (33) f -value corrections apply to HD 100340; (34) f -value correction applies to an average of both lines in the Mg II 1240Å doublet, using values given by Sofia et al. (1994); (35) No statement on f -values, so we assume they used Morton (1991); column density values taken from their Table 3 and errors from Table 4; (two tables disagree for column densities, but the values in Table 4 are correct (Welsh, private communication); (36) S II lines too saturated; C II and Mg II measured from weak damping wings; (37) Applies to o Per, β^1 Sco; (38) Applies to α^1 Cru, ϵ Cen, and ζ Cen; (39) Applies to η Cen. (40) H₂ only, errors not stated, but are unimportant. (41) H I recordings made at high resolution (U1 detector), which allowed interstellar profiles to be separated from stellar ones. Also, higher Lyman series lines were studied.

Table 2. Stellar Data and Line of Sight Information

HD (1)	Name (2)	Gal. Coord.		V (5)	Spectral Type		$E(B - V)$ (8)	dist. (kpc) (9)	z (kpc) (10)	log $N(\text{H I})$			Ref. ^b (14)	log $N(\text{H}_2)$			
		ℓ (3)	b (4)		Value (6)	ref. ^a (7)				l.l. (11)	best (12)	u.l. (13)		l.l. (15)	best (16)	u.l. (17)	Ref. ^b (18)
1383	HD 1383	119.02	-0.89	7.63	B1 II	JM53	0.37	2.94	-0.05	21.33	21.42	21.51	CLMS04	20.38	20.45	20.52	CLMS04
2905	κ Cas	120.84	0.14	4.19	B0.7 Ia	W72	0.29	1.18	0.00	21.05	21.20	21.32	BSD78	20.09	20.27	20.45	BSD78
5394	γ Cas	123.58	-2.15	2.39	B0 IVe	B++08	0.21	0.17	-0.01	20.06	20.16	20.24	BSD78	16.48	16.53	16.58	S98
12323	HD 12323	132.91	-5.87	8.92	O9 V	B++08	0.21	4.4	-0.45	21.09	21.18	21.27	CLMS04	20.24	20.32	20.40	CLMS04
13268	HD 13268	133.96	-4.99	8.18	O8 Vnn	B++08	0.23	2.1	-0.18	21.23	21.32	21.41	CLMS04	20.35	20.42	20.49	CLMS04
13745	HD 13745	134.58	-4.96	7.90	O9.7 IIIn	B++08	0.34	3.2	-0.28	21.15	21.25	21.35	DS94	20.42	20.47	20.52	S++08a
14434	HD 14434	135.08	-3.82	8.59	O5.5 Vnfp	B++08	0.38	3.5	-0.23	21.28	21.37	21.46	CLMS04	20.40	20.47	20.54	CLMS04
15137	HD 15137	137.46	-7.58	7.86	O9.5 II-IIIn	B++08	0.24	3.5	-0.46	20.95	21.11	21.27	DS94	20.24	20.27	20.30	S++08a
18100	HD 18100	217.93	-62.73	8.44	B1 V	SMS01	0.02	1.7	-1.48	20.02 ^c	20.15 ^c	20.29 ^c	DS94	14.80	R++00
21278	HD 21278	147.52	-6.19	4.97	B5 V	MHG71	0.06	0.16	-0.02	...	20.64 ^c	21.07 ^c	SV85	19.25	19.48	19.71	BSD78
21856	HD 21856	156.32	-16.75	5.90	B1 V	L68	0.15	0.50	-0.14	20.92 ^c	21.02 ^c	21.11 ^c	BSD78	19.89	20.04	20.19	BSD78
22586	HD 22586	264.19	-50.36	8.01	B2 III	H70	0.01	2.02	-1.56	20.21 ^d	20.36 ^d	20.50 ^d	DS94
22928	δ Per	150.28	-5.77	2.99	B5 III	B++08	0.05	0.16	-0.02	...	21.21 ^e	...	SV85	19.10	19.30	19.50	BSD78
22951	40 Per	158.92	-16.70	4.98	B0.5 V	JM53	0.19	0.32	-0.09	20.89	21.04	21.16	BSD78	20.28	20.46	20.64	BSD78
23180	o Per	160.36	-17.74	3.86	B1 III	L68	0.22	0.38	-0.12	20.72 ^d	20.88 ^d	21.01 ^d	BSD78	20.45	20.60	20.75	BSD78
23408	20 Tau	166.17	-23.51	3.87	B7 III	JM53	0.06	0.12	-0.05	19.49	19.75	20.01	BSD78
23478	HD 23478	160.76	-17.42	6.69	B3 IV	H56b	0.20	0.47	-0.14	20.25 ^c	20.71 ^c	20.88 ^c	C++08	20.41	20.48	20.55	C++08
23480	23 Tau	166.57	-23.75	4.16	B6 IVnn	JM53	0.07	0.12	-0.05	19.94	20.12	20.30	BSD78
23630	η Tau	166.67	-23.46	2.87	B7 IIIe	B++08	0.05	0.12	-0.05	19.36	19.54	19.72	BSD78
24190	HD 24190	160.39	-15.18	7.45	B2 Vn	W71	0.23	0.82	-0.22	21.12	21.18	21.24	C++08	20.31	20.38	20.45	C++08
24398	ζ Per	162.29	-16.69	2.88	B1 Ib	B++08	0.27	0.23	-0.07	20.75 ^d	20.80 ^d	20.84 ^d	BSD78	20.49	20.67	20.85	BSD78
24534	X Per	163.08	-17.14	6.10	O9.5 III	S82	0.31	2.07	-0.61	20.67	20.73	20.79	DS94	20.88	20.92	20.96	R++02
24760	ϵ Per	157.35	-10.09	2.90	B0.5 IV	B++08	0.07	0.20	-0.03	20.30	20.40	20.48	BSD78	19.26	19.52	19.78	BSD78
24912	ξ Per	160.37	-13.11	4.04	O7.5 IIIIn	B++08	0.26	0.59	-0.13	21.02	21.11	21.19	BSD78	20.38	20.53	20.68	BSD78
27778	62 Tau	172.76	-17.39	6.33	B3V	SMS01	0.34	0.23	-0.07	...	20.35 ^c	20.89 ^c	CLMS04	20.64	20.72	20.80	CLMS04
28497	228 Eri	208.78	-37.40	5.59	B1.5 Ve	B++08	0.02	0.43	-0.26	...	19.53 ^f	20.13 ^f	SV85	15.00	15.11	15.20	SY77
29248	ν Eri	199.31	-31.38	3.92	B2 III	L68	-0.02	0.21	-0.11	20.03 ^d	20.35 ^d	20.52 ^d	B++83	17.41	B++83
30614	α Cam	144.07	14.04	4.30	O9.5 Iae	B++08	0.23	1.73	0.42	20.81 ^d	20.90 ^d	20.98 ^d	BSD78	20.19	20.34	20.49	BSD78
31237	π^5 Ori	196.27	-24.56	3.72	B2 III	L68	0.03	0.35	-0.14	19.65 ^d	20.16 ^d	20.37 ^d	B++83	17.45	B++83
34029	α Aur	162.59	4.57	0.08	G1 III+K0 III	SF90	0.80	0.01	0.00	18.15	18.24	18.30	VF02
34816	λ Lep	214.83	-26.24	4.27	B0.5 IV	L68	-0.03	0.26	-0.12	20.08	20.18	20.26	B++83	15.04	B++83
34989	HD 34989	194.62	-15.61	5.78	B1 V	L68	0.11	0.49	-0.13	21.00 ^c	21.10 ^c	21.18 ^c	BSD78	18.45	BSD78
35149	23 Ori	199.16	-17.86	5.00	B1 Vn	L68	0.08	0.36	-0.11	20.47 ^c	20.63 ^c	20.74 ^c	BSD78	18.53	BSD78
35439	25 Ori	200.96	-18.29	4.87	B1 Vne	B++08	0.06	0.35	-0.11	20.06	20.36	20.49	B++83	14.63	14.78	14.93	B++83
35715	ψ Ori	200.09	-17.22	4.60	B1 V	L68	0.03	0.37	-0.11	20.26 ^c	20.49 ^c	20.64 ^c	B++83	14.63	14.78	14.93	B++83
36166	HD 36166	201.67	-17.19	5.74	B2 V	L68	0.01	0.40	-0.12	...	20.11 ^c	...	B++83	15.00	B++83
36486	δ Ori A	203.86	-17.74	2.23	O9.5 II	B++08	0.08	0.42	-0.13	20.15	20.19	20.23	ST++00	14.42	14.68	14.94	BSD78
36822	ϕ^1 Ori	195.40	-12.29	4.40	B0.5 IV-V	L68	0.07	0.33	-0.07	20.72	20.81	20.89	BSD78	19.17	19.32	19.47	BSD78
36841	HD 36841	204.26	-17.22	8.58	O8	SMS01	0.31	4.92	-1.46	21.40	21.70	22.00	SV85
36861	λ Ori A	195.05	-12.00	3.30	O8 IIIIn	B++08	0.10	0.55	-0.11	20.65	21.78	20.88	BSD78	18.92	19.12	19.32	BSD78
37021	θ^1 Ori	209.01	-19.38	7.96	B3 V	LA76	0.42	0.56	-0.19	21.52 ^c	21.65 ^c	21.78 ^c	CLMS04	CLMS04
37043	ι Ori	209.52	-19.58	2.77	O9 III	B++08	0.06	0.43	-0.14	20.08	20.15	20.21	BSD78	14.49	14.69	14.89	BSD78
37061	ν Ori	208.92	-19.27	6.87	B0.5 V	LA76	0.44	0.64	-0.21	21.64	21.73	21.82	CLMS04
37128	ϵ Ori	205.21	-17.24	1.70	B0 Iae	B++08	0.10	0.48	-0.14	20.35	20.45	20.53	BSD78	16.37	16.57	16.77	BSD78
37367	HD 37367	179.04	-1.03	5.99	B2 IV-V	L68	0.33	0.34	-0.01	21.02 ^c	21.17 ^c	21.29 ^c	CLMS04	20.44	20.53	20.62	CLMS04
37468	σ Ori	206.82	-17.34	3.80	O9.5 V	L68	0.03	0.37	-0.11	20.42	20.52	20.60	B++83	18.30	B++83
37742	ζ Ori A	206.45	-16.59	1.70	O9.5 Ib	B++08	0.13	0.25	-0.07	20.32	20.41	20.49	BSD78	15.56	15.71	15.86	SCH75
37903	HD 37903	206.85	-16.54	7.84	B1.5 V	SMS01	0.29	0.83	-0.24	21.02 ^c	21.12 ^c	21.22 ^c	CLMS04	20.78	20.85	20.92	CLMS04
38666	μ Col	237.29	-27.10	5.15	O9.5 V	B++08	0.01	0.41	-0.19	19.84	19.86	19.88	HSF99	15.35	15.50	15.65	SCH75

27

Table 2—Continued

HD (1)	Name (2)	Gal. Coord.		V (5)	Spectral Type		$E(B - V)$ (8)	dist. (kpc) (9)	z (kpc) (10)	$\log N(\text{H I})$				$\log N(\text{H}_2)$			
		ℓ (3)	b (4)		Value (6)	ref. ^a (7)				l.l. (11)	best (12)	u.l. (13)	Ref. ^b (14)	l.l. (15)	best (16)	u.l. (17)	Ref. ^b (18)
38771	κ Ori	214.51	-18.50	2.05	B0.5 Ia	B++08	0.09	0.20	-0.06	20.47	20.52	20.56	BSD78	15.48	15.68	15.88	BSD78
40111	139 Tau	183.97	0.84	4.82	B1 Ib	B++08	0.10	0.48	0.01	20.81 ^d	20.90 ^d	20.98 ^d	BSD78	19.53	19.73	19.93	BSD78
40893	HD 40893	180.09	4.34	8.99	B0 IV	MCW55	0.31	3.07	0.23	21.36	21.45	21.54	C++08	20.42	20.49	20.56	C++08
41161	HD 41161	164.97	12.89	6.76	O8 Vn	B++08	0.19	1.4	0.31	20.91	21.00	21.09	OH06	19.89	19.98	19.18	OH06
42933	δ Pic	263.30	-27.68	4.81	B0.5 IV	B++08	0.02	0.40	-0.19	20.15	20.23	20.31	DS94
43818	LU Gem	188.49	3.87	6.92	B0 II	JM53	0.45	1.85	0.12
44506	HD 44506	241.63	-20.78	5.53	B1.5 III _n	B++08	0.02	0.75	-0.27	19.49 ^d	20.09 ^d	20.32 ^d	B++83	14.85	B++83
44743	β CMa	226.06	-14.27	1.97	B1 II-III	L68	-0.04	0.15	-0.04	18.26 ^g	18.30 ^g	18.34 ^g	C++96
47839	15 Mon	202.94	2.20	4.66	O7 Vf	B++08	0.07	0.86	0.03	20.21	20.31	20.41	DS94	15.45	15.55	15.65	BDS78
48915 (+12)	α CMa	227.23	-8.89	-1.47	A0 IV	L72	0.00	0.003	0.00	17.18	17.40	17.54	H++99
(+18)										17.48	17.60	17.74	H++99
49798	HD 49798	253.71	-19.14	8.29	sdO	KM89	0.03	0.57	-0.19
52089	ϵ CMa	239.83	-11.33	1.51	B2 II	MR50	-0.05	0.12	-0.02	17.85 ^g	17.96 ^g	18.08 ^g	C++95	17.66	BSD78
52266	HD 52266	219.13	-0.68	7.23	O9 IV _n	W73	0.22	1.84	-0.02
52918	19 Mon	218.01	0.61	4.99	B1 IVe	B++08	0.04	0.37	0.00	19.75	20.20	20.35	B++83	14.63	14.78	14.93	B++83
53138	σ^2 Cma	235.55	-8.23	3.00	B3 Ia	MR50	0.05	0.98	-0.14	17.95 ^d	19.78 ^d	20.04 ^d	BSD78
53975	HD 53975	225.68	-2.32	6.48	O7.5 V	W72	0.16	1.40	-0.06	21.07	21.13	21.19	OH06	19.14	19.18	19.22	OH06
54662	HD 54662	224.17	-0.78	6.23	O6.5 V	W72	0.27	1.22	-0.02	21.23	21.38	21.49	BSD78	19.82	20.00	20.18	BSD78
55879	HD 55879	224.73	0.35	6.00	O9.5 II-III	W72	0.08	1.78	0.01	20.75	20.90	21.02	BSD78	18.90	BSD78
57060	29 CMa	237.82	-5.37	4.98	O7 Iabfp	B++08	0.15	1.87	-0.17	20.60	20.70	20.78	BSD78	15.60	15.78	15.96	BSD78
57061	τ CMa	238.18	-5.54	4.39	O9 II	B++08	0.11	1.57	-0.15	20.65	20.70	20.74	BSD78	15.30	15.48	15.66	BSD78
62542	HD 62542	255.92	-9.24	8.03	B5 V	FTW55	0.31	0.38	-0.06	20.60	20.81	21.02	R++02
63005	HD 63005	242.47	-0.93	9.13	O6 Vf	B++08	0.22	5.4	-0.09	21.18	21.24	21.30	CLMS04	20.14	20.23	20.32	CLMS04
64740	HD 64740	263.38	-11.19	4.61	B1.5 Vp	B++08	0.01	0.23	-0.05	19.64 ^c	20.05 ^c	20.23 ^c	B++83	14.95	B++83
64760	HD 64760	262.06	-10.42	4.23	B0.5 Ib	B++08	0.05	0.51	-0.09	20.13	20.26	20.35	B++83	14.60	B++83
65575	χ Car	266.68	-12.32	3.44	B3 IVp	HGS69	0.01	0.14	-0.03	20.74 ^e	B++83	14.78	B++83
65818	V Pup	263.48	-10.28	4.45	B1V+B3V	P43	0.07	0.29	-0.05	20.36 ^c	20.52 ^c	20.65 ^c	B++83	14.78	15.08	15.38	B++83
66788	HD 66788	245.43	2.05	9.43	O8 V	SMS01	0.20	4.85	0.17	21.13	21.23	21.33	JS07a	19.69	19.72	19.75	S++08a
66811	ζ Pup	255.98	-4.71	2.21	O5 Ibnf	B++08	0.12	0.33	-0.03	19.92	19.96	20.00	ST++00	14.40	14.45	14.50	MD76
68273	γ^2 Vel	262.80	-7.69	1.81	WC8+O9 I	B++08	0.00	0.47	-0.06	19.67	19.71	19.75	ST++00	14.03	14.23	14.43	BSD78
69106	HD 69106	254.52	-1.33	7.13	B0.5 IV _{nn}	B++08	0.14	1.5	-0.03	21.00	21.06	21.12	C++08	19.57	19.64	19.71	C++08
71634	HD 71634	273.32	-11.52	6.65	B7 IV	M61	0.09	0.32	-0.06
72089 (+5)	HD 72089	263.21	-3.89	8.01	B5 II-III	MSS78	0.03	0.80	-0.05
72127	HD 72127	262.57	-3.36	4.99	B2 IV	HGS69	0.03	0.40	-0.02
72754	FY Vel	266.83	-5.82	6.90	B2 I: pe	T71	0.31	3.91	-0.40	21.05 ^h	21.17 ^h	21.29 ^h	CLMS04	20.25	20.35	20.45	CLMS04
73882	HD 73882	260.18	0.64	7.27	O8.5 Vn	W73	0.59	0.96	0.01	21.04	21.11	21.22	FM90	20.98	21.08	21.18	SR++00
74375	HD 74375	275.82	-10.86	4.32	B1.5 III	HGS69	0.16	0.44	-0.08	20.67 ^d	20.78 ^d	20.87 ^d	BSD78	18.34	BSD78
74575	α Pyx	254.99	5.77	3.68	B1.5 III	HGS69	0.04	0.27	0.03	20.27 ^d	20.46 ^d	20.59 ^d	B++83	15.04	B++83
75309	HD 75309	265.86	-1.90	7.84	B1 IIp	B++08	0.18	2.9	-0.10	20.98 ^h	21.07 ^h	21.17 ^h	CLMS04	20.08	20.20	20.32	CLMS04
79186	GX Vel	267.36	2.25	5.02	B5 Ia	GHS77	0.23	1.91	0.07	21.08 ^d	21.18 ^d	21.27 ^d	CLMS04	20.63	20.72	20.81	CLMS04
79351	a Car	277.69	-7.37	3.40	B2.5 V	S82	0.04	0.14	-0.02	20.44 ^c	B++83	17.90	B++83
81188	κ Vel	275.88	-3.54	2.46	B2 IV-V	HGS69	0.02	0.18	-0.01	19.50 ^c	B++83	17.70	B++83
88115	HD 88115	285.32	-5.53	8.31	B1.5 II _n	B++08	0.12	3.7	-0.36	20.86 ^h	20.98 ^h	21.06 ^h	A++03	19.00	19.30	19.48	A++03
91316	ρ Leo	234.89	52.77	3.84	B1 Iab	B++08	0.04	1.09	0.87	20.14 ^d	20.25 ^d	20.32 ^d	BSD78	15.31	15.61	15.91	BSD78
91597	HD 91597	286.86	-2.37	9.61	B1 III _{ne}	B++08	0.30	3.9	-0.16	21.34 ^h	21.40 ^h	21.46 ^h	DS94	19.65	19.70	19.75	S++08a
91651	HD 91651	286.55	-1.72	8.87	O9 V:n	B++08	0.25	2.8	-0.08	21.09	21.15	21.21	DS94	19.04	19.07	19.10	S++08a
91824	HD 91824	285.70	0.07	8.15	O7 V	GHS77	0.22	2.99	0.00	21.06	21.12	21.18	CLMS04	19.78	19.85	19.92	CLMS04
91983	HD 91983	285.88	0.05	8.58	B1 III	F58	0.14	3.03	0.00	21.07 ^d	21.16 ^d	21.26 ^d	CLMS04	20.07	20.14	20.21	CLMS04
92554	HD 92554	287.60	-2.02	9.50	O9.5 II _n	B++08	0.34	6.9	-0.24	21.18	21.28	21.38	DS94	18.88	18.93	18.98	S++08a

Table 2—Continued

HD (1)	Name (2)	Gal. Coord.		<i>V</i> (5)	Spectral Type		<i>E(B - V)</i> (8)	dist. (kpc) (9)	<i>z</i> (kpc) (10)	log <i>N</i> (H I)				log <i>N</i> (H ₂)				
		<i>ℓ</i> (3)	<i>b</i> (4)		Value (6)	ref. ^a (7)				l.l. (11)	best (12)	u.l. (13)	Ref. ^b (14)	l.l. (15)	best (16)	u.l. (17)	Ref. ^b (18)	
93030	<i>θ</i> Car	289.60	-4.90	2.78	B0 V	H56a	0.04	0.14	-0.01	20.18	20.26	20.34	DS94	14.90	15.02	15.26	AJS92	
93205	V560 Car	287.57	-0.71	7.76	O3 Vf+	B++08	0.34	3.3	-0.04	21.34	21.38	21.42	A++03	19.70	19.78	19.85	A++03	
93222	HD 93222	287.74	-1.02	8.11	O7 IIIf	B++08	0.32	3.6	-0.06	21.33	21.40	21.46	A++03	19.70	19.78	19.85	A++03	
93521	(-66)	HD 93521	183.14	62.15	7.06	O9 Vp	B++08	0.05	1.76	1.56	18.21	18.51	18.82	SF93
	(-58)										19.28	19.34	19.40	SF93
	(-51)										19.11	19.20	19.29	SF93
	(-39)										18.70	18.88	19.06	SF93
	(-29)										18.06	18.38	18.70	SF93
	(-18)										19.23	19.28	19.33	SF93
	(-10)										19.31	19.36	19.41	SF93
	(+3)										19.24	19.30	19.36	SF93
	(+7)										18.56	18.79	19.02	SF93
	(total)										20.06 ⁱ	20.10 ⁱ	20.16 ⁱ	DS94
93843	HD 93843	288.24	-0.90	7.33	O5 IIIf	B++08	0.24	3.5	-0.06	21.25	21.33	21.41	DS94	19.58	19.61	19.64	S++08a	
94493	HD 94493	289.01	-1.18	7.27	B1 Ib	B++08	0.15	3.4	-0.07	21.03 ^h	21.08 ^h	21.12 ^h	A++03	20.08	20.15	20.20	A++03	
94454	HD 94454	295.69	-14.73	6.70	B8 III	HC75	0.19	0.30	-0.08	20.66	20.76	20.86	S++08b	
99171	HD 99171	286.33	17.38	6.11	B2 IV-V	HGS69	0.03	0.54	0.16	...	20.06 ^c	20.43 ^c	BSD78	15.10	15.25	15.40	BSD78	
99857	HD 99857	294.78	-4.94	7.47	B0.5 Ib	B++08	0.27	3.5	-0.30	21.16	21.24	21.31	A++03	20.36	20.43	20.49	A++03	
99872	HD 99872	296.69	-10.62	6.11	B3 V	HGS69	0.29	0.24	-0.04	20.41	20.51	20.61	S++07	
99890	HD 99890	291.75	4.43	8.31	B0 III _n	GHS77	0.17	3.59	0.28	20.80	20.93	21.06	DS94	19.42	19.47	19.52	S++08a	
100340	HD 100340	258.85	61.23	10.07	B1 V	B++08	0.00	3.0	2.63	20.38 ^c	20.46 ^c	20.54 ^c	DS94	29	
102065	HD 102065	300.03	-18.00	6.61	B2 V	BFM07	0.28	0.18	-0.05	20.53	20.63	20.73	BFM07	
103779	HD 103779	296.85	-1.02	7.22	B0.5 Iab	GHS77	0.17	4.34	-0.08	21.06	21.16	21.26	DS94	19.77	19.82	18.87	S++08a	
104705	DF Cru	297.45	-0.34	7.83	B0 Ib	B++08	0.17	5.0	-0.03	21.00	21.10	21.18	A++03	20.04	20.08	20.11	A++03	
106490	<i>δ</i> Cru	298.23	3.79	2.78	B2 IV	B++08	0.02	0.11	0.01	...	20.60	19.69 ^c	B++83	14.08	B++83	
108248	<i>α</i> ¹ Cru	300.13	-0.36	1.40	B0.5 IV	HGS69	0.22	0.10	0.00	19.50	19.60	19.70	YR76	14.18	B++83	
108639	HD 108639	300.22	1.95	7.81	B0.2 III	W72	0.26	2.41	0.08	21.26	21.35	21.44	C++08	19.88	19.95	20.02	C++08	
109399	HD 109399	301.71	-9.88	7.63	B0.7 II	GHS77	0.19	2.94	-0.50	21.05	21.11	21.17	DS94	19.84	20.04	20.24	JS07a	
110432	BZ Cru	301.96	-0.20	5.32	B0.5 IIIe	B++08	0.39	0.6	0.00	20.70	20.85	21.00	R++01	20.60	20.64	20.68	R++02	
111934	BU Cru	303.20	2.51	6.92	B1.5 Ib	D++06	0.32	2.29	0.10	
112999	V946 Cen	304.17	2.18	7.38	B6 V	GHS77	0.17	0.45	0.02	20.01	20.11	20.21	S++08b	
113904	<i>θ</i> Mus	304.67	-2.49	5.69	WC5+B0 Ia	HGS69	0.18	2.66	-0.12	20.98	21.08	21.16	BSD78	19.72	19.83	19.94	BSD78	
114886	HD 114886	305.52	-0.83	6.89	O9 III _n	GHS77	0.32	1.84	-0.03	21.28	21.34	21.40	C++08	20.15	20.23	20.30	C++08	
115071	V961 Cen	305.76	0.15	7.97	B0.5 V _n	GHS77	0.40	2.70	0.01	21.30	21.36	21.42	C++08	20.55	20.63	20.70	C++08	
116658	<i>α</i> Vir	316.11	50.84	1.04	B1 IV	B++08	0.10	0.08	0.06	18.90 ^j	19.00 ^j	19.10 ^j	YR76	12.65	12.95	13.25	Y76	
116781	V967 Cen	307.05	-0.07	7.45	B0 III _{ne}	B++08	0.31	2.2	0.00	21.08	21.18	21.28	JS07a	20.03	20.08	20.13	S++08a	
116852	HD 116852	304.88	-16.13	8.49	O9 III	B++08	0.14	4.5	-1.25	20.87	20.96	21.05	CLMS04	19.68	19.79	19.90	CLMS04	
118716	<i>ε</i> Cen	310.19	8.72	2.27	B1 III	HGS69	0.04	0.13	0.02	19.10 ^d	19.60 ^d	19.79 ^d	B++83	14.08	B++83	
119608	HD 119608	320.35	43.13	7.50	B1 Ib	SMS01	0.11	4.20	2.87	20.79 ^d	20.85 ^d	20.90 ^d	SV85	
120086	HD 120086	329.61	57.50	7.82	B2 V	SMS01	0.04	0.99	0.83	20.07 ^c	SV85	
120324	<i>μ</i> Cen	314.24	19.12	3.46	B2 IV-Ve	S82	0.04	0.16	0.05	4.00 ^f	18.76 ^f	20.22 ^f	B++83	14.78	B++83	
121263	<i>ζ</i> Cen	314.07	14.19	2.52	B2.5 IV	B++08	0.02	0.12	0.03	20.02 ^e	BSD78	12.62	12.80	12.98	BSD78	
121968	HD 121968	333.97	55.84	10.16	B1 V	B++08	0.11	3.8	3.14	20.43 ^c	20.58 ^c	20.70 ^c	DS94	18.60	18.70	18.80	BFM07	
122451	<i>β</i> Cen	311.77	1.25	0.60	B1 III	B++08	0.06	0.12	0.00	19.49 ^j	19.54 ^j	19.59 ^j	YR76	12.70	12.80	12.90	Y76	
122879	HD 122879	312.26	1.79	6.43	B0 Ia	B++08	0.29	3.3	0.10	21.14	21.26	21.38	CLMS04	20.15	20.24	20.33	CLMS04	
124314	HD 124314	312.67	-0.42	6.64	O6 V _{nf}	B++08	0.43	1.4	-0.01	21.31	21.41	21.49	A++03	20.46	20.52	20.57	A++03	
125924	HD 125924	338.16	48.28	9.66	B2 IV	SMS01	0.01	3.51	2.62	20.47 ^c	20.63 ^c	20.74 ^c	DS94	
127972	<i>η</i> Cen	322.77	16.67	2.32	B2 IVe	S82	0.00	0.09	0.03	19.48 ^f	B++83	14.18	B++83	
135591	HD 135591	320.13	-2.64	5.43	O7.5 IIIf	B++08	0.18	1.25	-0.06	20.92	21.08	21.19	BSD78	19.66	19.77	19.88	BSD78	

Table 2—Continued

HD (1)	Name (2)	Gal. Coord.		<i>V</i> (5)	Spectral Type		<i>E</i> (<i>B</i> − <i>V</i>) (8)	dist. (kpc) (9)	<i>z</i> (kpc) (10)	log <i>N</i> (H I)				log <i>N</i> (H ₂)				
		<i>ℓ</i> (3)	<i>b</i> (4)		Value (6)	ref. ^a (7)				l.l. (11)	best (12)	u.l. (13)	Ref. ^b (14)	l.l. (15)	best (16)	u.l. (17)	Ref. ^b (18)	
177989	HD 177989	17.81	−11.88	9.34	B0 III	B++08	0.11	6.0	−1.24	20.86	20.96	21.04	A++03	20.11	20.18	20.23	A++03	
179406	20 Aql	28.23	−8.31	5.36	B3 V	L68	0.26	0.30	−0.04	20.57	20.62	20.65	S++08a	
179407	HD 179407	24.02	−10.40	9.44	B0.5 Ib	SMS01	0.23	9.21	−1.66	21.00	21.11	21.22	DS94	20.16	20.21	20.27	S++08a	
184915	κ Aql	31.77	−13.29	4.96	B0.5 IIIne	B++08	0.17	0.70	−0.16	20.77	20.85	20.93	DS94	20.16	20.31	20.46	BSD78	
185418	HD 185418	53.60	−2.17	7.52	B0.5 V	B++08	0.38	1.2	−0.05	21.10	21.19	21.28	CLMS04	20.59	20.71	20.83	CLMS04	
188209	HD 188209	80.99	10.09	5.63	O9.5 Iab	W72	0.14	2.21	0.39	20.75	20.90	21.02	BSD78	19.90	20.01	20.12	BSD78	
190918	V1676 Cyg	72.65	2.07	6.81	WN4+O9.7Iab	B++08	0.44	2.1	0.08	21.32	21.38	21.44	CLMS04	19.76	19.84	19.92	CLMS04	
191877	HD 191877	61.57	−6.45	6.27	B1 Ib	B++08	0.14	2.3	−0.26	20.95 ^d	21.05 ^d	21.15 ^d	H++03	19.97	20.02	20.07	S++08a	
192035	RX Cyg	83.33	7.76	8.22	B0 III - IVn	B++08	0.28	2.7	0.36	21.11	21.20	21.29	CLMS04	20.55	20.62	20.69	CLMS04	
192639	HD 192639	74.90	1.48	7.11	O7 Ibf	B++08	0.56	2.1	0.05	21.20	21.29	21.38	CLMS04	20.63	20.73	20.83	CLMS04	
193322	HD 193322	78.10	2.78	5.82	O9 V	L68	0.33	0.70	0.03	20.86	21.08	21.23	BSD78	19.90	20.08	20.26	BSD78	
195455	HD 195455	20.27	−32.14	9.20	B0.5 III	SMS01	0.07	5.76	−3.07	20.57	20.67	20.77	DS94	
195965	HD 195965	85.71	5.00	6.98	B0 V	B++08	0.19	1.1	0.10	20.92	20.95	20.98	H++03	20.34	20.37	20.40	JS07b	
197512	HD 197512	87.89	4.63	8.55	B0.5 V	J78	0.30	1.70	0.14	
198478	55 Cyg	85.75	1.49	4.86	B3 Ia	L68	0.43	1.34	0.03	21.15 ^d	21.31 ^d	21.46 ^d	CLMS04	20.72	20.87	21.02	CLMS04	
198781	HD 198781	99.94	12.61	6.46	B0.5 V	L68	0.26	0.69	0.15	20.82	20.91	21.00	CLMS04	20.41	20.48	20.55	CLMS04	
199579	HD 199579	85.70	−0.30	5.97	O6 Vf	B++08	0.31	1.4	−0.01	20.93	21.04	21.15	DS94	20.49	20.53	20.57	R++02	
200120	59 Cyg	88.03	0.97	4.74	B1.5 Ve	B++08	0.02	0.34	0.01	...	19.20 ^f	20.07 ^f	BSD78	19.12	19.30	19.48	BSD78	
201345	HD 201345	78.44	−9.54	7.75	O9 V	B++08	0.14	2.2	−0.36	20.88	20.97	21.06	CLMS04	19.42	19.55	19.68	CLMS04	
202347	HD 202347	88.22	−2.08	7.50	B1.5 V	B++08	0.11	1.0	−0.04	20.68 ^c	20.83 ^c	20.94 ^c	A++03	19.85	19.95	20.04	CLMS04	
202904	ν Cyg	80.98	−10.05	4.43	B2.5 Ve	S82	0.09	0.16	−0.03	...	20.37 ^f	20.65 ^f	B++83	18.97	19.15	19.33	CA++83	
203064	68 Cyg	87.61	−3.84	5.04	O7.5 III: n((f))	W72	0.22	1.28	−0.09	20.85	21.00	21.11	BSD78	20.15	20.30	20.45	BSD78	
203374	HD 203374	100.51	8.62	6.69	B2 Vne	A81	0.43	0.34	0.05	20.96 ^f	21.13 ^f	21.23 ^f	C++08	20.51	20.60	20.69	C++08	
203532	HD 203532	309.46	−31.74	6.36	B3 IV	HGS69	0.24	0.22	−0.11	...	20.22 ^c	20.97 ^c	CLMS04	20.56	20.64	20.72	CLMS04	
203938	HD 203938	90.56	−2.23	7.10	B0.5 IV	MCW55	0.59	0.79	−0.03	21.33	21.48	21.63	FM90	20.94	21.00	21.06	R++02	
206144 ^o	HD 206144	34.82	−45.12	9.36	B2 II	MSS88	0.05	5.98	−4.23	20.26 ^d	20.49 ^d	20.65 ^d	DS94	
206267	HD 206267	99.29	3.74	5.62	O6 V	W72	0.45	0.86	0.06	21.15	21.30	21.45	R++02	20.82	20.86	20.90	R++02	
206773	HD 206773	99.80	3.62	6.93	B0 V:nnep	GK76	0.39	0.82	0.05	21.03	21.09	21.15	CLMS04	20.34	20.44	20.54	CLMS04	
207198	HD 207198	103.14	6.99	5.96	O9.5 Ib-II	B++08	0.47	1.3	0.16	21.46	21.53	21.60	CLMS04	20.79	20.83	20.87	R++02	
207308	HD 207308	103.11	6.82	7.49	B0.7 III-IV(n)	W71	0.44	1.24	0.15	21.10	21.20	21.30	JS07a	20.71	20.76	20.81	S++08a	
207538	HD 207538	101.60	4.67	7.30	O9.5 V	GK76	0.51	0.94	0.08	21.22	21.34	21.46	DS94	20.85	20.91	20.97	R++02	
208440	HD 208440	104.03	6.44	7.91	B1 V	S68	0.27	1.05	0.12	21.12 ^f	21.21 ^f	21.31 ^f	CLMS04	20.22	20.29	20.36	CLMS04	
208947	HD 208947	106.55	9.00	6.40	B2 V	L68	0.16	0.56	0.09	20.72 ^c	20.91 ^c	21.03 ^c	C++08	
209339	HD 209339	104.58	5.87	6.69	B0 IV	L68	0.24	1.22	0.13	21.10	21.17	21.24	C++08	20.16	20.24	20.32	C++08	
209975	19 Cep	104.87	5.39	5.11	O9.5 Ib	W72	0.27	1.23	0.12	20.96	21.11	21.23	BSD78	19.90	20.08	20.26	BSD78	
210809	HD 210809	99.85	−3.13	7.56	O9 Iab	B++08	0.28	4.3	−0.23	21.20	21.29	21.38	CLMS04	19.91	20.00	20.09	CLMS04	
210839	λ Cep	103.83	2.61	5.09	O6 Infp	B++08	0.49	1.1	0.05	21.03	21.15	21.27	DS94	20.80	20.84	20.88	R++02	
212571	π Aqr	66.01	−44.74	4.79	B1 V(e)	L68	0.07	0.24	−0.17	20.32 ^f	20.50 ^f	20.62 ^f	DS94	
212791	V408 Lac	101.64	−4.30	8.02	B3ne	KW99	0.18	0.62	−0.05	20.85 ^f	21.11 ^f	21.23 ^f	CLMS04	19.31	19.42	19.53	CLMS04	
214080	HD 214080	44.80	−56.92	6.82	B1 Ib	B++08	0.05	3.42	−2.87	20.38 ^d	20.61 ^d	20.77 ^d	BSD78	19.00	BSD78	
214680	10 Lac	96.65	−16.98	4.88	O9 V	W72	0.08	0.61	−0.18	20.54	20.70	20.81	BSD78	19.11	19.22	19.33	BSD78	
214993	12 Lac	97.65	−16.18	5.23	B1.5 III _n	L68	0.06	0.61	−0.17	20.60 ^d	20.76 ^d	20.89 ^d	B++83	19.45	19.63	19.81	B++83	
215733	(−93) (−83) (−61) (−59) (−54) (−47) (−45)	HD 215733	85.16	−36.35	7.34	B1 II	SMS01	0.06	2.79	−1.65	16.91	17.39	17.63	FS97
											17.60	18.40	18.55	FS97
											18.91	19.44	19.56	FS97
											18.75	18.95	19.25	FS97
											19.09	19.63	19.88	FS97
											...	18.94	19.69	FS97
											17.37	18.06	18.38	FS97

Table 2—Continued

HD (1)	Name (2)	Gal. Coord.		V (5)	Spectral Type		$E(B - V)$ (8)	dist. (kpc) (9)	z (kpc) (10)	$\log N(\text{H I})$				$\log N(\text{H}_2)$			
		ℓ (3)	b (4)		Value (6)	ref. ^a (7)				l.l. (11)	best (12)	u.l. (13)	Ref. ^b (14)	l.l. (15)	best (16)	u.l. (17)	Ref. ^b (18)
(-42)										17.23	18.53	18.90	FS97
(-40)										18.06	18.81	19.23	FS97
(-32)										19.50	19.64	19.74	FS97
(-31)									
(-28)										18.85	18.91	19.02	FS97
(-26)										18.99	19.11	19.19	FS97
(-23)										19.21	19.25	19.29	FS97
(-21)										19.32	19.37	19.42	FS97
(-19)									
(-16)										20.08	20.11	20.14	FS97
(-11)										19.57	19.60	19.63	FS97
(-9)										20.01	20.07	20.13	FS97
(-5)										19.50	19.58	19.66	FS97
(+1)										19.68	19.71	19.74	FS97
(+9)									
(+15)										18.35	18.42	18.49	FS97
(total)										20.66 ^P	20.75 ^P	20.84 ^P	DS94
217675	o And	102.21	-16.10	3.63	B6 III	S82	0.05	0.12	-0.03	19.49	19.67	19.85	BSD78
218376	1 Cas	109.95	-0.78	4.84	B0.5 III	L68	0.16	0.35	0.00	20.80	20.95	21.07	BSD78	19.97	20.15	20.33	BSD78
218915	HD 218915	108.06	-6.89	7.20	O9.5 Iab	B++08	0.21	5.0	-0.60	21.13	21.17	21.21	A++03	20.15	20.20	20.26	A++03
219188	HD 219188	83.03	-50.17	7.00	B0.5 IIIIn	B++08	0.09	2.08	-1.60	20.62	20.85	20.99	BSD78	19.16	19.34	19.52	BSD78
220057	HD 220057	112.13	0.21	6.95	B3 IV	CLMS04	0.17	0.77	0.00	20.83 ^q	21.02 ^q	21.15 ^q	CLMS04	20.21	20.28	20.35	CLMS04
224151	V373 Cas	115.44	-4.64	6.05	B0.5 II-III	L68	0.34	1.30	-0.11	21.24	21.32	21.39	A++03	20.54	20.61	20.67	A++03
224572	σ Cas	115.55	-6.36	5.00	B1 V	L68	0.13	0.34	-0.04	20.64 ^c	20.79 ^c	20.88 ^c	BSD78	20.05	20.23	20.41	BSD78
232522	HDE 232522	130.70	-6.71	8.70	B1 II	B++08	0.14	6.1	-0.71	21.02	21.08	21.14	CLMS04	20.13	20.22	20.31	CLMS04
303308	HDE 303308	287.59	-0.61	8.21	O3 Vf	B++08	0.33	3.8	-0.04	21.33	21.41	21.48	A++03	20.26	20.34	20.41	A++03
308813	HDE 308813	294.79	-1.61	9.32	O9.5 V	B++08	0.26	3.1	-0.09	21.11	21.20	21.29	CLMS04	20.18	20.25	20.32	CLMS04
...	BD +35 4258	77.19	-4.74	9.46	B0.5 Vn	MCW55	0.22	2.90	-0.24	21.18	21.28	21.38	JS07a	19.53	19.56	19.59	S++08a
...	BD +53 2820	101.24	-1.69	9.96	B0 IV:n	H56b	0.28	5.07	-0.15	21.26	21.35	21.44	CLMS04	19.90	20.01	20.12	CLMS04
...	CPD -59 2603	287.59	-0.69	8.75	O5 V((f))	W73	0.36	3.5	-0.04	21.01	21.12	21.23	DS94	20.05	20.15	20.25	S++08b
...	CPD -69 1743	303.71	-7.35	9.46	B0.5 IIIIn	SMS01	0.19	5.45	-0.70	21.02	21.11	21.20	CLMS04	19.81	19.90	19.99	CLMS04

^aCodes in this column are linked to references listed in Table 3

^bCodes in this column are linked to references listed in Table 1

^cPublished $N(\text{H I})$ corrected for contamination by the stellar $\text{L}\alpha$ line using the prescription of Diplax & Savage (1994) for $\log g = 4$ and the $[c_1]$ value in the catalog of Hauck & Mermilliod (1998); see §4.6.2 for details.

^dSame as with note *c* except that $\log g = 3$ instead of 4.

^eAfter computing the correction for contamination by the stellar $\text{L}\alpha$ feature, the upper limit value was a negative number, so the upper limit was set equal to the upper limit for $N(\text{H I})_{\text{obs.}}$.

^fCorrection for stellar $\text{L}\alpha$ contamination was based on the stellar spectral type and a generic correction for that type with $\log g = 4$, since either a measurement of $[c_1]$ was not available or the star had emission lines that made photometric measurements unreliable; see §4.6.2 for details.

^gNormally this value of $N(\text{H I})$ would require a correction for stellar $\text{L}\alpha$ contamination, but in this case the column density was determined from the shape of the star's energy distribution in the EUV after accounting for hydrogen absorption in the star's photosphere, so the published number was accepted at face value.

^hSame as for note *f* except that $\log g = 3$ was used instead of 4.

ⁱThese values are taken from a measurement of the $\text{L}\alpha$ feature. Numbers listed above for individual velocity components are from 21-cm emission measurements. The sums of the 21-cm values give

$\log N(\text{H I}) = 19.99, 20.08, 20.17.$

^jNormally this value of $N(\text{H I})$ would require a correction for stellar $L\alpha$ contamination, but in this case the interstellar feature could be measured at the bottom of the stellar one, so the published number was accepted at face value.

^k $[c_1]$ taken from Tobin, Viton & Sivan (1994).

^l $[c_1]$ measurement is not available, and the spectral classification could range between B3 V and B5 V. The correction for stellar $L\alpha$ contamination is based on a compromise value for the generic correction, but with an increase in the Δ uncertainty parameter to 0.54 dex (see Eq. 20).

^m $[c_1]$ taken from Tobin (1985)

ⁿ $[c_1]$ taken from Tobin & Kaufmann (1984)

^oThis star was misidentified as HD 206114 by Diplas & Savage (1994).

^pThese values are taken from a measurement of the $L\alpha$ feature. Numbers listed above for individual velocity components are from 21-cm emission measurements. The sums of the 21-cm values give $\log N(\text{H I}) = 20.66, 20.77, 20.88.$ $[c_1]$ taken from Tobin (1985)

^q $[c_1]$ evaluated from the Vilnius photometric indices of Sudzius & Bobinas (1992), followed by a conversion to the Strömngren system using the recipe given by Kaltcheva & Knude (2002).

Table 3. Reference Codes for Spectral Types Listed in Table 2

Code	Reference
A81	Abt 1981
ACNP85	Andersen et al. 1985
B++08	Bowen et al. 2008
B54	Bidelman 1954
B58	Bertiau 1958
BFM07	Burgh, France, & McCandliss 2007
CLMS04	Cartledge et al. 2004
D++06	Dufton et al. 2006
F58	Feast 1958
FTW55	Feast, Thackeray, & Wesselink 1955
GG94	Garrison & Gray 1994
GK76	Garrison & Kormendy 1976
GMB77	Golay, Mandwewala, & Bartholdi 1977
H56a	Hoffleit 1956
H56b	Hiltner 1956
H70	Hill 1970
HGS69	Hiltner, Garrison, & Schild 1969
J81	Jensen, 1981
JJ92	Jaschek & Jaschek 1992
JM53	Johnson & Morgan 1953
KM89	Kilkenny & Muller 1989
KW99	Kohoutek & Wehmeyer 1999
L68	Lesh 1968
L72	Levato 1972
LA76	Levato & Abt 1976
M61	Morris 1961
MCW55	Morgan, Code, & Whitford 1955
MHG71	Morgan, Hiltner, & Garrison 1971
MR50	Morgan & Roman 1950
P43	Popper 1943
S68	Simonson 1968
S82	Slettebak 1982
SF90	Strassmeier & Fekel 1990

Table 3—Continued

Code	Reference
SMM85	Savage, Massa, & Meade 1985
SMS01	Savage, Meade, & Sembach 2001
T71	Thackeray 1971
W71	Walborn 1971
W72	Walborn 1972
W73	Walborn 1973

4.5. Characteristics of the Sight Lines and Target Stars

Table 2 lists some fundamental information on the stars included in this investigation, along with determinations of the amount of foreground hydrogen in both atomic and molecular form. The stars are identified by both their HD numbers and their alternate representations [columns (1) and 2], followed by their Galactic coordinates [columns (3) and (4)]. Column (5) lists visual magnitudes of the stars taken from the Simbad database. Except for a few stars, these V magnitudes were not used for calculating the reddenings or spectroscopic parallaxes discussed in §4.5.1; the tabulated values are therefore of uncertain origin and meant only as an approximate guide. Column (6) lists the spectral types of the stars, followed by codes in column (7) that designate their sources in the literature according to the matches to references given in Table 3. Column (8) lists the $B - V$ color excess toward each star, which is one indication of the total amount of dust along the sight line. Column (9) shows the distances toward the stars, computed according to the principles given below in §4.5.1, followed by the corresponding distances z from the Galactic plane [column (10)]. Columns (11) through (18) show the lower limits, best values, and upper limits for atomic and molecular hydrogen, in each case followed by codes that give the sources for these values. Note that many atomic hydrogen column densities had adjustments applied to account for stellar contamination of the $L\alpha$ profile, as will be explained later in §4.6.2.

Figure 4 shows the distribution of F_* values for all of the stars considered, including those which did not meet the eligibility requirements for helping to determine the element parameters A_X , B_X , and z_X as outlined under point nrs. 3, 4, and 7 in §4.2. Note that there are values of F_* below zero, but the sightlines for these cases have $\log N(\text{H}) < 19.5$, which violates one of the conditions needed for participation in the estimation of the element parameters. Actual numerical values of F_* (and their uncertainties) toward the specific target stars appear later in Table 5.

4.5.1. Calculations of Distances and Reddenings

For determining the distances to early-type stars, one must make use of different sources of information, depending on the circumstances. At the most basic level, we note that trigonometric parallaxes provide the most accurate measures of distance for nearby stars, but when the errors in these parallaxes are not considerably smaller than the measured values, it is better to rely on spectroscopic parallaxes. For trigonometric parallaxes, we rely on the second reduction of the Hipparcos data (nr. I/311 in the Strasbourg CDS VizieR on-line catalog)⁸ (van Leeuwen 2007), but accept the values only if $\pi/\sigma(\pi) > 10$. For stars that do not meet this standard, we revert to distance derivations based on spectroscopic parallaxes, as described below.

As a part of an investigation of O VI absorptions in the Galactic disk, Bowen et al. (2008)

⁸The faulty version of this catalog that appeared during July to Sept 2008 was not used.

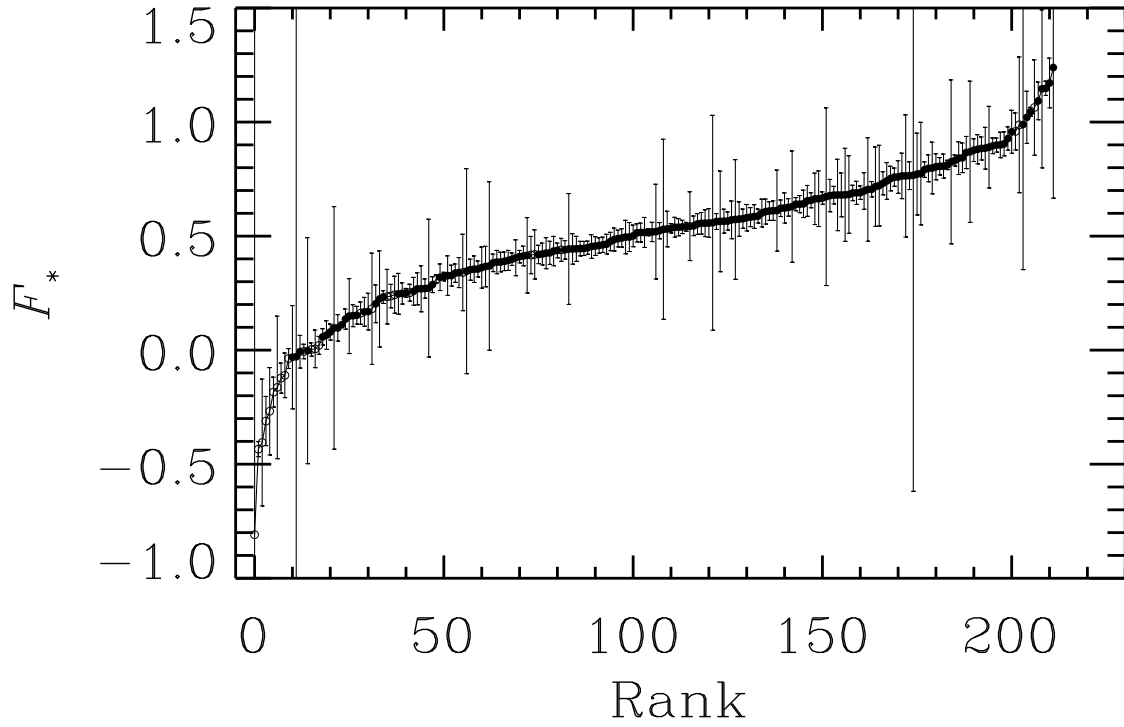


Fig. 4.— The outcomes for F_* and their respective 1σ errors in this study, arranged in a sequence according to their rank in value. Solid points apply to cases where $N(\text{H}) > 10^{19.5}\text{cm}^{-2}$, and hollow ones indicate measurements below this range.

(hereafter B08) carried out a rigorous process for determining the distances to stars based on spectroscopic parallaxes with many additional refinements, as described in Appendix B of their article. We adopt here many of the principles that they did, but with some simplifications since the standard of accuracy here is not as demanding as that for one of the objectives of the O VI survey. Some of the stars in the current survey were listed by B08. For those cases, Table 2 simply duplicates the values of distance and reddening that they listed, except for cases where they adopted Hipparcos parallaxes. The reason for rejecting their distances based on Hipparcos data is that (1) they used results from the earlier, less accurate solutions that were incorporated into the first catalog (Schrijver 1997), and (2) their acceptance threshold was set to $\pi/\sigma(\pi) > 5$ instead of 10.

Stars for which neither the Hipparcos parallaxes nor the determinations by B08 were applicable had their spectroscopic parallaxes determined with the standard formula for the distance d (in kpc),

$$\log d = (m_V - A_V - M_V - 10)/5 \tag{17}$$

where m_V is the apparent V magnitude of the star, A_V is the extinction by dust in the visible (assumed to be $3.1E(B - V)$), and M_V is the absolute V magnitude of the star. We follow the recommendation of B08 in adopting, when available, the two-color photometric measurements from the *Tycho* Starmapper catalog (Schrijver 1997) to obtain values for the B and V magnitudes, after a suitable transformation from the *Tycho* magnitude system B_T and V_T (see Appendix B1 of B08). The premise here is that these magnitudes represent a uniform set of measurements where both colors were determined at a single epoch (which can be important for variable stars). If *Tycho* magnitudes were not available, we use values of B and V listed in the catalog of Johnson et al. (1966). Finally, if neither of the above two sources had listings for the stars, we used the magnitudes given by the Simbad web site.

Column (6) of Table 2 lists the adopted spectral classifications of the target stars, along with the respective sources of the assignments in the column that follows. (Many of these classifications were taken from either B08 or Savage, Meade & Sembach (2001), who made judgments on the most reliable sources and listed them in their tables.) For these chosen spectral types, we link them to values of M_V in the consolidation from many sources made by B08 and adopt the intrinsic colors from Wegner (1994). A fraction of the stars are recognized as spectroscopic binaries and thus must have their distances adjusted outward to compensate for the fact that their brightnesses are greater than that of the primary star alone. B08 outline a procedure for implementing this correction (see their Appendix B1.2).

4.6. Determinations of $N(\text{H})$

For most stars, we can draw upon measurements of both H I and H₂ and evaluate the quantity $N(\text{H I}) + 2N(\text{H}_2)$ to find the total number of hydrogen atoms $N(\text{H})$ along a given sight line. Since the errors in $N(\text{H I})$ and $N(\text{H}_2)$ are uncorrelated, we can simply add them in quadrature to find

the net uncertainty in $N(\text{H})$. Unfortunately, for some of the stars of potential value for this survey, there were no measurements of the foreground H I, H₂ (or both), or there were just upper limits thereof. For other stars, corrections had to be made for the upward shift in the apparent $N(\text{H I})$ caused by L α absorption in the stellar atmospheres. The handling of these special circumstances is discussed in the following subsections.

4.6.1. Missing Information

At the most fundamental level, sight lines without information on both H I and H₂ were not suitable for measuring depletions directly. However, for about half of these stars $N(\text{H I})$ is known, and values of $N(\text{H})$ could be salvaged on the premise that empirically the fraction of hydrogen in molecular form is very small ($f(\text{H}_2) \equiv 2N(\text{H}_2)/[N(\text{H I}) + 2N(\text{H}_2)] < 0.1$) when the star's $B - V$ color excess is less than 0.05 (Savage et al. 1977); see also Rachford et al. (2009). An equivalent cutoff can be established on the basis of just the measurement of $N(\text{H I})$: In a survey of stars using the *Copernicus* satellite, Bohlin, Savage & Drake (1978) found that

$$\langle \{N(\text{H I}) + 2N(\text{H}_2)\}/E(B - V) \rangle = 5.8 \times 10^{21} \text{ atoms cm}^{-2}\text{mag}^{-1}, \quad (18)$$

which is approximately consistent with

$$\langle N(\text{H I})/E(B - V) \rangle = 5.2 \times 10^{21} \text{ atoms cm}^{-2}\text{mag}^{-1}, \quad (19)$$

derived for an *IUE* survey conducted by Shull & Van Steenberg (1985) for a larger number of stars. For such stars with no explicit H₂ data, but which had $\log N(\text{H I}) < 20.4$ the value for $N(\text{H})$ was set equal to $N(\text{H I})$, but with an increase in the upper error bar by 0.04 dex to allow for the fact that an unseen additional 10% of the hydrogen atoms could be in molecular form.

Many stars had no reported values for $N(\text{H I})$ because either the L α absorption was not observed or the star was of a late enough spectral type that there was a good chance that the L α feature was strongly dominated by a stellar contribution. It is important to emphasize that for such cases we did not use $E(B - V)$ to determine $N(\text{H})$ on the basis of the empirical relationship given in Eq. 18. This choice makes the survey immune to possible misleading effects caused by real deviations from the general connection between selective extinction and the amount of gas present. This can be important for future studies that might attempt to relate depletions to various observable properties of the dust (i.e., A_V , R_V , wavelength of maximum polarization, etc.). It also avoids our being deceived by photometric errors arising from the occasional presence of emission lines in the spectra of stars.

We avoided the practice of estimating $N(\text{H})$ simply by using the column density of a supposedly undepleted element and assuming a solar abundance ratio, since the lack of any depletion for that element could be subject to question. For example, we did not accept values of $N(\text{H})$ listed by Cartledge et al. (2004, 2006) based on the column densities of Kr. (Later, it will be shown that Kr may exhibit some very mild depletion.)

Ultimately, stars for which $N(\text{H})$ could not be recovered from data in the literature were not useless. A means for calculating an indirect, synthetic value for this quantity is discussed in §7, and it will be demonstrated that this outcome offers a reasonably accurate replacement for an observed value of $N(\text{H})$.

4.6.2. Corrections for Stellar $L\alpha$ Absorption

A significant proportion of the sight lines covered in this study (102 cases) made use of stars that had spectral types B1 or cooler. In such instances, there is a danger that the equivalent width of the observed $L\alpha$ absorption feature is enhanced by an underlying stellar contribution (Savage & Panek 1974). It is important to account for this effect, since there will be a systematic shift in the measurement of $N(\text{H I})$, sometimes quite small, to some amount that is above the true value that belongs to the ISM. Many investigators who reported or used values of $N(\text{H I})$ recognized this problem and provided cautions that some of their results were probably contaminated by a stellar contribution, but they did not attempt to apply compensations (Bohlin, Savage, & Drake 1978; Shull & Van Steenberg 1985; André et al. 2003; Cartledge et al. 2004, 2008). However Bohlin, et al. (1983) appear to have overlooked this problem when they derived additional values of $N(\text{H I})$.

In a study of $L\alpha$ absorption toward a large number of stars, Diplas & Savage (1994) devised a means for estimating the stellar $L\alpha$ absorption and corrected many of their measurements to compensate for it. Their method was based on the findings of Savage & Panek (1974) with some additional guidance from NLTE stellar atmosphere calculations, and it used as a yardstick the reddening-corrected measure of the Balmer discontinuity based on a combination of narrow-band Strömrgren photometric indices $[c_1] = c_1 - 0.2(b - y)$, where the uncorrected Balmer jump index $c_1 = (u - v) - (v - b)$.

In making corrections for stellar $L\alpha$ absorption in the present study, we assume that the stellar profile is well approximated by a Lorentzian shape, as did Diplas & Savage, so that we may simply subtract from the observed $N(\text{H I})$ the equivalent column density for the stellar line to obtain the interstellar value. In estimating the strength of the stellar line, we follow exactly the recipe given by Diplas & Savage. Our only departure from their practice was that we did not exclude from consideration cases where $\log N(\text{H I})_{\text{obs.}} - \log N(\text{H I})_{\text{stellar}} \leq 0.5$ dex. We justify this action on the grounds that the larger uncertainties are well accounted for in the error estimation technique described below, which then influences the weight factors in the parameter estimations described in §§3.1 and 3.2 without totally discarding the results at an arbitrary level.

After subtraction of $N(\text{H I})_{\text{stellar}}$ from $N(\text{H I})_{\text{obs.}}$ to obtain $N(\text{H I})_{\text{ISM}}$, we define the error in the result $\sigma[N(\text{H I})]_{\text{ISM}}$ in terms of a combination of errors in both the observed column density and the estimate for the stellar contribution, given by the relation

$$\sigma[N(\text{H I})]_{\text{ISM}} = \sqrt{\sigma_{\pm}[N(\text{H I})]_{\text{obs.}}^2 + [N(\text{H I})_{\text{stellar}}(1 - 10^{\mp\Delta})]^2}, \quad (20)$$

where $\sigma_{\pm}[N(\text{H I})]_{\text{obs.}}$ represents the differences between the best values of the observed column densities and their respective upper and lower bounds, and Δ is the logarithm of the relative uncertainty in $N(\text{H I})_{\text{stellar}}$. We adopted a value $\Delta = 0.20$ dex for all of the correction calculations.⁹

For most of the stars that needed an evaluation of $N(\text{H I})_{\text{stellar}}$, values of the critical parameter $[c_1]$ could be retrieved from the catalog of Hauck & Mermilliod (1998).¹⁰ In a few cases, other sources were needed, as indicated in the endnotes of Table 2. The photometry for stars whose spectral classifications indicated the presence of emission lines (i.e., with an “e” appended) are probably untrustworthy. For these stars, as well as others for which no measurements of $[c_1]$ could be found, the estimates for $N(\text{H I})_{\text{stellar}}$ had to be based on the stars’ spectral types, using mean values of $[c_1]$ found for other stars with similar classifications. From the dispersion of individual results about these means, we judge that the uncertainty of any outcome using only the spectral classification is about 0.38 dex; hence we used this value for Δ in Eq. 20 for the small number of cases where a spectral type had to be used instead of $[c_1]$. These stars with reduced accuracy are also identified explicitly in the table.

In a number of instances, we found that $\sigma[N(\text{H I})]_{\text{ISM}} > N(\text{H I})_{\text{ISM}}$, but $N(\text{H I})_{\text{ISM}} > 0$. When this happened, lower limits were not stated in Table 2 and should thus be considered to be zero (the preferred values and upper limits were retained however). In other cases, $N(\text{H I})_{\text{ISM}} < 0$ but $N(\text{H I})_{\text{ISM}} + \sigma[N(\text{H I})]_{\text{ISM}} > 0$; under these circumstances only upper limits set equal to $N(\text{H I})_{\text{ISM}} + \sigma[N(\text{H I})]_{\text{ISM}}$ were stated. Finally, there were 6 instances where $N(\text{H I})_{\text{ISM}} + \sigma[N(\text{H I})]_{\text{ISM}} < 0$; when this happened, only upper limits were stated and they were simply set equal to the upper limits for $N(\text{H I})_{\text{obs.}}$. The fact that this occurred for only 6 out of the 95 cases considered for the correction offers a rough indication that the estimates for the 1σ uncertainties in $N(\text{H I})_{\text{ISM}}$ are probably not unrealistically small.

There are a few determinations of $N(\text{H I})$ for the cooler stars that could be accepted at their stated values because either (1) their interstellar features could be seen as distinct absorptions at the bottoms of the photospheric features (α CMa, α Vir, β Cen and λ Sco) (York & Rogerson 1976; York 1983; Hébrard et al. 1999) or (2) the H I column density was determined by the observed shape of the star’s energy distribution in the EUV after accounting for hydrogen absorption in the star’s photosphere (β and ϵ CMa) (Cassinelli et al. 1995, 1996).

⁹The best value of Δ , an error parameter that must include both random and systematic errors, is difficult to quantify with much precision. Our choice of $\Delta = 0.20$ dex is a conservative one based on 3 considerations: (1) An estimate by Savage & Panek (1974) that their rms errors in equivalent widths of the stellar $\text{L}\alpha$ feature are about 20%, which translates into (+0.16, -0.19) dex errors in $N(\text{H I})_{\text{stellar}}$, (2) An rms deviation of approximately 0.08 dex in $N(\text{H I})$ at $[c_1] \approx 0.3$ on either side of the theoretical line shown in Fig. 2 of Diplas & Savage (1994) (where the stellar line probably dominates over the interstellar contribution), but with 4 outliers elsewhere that were more than three times this value in the negative direction, and (3) the size of the transition between the two discrete choices for factoring in the stellar surface gravity, one at $\log g = 3$ and the other at $\log g = 4$, in the recipe of Diplas & Savage.

¹⁰The photometric data are available in the Strasbourg CDS VizieR on-line catalog nr. II/215.

5. Solutions for the Element Coefficients

Compilations of the atomic column density measurements (corrected for f -value changes) and their sources in the literature appear in Appendix B with a series of tables organized according to the different elements studied in this survey. These same tables also show the outcomes for F_* , together with information on how well the individual measurements conform to the best-fit solutions within our generalized framework.

For the depletion parameters that pertain to the just the elements, Table 4 presents the outcomes of the weighted least squares fits described in §3.2. (Sulfur is an element that presents special challenges and will be handled separately in §9.) Column (2) of this table lists the assumed reference abundances taken from Lodders (2003) for the proto-Sun (see §2.1). The fundamental parameters of the linear fits are A_X , B_X and z_X listed in columns (3) to (5), but the secondary quantities $[X_{\text{gas}}/\text{H}]_0$ and $[X_{\text{gas}}/\text{H}]_1$ in columns (6) and (7) allow us to understand how these parameters translate into the expected depletions near the two extremes of F_* , $F_* = 0$ and 1 (values of F_* greater than 1 do show up for a few stars however – see Figure 4). The last three columns of the table present information on how well the observations fit their respective best-fit trends. For each element, we can use the values of χ^2 [column (8)] with their appropriate degrees of freedom ν (number of observations minus 2) listed in the next column to compute the probability shown in column (10) that the fit could have been worse than what we obtained. These probabilities are based on the assumptions that (1) the basic model for depletions expressed in Eq. 10 is correct and that (2) the errors in the observed depletions were estimated correctly. For Mn, this probability value seems rather low, which may indicate that either there are complicating factors that render the model as inappropriate for this element or that the errors in measuring column densities were underestimated (or both). Conversely, unreasonably high values for these probabilities (e.g., Mg, Fe, Cu, and Ge) indicate that the measurement errors have probably been overestimated.

Table 4. Element Depletion Parameters^a

Elem.	Adopted								Prob.
X	$(X/H)_{\odot}^b$	A_X	B_X^c	z_X	$[X_{\text{gas}}/H]_0^c$	$[X_{\text{gas}}/H]_1^c$	χ^2	ν	worse
(1)	(2)	(3)	(4)	(5)	(6)	(7)	(8)	(9)	fit
(1)	(2)	(3)	(4)	(5)	(6)	(7)	(8)	(9)	(10)
C	8.46 ± 0.04	-0.101 ± 0.229	-0.193 ± 0.060	0.803	-0.112 ± 0.194	-0.213 ± 0.075	3.7	8	0.881
N	7.90 ± 0.11	-0.000 ± 0.079	-0.109 ± 0.111	0.550	-0.109 ± 0.119	-0.109 ± 0.117	28.8	32	0.628
O	8.76 ± 0.05	-0.225 ± 0.053	-0.145 ± 0.051	0.598	-0.010 ± 0.060	-0.236 ± 0.055	75.0	64	0.164
Mg	7.62 ± 0.02	-0.997 ± 0.039	-0.800 ± 0.022	0.531	-0.270 ± 0.030	-1.267 ± 0.029	79.0	103	0.962
Si	7.61 ± 0.02	-1.136 ± 0.062	-0.570 ± 0.029	0.305	-0.223 ± 0.035	-1.359 ± 0.052	19.4	16	0.247
P	5.54 ± 0.04	-0.945 ± 0.051	-0.166 ± 0.042	0.488	0.296 ± 0.049	-0.649 ± 0.050	69.5	65	0.330
Cl	5.33 ± 0.06	-1.242 ± 0.129	-0.314 ± 0.065	0.609	0.442 ± 0.102	-0.800 ± 0.082	38.9	44	0.688
Ti	5.00 ± 0.03	-2.048 ± 0.062	-1.957 ± 0.033	0.430	-1.077 ± 0.043	-3.125 ± 0.049	50.7	43	0.195
Cr	5.72 ± 0.05	-1.447 ± 0.064	-1.508 ± 0.055	0.470	-0.827 ± 0.062	-2.274 ± 0.064	24.1	20	0.239
Mn	5.58 ± 0.03	-0.857 ± 0.041	-1.354 ± 0.032	0.520	-0.909 ± 0.038	-1.765 ± 0.038	106.3	83	0.043
Fe	7.54 ± 0.03	-1.285 ± 0.044	-1.513 ± 0.033	0.437	-0.951 ± 0.038	-2.236 ± 0.041	48.5	66	0.948
Ni	6.29 ± 0.03	-1.490 ± 0.062	-1.829 ± 0.035	0.599	-0.937 ± 0.051	-2.427 ± 0.043	30.7	34	0.630
Cu	4.34 ± 0.06	-0.710 ± 0.088	-1.102 ± 0.063	0.711	-0.597 ± 0.089	-1.307 ± 0.068	15.3	32	0.995
Zn	4.70 ± 0.04	-0.610 ± 0.066	-0.279 ± 0.045	0.555	0.059 ± 0.058	-0.551 ± 0.054	25.6	19	0.142
Ge	3.70 ± 0.05	-0.615 ± 0.083	-0.725 ± 0.054	0.690	-0.301 ± 0.078	-0.916 ± 0.059	12.4	24	0.975
Kr	3.36 ± 0.08	-0.166 ± 0.103	-0.332 ± 0.083	0.684	-0.218 ± 0.109	-0.384 ± 0.089	18.9	26	0.839

^aAs defined in Eqs. 10, 11, 13 & 15. Coefficients for S do not appear in this table because a nonstandard approach was required. The coefficients are given in the text of §9.

^bOn a logarithmic scale with $H = 12$. Values and their errors taken from the recommended solar abundances of Lodders

(2003).

^cUnlike the convention for listing errors in the fit outcomes in Tables 7 to 23, the uncertainties with the terms listed here include both the formal errors of the fit coefficients and the error in the adopted value of $(X/H)_{\odot}$, added together in quadrature.

6. The Buildup of Dust Grains

The strengths of chemical bonds for compounds that are most likely to form in dust grains vary over a large range. As a consequence, the propensity of different elements to condense into solid form, or the likelihood that they can subsequently be liberated back into the gas phase, are strongly dependent on physical conditions and time scales for creating or destroying the compounds. One popular paradigm is that the most refractory compounds are formed early in the nucleation process (possibly in the mass-loss outflows of stars or in the ejecta of supernovae), forming a core of the dust grain, and this is followed by the accumulation in dense molecular clouds of more loosely bound compounds that form a mantle around this core (Greenberg 1989; Jones, Duley, & Williams 1990; Mathis 1990; Dwek 1998; Tielens 1998; Draine 2003a). However, in approaching the issue of relative depletions in different regions of space, we can bypass the question of how the grains are structured, i.e., whether they have a core-mantle assembly or a more amorphous configuration, and simply focus on the empirical relationships between different element abundances when the overall severity of the depletions change.

Since we define lines of sight with $F_* = 0$ to represent the circumstances that exhibit the minimum general level of depletion, we can regard values of $[X_{\text{gas}}/\text{H}]_0$ to represent a “base depletion” that, by virtue of it being found everywhere, probably indicates the composition of the most durable constituents of grains (or in the parlance of the core-mantle picture, the disappearance of elements in the gas phase to make up the “core” of a grain). As the composition of the grains evolve from being dominated by refractory compounds to more volatile ones, different elements increase the absolute values of their depletions at different rates. One way to characterize the makeup of the more developed grains that have incorporated these volatile compounds might be to consider the depletions at some much larger level of depletion, say at $F_* = 1$.

An important drawback of any declaration of an absolute level of depletion is that it depends on the assumed abundance of an element in the ISM when no grains exist at all, for which there have been some inconsistent quantitative conclusions, as discussed earlier in §2.1. As a result, there have been conflicting views on the makeup of the grains, which in turn have created some challenges in constructing representations of the number, sizes and compositions of dust grains that had to be reconciled with the observed absorption, scattering and polarization at visible, UV and X-ray wavelengths (Mathis 1996; Smith & Dwek 1998; Draine 2003b,c).

While our expressions of the base depletions $[X_{\text{gas}}/\text{H}]_0$ must depend on the adopted values of the reference abundances, we can dispense with this relationship for more strongly developed depletions by not attempting to characterize the total composition of grains in the more advanced stages of growth, but instead simply by measuring the additional consumptions of different elements as they are incorporated into the newly formed grain materials. That is, by determining how rapidly the abundances of different elements decrease as F_* advances, we become insensitive to ambiguities that arise from uncertainties in the reference abundances.

If we substitute the right-hand side of Eq. 10 for $[X_{\text{gas}}/\text{H}]$ into Eq. 2 and differentiate it with

respect to F_* , we find that

$$\begin{aligned} d(X_{\text{dust}}/H)/dF_* &= -(\ln 10)(X/H)_\odot A_X 10^{B_X + A_X(F_* - z_X)} \\ &= -(\ln 10)A_X (X_{\text{gas}}/H)_{F_*} \end{aligned} \tag{21}$$

The first equality gives the result in terms of variables defined earlier in this paper, while the second shows that this outcome is independent of the adopted solar abundances – only the actual expectation of (X_{gas}/H) and its slope (A_X) with F_* matter. (Note that the term (X_{gas}/H) refers to the actual gas-phase abundance of an element X relative to H, whereas the notation used in earlier equations, $[X_{\text{gas}}/H]$, refers to the logarithm of the element’s depletion factor.)

Figures 5 through 8 show two fundamental results for all of the elements except sulfur. (Again, sulfur is a difficult case that will be treated separately in §9.) For each element, the upper panel depicts the observed depletions as a function of F_* . Individual observed depletions are plotted as points with diameters that indicate their respective levels of accuracy. Dashed lines follow the linear trends with F_* represented by the best fits defined by the parameters A_X , B_X , and z_X listed in Table 4. The quantities $[X_{\text{gas}}/H]_0$ and $[X_{\text{gas}}/H]_1$ in columns (6) and (7) in that table are equal to the intercepts of these lines at $F_* = 0$ and $F_* = 1$, respectively; see Eqs. 13 through 16. The lower panels show the differential grain compositions, expressed in terms of the number of atoms per H atom that condense onto the grains per unit change in F_* . The cross-hatched regions show the allowed combinations of this differential composition for 1 and 2σ deviations in the errors for A_X and B_X . (Note that the portion of $\sigma(B_X)$ that is attributable to $\sigma(X/H)_\odot$ drops out of Eq. 21, thus leaving only the formal uncertainty in the least-squares solution for the intercept of the fit at z_X . These values of $\sigma(B_X)$ can be recovered by subtracting in quadrature the error values listed in column (2) of Table 4 from those listed in column (4) of the same table.)

Clearly, the slopes of the logarithms of the consumption rates of free atoms exhibit large variations from one element to the next, indicating that as the gas becomes more depleted the composition of the grains must change (or, put differently, that the material in the outer portions of the grain mantles differs from that in or near the cores). Our outlook on plausible mixtures of compounds within the grains must be constrained by not only the consumption information presented here, but also the chemical properties of the compounds themselves (Mathis 1996; Draine 2003a, 2004).

Fig. 5.— (Shown on next page) *Top row of panels:* Measured depletions (points) and the linear trends defined by the parameters A_X , B_X and z_X in Eq. 10 (dashed lines), as listed in Table 4, shown as a function of the generalized depletion parameter F_* for the elements C, N, O, Mg and Si. Solid points have $N(\text{H}) > 10^{19.5} \text{cm}^{-2}$, while open ones have $N(\text{H})$ values below this range. Gray points represent sightlines that had only 3 elements to define their F_* parameters, while black ones represent those that had 4 or more elements. Upper and lower limit measurements are depicted with arrows (and were not included in any analysis). Sight lines that crossed the galactocentric limits $R_{\text{GC}} < 7 \text{kpc}$ or $R_{\text{GC}} > 10 \text{kpc}$ are overlaid with crosses (+) or x's (×), respectively, to indicate that they were not used to define the linear trends for the elements. *Bottom row of panels:* Differential consumptions of elements by number (relative to hydrogen) by dust grains for small changes in F_* , again plotted as a function of F_* . The trend lines that follow Eq. 21 with the best values of A_X and B_X are shown with dark lines, while the allowable changes that can arise from the uncertainties in A_X and B_X are shown by the shaded regions. Uncertainties at the 1σ level are shown by the cross-hatched areas, while the envelopes for 2σ deviations have simple line shading in only one direction.

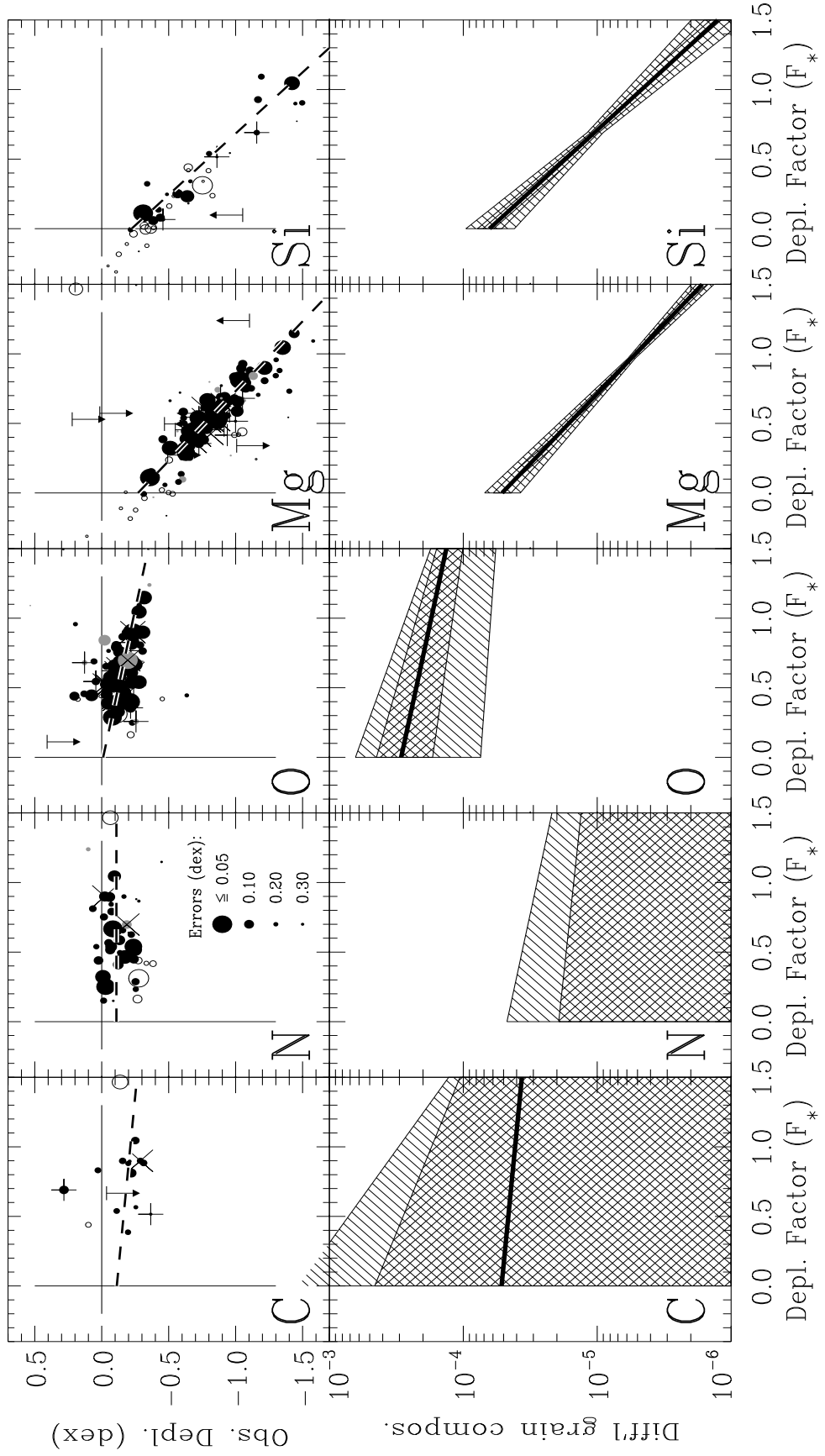


Fig. 5.— (Caption on previous page.)

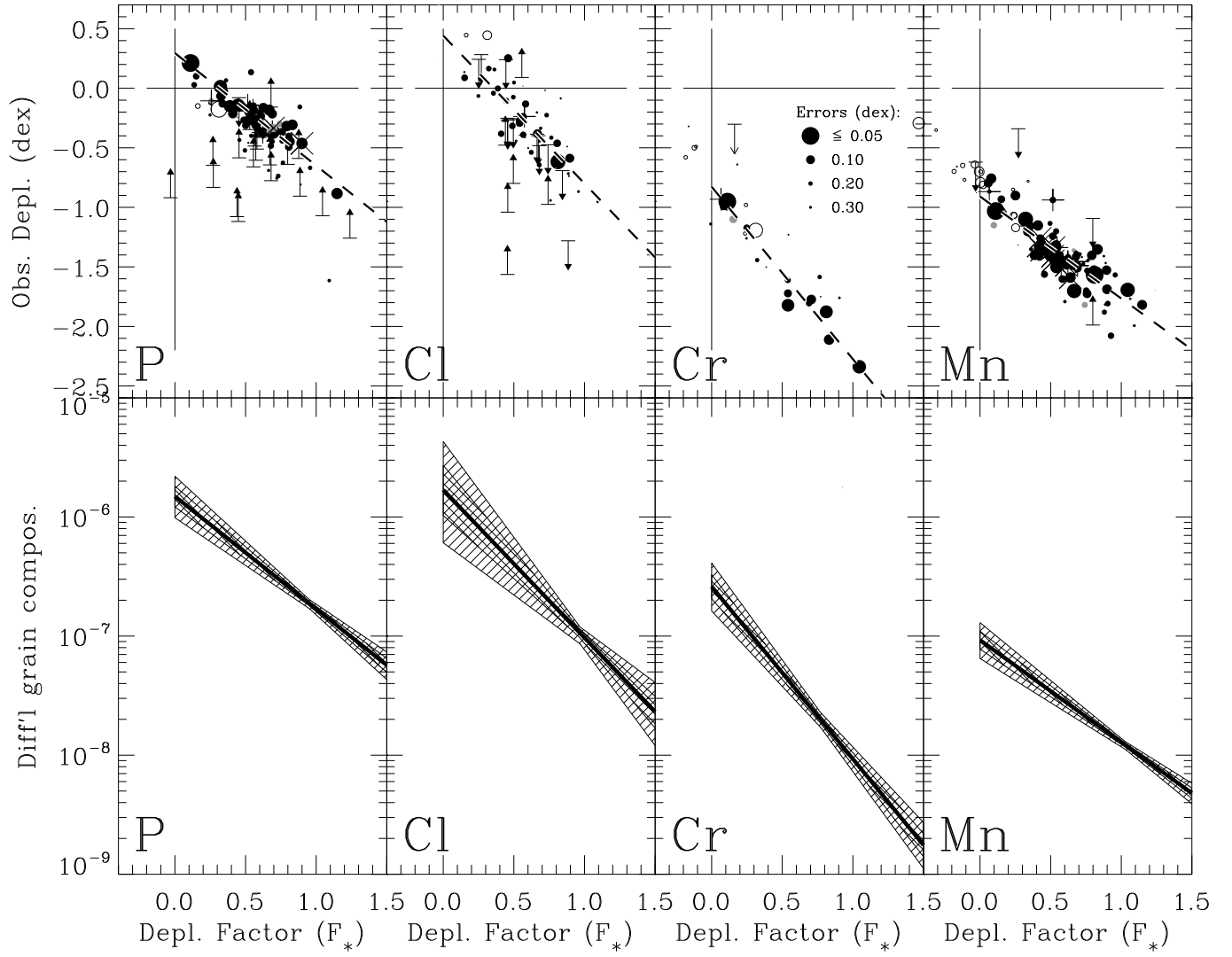


Fig. 6.— Same as for Fig. 5 for the elements P, Cl, Cr, and Mn.

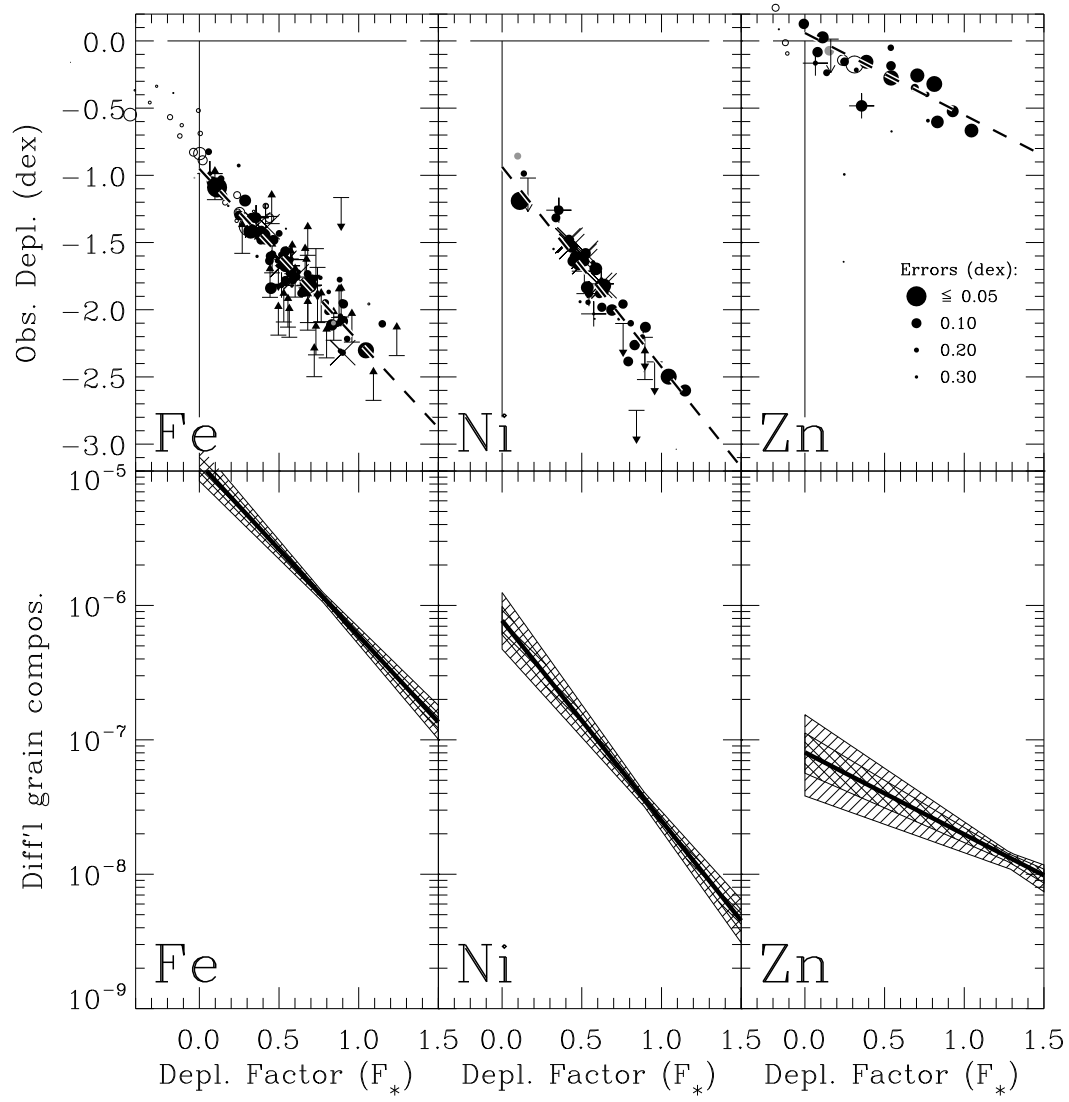


Fig. 7.— Same as for Fig. 5 for the elements Fe, Ni, and Zn.

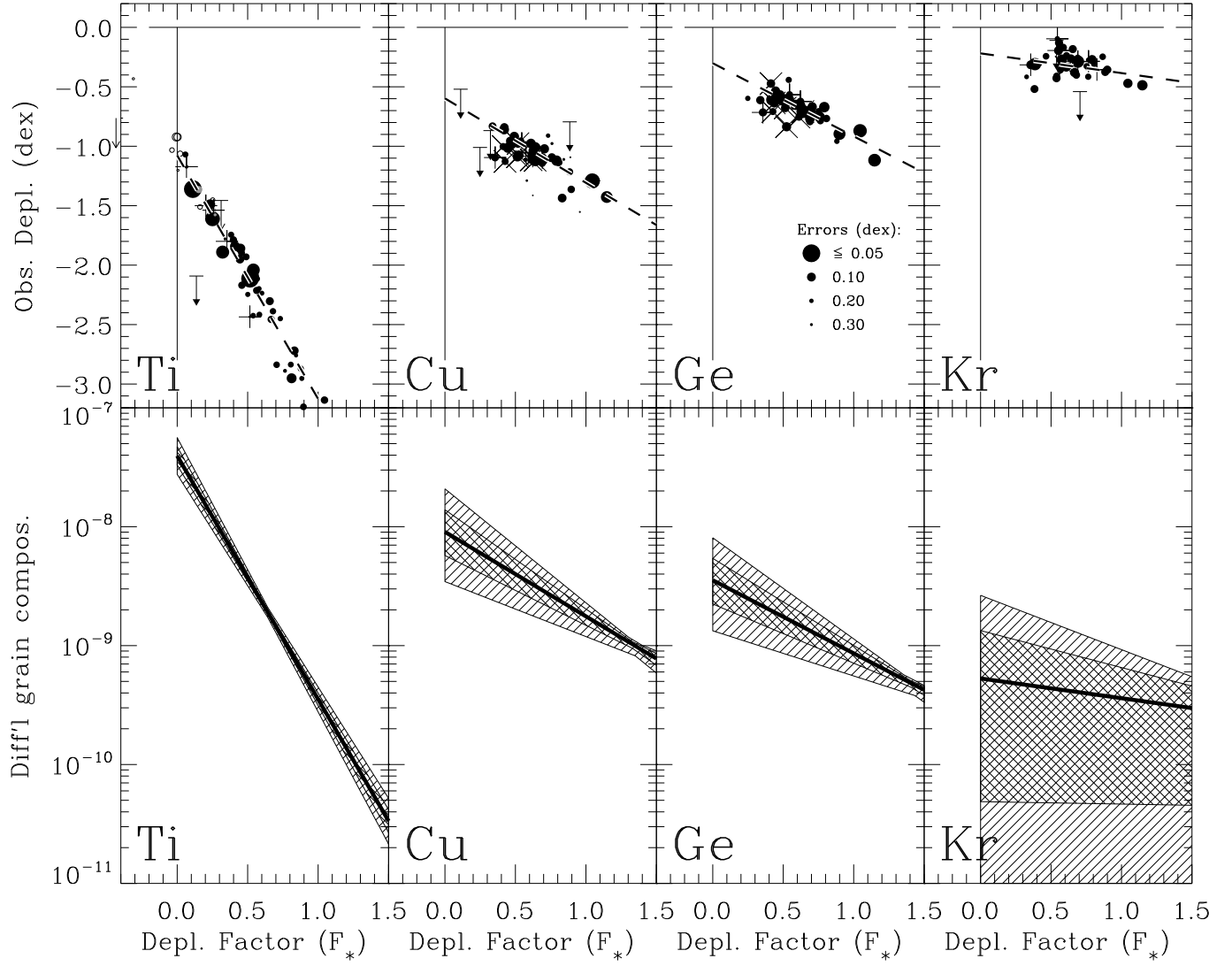


Fig. 8.— Same as for Fig. 5 for the elements Ti, Cu, Ge, and Kr.

7. Derivation of $N(\text{H})$ and F_* when $N(\text{H})$ is not Observed

7.1. Method

There are a number of applications where we can use the information on the depletion trends either to make up for the fact that $N(\text{H})$ is not known, or, if it is known, to make an independent determination of the overall total abundances of heavier elements in the gas (usually referred to as the metallicity of the gas). In this section, we describe a means for processing information on the relative gas phase abundances to recover both $N(\text{H})$, assuming a metallicity equal to the solar value, and the depletion strength F_* . Later, we will touch upon the relevance of this analysis for specific issues ranging from determinations of depletions of gas not far from the Sun (§8), to interpretations of the metallicity of gas out to several kpc from the Sun (§10.3), to the general behavior of sulfur depletions (§9), and, finally to the metallicity in absorption systems at high redshifts (§10.4). Even within the current survey, a reconstruction of $N(\text{H})$ and F_* is of some utility: out of all of the sightlines (or specific velocity components) studied here, there are 97 cases where information is missing on the observed column densities of H I, H₂, or both. For 39 of them, the fact that $N(\text{H}_2)$ was not observed did not present a problem, since H₂ was unlikely to contribute much to $N(\text{H})$, as discussed in §4.6.1. For the remaining 58, the lack of information on the observed $N(\text{H})$ prevented the determination of $[X_{\text{gas}}/\text{H}]_{\text{obs}}$ for any of the elements, values of which are essential for calculating F_* through the use of Eq. 4.

If it were true that all of the elements depleted logarithmically in unison as the general level of depletion became more severe (i.e., their values of A_X were virtually identical), without information on $N(\text{H})$ it would be impossible to distinguish between a line of sight with a modest level of depletion and a certain estimated $N(\text{H})$, as opposed to a situation where the depletions were very strong and $N(\text{H})$ was much higher. Fortunately, this is usually not the case. Given that many sight lines have measured abundances of elements with different A_X values, it is possible to estimate with reasonable accuracy the quantities $N(\text{H})$ and F_* , even when $N(\text{H})$ is not known from the observations.

If we substitute $[X_{\text{gas}}/\text{H}]_{\text{obs}}$ for $[X_{\text{gas}}/\text{H}]_{\text{fit}}$ in Eq. 10, we obtain

$$[X_{\text{gas}}/\text{H}]_{\text{obs}} = B_X + A_X(F_* - z_X) . \quad (22)$$

Noting that

$$[X_{\text{gas}}/\text{H}]_{\text{obs}} = \log N(X) - \log N(\text{H}) - \log(X/\text{H})_{\odot} \quad (23)$$

(this is simply a restatement of Eq. 1), we can rearrange the terms in this equation to obtain a simple linear expression

$$y = a + bx , \quad (24a)$$

where

$$y = \log N(X) - \log(X/\text{H})_{\odot} - B_X + A_X z_X , \quad (24b)$$

$$x = A_X , \quad (24c)$$

and the coefficients of the equation have the meaning

$$a = \log N(\text{H}) , \quad (24\text{d})$$

and

$$b = F_* . \quad (24\text{e})$$

This set of equations allows us to derive the most likely values of $\log N(\text{H})$ and F_* through the method of finding a (weighted) least-squares fit, once again using the routine `FITEXY` (Press et al. 2007) that recognizes the existence of errors in the measurements of both x and y when minimizing the χ^2 of the fit. Note that the uncertainty in $\log(X/\text{H})_\odot$ does not contribute to the errors in y , since excursions in this term are exactly canceled by opposing changes in the derived values of B_X . Any combination of elements that does not give large differences for the A_X values will yield a value for b (i.e., F_*) that is very uncertain. For this reason, lines of sight where the A_X values span a range of less than 0.5 were not evaluated. Also, at least 3 elements were required for the analysis to proceed. (In principle, only 2 elements are needed to obtain a solution, but then we have no information on the goodness of fit.) The element sulfur was not considered. Henceforth, we will refer to the outcomes of the above set of equations as synthetic versions of $N(\text{H})$ and F_* .

7.2. Outcomes and Performance

Table 5 allows us to compare the observed values of $\log N(\text{H})$ and values of F_* computed according to Eq. 4 in §3.1 [columns (3)–(6)] to the synthetic ones obtained from the best-fit calculations described above [columns (7) and (8)]. This table also lists synthetic values for these two quantities for the stars that had incomplete or no information on the observed $N(\text{H})$. Stars for which F_* could not be computed either from Eqs. 4 or 24a do not appear in the table.

As stated in §3, the highly depleted velocity component at -15 km s^{-1} in the direction of $\zeta \text{ Oph}$ was adopted as an approximate fiducial point for defining the scale of F_* . In the initial analysis, we had assumed that this component is responsible for most of the hydrogen along the sight line. We are now in a position to test this assumption. The least-squares fit outcome for Eq. 24a evaluated for the other component at -27 km s^{-1} yields $\log N(\text{H})_{\text{syn.}} = 19.53 \pm 0.06$, which is well below $\log N(\text{H})_{\text{obs.}} = 21.15$ determined from the damped $L\alpha$ profile and the Lyman series lines of H_2 in the spectrum of this star. This value is even lower than the estimate of $\log N(\text{H}) = 19.74$ that was adopted by Savage, Cardelli & Sofia (1992).

For most of the determinations the trends of y vs. x appear to be well defined, and the scatter of y values on either side of the best-fit line are consistent with the measurement errors. However, on some occasions the minimum χ^2 values indicated that the fit was poor, as shown by small values for the probabilities of a worse fit given in column (9) of the table. When this happens, we must be cautious about the reliability of the outcomes for the synthetic $N(\text{H})$ and F_* . Two examples illustrate some common reasons for this sort of outcome.

Table 5. Observed and Synthetic $\log N(\text{H})$ and F_*

HD (1)	Name (2)	Observed				Synthetic		Prob. worse fit (9)	Elements Considered (10)
		$\log N(\text{H})$			F_* (6)	$\log N(\text{H})$ (7)	F_* (8)		
		l.l. (3)	best (4)	u.l. (5)					
1383	HD 1383	21.43	21.50	21.58	0.61 ± 0.04	21.49 ± 0.08	0.59 ± 0.08	0.510	O Mg Mn Ni Cu Ge
2905	κ Cas	21.17	21.29	21.40	0.58 ± 0.06	21.00 ± 0.26	0.41 ± 0.14	0.989	Mg Cl Ti Mn Fe Ni Cu
5394	γ Cas	20.06	20.16	20.24	0.52 ± 0.04	20.15 ± 0.05	0.51 ± 0.05	0.306	N O Mg P Cl Ti Mn Fe
12323	HD 12323	21.21	21.29	21.36	0.52 ± 0.04	21.24 ± 0.08	0.48 ± 0.07	0.011	O Mg Mn Fe Ni Cu Ge
13268	HD 13268	21.35	21.42	21.49	0.51 ± 0.04	21.38 ± 0.07	0.48 ± 0.08	0.147	O Mg Mn Ni Cu Ge
13745	HD 13745	21.30	21.37	21.45	0.43 ± 0.07	Mg Fe
14434	HD 14434	21.40	21.47	21.54	0.52 ± 0.04	21.45 ± 0.09	0.51 ± 0.09	0.301	O Mg Mn Ni Cu
15137	HD 15137	21.10	21.22	21.35	0.37 ± 0.09	Mg Fe
18100	HD 18100	20.02	20.15	20.29	0.14 ± 0.04	19.75 ± 0.09	-0.21 ± 0.08	0.000	Mg Si P Cr Mn Fe Ni Zn
21856	HD 21856	21.02	21.11	21.18	0.67 ± 0.39	Mg Mn
22586	HD 22586	20.21	20.36	20.54	0.34 ± 0.07	20.24 ± 0.35	0.20 ± 0.24	0.240	Si Ti Fe Ni
22928	δ Per	19.40	...	21.22	...	19.64 ± 0.11	0.23 ± 0.11	0.028	N Mg P Ti Mn Fe
22951	40 Per	21.11	21.22	21.33	0.73 ± 0.05	20.89 ± 0.15	0.52 ± 0.10	0.007	Mg P Cl Ti Mn Ni Cu
23180	o Per	21.09	21.19	21.30	0.84 ± 0.06	21.28 ± 0.09	0.92 ± 0.09	0.362	N O Mg P Ti Mn Cu
23478	HD 23478	20.89	21.05	21.14	-0.00 ± 0.50	O Kr
23630	η Tau	20.40 ± 0.14	0.89 ± 0.10	0.005	Ti Cr Zn
24190	HD 24190	21.25	21.30	21.35	0.63 ± 0.24	O Kr
24398	ζ Per	21.10	21.20	21.31	0.88 ± 0.05	21.23 ± 0.07	0.90 ± 0.07	0.163	C O Mg P Ti Mn Fe Cu Kr
24534	X Per	21.31	21.34	21.38	0.90 ± 0.06	21.37 ± 0.07	0.93 ± 0.11	0.228	C N O P Fe
24760	ϵ Per	20.41	20.50	20.59	0.68 ± 0.04	20.45 ± 0.05	0.62 ± 0.05	0.375	N O Mg P Cl Ti Mn Fe Kr
24912	ξ Per	21.22	21.29	21.37	0.83 ± 0.02	21.46 ± 0.06	0.95 ± 0.05	0.000	C O Mg P Cl Ti Cr Mn Fe Ni Cu Zn
27778	62 Tau	20.99	...	21.27	...	21.38 ± 0.07	1.19 ± 0.07	0.640	N O Mg P Mn Fe Ni Cu Ge Kr
30614	α Cam	21.02	21.09	21.17	0.46 ± 0.04	21.02 ± 0.09	0.41 ± 0.07	0.001	O Mg P Ti Mn
31237	π^5 Ori	19.65	20.16	20.37	0.52 ± 0.21	Mg P Mn Fe
34029	α Aur	18.15	18.24	18.34	0.44 ± 0.05	18.71 ± 0.13	0.95 ± 0.12	0.000	C N O Mg Si Fe
34816	λ Lep	20.08	20.18	20.26	0.45 ± 0.05	Ti

Table 5—Continued

HD (1)	Name (2)	Observed			F_* (6)	Synthetic		Prob. worse fit (9)	Elements Considered (10)
		log $N(\text{H})$				log $N(\text{H})$ (7)	F_* (8)		
		l.l. (3)	best (4)	u.l. (5)					
34989	HD 34989	21.00	21.10	21.18	0.72 ± 0.17	Fe
35149	23 Ori	20.47	20.63	20.74	0.54 ± 0.04	21.03 ± 0.05	0.85 ± 0.05	0.000	C N O Mg Si P Cl Ti Cr Mn Fe Ni Cu Zn Ge
35439	25 Ori	20.06	20.36	20.49	0.72 ± 0.18	Mg P Cl Mn
35715	ψ Ori	20.26	20.49	20.64	0.66 ± 0.11	Mg P Cl Mn Fe
36486	δ Ori A	20.15	20.19	20.23	0.54 ± 0.02	20.07 ± 0.04	0.45 ± 0.04	0.004	N O Mg P Cl Ti Cr Mn Fe Zn
36822	ϕ^1 Ori	20.75	20.84	20.91	0.74 ± 0.08	Mg P Mn
36841	HD 36841	20.90 ± 0.19	0.81 ± 0.18	0.937	Mg P Mn Ni Cu
36861	λ Ori A	20.67	20.80	20.90	0.57 ± 0.04	20.77 ± 0.04	0.53 ± 0.04	0.144	C N O Mg P Cl Ti Mn Fe Kr
37021	θ^1 Ori	21.52 ± 0.06	0.75 ± 0.06	0.000	C O Mg Si P Fe Ni Cu Ge Kr
37043	ι Ori	20.08	20.15	20.21	0.41 ± 0.03	20.09 ± 0.05	0.36 ± 0.04	0.040	N O Mg P Cl Ti Mn Fe
37061	ν Ori	21.69 ± 0.06	0.82 ± 0.07	0.000	C O Mg Si Fe Cu Ge Kr
37128	ϵ Ori	20.35	20.45	20.53	0.54 ± 0.03	20.40 ± 0.05	0.49 ± 0.04	0.022	O Mg P Cl Ti Cr Mn Fe Zn Kr
37367	HD 37367	21.23	21.33	21.42	0.65 ± 0.07	21.49 ± 0.09	0.86 ± 0.12	0.991	O Mg Mn Cu Ge Kr
37468	σ Ori	20.42	20.52	20.60	0.58 ± 0.04	20.78 ± 0.11	0.78 ± 0.11	0.000	Mg P Cl Ti Mn
37742	ζ Ori A	20.32	20.41	20.49	0.57 ± 0.05	Ti
37903	HD 37903	21.38	21.44	21.50	1.15 ± 0.03	21.34 ± 0.06	1.03 ± 0.07	0.297	N O Mg P Mn Fe Ni Cu Ge Kr
38666	μ Col	19.84	19.86	19.88	0.11 ± 0.01	19.92 ± 0.04	0.16 ± 0.04	0.589	Mg Si P Ti Cr Mn Fe Ni Zn
38771	κ Ori	20.47	20.52	20.56	0.67 ± 0.03	20.50 ± 0.05	0.65 ± 0.05	0.000	N O Mg P Cl Ti Mn Fe Kr
40111	139 Tau	20.87	20.95	21.03	0.49 ± 0.04	20.77 ± 0.09	0.34 ± 0.08	0.718	Mg P Cl Ti Mn Fe Ni Cu
40893	HD 40893	21.46	21.54	21.61	0.61 ± 0.05	21.47 ± 0.06	0.52 ± 0.07	0.372	O Mg Fe Kr
41161	HD 41161	21.00	21.08	21.17	0.44 ± 0.04	21.30 ± 0.06	0.57 ± 0.04	0.002	N O Ti Fe
42933	δ Pic	20.15	20.23	20.35	0.32 ± 0.06	Ti
43818	LU Gem	21.65 ± 0.06	0.66 ± 0.07	0.032	O Mg Mn Ni Cu Ge
44506	HD 44506	19.49	20.09	20.32	-0.03 ± 0.23	Mg Cl Fe
44743	β CMa	18.26	18.30	18.38	-0.43 ± 0.03	18.23 ± 0.04	-0.46 ± 0.05	0.000	N O Si Mn Fe
47839	15 Mon	20.21	20.31	20.41	0.25 ± 0.05	20.13 ± 0.08	0.12 ± 0.06	0.854	O P Cl Ti Cr Zn Ge

Table 5—Continued

HD (1)	Name (2)	Observed			F_* (6)	Synthetic		Prob. worse fit (9)	Elements Considered (10)
		log $N(\text{H})$				log $N(\text{H})$ (7)	F_* (8)		
		l.l. (3)	best (4)	u.l. (5)					
48915 (+12)	α CMa	17.18	17.40	17.58	0.42 ± 0.11	16.96 ± 0.08	-0.01 ± 0.07	0.000	N O Mg Si Fe
(+18)		17.48	17.60	17.78	0.42 ± 0.08	17.26 ± 0.06	0.06 ± 0.05	0.000	N O Mg Si Fe
52266	HD 52266	21.37 ± 0.10	0.65 ± 0.10	0.503	Mg Mn Ni Cu Ge
52918	19 Mon	19.75	20.20	20.35	0.44 ± 0.24	Mg P Mn
53138	o^2 Cma	17.95	19.78	20.08	0.10 ± 0.53	Ti
53975	HD 53975	21.08	21.14	21.20	0.45 ± 0.03	21.06 ± 0.06	0.41 ± 0.05	0.000	N O Mg Ti Fe
54662	HD 54662	21.28	21.41	21.52	0.89 ± 0.09	21.17 ± 0.66	0.67 ± 0.62	0.970	Mg Cl Mn Fe Ni
57060	29 CMa	20.60	20.70	20.78	0.50 ± 0.05	20.80 ± 0.16	0.58 ± 0.12	0.063	Mg P Cl Ti Mn Fe
57061	τ CMa	20.65	20.70	20.74	0.39 ± 0.04	20.67 ± 0.06	0.36 ± 0.08	0.225	C O Mg Cl Cr Mn Fe Zn Kr
63005	HD 63005	21.27	21.32	21.37	0.64 ± 0.03	21.28 ± 0.06	0.61 ± 0.07	0.261	O Mg Mn Ni Cu Ge
64740	HD 64740	19.64	20.05	20.23	0.27 ± 0.30	Cl Fe
64760	HD 64760	20.13	20.26	20.35	0.35 ± 0.06	Mg P Cl Mn Fe
65818	V Pup	20.36	20.52	20.65	0.36 ± 0.09	Mg P Cl Mn Fe
66788	HD 66788	21.16	21.26	21.35	0.53 ± 0.08	Mg Fe
66811	ζ Pup	19.92	19.96	20.00	0.32 ± 0.02	20.14 ± 0.05	0.47 ± 0.04	0.628	N Mg Si P Cl Ti Cr Mn Fe Ni Zn
68273	γ^2 Vel	19.67	19.71	19.75	0.25 ± 0.02	19.80 ± 0.05	0.31 ± 0.04	0.152	N Mg Si P Ti Mn Fe
69106	HD 69106	21.04	21.09	21.15	0.64 ± 0.06	21.10 ± 0.08	0.65 ± 0.09	0.818	O Mg Fe Kr
71634	HD 71634	21.34 ± 0.16	0.90 ± 0.16	0.389	Mg P Mn Ni Cu Ge
72127	HD 72127	20.25 ± 0.11	0.40 ± 0.08	0.021	Ti Cr Zn
72754	FY Vel	21.19	21.28	21.38	0.76 ± 0.10	21.13 ± 0.08	0.54 ± 0.12	0.913	O P Ge Kr
73882	HD 73882	21.50	21.57	21.65	0.68 ± 0.07	N Fe
74375	HD 74375	20.67	20.78	20.87	0.61 ± 0.18	Fe
74575	α Pyx	20.27	20.46	20.59	0.33 ± 0.09	Ti
75309	HD 75309	21.10	21.18	21.26	0.63 ± 0.04	21.18 ± 0.06	0.61 ± 0.07	0.173	N O Mg P Mn Ni Cu Ge Kr
79186	GX Vel	21.34	21.41	21.48	0.69 ± 0.03	21.46 ± 0.07	0.73 ± 0.07	0.532	O Mg P Mn Ni Cu Ge
88115	HD 88115	20.89	20.99	21.08	0.35 ± 0.45	N O

Table 5—Continued

HD (1)	Name (2)	Observed			F_* (6)	Synthetic		Prob. worse fit (9)	Elements Considered (10)
		log $N(\text{H})$				log $N(\text{H})$ (7)	F_* (8)		
		l.l. (3)	best (4)	u.l. (5)					
91316	ρ Leo	20.14	20.25	20.32	0.15 ± 0.04	20.16 ± 0.09	0.11 ± 0.06	0.497	Ti Cr Zn
91597	HD 91597	21.36	21.41	21.47	0.44 ± 0.05	Mg Fe
91651	HD 91651	21.10	21.16	21.22	0.27 ± 0.04	Mg Fe
91824	HD 91824	21.11	21.16	21.22	0.45 ± 0.03	21.34 ± 0.07	0.61 ± 0.08	0.292	O Mg P Mn Ni Cu Ge
91983	HD 91983	21.16	21.24	21.32	0.48 ± 0.04	21.32 ± 0.06	0.55 ± 0.07	0.821	O Mg P Mn Ni Cu Ge
92554	HD 92554	21.18	21.28	21.38	0.27 ± 0.07	Mg Fe
93030	θ Car	20.18	20.26	20.34	0.45 ± 0.03	20.10 ± 0.09	0.34 ± 0.05	0.342	O Mg P Cl Ti Mn Fe
93205	V560 Car	21.36	21.40	21.44	0.40 ± 0.03	21.26 ± 0.05	0.28 ± 0.05	0.958	O Mg Ti Fe
93222	HD 93222	21.35	21.42	21.48	0.39 ± 0.04	21.48 ± 0.06	0.46 ± 0.06	0.055	O Mg P Fe
93521	HD 93521	18.21	18.51	18.86	-0.31 ± 0.11	18.79 ± 0.14	-0.14 ± 0.11	0.000	Mg Si Ti Mn Fe
(-58)		19.28	19.34	19.44	-0.01 ± 0.03	19.36 ± 0.08	-0.04 ± 0.06	0.000	Mg Si Ti Mn Fe
(-51)		19.11	19.20	19.33	-0.04 ± 0.04	19.61 ± 0.12	0.24 ± 0.11	0.007	Mg Si Ti Mn Fe
(-39)		18.70	18.88	19.10	0.01 ± 0.08	18.04 ± 0.17	-0.82 ± 0.15	0.000	Mg Si Ti Mn Fe
(-29)		18.06	18.38	18.74	0.34 ± 0.17	Si Mn Fe
(-18)		19.23	19.28	19.37	0.00 ± 0.03	19.16 ± 0.11	-0.14 ± 0.09	0.000	Mg Si Ti Mn Fe
(-10)		19.31	19.36	19.45	0.02 ± 0.04	19.38 ± 0.17	0.01 ± 0.12	0.282	Mg Si Ti Mn Fe
(+3)		19.24	19.30	19.40	0.25 ± 0.04	19.10 ± 0.17	0.10 ± 0.18	0.948	Mg Si Ti Mn Fe
(+7)		18.56	18.79	19.06	0.23 ± 0.12	Si Mn Fe
(total)		20.06	20.10	20.20	0.06 ± 0.04	20.14 ± 0.13	0.05 ± 0.11	0.009	Mg Si Ti Mn Fe
93843	HD 93843	21.27	21.35	21.42	0.39 ± 0.05	Mg Fe
94493	HD 94493	21.13	21.17	21.20	0.29 ± 0.03	21.11 ± 0.06	0.25 ± 0.06	0.013	N O Mg Fe
99857	HD 99857	21.30	21.36	21.41	0.54 ± 0.04	21.28 ± 0.05	0.47 ± 0.06	0.357	N O Mg P Fe Kr
99890	HD 99890	20.84	20.96	21.08	0.17 ± 0.08	Mg Fe
100340	HD 100340	20.38	20.46	20.58	0.10 ± 0.06	19.59 ± 0.20	-0.63 ± 0.17	0.118	Mg Mn Ni
103779	HD 103779	21.11	21.20	21.29	0.43 ± 0.06	Mg Fe
104705	DF Cru	21.09	21.18	21.24	0.33 ± 0.05	21.10 ± 0.05	0.26 ± 0.06	0.583	O Mg P Fe Kr

Table 5—Continued

HD (1)	Name (2)	Observed			F_* (6)	Synthetic		Prob. worse fit (9)	Elements Considered (10)
		log $N(\text{H})$				log $N(\text{H})$ (7)	F_* (8)		
		l.l. (3)	best (4)	u.l. (5)					
108248	α^1 Cru	19.50	19.60	19.70	0.15 ± 0.05	19.78 ± 0.09	0.30 ± 0.09	0.240	N Mg P Cl Mn Fe
108639	HD 108639	21.30	21.38	21.47	0.37 ± 0.37	O Kr
109399	HD 109399	21.12	21.18	21.24	0.48 ± 0.05	Mg Fe
110432	BZ Cru	21.13	21.20	21.28	1.17 ± 0.11	N Fe
111934	BU Cru	21.48 ± 0.14	0.57 ± 0.15	0.879	Mg P Mn Ni Cu Ge
114886	HD 114886	21.35	21.40	21.46	0.87 ± 0.31	O Kr
115071	V961 Cen	21.45	21.50	21.55	0.22 ± 0.21	O Kr
116658	α Vir	18.90	19.00	19.10	0.16 ± 0.05	18.84 ± 0.06	0.11 ± 0.06	0.658	N O Si P Cl Ti Mn Fe
116781	V967 Cen	21.16	21.24	21.33	0.44 ± 0.07	Mg Fe
116852	HD 116852	20.94	21.02	21.10	0.36 ± 0.04	20.71 ± 0.05	0.07 ± 0.05	0.000	O Mg Mn Fe Ni Cu Zn Ge Kr
118716	ϵ Cen	19.10	19.60	19.79	0.15 ± 0.16	19.67 ± 0.12	0.20 ± 0.12	0.801	N Mg P Cl Fe
120086	HD 120086	20.07	...	19.38 ± 0.23	-0.56 ± 0.18	0.000	Mg Si Ti Fe Ni
120324	μ Cen	...	18.76	20.22	-0.81 ± 3.74	Mg P Cl Fe
121263	ζ Cen	12.92	...	20.02	...	19.84 ± 0.14	0.48 ± 0.14	0.295	N Mg P Mn Fe
121968	HD 121968	20.45	20.60	20.71	0.26 ± 0.06	20.31 ± 0.09	0.09 ± 0.06	0.468	O P Ti
122451	β Cen	19.49	19.54	19.59	0.23 ± 0.03	19.23 ± 0.10	0.06 ± 0.06	0.174	N Si Ti
122879	HD 122879	21.24	21.34	21.44	0.55 ± 0.04	21.58 ± 0.07	0.75 ± 0.07	0.640	O Mg Mn Fe Ni Cu Ge Kr
124314	HD 124314	21.43	21.51	21.58	0.59 ± 0.05	21.57 ± 0.05	0.64 ± 0.06	0.502	N O Mg P Fe Kr
125924	HD 125924	20.47	20.63	20.78	0.20 ± 0.08	Ti
127972	η Cen	19.48	...	20.23 ± 0.10	0.86 ± 0.10	0.000	N Mg P Mn Fe
135591	HD 135591	20.98	21.12	21.22	0.56 ± 0.22	Mg Cl Mn
137595	HD 137595	21.18	21.22	21.27	0.77 ± 0.22	O Kr
141637	1 Sco	21.01	21.13	21.23	0.69 ± 0.05	21.22 ± 0.08	0.78 ± 0.09	0.762	O Mg P Cl Cr Mn Fe Cu Zn Ge Kr
143018	π Sco	20.62	20.69	20.74	0.71 ± 0.03	20.95 ± 0.10	0.91 ± 0.08	0.521	Mg P Ti Cr Mn Fe Cu Zn Ge
143275	δ Sco	21.07	21.17	21.24	0.90 ± 0.03	21.34 ± 0.06	1.01 ± 0.06	0.038	C N O Mg P Cl Ti Mn Fe Cu
144217	β^1 Sco	21.10	21.14	21.17	0.81 ± 0.02	21.27 ± 0.06	0.91 ± 0.06	0.507	C N O Mg P Cl Ti Cr Mn Fe Zn

Table 5—Continued

HD (1)	Name (2)	Observed			F_* (6)	Synthetic		Prob. worse fit (9)	Elements Considered (10)
		$\log N(\text{H})$				$\log N(\text{H})$ (7)	F_* (8)		
		l.l. (3)	best (4)	u.l. (5)					
144470	σ^1 Sco	21.14	21.23	21.30	0.81 ± 0.04	21.36 ± 0.08	0.91 ± 0.08	0.938	O Mg P Cl Ti Mn Fe
144965	HD 144965	21.23	21.32	21.38	1.15 ± 0.35	O Kr
145502	ν Sco	20.87	21.13	21.28	0.80 ± 0.11	21.49 ± 0.84	0.98 ± 0.44	0.707	Mg Cl Ti
147165	σ Sco	21.16	21.36	21.51	0.76 ± 0.06	21.50 ± 0.08	0.87 ± 0.07	0.000	O Mg P Cl Ti Cr Mn Zn Kr
147683	V760 Sco	21.25	21.41	21.51	0.56 ± 0.47	O Kr
147888	ρ Oph D	21.55	21.74	21.84	0.88 ± 0.06	21.59 ± 0.05	0.71 ± 0.06	0.000	C N O Mg Mn Fe Ni Ge Kr
147933	ρ Oph A	21.62	21.70	21.78	1.09 ± 0.08	21.62 ± 0.23	1.00 ± 0.26	0.001	O Mg Si P Cl Mn Ni Cu
148184	χ Oph	21.17	21.31	21.41	0.96 ± 0.09	21.89 ± 0.23	1.57 ± 0.26	0.739	O Mg P Cl Mn Cu
148594	HD 148594	21.31 ± 0.07	0.95 ± 0.07	0.382	O Mg P Mn Ni Cu Ge Kr
148605	22 Sco	20.28	20.69	20.86	0.53 ± 0.39	Cl Mn
149038	μ Nor	21.11	21.19	21.27	0.56 ± 0.05	Ti
149757 (−27)	ζ Oph	19.53 ± 0.06	0.11 ± 0.05	0.000	O Mg Si P Ti Cr Mn Fe Ni Cu Zn
(−15)		21.10	21.15	21.20	1.05 ± 0.02	21.15 ± 0.05	1.04 ± 0.05	0.881	C N O Mg Si Ti Cr Mn Fe Ni Cu Zn Ge Kr
149881	V600 Her	20.43	20.65	20.80	0.07 ± 0.06	20.52 ± 0.08	-0.03 ± 0.06	0.030	Si Ti Cr Mn Fe Zn
151804	V973 Sco	21.07	21.19	21.29	0.57 ± 0.08	21.21 ± 0.42	0.57 ± 0.37	0.867	Mg Cl Mn Fe Ni Cu
151805	HD 151805	21.36	21.41	21.46	0.83 ± 0.36	O Kr
151890	μ^1 Sco	...	19.59	20.12	-0.03 ± 3.47	Mg P Cl Mn Fe
152236	ζ^1 Sco	21.73	21.84	21.96	0.80 ± 0.06	Ti Fe
152590	HD 152590	21.42	21.47	21.52	0.69 ± 0.03	21.46 ± 0.06	0.68 ± 0.06	0.669	C O Mg Si P Mn Fe Cu Ge Kr
154368	V1074 Sco	21.54	21.59	21.64	0.52 ± 0.07	21.79 ± 0.16	0.69 ± 0.16	0.026	C O Mg Si P Ti Mn Fe Ni
155806	V1075 Sco	21.00	21.14	21.24	0.62 ± 0.07	21.29 ± 0.24	0.73 ± 0.25	0.401	Mg Cl Mn Fe Ni Cu
157246	γ Ara	20.61	20.71	20.78	0.46 ± 0.03	20.75 ± 0.05	0.53 ± 0.05	0.015	O Mg P Cl Ti Mn Fe
157857	HD 157857	21.38	21.44	21.51	0.62 ± 0.04	21.47 ± 0.07	0.65 ± 0.07	0.591	O Mg P Mn Ni Cu Ge
158926	λ Sco	19.20	19.23	19.26	0.31 ± 0.02	19.13 ± 0.04	0.28 ± 0.04	0.000	N O Si P Cl Cr Fe Zn
160578	κ Sco	20.03	20.22	20.34	0.50 ± 0.07	20.27 ± 0.09	0.52 ± 0.09	0.000	N Mg P Cl Mn Fe
164284	66 Oph	20.23	20.75	20.90	0.89 ± 0.18	21.74 ± 0.83	1.88 ± 0.88	0.263	Mg P Cl Mn Ni Cu

Table 5—Continued

HD (1)	Name (2)	Observed				Synthetic		Prob. worse fit (9)	Elements Considered (10)
		log $N(\text{H})$			F_* (6)	log $N(\text{H})$ (7)	F_* (8)		
		l.l. (3)	best (4)	u.l. (5)					
165024	θ Ara	20.74	20.84	20.91	0.56 ± 0.03	20.80 ± 0.09	0.53 ± 0.07	1.000	Mg P Cl Ti Mn Fe
165246	HD 165246	20.70	21.46	21.52	0.77 ± 1.39	O Kr
165955	HD 165955	21.04	21.10	21.16	0.42 ± 0.04	21.04 ± 0.09	0.38 ± 0.10	0.460	O Mg Mn Ni Cu Ge
167264	15 Sgr	21.13	21.25	21.34	0.68 ± 0.16	21.66 ± 0.21	1.17 ± 0.28	0.796	O Mg Mn
167756	HD 167756	20.54 ± 0.08	0.12 ± 0.08	0.061	Mg Si Cr Zn
167971	MY Ser	21.53	21.73	21.97	0.70 ± 0.23	Fe
168076	HD 168076	21.55	21.73	21.93	0.68 ± 0.17	Fe
168941	HD 168941	21.11	21.19	21.62	0.42 ± 0.17	Mg Fe
170740	HD 170740	21.30	21.40	21.50	1.02 ± 0.11	Fe
175360	HD 175360	21.00 ± 0.07	0.70 ± 0.08	0.463	O Mg P Mn Ni Cu Ge Kr
177989	HD 177989	21.01	21.08	21.15	0.55 ± 0.05	21.19 ± 0.06	0.67 ± 0.07	0.623	O Mg P Fe Kr
179406	20 Aql	21.09 ± 0.12	0.14 ± 0.08	0.000	N Ti Fe
179407	HD 179407	21.12	21.21	21.30	0.35 ± 0.05	Ti
184915	κ Aql	20.98	21.05	21.13	0.88 ± 0.05	21.23 ± 0.29	0.97 ± 0.16	0.869	Mg Cl Ti Mn
185418	HD 185418	21.34	21.41	21.49	0.79 ± 0.03	21.61 ± 0.06	0.98 ± 0.07	0.046	N O Mg P Mn Fe Ni Cu Ge Kr
188209	HD 188209	20.88	21.00	21.10	0.66 ± 0.12	Mg P Mn
190918	V1676 Cyg	21.35	21.40	21.46	0.46 ± 0.03	21.43 ± 0.09	0.48 ± 0.08	0.531	O Mg Mn Ni Cu
191877	HD 191877	21.04	21.12	21.21	0.39 ± 0.04	N Ti
192035	RX Cyg	21.32	21.38	21.45	0.76 ± 0.04	21.39 ± 0.07	0.78 ± 0.08	0.130	O Mg Mn Ni Cu Ge
192639	HD 192639	21.41	21.48	21.55	0.64 ± 0.04	21.54 ± 0.07	0.70 ± 0.07	0.906	N O Mg Mn Fe Ni Cu
195965	HD 195965	21.11	21.13	21.16	0.52 ± 0.02	21.06 ± 0.05	0.48 ± 0.04	0.297	N O Mg Ti
198478	55 Cyg	21.44	21.55	21.66	0.81 ± 0.05	21.52 ± 0.07	0.80 ± 0.08	0.129	O Mg P Mn Ni Cu Ge Kr
198781	HD 198781	21.09	21.15	21.21	0.59 ± 0.03	21.07 ± 0.08	0.53 ± 0.08	0.017	O Mg P Mn Ni Ge
199579	HD 199579	21.18	21.25	21.32	0.76 ± 0.27	N Fe
200120	59 Cyg	19.54	...	20.20	...	20.12 ± 0.22	0.27 ± 0.14	0.489	Mg P Cl Ti Mn Fe
201345	HD 201345	20.92	21.00	21.09	0.34 ± 0.04	20.89 ± 0.07	0.24 ± 0.07	0.220	O Mg P Mn Ni Cu Ge

Table 5—Continued

HD	Name	Observed			F_*	Synthetic		Prob. worse fit	Elements Considered
		log $N(\text{H})$				log $N(\text{H})$	F_*		
(1)	(2)	l.l. (3)	best (4)	u.l. (5)	(6)	(7)	(8)	(9)	(10)
202347	HD 202347	20.81	20.94	21.02	0.56 ± 0.06	20.93 ± 0.09	0.56 ± 0.09	0.059	O Mg P Fe
202904	ν Cyg	19.45	...	20.67	...	20.24 ± 0.14	0.39 ± 0.11	0.431	Mg P Cl Ti Mn Fe
203064	68 Cyg	21.04	21.15	21.24	0.68 ± 0.20	Mg Cl Mn
203374	HD 203374	21.22	21.33	21.40	0.56 ± 0.06	21.43 ± 0.07	0.66 ± 0.07	0.181	O Mg Fe Kr
203532	HD 203532	20.91	...	21.26	...	21.37 ± 0.08	1.14 ± 0.09	0.907	O Mg P Mn Ni Cu Ge Kr
203938	HD 203938	21.61	21.70	21.80	0.99 ± 0.64	Fe
206267	HD 206267	21.45	21.54	21.63	0.87 ± 0.07	21.60 ± 0.09	0.92 ± 0.10	0.810	N O Mg Fe Kr
206773	HD 206773	21.20	21.25	21.30	0.53 ± 0.02	21.21 ± 0.05	0.51 ± 0.04	0.105	O Mg P Ti Mn Ni Ge
207198	HD 207198	21.63	21.68	21.73	0.90 ± 0.03	21.57 ± 0.06	0.81 ± 0.07	0.864	C N O Mg Si Mn Fe Ni Ge Kr
207308	HD 207308	21.38	21.44	21.50	0.80 ± 0.06	Mg Fe
207538	HD 207538	21.51	21.58	21.66	0.84 ± 0.07	21.81 ± 0.09	1.09 ± 0.11	0.869	O Mg Fe
208440	HD 208440	21.23	21.31	21.38	0.61 ± 0.04	21.37 ± 0.07	0.68 ± 0.08	0.989	O Mg P Mn Ni Cu Ge Kr
209339	HD 209339	21.20	21.26	21.32	0.58 ± 0.04	21.35 ± 0.07	0.66 ± 0.07	0.951	O Mg Fe Kr
209975	19 Cep	21.06	21.18	21.29	0.57 ± 0.26	Cl Mn
210809	HD 210809	21.25	21.33	21.42	0.41 ± 0.04	21.27 ± 0.07	0.36 ± 0.07	0.359	O Mg Mn Ni Cu Ge
210839	λ Cep	21.39	21.45	21.51	0.66 ± 0.03	21.44 ± 0.05	0.67 ± 0.05	0.035	N O Mg Ti Fe
212571	π Aqr	20.64 ± 0.11	0.52 ± 0.11	0.045	Cr Cu Zn Ge
212791	V408 Lac	20.88	21.12	21.24	0.57 ± 0.08	21.13 ± 0.08	0.61 ± 0.09	0.253	O Mg P Mn Ni Cu Ge
214080	HD 214080	20.38	20.61	20.77	0.27 ± 0.10	20.06 ± 0.55	-0.03 ± 0.20	0.629	Mg Ti Mn
214680	10 Lac	20.58	20.73	20.83	0.50 ± 0.06	P Ti
214993	12 Lac	20.68	20.82	20.94	0.68 ± 0.10	Mg P Cl Mn
215733 (-93)	HD 215733	16.91	17.39	17.67	-0.27 ± 0.19	Si Fe
(-83)		17.60	18.40	18.59	0.99 ± 0.30	Si Fe
(-61)		18.91	19.44	19.60	1.06 ± 0.21	Si Mn Fe
(-59)		18.75	18.95	19.29	-0.11 ± 0.10	18.42 ± 0.15	-0.62 ± 0.13	0.193	Mg Si Cr Mn Fe Zn
(-54)		19.09	19.63	19.92	0.54 ± 0.15	18.63 ± 0.15	-0.40 ± 0.13	0.013	Mg Si Cr Mn Fe Zn

Table 5—Continued

HD (1)	Name (2)	Observed				Synthetic		Prob. worse fit (9)	Elements Considered (10)
		log $N(\text{H})$			F_* (6)	log $N(\text{H})$ (7)	F_* (8)		
		l.l. (3)	best (4)	u.l. (5)					
(−47)		...	18.94	19.73	...	18.85 ± 0.16	-0.39 ± 0.14	0.199	Mg Si Cr Mn Fe Zn
(−45)		17.37	18.06	18.42	-0.40 ± 0.28	Mg Si Mn Fe
(−42)		17.23	18.53	18.94	-0.16 ± 0.31	18.08 ± 0.33	-0.72 ± 0.29	0.336	Mg Si Cr Mn Fe Zn
(−40)		18.06	18.81	19.27	0.18 ± 0.24	18.09 ± 0.57	-0.48 ± 0.48	0.146	Si Cr Mn Fe
(−32)		19.50	19.64	19.78	0.25 ± 0.09	18.99 ± 0.46	-0.40 ± 0.41	0.057	Mg Si Cr Mn Fe Zn
(−31)		18.14 ± 0.35	-0.76 ± 0.29	0.364	Mg Si Cr Mn Fe Zn
(−28)		18.85	18.91	19.06	-0.18 ± 0.07	19.00 ± 0.20	-0.12 ± 0.19	0.643	Mg Si Cr Mn Fe Zn
(−26)		18.99	19.11	19.23	-0.12 ± 0.07	18.83 ± 0.21	-0.39 ± 0.20	0.361	Mg Si Cr Mn Fe Zn
(−23)		19.21	19.25	19.33	0.24 ± 0.08	19.07 ± 0.41	0.06 ± 0.37	0.389	Mg Si Cr Mn Fe Zn
(−21)		19.32	19.37	19.46	0.24 ± 0.05	19.27 ± 0.16	0.15 ± 0.17	0.289	Mg Si Cr Mn Fe Zn
(−19)		19.22 ± 0.41	0.27 ± 0.40	0.989	Si Cr Mn Fe
(−16)		20.08	20.11	20.18	0.93 ± 0.05	20.02 ± 0.21	0.83 ± 0.22	0.013	Mg Si Cr Mn Fe Zn
(−11)		19.57	19.60	19.67	-0.01 ± 0.07	19.84 ± 0.21	0.27 ± 0.23	0.716	Mg Si Cr Zn
(−9)		20.01	20.07	20.17	0.08 ± 0.04	20.52 ± 0.10	0.45 ± 0.10	0.000	Mg Si Cr Mn Fe Zn
(−5)		19.50	19.58	19.70	0.77 ± 0.18	19.17 ± 0.53	0.34 ± 0.55	0.621	Mg Si Cr Zn
(+1)		19.68	19.71	19.78	0.90 ± 0.05	18.90 ± 0.42	0.18 ± 0.34	0.251	Mg Si Cr Mn Fe
(+15)		18.35	18.42	18.53	0.96 ± 0.08	Si Fe
(total)		20.41 ± 0.17	-0.05 ± 0.16	0.589	Mg Si Cr Mn Fe Zn
218376	1 Cas	20.95	21.07	21.17	0.60 ± 0.06	20.66 ± 0.27	0.37 ± 0.15	0.602	Mg Cl Ti Mn
218915	HD 218915	21.22	21.25	21.29	0.70 ± 0.08	21.20 ± 0.06	0.60 ± 0.12	0.809	N O P
219188	HD 219188	20.66	20.88	21.01	1.24 ± 0.57	20.99 ± 0.14	1.77 ± 0.62	0.268	N O Mn
220057	HD 220057	21.02	21.16	21.26	0.75 ± 0.05	21.21 ± 0.06	0.83 ± 0.06	0.131	N O Mg P Mn Ni Cu Ge Kr
224151	V373 Cas	21.40	21.46	21.52	0.46 ± 0.04	21.40 ± 0.04	0.42 ± 0.05	0.666	N O Mg P Fe Kr
224572	σ Cas	20.87	20.98	21.07	0.76 ± 0.07	21.09 ± 0.39	0.86 ± 0.40	0.559	Mg P Cl Mn Fe Cu
232522	HDE 232522	21.14	21.19	21.24	0.44 ± 0.03	21.07 ± 0.08	0.33 ± 0.08	0.797	O Mg Mn Ni Ge
303308	HDE 303308	21.41	21.48	21.54	0.38 ± 0.04	21.37 ± 0.05	0.30 ± 0.05	0.169	O Mg Ti Fe Kr

Table 5—Continued

HD (1)	Name (2)	Observed			F_* (6)	Synthetic		Prob. worse fit (9)	Elements Considered (10)
		$\log N(\text{H})$				$\log N(\text{H})$ (7)	F_* (8)		
		l.l. (3)	best (4)	u.l. (5)					
308813	HDE 308813	21.21	21.29	21.36	0.49 ± 0.04	21.22 ± 0.08	0.43 ± 0.08	0.679	O Mg Mn Ni Cu Ge
	BD +35 4258	21.20	21.30	21.39	0.40 ± 0.08	Mg Fe
	BD +53 2820	21.31	21.39	21.47	0.43 ± 0.05	21.23 ± 0.10	0.27 ± 0.09	0.204	O Mn Ni Cu Ge
	CPD -59 2603	21.11	21.20	21.30	0.17 ± 0.06	Mg Fe
	CPD -69 1743	21.08	21.16	21.24	0.42 ± 0.05	21.02 ± 0.09	0.30 ± 0.09	0.113	O Mn Ni Cu Ge

First, as the top panel of Fig. 9 shows for the star ξ Per, the poor fit may simply be due to the fact that many of the observational errors for the column densities are remarkably small (Cardelli et al. 1991), which results in a large value for χ^2 for the fit even when the overall trend seems to be reasonably well defined. Here, there is a moderate but tolerable disagreement between the intercepts and slopes of two lines, one representing the trend that conforms to $\log N(\text{H})_{\text{obs}} = 21.29 \pm 0.08$ and $F_* = 0.83 \pm 0.02$ derived using Eq. 4 (solid gray line) and the other arising from the best-fit solution to Eq. 24a (dashed gray line), yielding $\log N(\text{H})_{\text{syn.}} = 21.46 \pm 0.06$ and $F_{*\text{syn.}} = 0.95 \pm 0.05$. (It is important to note that the quoted uncertainties in the results are based on only the measurement errors, with no reference to how much the points scatter about the fit line. If one repeats the analysis using just the measurements with no errors and assumes that the model is perfectly correct, the anticipated uncertainties in $\log N(\text{H})_{\text{syn.}}$ and $F_{*\text{syn.}}$ increase to 0.14 and 0.12, respectively.)

A second reason for a poor outcome is that there may be fundamental problems arising from the fact that different regions with markedly different depletion levels are being grouped together. For example, the line of sight toward the star HD 116852 in the lower halo of the Galaxy traverses regions at different radial velocities that have markedly different relative abundances (Sembach & Savage 1996). When such a mixture is considered as a whole, the basic premise that the relative abundances should obey the simple relation given by Eq. 10 starts to break down. It is clear from the lower panel of Fig. 9 that the disagreements between the two variable pairs is far worse: $\log N(\text{H})_{\text{obs}} = 21.02 \pm 0.08$ vs. $\log N(\text{H})_{\text{syn.}} = 20.71 \pm 0.05$ (i.e., a factor of 2 in column density, which is well outside the quoted errors) and $F_* = 0.36 \pm 0.04$ from Eq. 4 vs. $F_{*\text{syn.}} = 0.07 \pm 0.05$ from Eq. 24a. The inset in the figure showing the apparent optical depths τ_a as a function of velocity for three species shows that the small changes in depletion for the lightly depleted elements O and Mg contrast sharply with strong changes in the usually heavily depleted Ni. If we could actually see a velocity profile for H, it would probably not look much different than the one for O. The broad peaks seen in the Ni profile centered at $v = -10$ and -35 km s^{-1} probably have a low depletion and an almost negligible amount of hydrogen associated with them, but they are conspicuous because they are seen alongside the component centered on $v = +10 \text{ km s}^{-1}$ where the Ni is highly depleted. If we repeat the analysis using just the information derived from the elements O, Cu, Zn, Ge and Kr, the y -intercept corresponds to $\log N(\text{H})_{\text{syn.}} = 21.01 \pm 0.09$ (dotted line), which almost exactly (fortuitously) equals the measured value. With the analysis restricted to this subset of elements with only light to moderate depletions, which gives greater emphasis to the velocity component that has the most hydrogen, the probability of a worse fit comes out at a satisfactory value of 0.674.

The two examples highlighted in the previous two paragraphs were carefully chosen to demonstrate two principal reasons for finding probability of worse fit outcomes at extremely low values (in these cases, lower than 0.001, as can be seen for the entries in column (9) of Table 5 for the respective stars). Other reasons for poor fits may include errors in the column densities that are well outside the quoted uncertainty limits (i.e., mistakes or poor judgment on the part of the observer) or perhaps some unusual effects that cause deviations in the element abundances so that they no longer conform to the simplified, general depletion trends among the elements being described here.

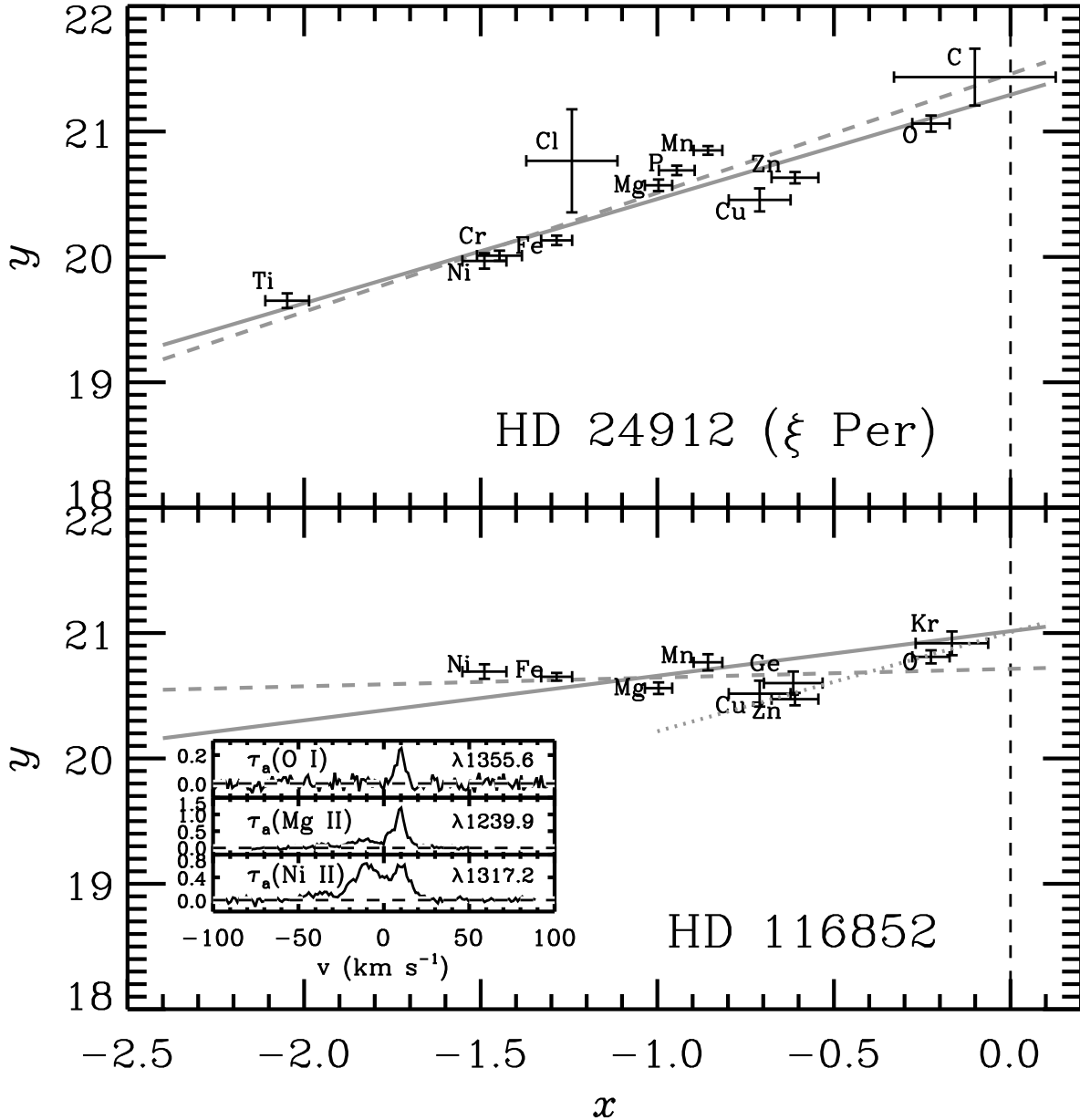


Fig. 9.— Illustrations of the fits obtained from the use of Eq. 24a, which can be used to estimate $N(\text{H})$ and F_* when $N(\text{H})$ is not observed. The dashed gray line in each case shows the best fit: its slope yields F_* and the y -intercept at $x = 0$ yields $N(\text{H})$. The solid gray line shows the slope and intercept obtained through from the observed value of $N(\text{H})$ and the value of F_* derived using the formulae given in §3.1. For HD 116852 (lower panel), a fit (dotted gray line) is also shown for just the elements O, Cu, Zn, Ge and Kr. The inset in this panel shows the shapes of the apparent optical depths vs. heliocentric radial velocity for the elements O I, Mg II, and Ni II. The two sight lines depicted in this figure highlight some special considerations that resulted in the poor fits discussed in the text.

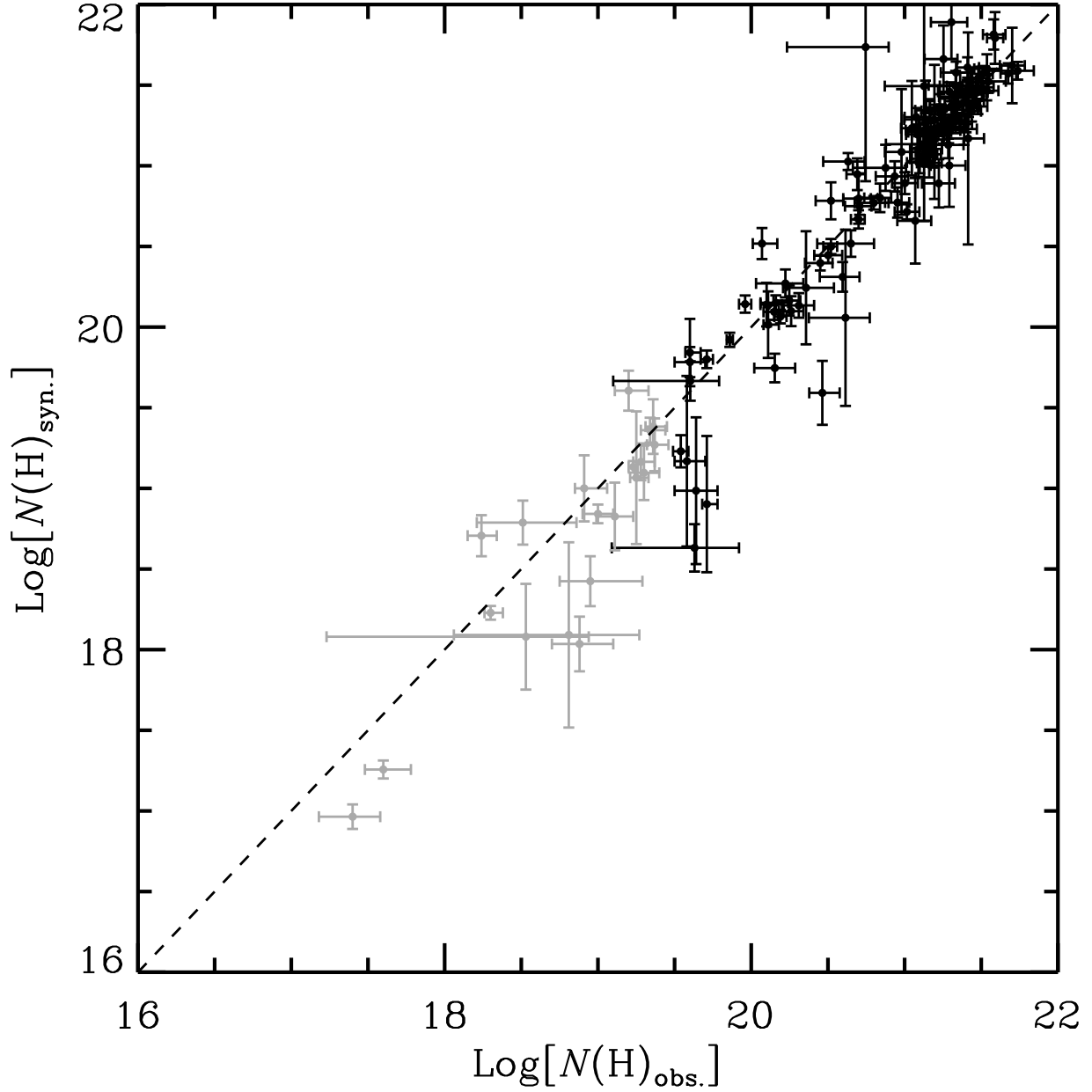


Fig. 10.— A comparison of the synthetic values of $N(\text{H})$ calculated using Eq. 24a (y axis) against their actual observed values (x axis), when known. See Columns (3–5) and Column (7) of Table 5. Gray points and error bars signify cases where $\log N(\text{H})_{\text{obs.}} < 19.5$ to emphasize the fact that their abundance measurements may not reliably indicate the true gas phase abundances in H I regions.

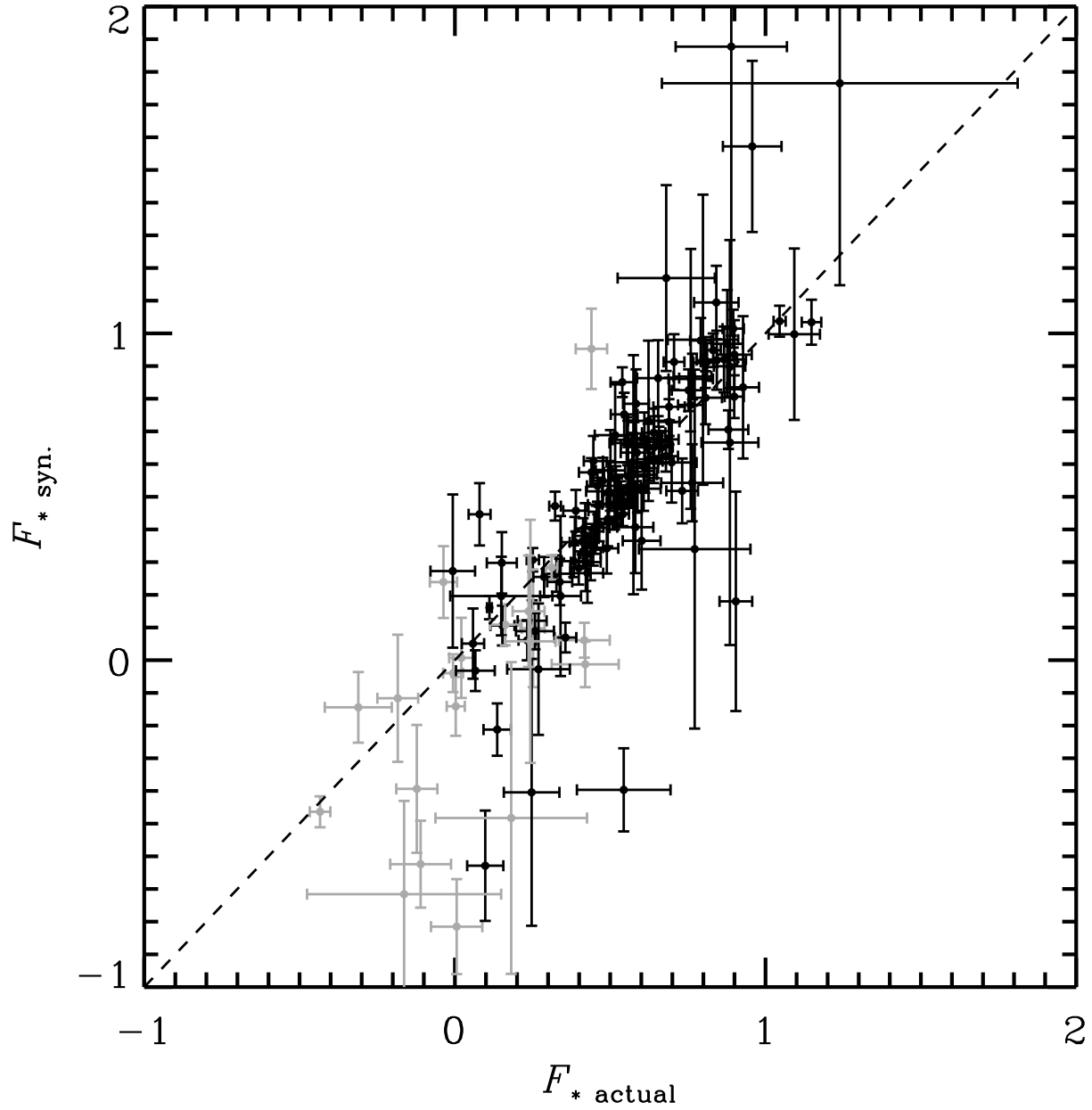


Fig. 11.— A comparison of the synthetic values of F_* computed using Eq. 24a (y axis), which would be used if $N(\text{H})$ were unknown, against computations of F_* obtained from Eq. 4 for all cases where $N(\text{H})$ has actually been observed. As in Fig. 10, gray symbols show cases where $\log N(\text{H})_{\text{obs.}} < 19.5$.

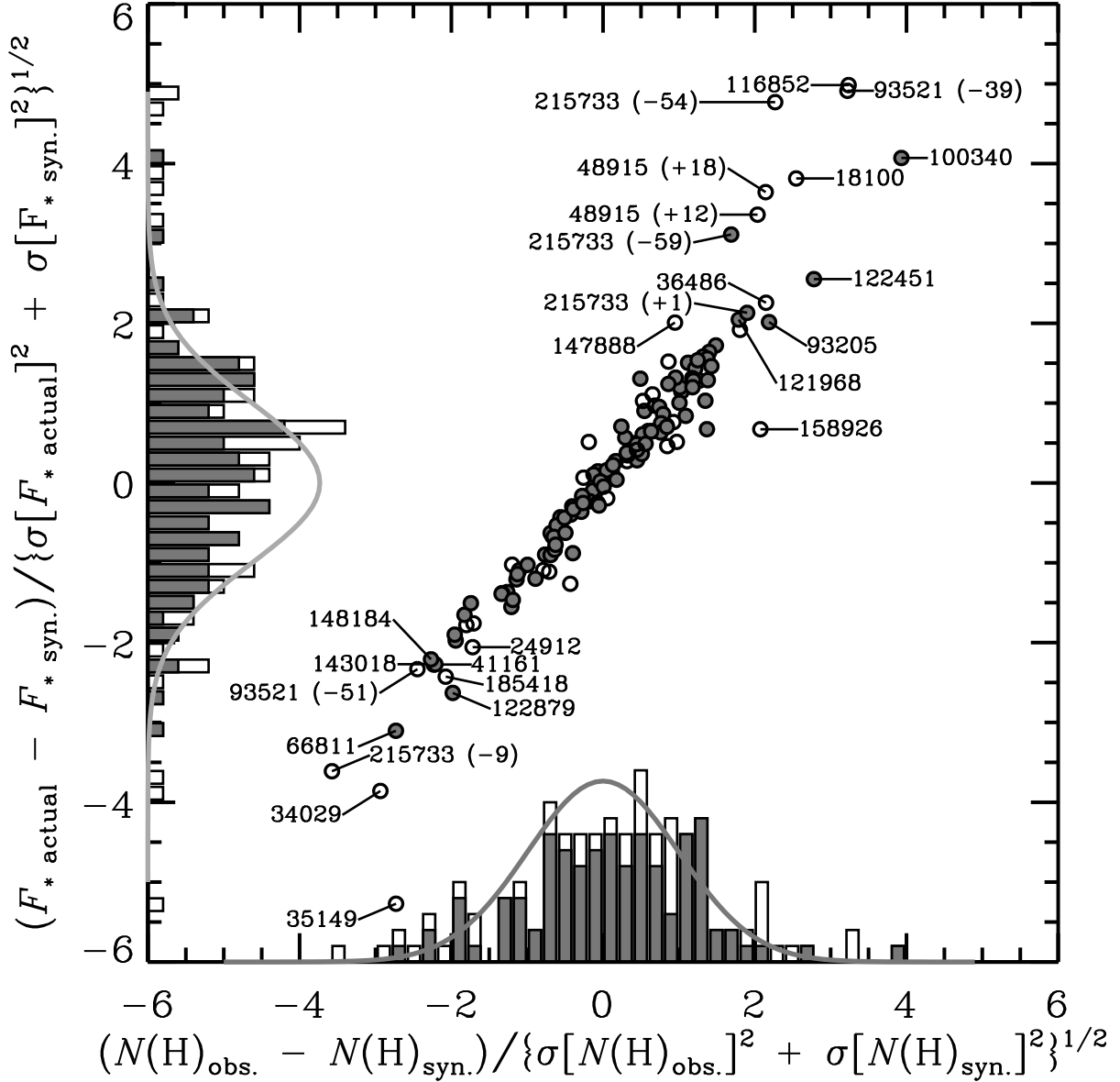


Fig. 12.— Deviations of $N(\text{H})$ and F_* (shown in Columns (3–6) of Table 5) from their synthetic counterparts derived from Eq. 24a (Columns 7 and 8 of the same table), divided by the respective uncertainties for the differences of the two quantities as defined by denominators shown in the x and y axis labels, for all cases where $N(\text{H})$ is known from observations. Points that are filled in have probabilities of worse fit (see Column (9) of Table 5) greater than 0.05, while open points are below this threshold. The HD numbers of stars (and the velocity components in parentheses, if appropriate) are labeled for outlier points that have deviations for either case that are more than 2σ away from zero. Histograms showing the distributions of all deviations are shown next to the x and y axes, with an overlay of a Gaussian distribution with a zero mean and standard deviation of 1 for comparison purposes. Solid and open portions of the bars are coded in the same manner as the points.

In making judgments on how well the applications of Eq. 24a are working, we can examine all cases where $N(\text{H})_{\text{obs}}$ is known and for which the right combination of elements were measured, and then simply compare the observed and synthetic values of $N(\text{H})$. We can also do the same for the two methods for determining F_* . Figures 10 and 11 show these comparisons. For both variables, a vast majority of stars show a good agreement between the two methods.

We can also examine the overall behavior of differences in the two ways of deriving both variables divided by the expected errors of such differences. This is shown in Figure 12. It is clear that the errors are highly correlated, which comes as no surprise if one imagines how errors in the slopes of the lines can have a large leverage in creating deviations for the locations of the y -intercepts at $x = 0$ (toward the far right-hand sides in the plots shown in Fig. 9), especially if there is no representation by elements with small depletions. (If one examines the errors in the synthetic $N(\text{H})$ values listed in Table 5, it is clear that they are generally larger than average if C, N, O or Kr are not represented in the list of elements shown in the last column.) Histograms on the sides of the plot box in the figure show how the deviations are distributed, with a Gaussian curve having a unit standard deviation and zero mean overlaid for comparison. While the distribution of the bars of these histograms seem generally consistent with this Gaussian curve, it is clear that the number of outliers beyond 2σ is larger than expected. Those cases are identified by their HD numbers (and velocities, if distinct). For both the histogram bars and the circle points in the diagram, the filled-in cases have probabilities of a worse fit that are larger than 0.05, while those that are open have lower probabilities.

8. Depletions toward White Dwarf Stars in the Local Bubble

It is clear from Fig. 3 that our coverage of distances exhibits an abrupt lower limit at about 100 pc. The volume of space out to about 100 pc from the Sun has an uncharacteristically low density; it is a region known as the Local Bubble (Cox & Reynolds 1987; Breitschwerdt et al. 1996; Vallerga 1996; Ferlet 1999; Lallement et al. 2003; Frisch 2007), and it contains a collection of isolated, warm clouds (Redfield & Linsky 2004a, b) embedded within and confined by a hot plasma (Breitschwerdt & de Avillez 2006; Savage & Lehner 2006). It was probably created by a series of supernova explosions that arose from an association of early-type stars that passed through our vicinity about 14 Myr ago (Maíz-Appelániz 2001; Berghöfer & Breitschwerdt 2002; Fuchs et al. 2006). Many white dwarf stars embedded in the Local Bubble were observed by the *Far Ultraviolet Spectroscopic Explorer (FUSE)* satellite. However, for all but a few of these targets, $N(\text{H I})$ was not observed. Thus, if we wish to obtain an understanding about the strength of the depletions toward these objects, we must rely on the analysis of synthetic F_* .

A large fraction of the sight lines studied in the Local Bubble probably have $\log N(\text{H I}) < 19.5$, and thus they violate the restriction that we imposed to lessen the chances that partial ionization effects could influence the outcomes (see rule nr. 3 in §4.2). Indeed, along the sight lines to white dwarf stars in the Local Bubble, it is not unusual to find that $N(\text{N II}) > N(\text{N I})$ (Kruk et al. 2002;

Lehner et al. 2003). However, for the elements Si and Fe, we can see from Figs 5 and 7 that most measurements with $\log N(\text{H I}) < 19.5$ (shown as open circles in the figures) seem to lie reasonably close to the trend established by the higher column density cases (or an extrapolation of it for $F_* < 0$), suggesting that, for these particular elements, our initial hesitation to include these low column density cases was more cautious than necessary. Moreover, ionization models of gas within the Local Bubble shown in Figure 6 of Lehner et al. (2003) indicate that for $\log N(\text{H I}) \gtrsim 18$, the influence of photoionization within the Local Bubble on the abundances of O I, P II, Si II and Fe II relative to H I is small. Comparisons of O I to H I are rather secure under almost all conditions because the ionizations of these two elements are coupled to each other by a strong charge exchange reaction (Field & Steigman 1971; Chambaud et al. 1980; Stancil et al. 1999).

In light of the above statements, we bypass here the column density restriction and proceed with derivations of synthetic values of $N(\text{H I})$ and F_* for sight lines toward white dwarf stars in the Local Bubble by using the prescription outlined in §7. In order to obtain a satisfactory spread in A_X , we require that information is available for O I and one or more of the species P II, Si II, and Fe II. Table 6 lists results for the stars that satisfy these conditions, based on observations reported by Oliveira et al (2003) and Lehner et al (2003). If errors in y of Eq. 24a were set to their formal values, unreasonably large values of χ^2 were obtained. This probably reflects the fact that the accuracy of the observations of $N(X)$, along with the formal errors in A_X and B_X , are far better than the precision of the assumption that Eq. 24a truly applies for gas parcels in the Local Bubble. For this reason, errors in y were artificially increased by 0.2 dex (added in quadrature to the original errors) to make the worse fit probabilities, as reflected by the values of χ^2 , evenly distributed over the interval 0 to 1.

Values of $\log N(\text{H I})_{\text{syn.}}$ listed in Table 6 range from 17.5 to 20.1. For three cases, observations of $N(\text{H I})$ are available for spot checks on the accuracy of the synthetic values: HZ 43A $\log N(\text{H I})_{\text{obs.}} = 17.93 \pm 0.03$ (Kruk et al. 2002) vs. $\log N(\text{H I})_{\text{syn.}} = 17.82 \pm 0.25$; Lan 23 $\log N(\text{H I})_{\text{obs.}} = 19.89^{+0.25}_{-0.04}$ (Wolff, Koester, & Lallement 1999) vs. $\log N(\text{H I})_{\text{syn.}} = 20.11 \pm 0.33$; GD 246 $\log N(\text{H I})_{\text{obs.}} = 19.11 \pm 0.03$ (Oliveira et al. 2003) vs. $\log N(\text{H I})_{\text{syn.}} = 18.94 \pm 0.25$. In all cases, the agreements are well within the estimated errors.

Figure 13 shows the distribution in the sky of the *FUSE* white dwarf observations along with the distances and derived values of $F_{*\text{syn.}}$. The construction of this figure is very similar to Fig. 1 of Lehner et al. (2003) so that one can easily compare their values of $\log N(\text{O I})$ (which are not very different from $N(\text{H I})_{\text{syn.}}$ aside from a constant factor) with our values of $F_{*\text{syn.}}$. It is also similar to Figs 7–12 of Redfield & Linsky (2004a), which show column densities of various species toward mostly late-type stars in the Local Bubble (these targets are generally much closer to us than the white dwarf stars). Our Fig. 13 indicates that there is a mild degree of coherence in the depletions: stars in the general direction of the south Galactic pole have light depletions, those toward the Galactic center have moderate depletions, and distant stars over a broad range of Galactic latitudes and at longitudes of around 90° have the largest values of $F_{*\text{syn.}}$. Six of the stars have $F_{*\text{syn.}} \geq 0.30$ and yet their values of $N(\text{H})_{\text{syn.}}$ are below our fiducial lower limit of $10^{19.5}\text{cm}^{-2}$ for the general

Table 6. Synthetic $\log N(\text{H})$ and F_* for Stars in the Local Bubble

WD nr. (1)	Alt. Name (2)	Gal. Coord.		V (5)	dist. ^a (pc) (6)	$\log N(\text{H})_{\text{syn.}}$ (7)	$F_{* \text{ syn.}}$ (8)	χ^2 (9)	Elem. Considered ^b (10)
		ℓ (3)	b (4)						
0004+330	GD 2	112.48	-28.69	13.8	97	19.69 ± 0.30	0.58 ± 0.33	0.61	O P Fe
0050-332	GD 659	299.14	-84.12	13.4	58	18.53 ± 0.26	0.03 ± 0.11	...	O Fe
0131-163	GD984	167.26	-75.15	14.0	96	19.21 ± 0.26	0.32 ± 0.27	2.49	O Si P Fe
0455-282	MCT 0455-2812	229.29	-36.17	14.0	102	18.09 ± 0.65	-0.18 ± 0.45	0.48	O Si Fe
0501+527	G191-B2B	155.95	7.10	11.8	69	18.05 ± 0.26	-0.22 ± 0.26	1.32	O Si Fe
0549+158	GD 71	192.03	-5.34	13.1	49	17.52 ± 0.28	-0.06 ± 0.20	...	O Si
0621-376		245.41	-21.43	12.1	78	18.56 ± 0.26	0.15 ± 0.34	...	O Fe
0715-703		281.62	-23.49	14.2	94	19.16 ± 0.27	0.28 ± 0.27	2.77	O Si P Fe
1017-138		256.48	34.74	14.6	90	18.93 ± 0.46	0.11 ± 0.39	4.72	O Si P Fe
1202+608	Feige 55	133.12	55.66	13.6	200	18.86 ± 0.25	-0.11 ± 0.23	1.54	O Si Fe
1211+332	HZ 21	175.04	80.02	14.7	115	18.97 ± 0.25	0.07 ± 0.21	0.84	O Si P Fe
1234+481		129.81	69.01	14.4	129	18.99 ± 0.27	0.40 ± 0.31	0.07	O Si P Fe
1314+293	HZ 43A	54.11	84.16	12.7	68	17.82 ± 0.25	0.22 ± 0.28	0.37	O Si Fe
1528+487		78.87	52.72	14.5	140	19.12 ± 0.27	0.39 ± 0.28	1.38	O Si P Fe
1615-154	EGGR 118	358.79	24.18	12.4	55	19.01 ± 0.28	0.17 ± 0.28	1.64	O P Fe
1631+781	IES 1631+78.1	111.30	33.58	13.0	67	19.29 ± 0.27	0.48 ± 0.29	0.05	O Si P Fe
1634-573	HD 149499B	329.88	-7.02	9.8	37	18.79 ± 0.25	0.35 ± 0.27	1.77	O Si P Fe
1636+351		56.98	41.40	14.9	109	18.77 ± 0.33	-0.31 ± 0.32	3.00	O Si P Fe
1800+685		98.73	29.78	14.6	159	19.35 ± 0.29	0.10 ± 0.25	1.34	O Si P Fe
1844-223		12.50	-9.25	14.0	62	19.23 ± 0.31	0.28 ± 0.31	1.14	O Si P Fe
2004-605		336.58	-32.86	13.4	58	18.93 ± 0.26	0.26 ± 0.29	0.75	O Si P Fe
2011+395	EUVE J2013+40.0	77.00	3.18	14.6	141	19.32 ± 0.26	0.31 ± 0.26	2.90	O Si P Fe
2111+498		91.37	1.13	13.1	50	18.26 ± 0.26	-0.07 ± 0.25	5.86	O Si Fe
2124-224		27.36	-43.76	14.6	224	19.05 ± 0.25	-0.20 ± 0.25	6.04	O Si P Fe
2152-548		339.73	-48.06	14.4	128	18.75 ± 0.27	0.03 ± 0.24	1.18	O Si Fe
2211-495		345.79	-52.62	11.7	53	18.54 ± 0.25	-0.01 ± 0.24	2.29	O Si P Fe
2247+583	Lan 23	107.64	-0.64	14.3	122	20.11 ± 0.33	0.56 ± 0.35	...	O Fe
2309+105	GD 246	87.26	-45.12	13.0	79	18.94 ± 0.25	0.29 ± 0.27	1.44	O Si P Fe
2331-475	MCT 2331-4731	334.84	-64.81	13.5	82	18.71 ± 0.26	0.12 ± 0.24	1.75	O Si P Fe

^aTaken from the papers that described the FUSE observations.

^bAll column density data from Lehner et al. (2003), except for HZ 21 (Oliveira et al. 2003).

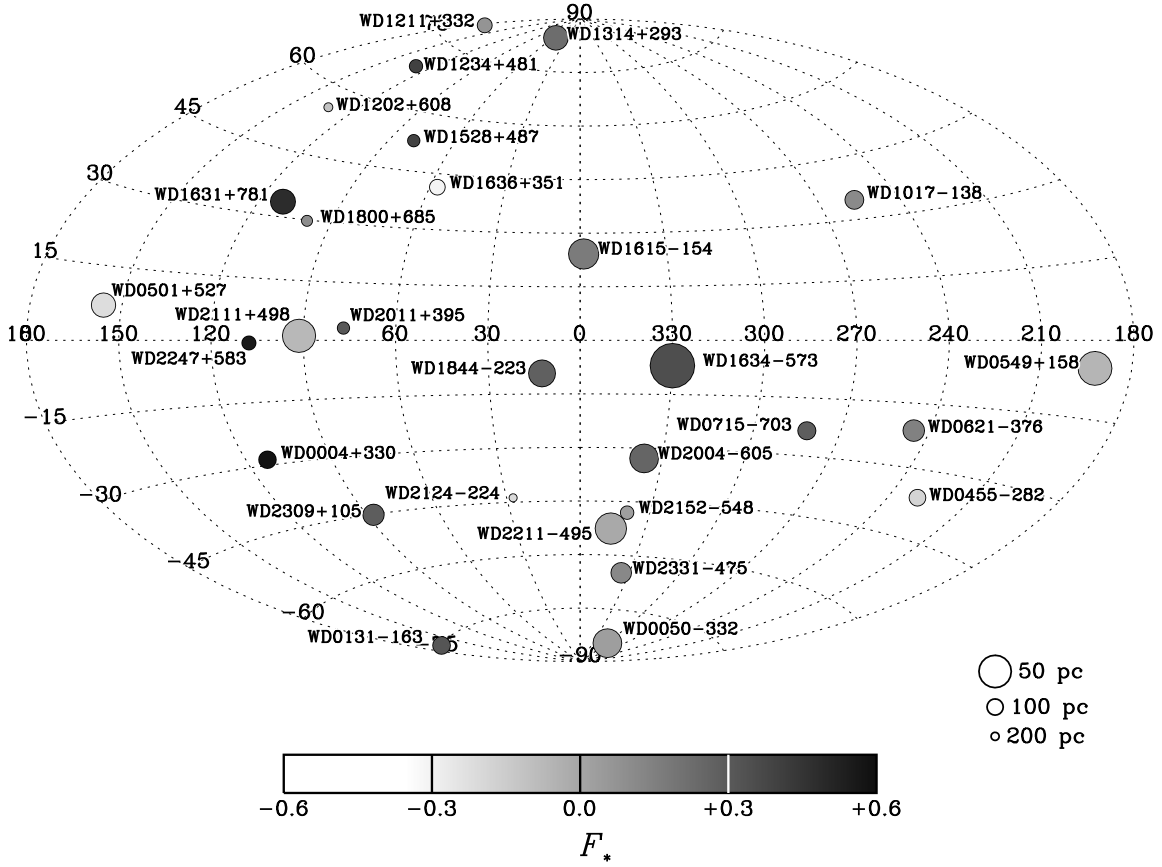


Fig. 13.— A depiction of F_{*syn} for the sight lines toward white dwarf stars observed with *FUSE*. The positions of the circles indicate the Galactic coordinates ($\ell = 0$, $b = 0$ at the center) and their sizes indicate the distances to the stars, according to the legend shown in the lower right-hand portion of the figure. The darkensses of the filled in portions of the circles indicate the derived values of F_{*syn} , according to the gray scale at the bottom.

study, indicating that, provided we are not being misled by ionization effects, moderately strong depletions can be found in the Local Bubble. This conclusion is consistent with the findings of Kimura et al. (2003) for very local, warm gas that surrounds our heliosphere.

9. Sulfur: A Troublesome Element

Our consideration of sulfur has been deferred until now because this element presents difficulties that warrant special treatment. A study of the depletion behavior of sulfur is especially important, since many studies of gas in both our Galaxy and very distant systems have relied on this element as a standard for what should be virtually zero depletion. We need to re-examine whether or not this is true. For instance, Calura et al. (2009) have summarized some recent findings reported in the literature that may revise our understanding of the status of sulfur depletions or possible lack thereof.

The singly-ionized form of sulfur is detected only through a triplet with transitions at 1250.6, 1253.8 and 1259.5 Å, with f -values of 0.00543, 0.0109, and 0.0166, respectively (Morton 2003). Unfortunately, for many lines of sight that contain moderately large amounts of gas, even the weakest line is partly or strongly saturated. Observations taken at low resolution (e.g., with the G160M configuration of the GHRS instrument on *HST*) often exhibited ratios for the equivalent widths of the two weaker lines of less than 1.5, and thus they were deemed to be saturated enough to violate one of the censorship guidelines for this study (rule nr. 2 in §4.2). However, a small number of observations showed that the saturations were not so severe, or that the S II column densities could be extracted from moderately saturated features recorded at high resolution and analyzed through their apparent optical depths.

Prominent in the limited selection of S II measurements were the individual velocity components of the stars HD 93521 and HD 215733 analyzed by Spitzer & Fitzpatrick (1993) and Fitzpatrick & Spitzer (1997). In a few instances, the velocity separations of adjacent components were small, which could lead to errors in the assignments of column densities between them. An additional drawback of using the individual velocity components toward these stars is the reliance on 21-cm emission line measurements of H I instead of $L\alpha$ absorption.

Table 13 in Appendix B shows the stars that had measurements of S II that were accumulated in the current study (but not all of which were suitable for determining depletion coefficients). Relative to the stars that could be used for other elements, they are few in number (12) and a substantial majority of them have hydrogen column densities that are either unknown or below the threshold $N(\text{H}) = 10^{19.5} \text{cm}^{-2}$ that qualifies them for consideration. As with the measurements of depletions of other elements, a reference abundance was adopted from Lodders (2003), $\log(\text{S}/\text{H})_{\odot} + 12 = 7.26 \pm 0.04$.

The left-hand panel of Fig. 14 shows the observed depletions as a function of F_* . A least-squares best fit to the observations with $\log N(\text{H}) > 19.5$ (the 8 solid points) yields $A_{\text{S}} = -1.261 \pm 0.165$,

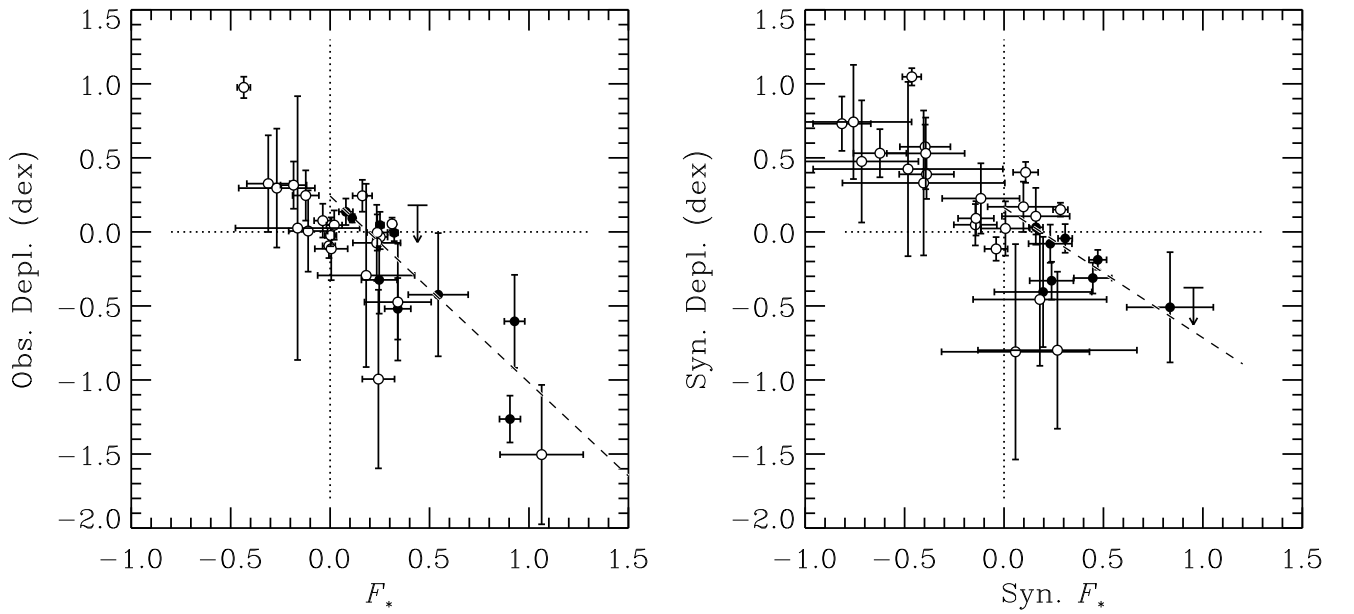


Fig. 14.— *Left-hand panel:* Observed depletions of S as a function of F_* . Cases with $N(\text{H}) < 10^{19.5} \text{ cm}^{-2}$ are shown with open symbols, while cases with larger values of $N(\text{H})$ have solid symbols. The dashed line shows the best least-squares fit to the solid points. *Right-hand panel:* Same as the left-hand panel, except that $N(\text{H})_{\text{syn.}}$ was used to derive the depletions and F_* derived from Eq. 4 was replaced by $F_{*\text{syn.}}$ calculated from the best fits to Eq. 24a.

$B_S = 0.028 \pm 0.047$, and $z_S = 0.170$, whose linear equation is represented by the dashed line. However, the probability of a worse fit is exceptionally low: $p = 0.005$.

There is a strong possibility that the 21-cm measurements that were used to set the H I column densities for the velocity components toward HD 93521 and HD 215733, which represent 26 of the points shown in the figure, are giving misleading outcomes. For instance, the beam width of the telescope was large (21'), and some H could be positioned inside the coverage of the beam but not in front of a star. Alternatively, some gas in front of the star that subtends a small solid angle in the sky could suffer severe beam dilution. Finally, some of the gas registered at 21 cm could be behind the star. (It was for these reasons that Fitzpatrick & Spitzer (1997) chose to disregard the hydrogen measurements and instead determined the depletions of elements other than S by making comparisons to the respective determinations of $N(\text{S II})$, on the presumption that S was always undepleted.)

To overcome the uncertainties in $N(\text{H I})$, we can resort to the tactic of deriving the synthetic versions of this quantity through the method outlined in §7 that made use of the relative abundances of other species. Likewise, F_* determinations that used $N(\text{H})_{\text{obs}}$ could be declared as suspect and instead we can use the synthetic values of F_* derived in conjunction with the calculations of $N(\text{H})$. The right-hand panel of Fig. 14 shows the outcomes with these different synthetic values of $N(\text{H})$ and F_* that were obtained from the fit to Eq. 24a. Here, we find that $A_S = -0.879 \pm 0.284$, $B_S = -0.091 \pm 0.042$, and $z_S = 0.290$. For the two fiducial points of F_* , we obtain from Eqs. 13 to 16 depletions $[\text{S}_{\text{gas}}/\text{H}]_0 = 0.163 \pm 0.092$ and $[\text{S}_{\text{gas}}/\text{H}]_1 = -0.715 \pm 0.206$. The chance of obtaining a worse fit for the 8 valid points in this case is 0.482 (from $\chi^2 = 5.5$ with 6 degrees of freedom), a considerable improvement over the earlier value that used the conventional determination of F_* and the observed values of $N(\text{H})$. Based on misgivings about the $N(\text{H})$ values derived from the 21-cm data and the improved fit using the synthetic values of $N(\text{H})$ and F_* , the numbers given immediately above are probably more reliable than those that were listed earlier, which were based on $N(\text{H})_{\text{obs}}$.

The ionization potential of S^+ is 23.4 eV; which, except for carbon, is the highest of the singly ionized species considered in this survey. For this reason, sulfur may be especially prone to the problem that its apparent abundance could be enhanced by its singly ionized form appearing in regions where the hydrogen is fully ionized by starlight photons (especially within H II regions created by stars with only moderately high effective temperatures, so that low energy photons that can ionize H are plentiful, while more energetic ones that are needed to ionize S^+ are not). One can therefore imagine that the appearance of readings of $[\text{S}_{\text{gas}}/\text{H}] > 0$ shown in Fig. 14 for $\log N(\text{H}) < 19.5$ (open circles) is caused by the invisibility of the accompanying hydrogen.

We could certainly benefit from some future, far more comprehensive survey of sulfur abundances. Not only do we find that the number of trustworthy determinations is small, but there may be a formidable selection bias that favors cases where $[\text{S}_{\text{gas}}/\text{H}]$ is lower than normal because we had to avoid cases where the sulfur absorption lines were not saturated and yet still satisfy our

requirement that $\log N(\text{H}) > 19.5$.

10. Discussion

10.1. The Composition of Interstellar Dust

10.1.1. General Remarks

The current study of depletions departs from most of the traditional ones that have emphasized the behavior of one or a few elements and how their abundance ratios change with such external factors as $\langle n(H) \rangle$, $f(\text{H}_2)$, and location. Our new perspective ignores these factors (except for retrospective studies reported later in §10.2) and recognizes that depletions change markedly from one sight line to the next but that among different elements they are well correlated. The objective now is to define how strongly each element participates in this collective behavior. In doing so, we can concentrate on only two properties of element depletions: (1) An initial depletion value $[X_{\text{gas}}/\text{H}]_0$, which serves as a minimum strength for all sight lines and (2) an index A_X that informs us about how rapidly individual elements deplete beyond this initial depletion compared to the others.

The existence of nonzero initial depletions $[X_{\text{gas}}/\text{H}]_0$ is an effect that has been known for some time (Jenkins, Savage, & Spitzer 1986; Joseph 1988; Fitzpatrick 1996), and it has commonly been identified with the gas phase abundances in a warm, low density medium (Spitzer 1985; Savage & Sembach 1996a). We can surmise that these minimum depletions indicate the composition of grains (through Eq. 2) that either have not had a chance to grow in dense interstellar media or have been partially stripped of certain elements by the recent passage of a shock at some point after such a growth phase.

The correctness of the values for $[X_{\text{gas}}/\text{H}]_0$ depend not only on the measured interstellar abundances, but also on the adopted values for the intrinsic abundance of the gas and dust put together, which in turn depend on the appropriateness and accuracy of the pre-solar abundance scale used in the current study. Also, it is important to remember that the definition of the zero point for F_* is probably strongly driven by our having adopted $N(\text{H}) > 10^{19.5} \text{cm}^{-2}$ as an artificial boundary condition in our assessment of the least severe levels of depletion. This requirement was imposed to minimize distortions in the abundance levels caused by the effects of ionization. As we look back to the open circles shown in the upper panels in Figs. 5 to 8, it appears that for the most part this rule may have been too conservative. Many of these open circles seem to be close to the trend lines or extrapolations thereof to negative values of F_* .

In contrast to the stated values of $[X_{\text{gas}}/\text{H}]_0$, the derivations of the progressive amounts of depletion represented by the various slopes A_X of elements X multiplied by their respective actual interstellar abundances (see Eq. 21) have no sensitivity to the choices for the reference abundances; they depend only on the magnitude of the adopted scale factor for the index F_* , which is an

index that we have created to define the collective depletion levels for the individual lines of sight. These differential rates for both the growth and destruction of grains allow us to determine the composition of the material that has been added to the cores responsible for the initial depletions. The elemental composition of this outer material (by number, not by mass) per unit change in the depletion index F_* , relative to the amount of hydrogen gas present, is represented by the lines and their error envelopes shown in the lower panels of Figs. 5 to 8.

Values of A_X listed in column (3) of Table 4 range between the extremes of zero (for A_N) to a large value for A_{Ti} , which is equal to 2.4 times the median value for all elements of -0.85 . The strong variability of A_X among the different elements allows us to rule out two explanations for the probable root cause of depletion differences in different sight lines: (1) errors in $N(H)$, which would cause all depletions in any given sight line to rise or fall in unison and (2) the dilution of elements in the gas within the Galactic disk caused by the infall and mixing of low metallicity material from the halo (Meyer et al. 1994; Meyer, Jura, & Cardelli 1998), which likewise would cause the logarithms of all element abundances to decrease in lock step with each other.

In §4.6.2, we discussed the corrections to $N(H I)_{obs.}$ to account for increases in the strengths of the $L\alpha$ absorption profiles caused by the stellar absorption features in stars of spectral type B1 and cooler. The median rank in F_* for these stars was 137, while for the hotter stars that did not need such a correction the median rank was 103. As a consequence, for elements that exhibited very mild progressive depletions (i.e., small absolute values of A_X), these corrections operated in a fashion to increase very slightly the numerical values of A_X and thus decrease the apparent contributions to grain growth. These systematic shifts were always smaller than the random errors associated with the fitting processes to derive A_X , as stated in Table 4, and, except for Kr, were not of much importance (see the footnote in §10.1.7).

In the following subsections, we discuss some noteworthy points about the depletions of a few specific elements.

10.1.2. Carbon

Carbon is a major constituent of grains, yet our knowledge of the actual differential consumption of C by grains still remains rudimentary, as is indicated by the large shaded region in Fig. 5. The paucity of data for C in our survey toward distant stars can be traced to the need to observe a weak intersystem transition at 2325 Å (Sofia et al. 2004) at a high S/N, since the allowed transitions at 1036 and 1335 Å are always strongly saturated. The strong transitions reveal reliable C II column densities for only a modest fraction of stars that are much closer to the Sun, i.e., those that have very low values of $N(H)$ (Wood & Linsky 1997; Lehner et al. 2003; Redfield & Linsky 2004a). There has been some concern expressed in the literature that not enough carbon is depleted to explain the optical properties of dust (Kim & Martin 1996; Mathis 1996; Dwek 1997). If we disregard the present large uncertainty in A_C and focus our attention on B_C to obtain a nominal

carbon depletion (at $F_* \approx 0.8$), we infer that the amount of C that is available for interstellar dust (and small molecules) is only 10^{-4} times the amount of H by number. About twice this amount is needed to explain the dust extinction (Draine 2003a). However, a recent, preliminary study by Sofia & Parvathi (2009) suggests that the strength of the intersystem line may be about twice as strong as that considered previously, which would lower the interstellar abundances by the same factor (and raise the dust carbon content by about 90%).

10.1.3. Nitrogen

The abundance of nitrogen is -0.109 ± 0.111 dex below its reference solar system abundance, regardless of the value of F_* , i.e., $A_N = 0.00 \pm 0.08$. Knauth, et al. (2003) claimed to have detected progressively stronger depletions of nitrogen as $N(\text{H})$ increased, but this effect may be indirectly related to an apparent enhancement of $N_{\text{gas}}/O_{\text{gas}}$ within 500 pc of the Sun discussed by Knauth et al. (2006). The latter result highlights the possible influence of regional differences in relative proportions of outputs from different nucleosynthesis sources (Type II SNe vs. AGB stellar winds) coupled with incomplete mixing in the ISM. However, if an effect such as this one were influential for our findings for N, it would probably have resulted in a poor outcome for the χ^2 value of the fit, which appears not to be the case (see Table 4). The fact that $A_N \approx 0$ suggests that the negative value of B_N might arise from the adopted value for $(\text{N}/\text{H})_{\odot}$ being too high, although the apparent deviation of B_N from zero is only at the 1σ level of significance.

Gail & Sedlmayr (1986) have pointed out that the condensation of N into any sort of solid compound could be inhibited by the production of N_2 , which is very stable. The saturated bond of this molecule results in a high activation energy barrier for gas phase reactions to form other molecules. While this may be an important theoretical consideration, the fact remains that the abundance of N_2 in the diffuse ISM is small (Knauth et al. 2004, 2006).

10.1.4. Oxygen

Cartledge et al. (2004) found that the abundance of oxygen exhibited a weak, but convincing downward trend of its abundance with respect to $\langle n(\text{H}) \rangle$. Thus, the fact that our value of $A_{\text{O}} = -0.225 \pm 0.053$ differs significantly from zero is not unexpected. However, what comes as a surprise is the finding that the extraction of oxygen from the gas phase seems, for the larger values of F_* , far out of proportion to the consumption of other, less abundant elements that can be thought to form solid compounds with oxygen. For instance, from Eq. 21 we find that when $F_* = 0$, $d(\text{O}_{\text{dust}}/\text{H})/dF_*$ is 1.6 times the sum of the solid phase accumulation rates (measured the same way) of Mg, Si and Fe, i.e., $d(\text{Mg} + \text{Si} + \text{Fe}_{\text{dust}}/\text{H})/dF_*$, and a factor of 16 greater when F_* reaches 1.0. Yet the conventional view is that oxygen is mostly incorporated into such refractory compounds as metallic oxides and amorphous silicates. However, even the most oxygen-rich of these compounds,

magnesium silicate (enstatite) MgSiO_3 , has only 3/2 times as much O as the other elements. Considering the uncertainties in the O consumption at $F_* = 0$, the 3/2 ratio, or even a somewhat lesser amount, could be satisfied. However, the divergence between the O consumption and those of the other elements makes this equality rapidly vanish when F_* becomes somewhat larger than 0. At even the lower edge of -2σ error zone for the O consumption at $F_* = 1$ shown in Fig. 5, we find that O atoms are taken out of the gas phase at a rate that is 6 times that of $\text{Mg} + \text{Si} + \text{Fe}$.

If we now switch our attention to absolute depletions instead of differential ones (this now relies on the premise that the pre-solar abundances are correct), our calculation of the value of $(\text{O}_{\text{dust}}/\text{H})$ at $F_* = 1$ is $2.41_{-0.66}^{+0.74} \times 10^{-4}$; the nominal value here is larger than a limit of 1.8×10^{-4} that is established by the *total* availability of other elements that can be incorporated into either the silicates, metallic oxides, or some combination of the two (Cardelli et al. 1996). However, the negative (1σ) error limit is consistent with this number. The uncertainty calculated for $(\text{O}_{\text{dust}}/\text{H})$ includes the presumption that $(\text{O}/\text{H})_{\odot}$ has a possible error as large as 0.05 dex.

We are drawn to the conclusion that O must be locked up in either some carbon or hydrogen compound (or as O_2), given that these are the only reactive elements with a sufficiently large cosmic abundance. (While it is abundant, the consumption of N during grain growth is nowhere near as much as O.) An initially attractive prospect was that O is incorporated in the form of amorphous H_2O ice on the grain surfaces (Ioppolo et al. 2008). Slightly more than 5% of the available oxygen atoms are found in the form of water in the material (with large extinction values) toward young stellar objects (van Dishoeck 1998), but various surveys indicate that the strength of the $3.05\mu\text{m}$ ice band shows a linear trend that extrapolates to zero when A_V decreases to values of around 2.6 to 5 (Whittet et al. 1988; Eiroa & Hodapp 1989; Smith, Sellgren, & Brooke 1993). The star Cygnus OB2 No. 12¹¹ has an extinction $A_V = 10.2 \pm 0.3$ but shows no detectable ice band in its spectrum ($\tau < 0.02$) (Gillett et al. 1975; Whittet et al. 1997). It may be possible that long term irradiation by cosmic ray particles and UV radiation modifies this ice layer in a way that inhibits the appearance of the infrared absorption feature (Greenberg 1982; Palumbo 2006). Other simple oxygen-bearing molecules in solid form, such as CO, CO_2 and O_2 generally have smaller abundances than that of H_2O , but they are not entirely negligible (van Dishoeck 2004).

An entirely separate method of determining what fraction of the oxygen is locked up in compounds is to examine the structure of absorptions in the vicinity of the K absorption edge at 23\AA in the spectra of x-ray binaries recorded by the grating spectrometers aboard *Chandra* and *XMM-Newton*. Molecular bonds shift the energies of bound-bound and bound-free transitions and create such complex structures, but unfortunately ionization of the atoms can play a similar role, which makes the analysis ambiguous (Costantini, Freyberg, & Predehl 2005). As a result, different investigators have arrived at differing interpretations of the observations. For instance, Paerels et al. (2001), Schulz et al (2002), and Takei et al (2002) have viewed their results on the O-edge structures in terms of specific compounds in the ISM, but these conclusions were later criticized

¹¹Sometimes called VI Cyg No. 12.

by Juett, Schulz & Chakrabarti (2004), who interpret the discrete features seen in a number of x-ray sources as arising simply from O I, O II, and O III. If their identification of absorption by compounds is correct, Takei et al. (2002) found that the amount of O in free atoms toward Cyg-X2 is $(8.6 \pm 2.8) \times 10^{17} \text{cm}^{-2}$, while O in bound form corresponds to $(5.2 \pm 2.2) \times 10^{17} \text{cm}^{-2}$, which is consistent with a depletion of atomic O of -0.205 dex. This amount of depletion is what we would expect for $F_* = 0.86$. However, Cunningham, McCray & Snow (2004) found that the total x-ray absorption by oxygen in all forms toward X Per (a sight line included here with $F_* = 0.90 \pm 0.06$; see Table 9) is consistent with just the gas-phase measurement, leaving no room for an appreciable amount of additional O in solid form.

A different approach is to use the x-ray absorption results to compare the total abundance of O with those of other elements, on the premise that perhaps large amounts of oxygen are locked within dust grains that have diameters of order or greater than $1 \mu\text{m}$. Grains this large have been detected in the local ISM by the dust sensors aboard the *Galileo* and *Ulysses* spacecrafts (Frisch et al. 1999; Landgraf et al. 2000; Krüger et al. 2006), and these measurements indicate that the large grains contribute a substantial portion of the total mass budget of material in solid form. The largest grains become optically thick to x-rays at energies near the K absorption edge. Takei et al (2002) found that $\log(\text{Ne}/\text{O}_{\text{gas} + \text{dust}}) = -0.84 \pm 0.18$ is consistent with the solar value of -0.81 ± 0.11 dex (Lodders 2003), indicating that all of the O absorption was evident in the observed edge absorption. In contrast, higher values that appear to indicate that some of the O is hidden have been derived in other investigations: $\log(\text{Ne}/\text{O}) = -0.52 \pm 0.21$ (Yao & Wang 2006), -0.66 ± 0.08 (Yao et al. 2009), and an outcome even as high as 0.1 (Paerels et al. 2001). Moreover, Ueda et al. (2005) found that Si/O and Mg/O were about 0.6 dex higher than their respective solar values (as adopted here, not as expressed in their article). The fact that the latter result is at variance with the UV absorption line data is consistent with the idea that while Si and Mg both reside mostly within small grains that individually have small optical depths for x-rays, significant amounts of O could be incorporated into grains or complexes thereof that are large enough to be fully opaque in x-rays.

Large dust grains having thick mantles of water ice should be extremely hard to detect by most astronomical methods. They contribute little to the extinction at visible and IR wavelengths, and their effectiveness in creating a distinctive $3.07 \mu\text{m}$ ice band absorption feature would be limited if the grain diameters exceeded $1 \mu\text{m}$ (B. T. Draine, private communication). About the only way to detect such large particles, if they are present, might be through very small angle scattering of x-rays from point sources (Smith & Dwek 1998; Witt, Smith, & Dwek 2001) or possibly even very faint scattering at larger angles at visible wavelengths for particles that are more than a few μm in diameter (Socrates & Draine 2008). However, various interpretations of the x-ray observations so far seem to indicate that the small-angle x-ray scattering data are consistent with dust grain populations composed of refractory compounds over a distribution of sizes smaller than $0.25 \mu\text{m}$ in diameter (Draine & Tan 2003; Dwek et al. 2004; Costantini, Freyberg, & Predehl 2005; Xiang, Zhang, & Yao 2005; Smith et al. 2006; Ling et al. 2009; Smith 2008).

10.1.5. Phosphorous

Phosphorous depletes more rapidly than oxygen, as is clear from the significant difference between the A_O and A_P values and their errors listed in Table 4. This finding is in conflict with the findings of Lebouteiller, Kuassivi & Ferlet (2005), who claim that $N(\text{P II})/N(\text{O I})$ always appears to be consistent with the solar abundance ratio over a large range of O I column densities.

10.1.6. Chlorine

The abundance trend of Cl is not as regular as for the other elements, as is evident from the scatter of points shown in Fig. 6 and the larger than usual errors for the parameters of Cl in Table 4. It should also be clear from the small dot sizes for Cl in Fig. 6 that the measurement errors are larger than usual. Some of the scatter in the Cl measurements may be due to the large fractions of Cl being in neutral form, compared to the singly ionized form. Jura (1974) has shown that chlorine ions can react with H_2 to produce $\text{HCl}^+ + \text{H}$ and eventually, through a chain of reactions that follow, revert to an amount of neutral chlorine that can even surpass the remaining concentration of chlorine ions. Indeed, there are a few lines of sight in the survey of JSS86 that indicate that $N(\text{Cl I}) > N(\text{Cl II})$. If these cases are predominantly at the largest values of F_* (which seems likely, since there will be a higher relative concentration of H_2), the slope of the best-fit line may be too steep (i.e., A_X is at too large a negative value), and this may be the dominant cause for our having found that $[\text{Cl}_{\text{gas}}/\text{H}]_0$ is positive.

10.1.7. Krypton

One apparently remarkable outcome is that Kr seems to show not only an offset below its solar system value, as indicated by the fact that $B_{\text{Kr}} = -0.332 \pm 0.083$, but that also there is an indication, not an entirely conclusive one, that there is some progressive depletion as F_* increases ($A_{\text{Kr}} = -0.166 \pm 0.103$). However it is clear that the nonzero value of this parameter is significant only at the 1.6σ level of significance.¹² A Pearson correlation coefficient of the 33 values $[\text{Kr}/\text{H}]_{\text{obs.}}$ vs. their respective F_* , which does not take into account the measurement errors, is only -0.225 . This value differs from zero correlation only at the 89.5% confidence level (we use a one-tail test here, since we reject the possibility that $A_{\text{Kr}} > 0$), which again supports the notion that this is a weak result. (Note that the determinations of F_* included measurements of Kr, but the weight factors W_X for Kr given in Eq. 5 are extremely small compared those of other elements because the

¹²In an earlier phase of this investigation, corrections for stellar $L\alpha$ absorption had not yet been implemented. The significance of the negative value for A_{Kr} was higher at that time. After the correction was added, a number of cases that supported stronger depletions of Kr at large F_* vanished because the calculated values of $N(\text{H I})_{\text{stellar}}$ were about equal to the uncorrected $N(\text{H I})_{\text{obs.}}$.

depletions have relatively large errors. Thus, there is a negligible influence of the Kr measurements on F_* , which in principle could have further weakened the conclusion on the significance of the correlation.)

The fact that the abundances of Kr seem to “pay attention to” the abundances of other elements with large values of A_X may signify that Kr is truly depleting and not exhibiting chance deviations caused either by real abundance variations or errors in measurement (either for Kr or H). This phenomenon was not evident in a conventional comparison of $(\text{Kr}_{\text{gas}}/\text{H})$ vs. $\langle n(\text{H}) \rangle$ in the most recent compilation of Kr abundances (Cartledge et al. 2008), and it indicates that this noble gas might either be attached to grains via physisorption or could possibly be trapped in a water clathrate (recall from the discussion in §10.1.4 that there might possibly be enough H_2O ice on large grains in the ISM to explain the depletion of O).

10.1.8. Trends with Condensation Temperatures

In trying to understand why different elements show different depletion strengths, a conventional approach is to compare them with their respective condensation temperatures. The condensation temperatures indicate the points at which the elements should show an appreciable deficit in the gaseous form as the result of forming compounds in a chemical equilibrium. However, apart from formation processes in stellar atmospheres and circumstellar envelopes, the formation and destruction of compounds within dust grains is not an equilibrium process. Even so, the condensation temperature may still be used as an approximate surrogate for the relative affinity of an element to form a solid compound and be resistant to destruction by shocks. As proposed by Dwek & Scalo (1980), the relative ease for the destruction of different compounds in grains is related to their respective sublimation energies, which are reflected by their formation temperatures through the Clausius-Clapeyron relation.

The left-hand panel of Fig. 15 shows the magnitudes of the initial depletions $[X_{\text{gas}}/\text{H}]_0$ as a function of the condensation temperatures T_c computed by Lodders (2003). Her values of T_c apply to a 50% decrease in the gas phase abundance at a pressure 10^{-4} bar with a pre-solar distribution of abundances. Values of $[X_{\text{gas}}/\text{H}]_0$ probably give the closest representation of the composition of grains that emerge from the atmospheres of late-type stars, supernovae, and circumstellar shells or disks. The relationship between the elements seen in this figure is similar to that for the highly depleted component toward ζ Oph: most elements show a trend of increasing depletion toward higher T_c , with the exception of P, Cl, Mg and Si, which seem to lie above the trend established by the other elements (Savage & Sembach 1996a).

If we now examine the differential depletions, the picture is a bit different. Recall that from Eq. 21 that the differential depletion scales in proportion to $A_X(X_{\text{gas}}/\text{H})_{F_*}$. If we normalize this rate to the concentration of atoms that are present, i.e., $(X_{\text{gas}}/\text{H})_{F_*}$, we get simply A_X . In effect, A_X represents a rate coefficient that applies to the quasiequilibrium state between the punctuated

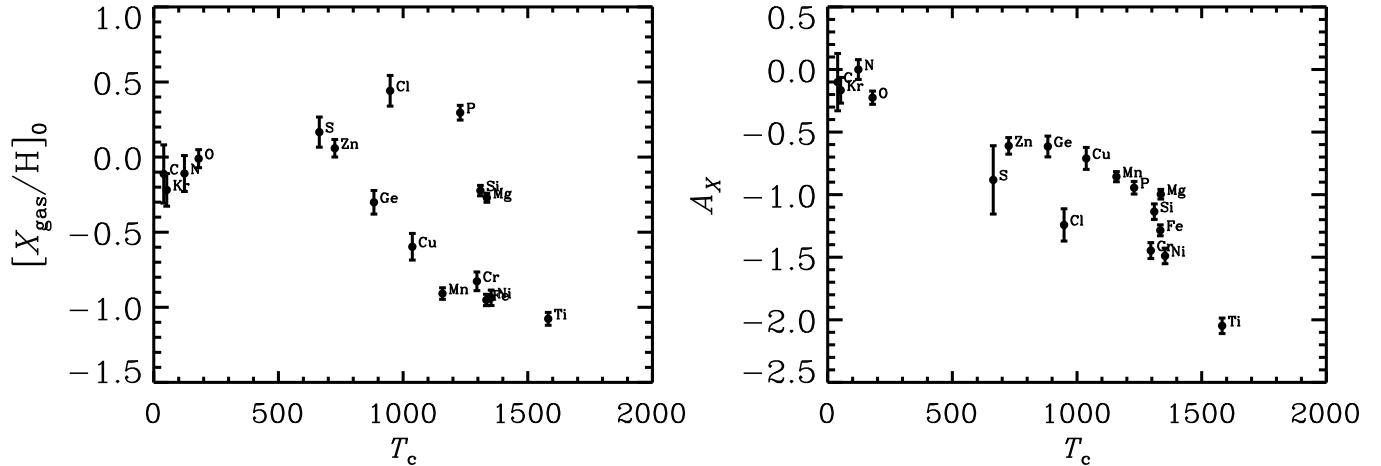


Fig. 15.— *Left-hand panel:* The trend of initial depletions as a function of the respective element condensation temperatures T_c listed by Lodders (2003). *Right-hand panel:* Values of A_X vs. T_c .

creation and destruction events of dust compounds (this is a loose concept because the condensation and destruction processes are physically different). The right-hand panel of Fig. 15 shows the values of A_X as a function of T_c . The placement of the points in this diagram seems more regular than what was seen for $[X_{\text{gas}}/H]_0$ (except for Cl, which seems to have flipped its position relative to the other elements – but recall the remarks about Cl made in §10.1.6).

10.2. The Relationship of F_* to Other Variables

We are in a position to repeat some of the comparisons mentioned in §1.2 using our generalized depletion index F_* for each sightline instead of just concentrating on the depletions of a single element (or several elements, but in an individual fashion), as has been done in the past. Figure 16 shows the trends of F_* against two popular extrinsic variables, the average density along the line of sight $\langle n(H) \rangle$ and the fraction of hydrogen atoms in molecular form $2N(\text{H}_2)/[N(\text{H I}) + 2N(\text{H}_2)]$. This figure shows that the relationship of F_* with the former seems more well defined than with the latter. Snow, Rachford & Figoski (2002) and Cartledge et al. (2006) arrived at a similar conclusion on the basis of their studies of the abundances of interstellar Fe, Ge, and Mg. As one would expect, target stars at some distance from the Galactic plane have lower than usual values of $\langle n(H) \rangle$, but the color coding of the symbols indicates that their depletion indices do not seem to show any distinct differences from other sight lines with the same average density. In contrast, Sembach & Savage (1996) found that gas identified with material in the lower halo of the Galaxy had smaller depletions than gas at comparable density in the disk [see also Savage & Sembach (1996a)]. The appearance of such a difference probably results from the fact that they treated separately the abundances in velocity components whose kinematics were consistent with being at large distances

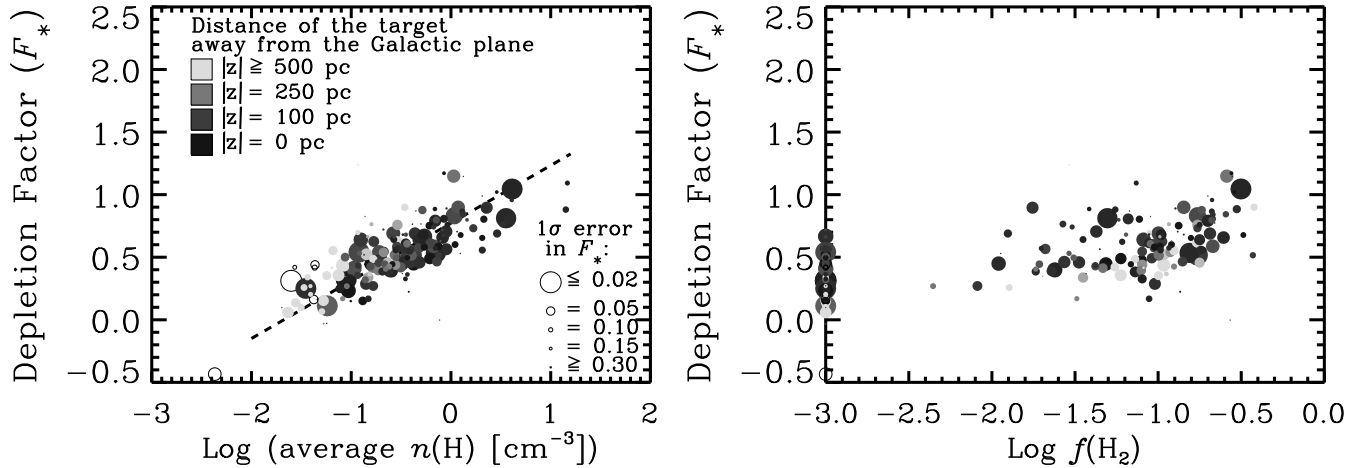


Fig. 16.— *Left-hand panel:* The trend of F_* as a function of the logarithm of the average density along the respective sight lines $\langle n(\text{H}) \rangle$. As indicated by the legends, the sizes of the circles indicate the errors in F_* , and their shades of gray indicate the distances of the stars from the Galactic plane. Open circles indicate cases where $\log N(\text{H}) < 19.5$. The least-squares best fit to the trend is indicated by the dashed line. *Right-hand panel:* The trend of F_* against the logarithm of the fraction of hydrogen in molecular form $f(\text{H}_2) \equiv 2N(\text{H}_2)/[N(\text{H I}) + 2N(\text{H}_2)]$. The sizes and gray levels of the points are the same as in the left-hand panel. Cases where $\log f(\text{H}_2) < -3.0$ are all bunched together on the y axis of the plot.

(i.e., far from the plane) instead of grouping all of the gas together, as in this study. An illustration of the importance of this distinction was shown earlier in Fig. 9 for the star HD 116852. Gas at progressively more negative velocities exhibited less depletion, and this material is farther from the Galactic plane (Sembach & Savage 1996).

A linear least-squares best fit to the trend shown in the left-hand panel of Fig. 16 follows the formula $F_* = 0.772 + 0.461 \log \langle n(\text{H}) \rangle$ indicated by the dashed line. This fit was evaluated in a way that minimized errors both in F_* and $\log \langle n(\text{H}) \rangle$. For the former, we take the actual estimates for the uncertainties in F_* [see column (6) of Table 5], and for the latter, we assume that the errors are dominated by the errors in the distances, which was assumed to be a uniform value of 0.2 dex (mostly from a 1 mag error in M_V ; see Appendix B3 of Bowen et al. (2008) for details on the probable errors in distances). In evaluating the fit, the protocol of accepting only sight lines where $N(\text{H}) > 10^{19.5} \text{cm}^{-2}$ was followed (see rule nr. 3 in §4.2). Such cases are indicated by the filled circles in the figure. The vertical dispersion of points on either side of the best fit line is 0.18. The χ^2 value for the fit is 285 for 175 degrees of freedom, indicating that the natural dispersion is somewhat larger than that created by our errors in F_* and $\log \langle n(\text{H}) \rangle$.

For the fit of F_* vs. $\log \langle n(\text{H}) \rangle$, there seems to be no departure from a simple linear trend, which seems contrary to the assertion by Cartledge et al. (2004, 2006) that a more complex association

between the two variables exists in the form of two plateaus with a transition between them at an intermediate value of $\log\langle n(\text{H})\rangle$ (they used a Boltzmann function to express this behavior). In their study of several different elements, the value of $\log\langle n(\text{H})\rangle$ for the transition region seemed to change somewhat from one element to the next, so the structure of this functional relationship may be lost when the generalized depletions based on many different elements are evaluated. Another alternative is that the extra parameters needed to define the Boltzmann function are not fully justified by the data, given the uncertainties present. The same remarks apply to the nonlinear forms shown by Jenkins, Savage & Spitzer (1986), who showed functions that fitted within the theoretical interpretation published earlier by Spitzer (1985).

We can repeat the comparison of F_* against the average of $n(\text{H})$ along sight lines for the white dwarf star sight lines that were analyzed in §8. Figure 17 shows this comparison and how it relates to the trend line shown in the left-hand panel of Fig. 16 for the early-type stars at greater distances. The correlation between $F_{*\text{syn.}}$ and $n(\text{H})_{\text{syn.}}$ is clear, and most of the points lie above the trend that was found for the more distant stars. Again, we express the caution that this difference could arise from the effects of photoionization.

Finally, a definition of our F_* parameter in the context of the summary of abundances given by Savage & Sembach (1996a) is presented in Appendix C.1. This comparison is presented to allow one to place later works that made use of these generalized abundance patterns into the framework of the present study.

10.3. Regional Differences in Total Abundances

In §4.2, we expressed reservations about using data from stars located at Galactocentric distances much different from that of the Sun. It is of interest to see if this concern was warranted, now that we have determined the coefficients F_* for all sight lines, but used only stars inside the range $7 < R_{\text{GC}} < 10$ kpc for determining the element parameters A_X and B_X . In essence, we wish to see if the interstellar line data show any hint of the gradient of overall abundances that have been detected for stars, planetary nebulae and H II regions [see the references cited within rule nr. 7 in §4.2 and also Table 1 of Rolleston et al. (2000)].

It also would be interesting to see if there are metallicity changes that mimic in any way the more specific abundance deviations reported in the literature for certain elements, such as an apparent enhancement of $N_{\text{gas}}/O_{\text{gas}}$ within 500 pc of the Sun reported by Knauth et al. (2006) or the increase in Kr_{gas}/H within an annulus $600 < r < 2500$ pc discussed by Cartledge et al. (2008).

A method for determining the overall metallicity of the gas that should be independent of the amount of depletion in a line of sight is to compare the synthetic determinations of hydrogen $N(\text{H})_{\text{syn.}}$, calculated on the basis of only the values of $N(X)$ in conjunction with their respective A_X and B_X in §7, with the observed counterparts $N(\text{H})_{\text{obs.}}$. The ratio of the two should indicate the relative excess or deficiency of the total heavy element abundances (gas + dust), compared to

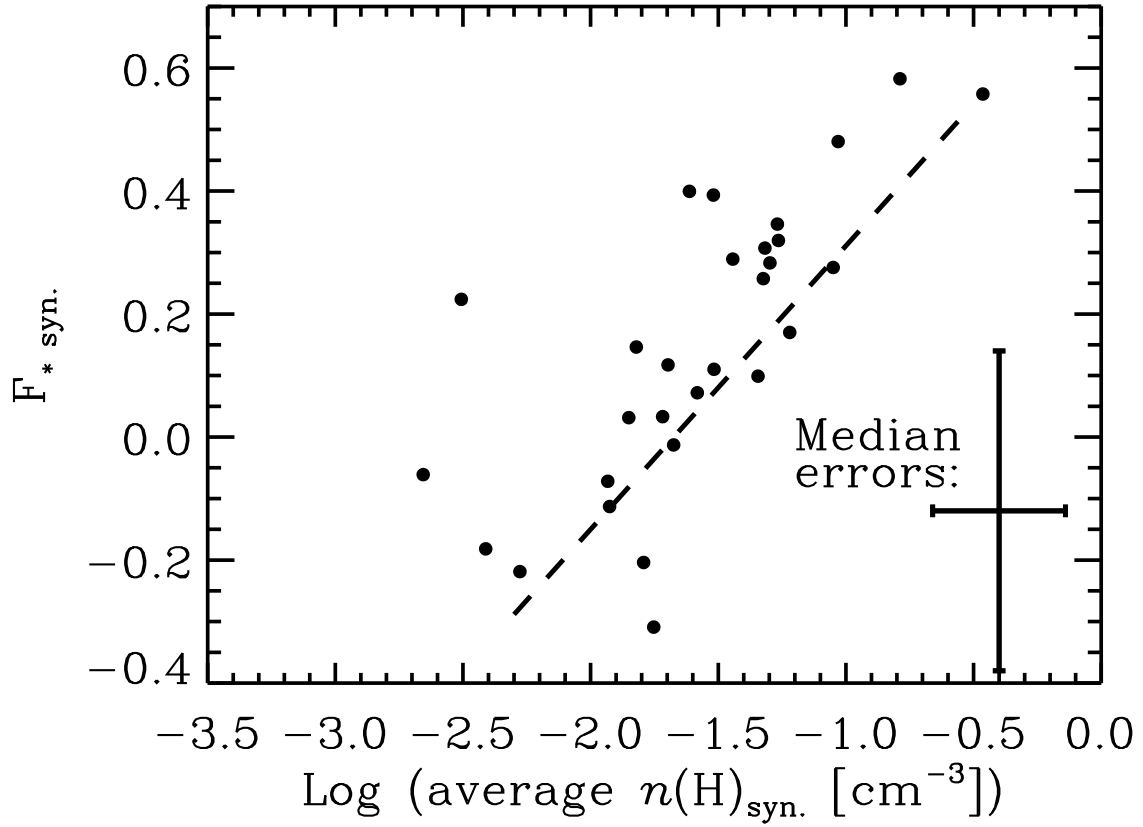


Fig. 17.— The relationship between $F_{* \text{ syn.}}$ and the average sight line density (determined from $N(\text{H})_{\text{syn.}}$) for the white dwarf stars in the Local Bubble, whose locations and distances are indicated in Fig. 13. Most of the estimated errors for the points in this figure have a size about equal to the bars shown in the lower right-hand portion of the plot. The diagonal dashed line indicates the location of the fit to the points shown in left-hand panel of Fig. 16.

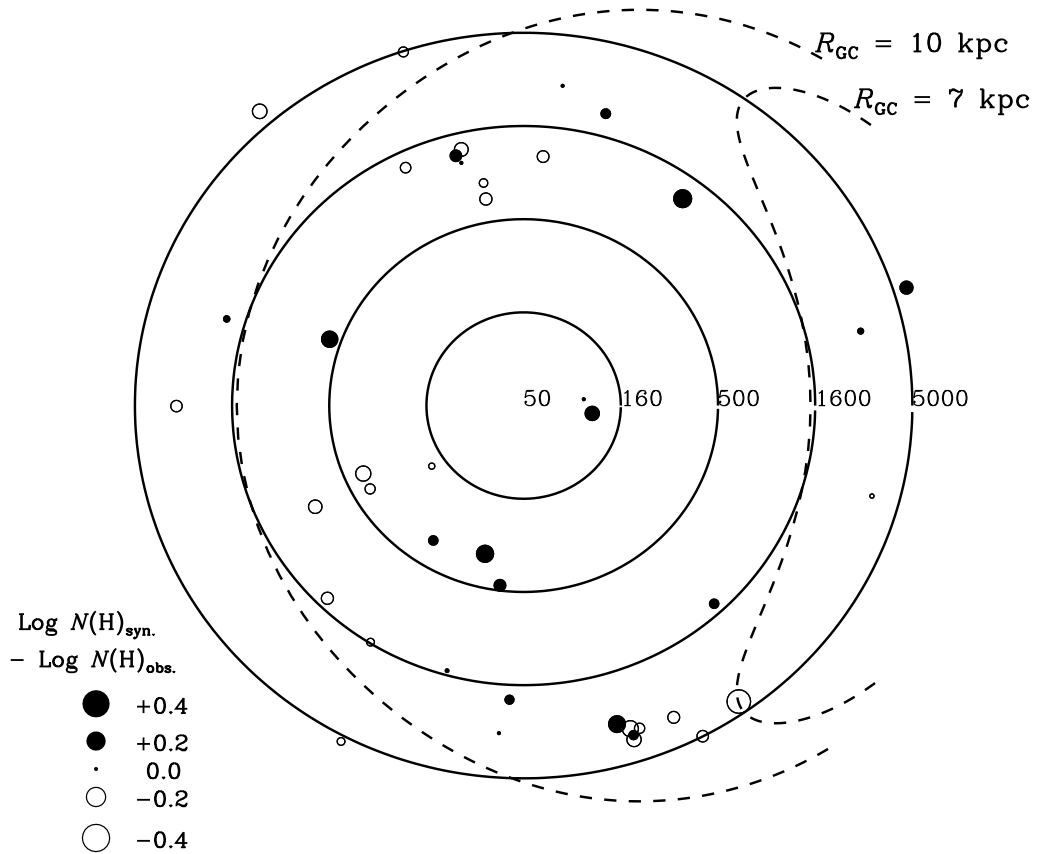


Fig. 18.— Differences in overall metallicity (gas + dust) with respect to locations relative to the Sun, as indicated by the quantity $\log N(\text{H})_{\text{syn.}} - \log N(\text{H})_{\text{obs.}}$. The only points that are shown are those with $N(\text{H})_{\text{obs.}} > 10^{19.5} \text{cm}^{-2}$ and where the ratio of the two values of $N(\text{H})$ is known to an accuracy of < 0.1 dex. Solid circles indicate gas that is metal rich, and open ones indicate the opposite condition. The Galactic center is to the right, and this polar representation has the distance from the Sun represented in a logarithmic fashion. The dashed lines indicate locations that are 7 and 10 kpc from the Galactic center.

their pre-solar values. That is, if $N(\text{H})_{\text{syn.}} < N(\text{H})_{\text{obs.}}$, we would conclude that the gas is metal poor.

Figure 18 shows a depiction of excesses and deficiencies of $\log N(\text{H})_{\text{syn.}} - \log N(\text{H})_{\text{obs.}}$ in a polar coordinate system that is logarithmic in radius and centered on the Sun. The points shown in this diagram are restricted to cases where both $N(\text{H})_{\text{syn.}}$ and $N(\text{H})_{\text{obs.}}$ are known, the error of their difference is less than 0.1 dex, and $N(\text{H})_{\text{obs.}} > 10^{19.5} \text{cm}^{-2}$. The locations of the solid and open circles appear to be random, indicating that no coherent changes in metallicity appear to be detected in different, readily identifiable locations. Of course, real differences may be masked by the averaging effect over the sight line that extends from the location of the Sun to that of the star. Unfortunately, there are too few sight lines that extend outside the zone $7 < R_{\text{GC}} < 10 \text{kpc}$ and that satisfy the restrictions given above to offer a good test of the metallicity gradient with galactocentric distance.

10.4. Applications for Abundances in Quasar and GRB Absorption Line Systems

10.4.1. Introductory Remarks

There have been many contemporary studies of element abundances in the Damped Lyman Alpha (DLA) and sub-DLA gas systems in front of quasars (Lu et al. 1996; Prochaska & Wolfe 2002; Pettini 2003; Prochaska, Howk, & Wolfe 2003; Dessauges-Zavadsky et al. 2004; Wolfe, Gawiser, & Prochaska 2005), as well as gases within or in front of the host galaxies of gamma-ray burst (GRB) sources that had bright afterglows in the visible part of the spectrum (Prochaska et al. 2007; Calura et al. 2009). A persistent problem with attempts to derive the intrinsic abundances of the elements has been the need to correct for the effect of depletion on the column density results. Early work on the abundances of these systems concentrated on the elements zinc and chromium (Meyer & Roth 1990; Pettini, Boksenberg, & Hunstead 1990), whose lines were easily accessible in the visible for low- z systems (Pettini 2003). Since it was known that the depletion of zinc is usually small and chromium large, approximate depletion corrections could be made by comparing the abundances of these elements to their solar abundance ratios.

Advances with larger, more sensitive telescopes and spectrographs led to studies of a wider range of elements, since transitions with short wavelengths in the rest frame could be viewed in systems at large redshifts in front of faint quasars. While opening up more elements for study has led to significant progress in chemical evolution studies of distant systems, investigators have still been hampered by a near degeneracy between the effects of dust depletion and those arising from shifts in the ratio of elements arising from α -capture processes compared to those associated with the iron peak (chiefly coming from Type 1a supernovae), since many of the iron peak elements are strongly susceptible to depletion while the α -process elements are usually much less so (Dessauges-Zavadsky, Prochaska, & D’Odorico 2002; Prochaska & Wolfe 2002). One can bypass the issue of dust by focusing on very mildly depleted elements such as C, N, O, Ar and Zn to measure the

overall metallicity of the gas, but except possibly for Zn, there is little leverage in learning about the α/Fe ratio, which is important for our understanding of the stellar initial mass functions and formation histories of the DLAs. Likewise, one may study systems that are known to contain very little dust, but this selection can introduce a sample bias that could lead to false conclusions on the chemical evolution of systems in general. Finally, one can take a broader approach by correcting for the effects of dust depletion, using information based on the empirical evidence on how element abundances change with the formation of dust in our Galaxy. We explain how to do this here.

10.4.2. *The Current Proposal to Correct for Dust Depletions*

As a way to interpret the abundances observed in an absorption system with an unknown overall metallicity and level of dust depletion, we can start with an initial guess that the intrinsic abundance pattern is not much different from that of our Galaxy, aside from an overall elevation or depression of all elemental abundances with respect to hydrogen. We then employ the method outlined in §7 to determine the severity of depletion, as represented by F_* (the slope of the trend of y vs. x). If $N(\text{H I})$ can be determined by observing the $\text{L}\alpha$ absorption (either from a space observatory for low- z absorption systems or from the ground for high- z systems), the difference between the synthetic $N(\text{H})$ and the real one indicates the metallicity of the system relative to that of the Galaxy. Next, we can examine the validity of the assumption that the pattern is not much different from that of our Galaxy by examining how well the element abundances conform to a straight line in y vs. x , as exemplified by Fig. 9 for two sight lines in our Galaxy (but recall that these two panels show special demonstrations of poor fits). Certain patterns of deviations from a straight line could serve as a warning that alternate intrinsic abundance patterns must be considered. (While this may be true, one must be watchful that one is not being deceived by effects of seeing mixtures of regions with different values of F_* , as exemplified by the lower panel of Fig. 9. It is noteworthy that on the one hand Prochaska (2003) found that abundance variations from all possible causes for different velocity components in 13 different DLA systems were less than 0.2 dex. On the other hand, Dessauges-Zavadsky et al. (2006) found that for some DLAs there were pronounced variations in some abundance ratios, sometimes >0.3 dex, which they interpreted to arise from changes in the depletion levels from one cloud to the next.)

As we move on to gas systems that we have good reason to believe to have intrinsic abundance patterns that are different from that of our Galaxy, we must rely on a more general approach, but one that still makes use of information provided by the current study. It is clear from the differences of the slopes of the trends shown in lower panels of Figs. 5 to 8 that the progressively increasing scarcity of certain elements starts to modify the composition of added material on the grains as they become larger or more numerous (i.e., as F_* increases). In such circumstances, it seems sensible to imagine that different atoms have their own proclivities to attach themselves to dust grains and form compounds, which forces the grain compositions to be regulated by the effective reaction rate constants of the elements (i.e., in a regime of only grain growth, we may

think of such rate constants in terms of the atomic sticking efficiencies times their mean velocities) multiplied by their respective concentrations at any given time. As we pointed out near the end of §10.1.8, the A_X terms derived here represent just such a collection of rate constants.

10.4.3. Possible Complications

A few cautionary remarks are in order for gas systems whose initial compositions differ appreciably from those in our Galaxy. In the following paragraphs, these cautions will be expressed, and it is important to emphasize that they apply to *any* dust correction scheme for abundances – not only the one proposed here.

One could imagine that for any arbitrary mixtures of gas-phase elements, one could simply integrate the equations for the condensations as a function of time (or grain growth), using the A_X values as rate constants. However, such an approach invokes the assumption that the retention of atoms after an initial sticking is in no way driven by the composition of the existing grain material. This may not be correct. Most elements probably depend on the presence of others to form chemically stable compounds that are durable enough to remain in solid form for long periods of time. For instance, Lodders (2003) presented examples where the elements Ni and Ge depend on the presence of a host element Fe to create an alloy. Likewise, Mg, Si and O are needed to form the host minerals forsterite and enstatite that are pathways to synthesize the most refractory compounds of Zn (Zn_2SiO_4 and ZnSiO_3) and Mn, (Mn_2SiO_4 and MnSiO_3). Thus, while we may note from Table 4 that A_{Zn} is about the same as A_{Ge} , in an environment where the α/Fe ratio differs appreciably from that of our Galaxy, one or the other of these two elements could be more starved for its respective host element(s) and could thus would probably behave differently from what we have observed here.

Another complication is the possibility that there could be large differences in dust-to-gas ratios and grain compositions in the ejecta of various kinds of sources that enrich a galaxy throughout its lifetime, such as evolved stars or different varieties of supernovae (Dwek 1998; Kozasa et al. 2009). It is well known that contributions of differing proportions from these sources throughout the history of a system’s chemical evolution will change the intrinsic mix of elements with time (Calura, Pipino, & Matteucci 2008), but they might also induce changes in the populations of either the primitive grains or the resilient cores of mature grains that do not normally grow or decline in the ISM. These primitive grains (or grain cores) are probably major contributors to the depletions seen at $F_* = 0$. Thus, while values of A_X might accurately describe how elements accrete onto grains as they grow in the ISM, the overall offsets represented by B_X could be influenced by the amounts and compositions of grains ejected by the sources.

As a simple illustration of how differing properties of grains in the ejecta of metal sources might create misleading conclusions, we can consider some comparisons of Si and Fe seen in the absorption spectra of DLAs. From entries in Table 4, we note that $A_{\text{Si}} \approx A_{\text{Fe}}$, so that differences in

the depletions of these two elements do not change much with differing values of F_* . The minimum separation between $[\text{Si}_{\text{gas}}/\text{H}]$ and $[\text{Fe}_{\text{gas}}/\text{H}]$ occurs at $F_* = 0$ and has a value of 0.73 dex. (A small decrease in this number could be realized by extrapolating the depletion trends to negative values of F_* , but not beyond that which makes $[\text{Si}_{\text{gas}}/\text{H}] > 0$.) Wolfe, Gawiser & Prochaska (Wolfe, Gawiser, & Prochaska 2005) show measurements of $[\text{Si}/\text{Fe}]$ in the gas phase (i.e., without any dust correction) as a function of $[\text{Si}/\text{H}]$ for a collection of high quality observations of DLAs (see their Fig. 8). Their plot shows that $[\text{Si}/\text{Fe}] \approx 0.3$ for $[\text{Si}/\text{H}] \lesssim -1.0$, and it increases somewhat for systems that have Si abundances that approach that of our Galaxy. On the one hand, if we simplistically apply our minimum correction for differences in dust depletion, we arrive at an intrinsic $[\text{Si}/\text{Fe}] \approx -0.4$. Correction factors of about the same magnitude were shown by Calura, Matteucci & Vladilo (2003), but their corrected $[\text{Si}/\text{Fe}]$ are not as low because their observed values of $[\text{Si}/\text{Fe}]$ started out at values that were generally higher than +0.3 dex. Of course, in this context it is possible that long, quiet periods between bursts of star formation could produce $[\alpha/\text{Fe}] < 0$ (Gilmore & Wyse 1991), and indeed the sequence of $[\alpha/\text{Fe}]$ as a function of $[\text{Fe}/\text{H}]$ for dwarf galaxies and the LMC is $\sim 0.1 - 0.3$ dex below that seen for stars in our Galaxy (Venn et al. 2004). On the other hand, it is quite possible that we could be misled in our interpretation if all of the following conditions apply: (1) Type Ia supernovae eject most of their Fe-peak elements eventually in the form of dust – a prospect that seems to have no observational support (Draine 2009), (2) this material is not significantly reprocessed through subsequent generations of stars and (3) core collapse supernovae do not form nearly as much dust in their ejecta as the Type Ia supernovae. In such circumstances, the depletion corrections could be distorted by the differing proportions of primitive grain production sites, compared to those in the present-day Galaxy (where the effects Type Ia supernovae are more influential than in the more primitive proto-disk galaxy systems), leading to corrected abundances that do not properly reflect the intrinsic gas + dust compositions of these other systems.

A strategy for checking on the complications discussed above is to examine many different elements simultaneously. For example, one might supplement the Si and Fe determinations discussed in the above paragraph with measurements of Ti (Dessauges-Zavadsky, Prochaska, & D’Odorico 2002; Ledoux, Bergeron, & Petitjean 2002), which is an α -process element that has large depletion parameters, even larger than those of Fe. If the depletion of Ti seems to be in the correct proportion to that of Fe, after correcting for a different intrinsic $[\alpha/\text{Fe}]$, then our misgivings about the effects of vastly different grain productions in different sources may be unwarranted.

Again, we suggest that to obtain the best general understanding of the complex processes that may influence the observed abundances in DLAs, the most productive insights may arise from examinations of the plots of y vs. x for individual absorbing systems. Such plots may be far more instructive than a battery of correlation plots that compare for many systems the various combinations of element abundance ratios.

10.4.4. Other Dust Correction Methods

In the recent past, investigations of DLA system abundances have relied on different schemes for correcting for dust depletion. For instance, Vladilo (2002b) devised a method to account for dust depletion in DLAs, using information on dust grain compositions derived from the summary of interstellar abundances under different conditions in our Galaxy given by Savage & Sembach (Savage & Sembach 1996a) (see Appendix C.1). Vladilo’s abundance corrections worked with parameters linked to the amounts of elements within the dust grains, with some recognition that these processes might change with different overall metallicities. Since this approach has been used to correct the observed abundances in a number of recent studies (Calura, Matteucci, & Vladilo 2003; Centurión et al. 2003; Dessauges-Zavadsky et al. 2004, 2007; Vladilo 2004; Vladilo et al. 2006; Quast, Reimers, & Baade 2008), it may be helpful re-express his abundance compensation parameters in the light of the parameters in the current study, so that we have a clearer understanding of what changes were made in the previous investigations. This is done in Appendix C.2.

In Appendix C.3 there is a similar cross calibration for two depletion parameters κ^{Zn} and κ^{Si} defined by Prochaska & Wolfe (2002) in their study of elements seen in their collection of DLAs. It is important to realize that there is no fundamental reason why distant DLAs could not have values of F_* less than zero, since their intrinsic metallicities $[\text{M}/\text{H}]$ range from about -2.5 to -0.5 dex (Wolfe, Gawiser, & Prochaska 2005). Our condition $F_* = 0$ applies to the arbitrary condition (but a practical one in our case) that the logarithm of the metallicity $[\text{M}/\text{H}] = 0$ and $N(\text{H}) \approx 10^{19.5} \text{cm}^{-2}$. While $F_* < 0$ might seem to be a reasonable outcome for such systems with very low concentrations of metals, especially those at the lower limit of $N(\text{H I}) = 10^{20.3} \text{cm}^{-2}$ for the standard definition of a DLA, in practice a comparison of our Fig. 21 with Fig. 22 of Prochaska & Wolfe (2002) indicates that F_* is always greater than zero.

11. Summary

The principal aim of this study has been to arrive at a simple, generalized description of the depletions of atoms in the interstellar medium of our Galaxy. The objective is not only to help us understand the elemental composition of dust grains, and how it changes as depletions increase, but also to provide the necessary guidance on how to correct for deviations in elemental abundances caused by dust grain depletions in distant gas systems that can be studied via their absorption lines in the spectra of quasars or GRB afterglows.

It has been known for some time that the strengths of depletions vary from one region to the next. However, to a remarkable degree of uniformity, we find that as these general depletion strengths vary, the logarithms of the depletion factors of different elements $[X_{\text{gas}}/\text{H}]$ are related to each other in a linear fashion that can be described by an equation

$$[X_{\text{gas}}/\text{H}] = B_X + A_X(F_* - z_X) \quad (25)$$

where B_X and A_X are empirically determined constants that apply to each element X , and F_* is a generalized depletion strength parameter that applies to the line of sight through the ISM that is under study. The zero-point offset for any element z_X that applies to F_* is added to the equation simply to make the measurement errors in B_X and A_X independent of each other (and its value is governed only by the distribution of F_* values and their errors in the sample).

A large accumulation of interstellar column densities gathered from the literature has been used to establish the validity of this simple model for depletions, as well as to provide the most likely values for the F_* line-of-sight parameters and the two constants B_X and A_X for 17 different elements. The data were screened to eliminate determinations that may have been compromised by uncertain corrections for line saturation, and in many cases the column densities were corrected in a manner to make them conform to a modern compilation of transition f -values. For all of the elements except sulfur, which was handled separately, the two constants are listed in Table 4. In establishing these constants, we considered only those sight lines that had $N(\text{H}) > 10^{19.5} \text{cm}^{-2}$, in order to decrease the chances that we could have been misled by unseen ionization stages, either for the element in question or hydrogen. Values of F_* and/or $F_{*\text{syn}}$ for 239 separate regions are listed in Table 5 (these include, for a few cases, some separate velocity components exhibited for some single sight lines and also sight lines that had $N(\text{H})$ below our established column density threshold). In a separate exercise, indirectly determined (synthetic) values of $N(\text{H})$ and F_* were evaluated for 29 white dwarf stars in the Local Bubble and listed in Table 6.

In conventional investigations of the elemental composition of dust grains, one compares the observed values of $N(X)$ to those expected from some adopted standard for the total abundance, most often taken from either a solar or meteoritic abundance (or the abundances of nearby B-type stars). The difference between a total abundance $(X/\text{H})_{\odot}$ and $(X/\text{H})_{\text{ISM}}$ indicates the quantity of the element that is locked up in solid form. One can apply this method to the measurements reported here, but the accuracy of the outcome is strongly driven by how well the adopted total abundance $(X/\text{H})_{\odot}$ conforms to reality. While this approach is needed to obtain the total makeup of the grains, another useful tactic is to study differences in specific elemental depletions as the overall levels of depletion increase. The outcome here is entirely independent of whatever one adopts for the total abundances. For any given value of F_* , the differential dust composition scales in proportion to $A_X(X_{\text{gas}}/\text{H})_{F_*}$.

For any sight line where $N(\text{H})$ has not been observed, one does not have explicit measurements of any depletions. Nevertheless, by making use of the information on how elements deplete in a collective manner, we can derive reasonably accurate (synthetic) values of F_* and $N(\text{H})$ if we have column density measurements $N(X)$ for several elements that have large differences in A_X and perform a least-squares fit of the quantities $\log N(X) - \log(X/\text{H})_{\odot} - B_X + A_X z_X$ against their respective values of A_X . While this is a useful tool for overcoming our inability to measure directly $N(\text{H})$ for any of several possible reasons, its greatest utility should be an application to the study of intrinsic element abundances in absorption-line systems seen in the spectra of distant quasars or the optical afterglows of GRBs. Specifically, one can compare the measured value of $N(\text{H})$,

obtained through an observation of the $L\alpha$ absorption, to the synthetic value of $N(\text{H})$ derived from the pattern of element column densities. The ratio of $N(\text{H})_{\text{syn.}}$ to $N(\text{H})_{\text{obs.}}$ yields the metallicity of the system relative to that of our Galaxy. The value of $F_{*\text{syn.}}$ indicates the dust content of the system. However, caution is advised for systems that are suspected to have a pattern of intrinsic abundances that differs appreciably from that of our Galaxy. For systems outside our Galaxy that are not too distant (e.g. the Magellanic Clouds), one should be able to validate the concept of using $N(\text{H})_{\text{syn.}}/N(\text{H})_{\text{obs.}}$ to obtain a metallicity by comparing the outcome to the average metallicity of the embedded stars.

The above paragraphs outline the basic themes contained in this paper. Some additional, more specific insights that came from this investigation are as follows:

1. Except for the elements C, N, O, P, Cl, S, and Zn, all elements show some measurable depletion at $F_* = 0$. For the elements Ti, Cr, Mn, Fe, and Ni, these base depletions $[X_{\text{gas}}/\text{H}]_0$ are of order -1 dex. They correlate moderately well with their respective condensation temperatures T_c , but the correlation of the depletion slopes A_X with T_c is even better.
2. Nitrogen appears to be the only element that does not show progressively stronger depletions as F_* approaches 1. There are too few measurements of carbon to establish whether or not the apparent strengthening of its depletion with F_* is real. For both of these elements, the errors are large enough to permit the progressive incorporation of these atoms (by number) to still exceed the accumulations of P, Cl, Cr, Mn, Fe, Ni, Zn, Ti, Cu, Ge or Kr when $F_* \approx 0$ and also Mg or Si when $F_* = 1$.
3. Until now, the observed small variations of $[\text{Kr}_{\text{gas}}/\text{H}]$ seemed random (and possibly driven either by changes in intrinsic abundances of this element from one place to the next or by observational uncertainties). The apparent correlation of this quantity with F_* in the current investigation suggests that the relative gas-phase abundance of this chemically inert element is coupled to those of other elements, but at a very low level. A possible means for depleting Kr is either physisorption on the surfaces of dust grains or locking within water ice clathrates.
4. For chlorine, there might be a mild misrepresentation of the relationship for its gas-phase abundance with respect to F_* . In part, the observational errors for $N(\text{Cl II})$ are larger than for other elements, but a more important effect is reversion of some of the atoms to a neutral form through a series of reactions with H_2 . This could be especially important at large values of F_* , where the fractional abundances of H_2 are large. There are some known cases where $N(\text{Cl I}) > N(\text{Cl II})$, according to JSS86.
5. The differential depletion of oxygen at low levels of F_* is just barely consistent with the consumption of O in the form of oxides and silicates. For $F_* \approx 1$ this is no longer true: the loss of O atoms from the gas phase far outstrips the production of silicates and oxides, suggesting that the formation of compounds involving abundant partner elements such as H or C may play an important role. While N is abundant, it does not have differential depletions

that are large enough to help explain the consumption of O. The large loss of oxygen atoms from the gas phase found in the present study is very difficult to reconcile with current models of interstellar grains.

6. Even though the average density $\langle n_{\text{H}} \rangle = N(\text{H})/d$ is a crude representation for the true local densities experienced by most of the atoms, we find that this quantity still exhibits a tight correlation with F_{\star} . This same correlation is seen for both the distant stars and for sight lines within a regime of generally low space densities within the Local Bubble. The surprisingly good relationship between average density and depletion strength supports the notion that either the lines of sight exhibiting high $\langle n_{\text{H}} \rangle$ have gas that is contained within, or has recently evolved from, very dense regions where rapid grain growth can occur or that these regions of space are better shielded from destructive, high velocity shocks, or both. The fraction of hydrogen in molecular form does not show a correlation that is probably any better than a secondary one that should arise from the correlation between $f(\text{H}_2)$ and $\langle n_{\text{H}} \rangle$.
7. By comparing synthetic values of $N(\text{H})$ with the observed ones, we see no evidence for changes in the intrinsic abundances of heavy elements in different regions around the Sun. The pattern of observed deviations seems random.
8. More needs to be done: additional data of good quality are needed to define better the differential depletion relationships of C, S and Kr, to see if their values of A_X are truly nonzero. Also, with the increase in sensitivity provided by the *Cosmic Origins Spectrograph* that will be installed on the forthcoming *HST* servicing mission, we should have an opportunity to observe lines of sight with greater extinctions (and hence probably much higher F_{\star}), so that we can obtain extend our reach to denser clouds and obtain a better understanding of chemically active environments that are better protected from uv dissociation.

This research was supported by Program number HST-AR-10279.01-A which was provided by NASA through a grant from the Space Telescope Science Institute, which is operated by the Association of Universities for Research in Astronomy, Incorporated, under NASA contract NAS5-26555. The author acknowledges the great utility of the SIMBAD and VizieR catalog databases, operated at CDS, Strasbourg, France, which provided critically important information on the target stars included in this survey. The author thanks B. T. Draine, J. X. Prochaska, B. D. Savage, U. J. Sofia and G. Wallerstein for providing helpful comments after reading a draft version of this article.

Facilities: HST(STIS), FUSE, Copernicus, IUE

A. Errors in Quotients

For several equations in §3, we must evaluate the uncertainties of quotients of two terms, each of which have their own errors. In order to do so, we make use of Geary’s (1930) approximation for the frequency distribution of the quotient of two quantities that each have normally distributed errors. According to Geary, for a quotient

$$z = \frac{b + y}{a + x} \quad (\text{A1})$$

involving a denominator a and numerator b that have respective normally distributed errors x with a standard deviation α and y with a standard deviation β , the quantity

$$t(z) = \frac{az - b}{\sqrt{\alpha^2 z^2 - 2r\alpha\beta z + \beta^2}} \quad (\text{A2})$$

has a normal distribution with a mean of zero and standard deviation of unity, provided that $a + x$ is unlikely to be negative (i.e., $a/\alpha \gtrsim 3$). (The quantity r in Eq. A2 is the correlation coefficient of x and y , which in our applications within §3 is always assumed to be zero.) After squaring both sides of Eq. A2 and collecting terms in z and z^2 , we have a quadratic equation,

$$(t^2\alpha^2 - a^2)z^2 + (2ab - 2t^2r\alpha\beta)z + (t^2\beta^2 - \beta^2) = 0 \quad (\text{A3})$$

whose roots give the extreme values of z that bound the possible combinations of b/a at the “ $t\sigma$ level of significance.” For the errors that appear in Eqs. 5 and 9, we evaluate half of the difference between the two roots for $t = 1$.

B. A Compilation of the Basic Data and Sight-Line Depletion Factors

Tables 7 through 23¹³ show the basic measurements of column densities (columns (3)–(5)) for each of the elements considered in this study, with the codes that signify the sources in the literature [column (6)] that are linked to references shown in column (2) in Table 1. All of the logarithms of the column densities have been corrected for changes in f -values (§4.4) by adding the factors expressed in dex for the appropriate elements given in Table 1. Column (7) of the element tables shows the value of the depletion index F_* and its error for the star in question, determined from Eqs. 4 and 6, respectively. This column is followed one that shows the expected depletion of the element $[X_{\text{gas}}/\text{H}]_{\text{fit}}$, calculated from Eq. 10 with the coefficients shown in Table 4. The error in this term,

$$\sigma([X_{\text{gas}}/\text{H}]_{\text{fit}}) = \sqrt{\sigma(B_X)^2 + [(F_* - z_X)\sigma(A_X)]^2 + [A_X\sigma(F_*)]^2} \quad (\text{B1})$$

¹³ These tables are placed at the end of this article, immediately after the references. When this article is published in the *Astrophysical Journal*, all of the tables will appear as a single, long table only in the electronic edition in the form of a machine-readable table.

combines in quadrature the various sources of errors arising from either the best-fit coefficients A_X and B_X of element X or the determination of F_* . (Recall from the discussion in §3.2 that $\sigma(B_X)$ here does not include the systematic error $\sigma(X/H)_\odot$.) Column (9) shows the amount by which the observed depletion $[X_{\text{gas}}/H]_{\text{obs}}$ differs from $[X_{\text{gas}}/H]_{\text{fit}}$, and column (10) shows this number divided by the combined uncertainty of $[X_{\text{gas}}/H]_{\text{obs}}$ and $[X_{\text{gas}}/H]_{\text{fit}}$ (with the two added together in quadrature), so that one can easily recognize deviations that seem to be unacceptably large. Values of $[X_{\text{gas}}/H]_{\text{obs}}$ can be obtained by adding together the numbers in columns (8) and (9), but asymmetrical error bars in the original data are not evident. To reconstruct the errors in $[X_{\text{gas}}/H]_{\text{obs}}$ one must take into account the uncertainties of both $N(X)$ and $N(H)$; for the latter, see Table 5. For each element, one can sense how well the calculated values $[X_{\text{gas}}/H]_{\text{fit}}$ agree with the observed ones by examining either individual deviations shown in the last two columns of the element tables or by inspecting the collective statistical information presented in Table 4 that was explained in §5. Missing entries in columns (7)–(10) are caused by a lack of information needed to calculate $N(H)$ (see Table 2).

C. Retrospectives on Earlier Characterizations

Many studies of gas abundances and dust compositions have made use of earlier descriptions of the depletion process. In order to recast these previous investigations in the light of the present work, we present in the subsections below the outcomes of the earlier depletion studies in terms of the parameters defined in §3. This should be useful in obtaining a better understanding of the earlier abundance works in the present context.

C.1. A Comparison with the Results of Savage & Sembach (1996a)

After the publication of the review paper by Savage & Sembach (1996a) on interstellar abundances from absorption line measurements using the *Hubble Space Telescope*, many investigations compared their own results with the generic depletions discussed in that review. We now offer a cross calibration between our F_* and the environments discussed by Savage & Sembach (1996a). We can do this through the application of Eq. 24a to their results, with mean values of the numbers given in their Table 6 replacing the expression $\log N(X) - \log(X/H)_\odot$ in our equation and by pinning $N(H)$ to a value of zero. Figure 19 shows this comparison for the four different representative environments specified by Savage & Sembach.

In order to obtain the values of F_* in each case, we evaluated a least-squares linear fit to the points, but without any weight factors to account for differing errors. For reasons given §9, sulfur was not included in the fit (but it is shown at the appropriate locations in the panels of the figure). Since depletions are known with respect to hydrogen, it is appropriate to add this element to the fit at the location $(x, y) = 0$. In order to make the comparison accurate, we made adjustments

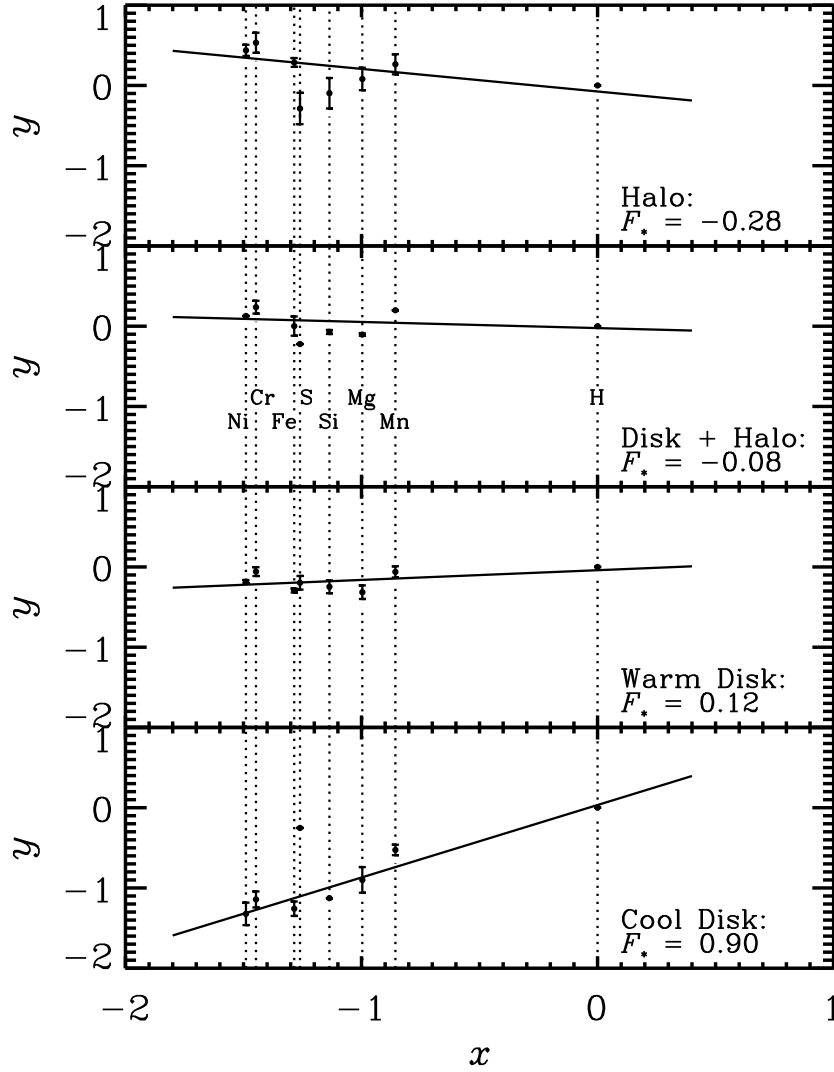


Fig. 19.— An application of Eq. 24a to the results shown in Table 6 of Savage & Sembach (1996a), so that their results for different environments can be calibrated to the F_* index of the present work. The values of x for each element are identified in the panel second from the top, with vertical dotted lines linking them across the remaining panels. In each case an unweighted least-squares linear fit to the points is shown by a slanted line whose slope yields the value of F_* listed in the respective panel. Error bars attached to some of the points do not represent uncertainties; instead they show the range of values that Savage & Sembach found for the respective elements in each environment.

to the numbers specified by Savage & Sembach, so that we can account for (1) small differences between their adopted reference abundances and the ones given by Lodders (2003), as listed in column (2) of our Table 4, and (2) the differences between the f -values that seemed appropriate in 1996 to the more recent ones published by Morton (2003) and Jenkins & Tripp (2006); see §4.4 for some considerations that applied to the f -value adjustments. The net changes are given by the following terms (expressed in dex) that were added to the original depletion values listed by Savage & Sembach: Mg = 0.23, Si = -0.04, S = -0.01, Mn = -0.05, Cr = 0.21, Fe = -0.03, and Ni = 0.34. The values of F_* that apply to each environment are given in the respective panels of Figure 19. As one would expect, there is a regular progression in F_* from the least dense environments to the most dense ones.

C.2. Dust Corrections of Vladilo (2002a, b)

Vladilo (2002b) used the summaries of element abundances in different environments given by Savage & Sembach (1996a) to characterize changes in $(X_{\text{dust}}/\text{H})$ (which he calls p_X) in terms of $(\text{Fe}_{\text{dust}}/\text{H})$ (which he calls r) by evaluating the derivatives of their logarithms and defining a parameter $\eta_X \equiv d \log p / d \log r$. We can evaluate the differentials of these two quantities with respect to F_* to obtain

$$\begin{aligned} \eta_X &= \frac{r}{p_X} \frac{dp_X/dF_*}{dr/dF_*} \\ &= (X/\text{H})_{\odot} \frac{(\text{Fe}_{\text{dust}}/\text{H})10^{[X/\text{H}]}A_X(\text{Fe}/\text{H})_{\odot}^{-1} - (X_{\text{dust}}/\text{H})10^{[\text{Fe}/\text{H}]}A_{\text{Fe}}(X/\text{H})_{\odot}^{-1}}{(X_{\text{dust}}/\text{H})10^{[\text{Fe}/\text{H}]}A_{\text{Fe}}} . \end{aligned} \quad (\text{C1})$$

Figure 20 shows how η_X varies as a function of F_* for the elements that Vladilo (2002a) chose to work with in his investigation of DLA abundances. It is clear from the figure that these quantities change with F_* , which makes it difficult to arrive at generalized dust correction factors for the DLA abundances using his method.

C.3. Dust Corrections of Prochaska & Wolfe (Prochaska & Wolfe 2002)

In their investigation of the relative amounts of dust as a function of $N(\text{H})$ in the DLA systems that they studied, Prochaska & Wolfe (2002) defined two dust parameters, $\kappa^X \equiv (1 - 10^{[X/\text{Fe}]})10^{[X/\text{H}]}$ for $X = \text{Zn}$ and $X = \text{Si}$, to characterize the dust-to-gas ratios in relation to those in our Galaxy. Figure 21 shows how these two parameters behave as a function of F_* , and these trends allow one to evaluate their findings in the context of the present study.

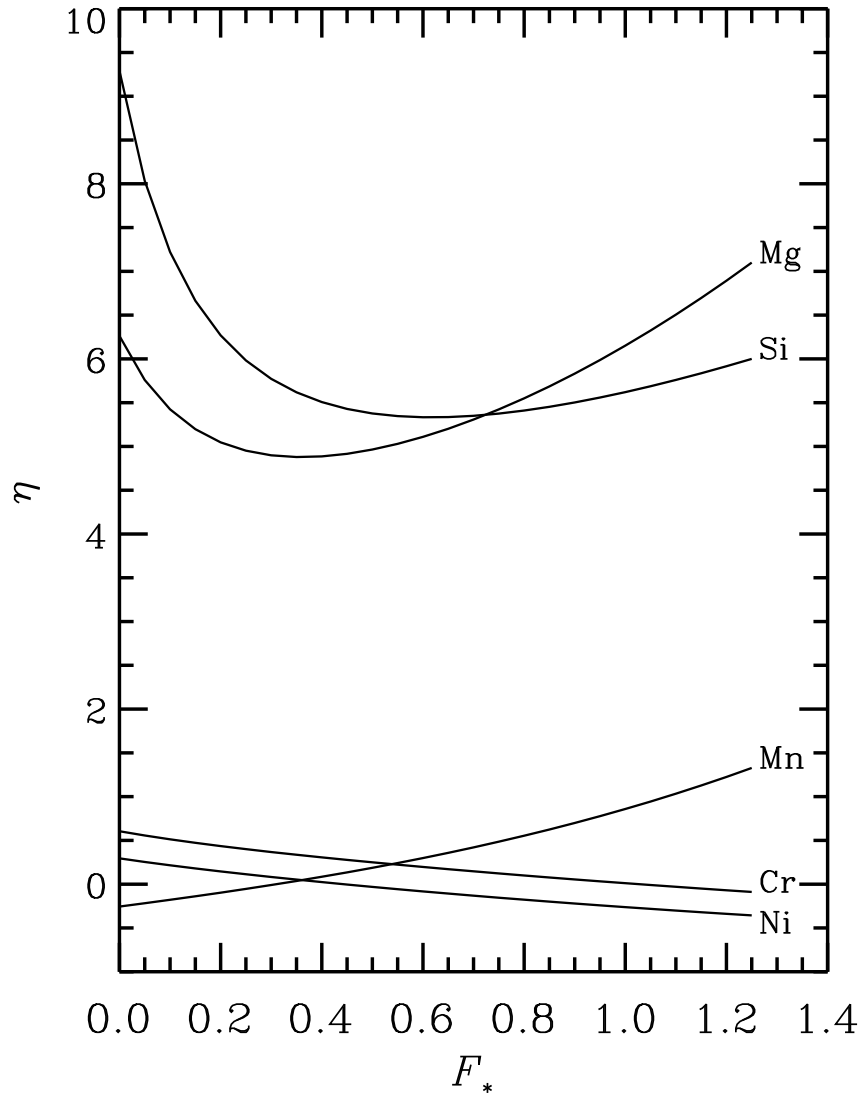


Fig. 20.— Values of the parameter η_X for various elements in the dust correction scheme of Vladilo (2002b), expressed in terms of our parameter F_* . η_{Zn} is off scale in this plot at values of around 20.

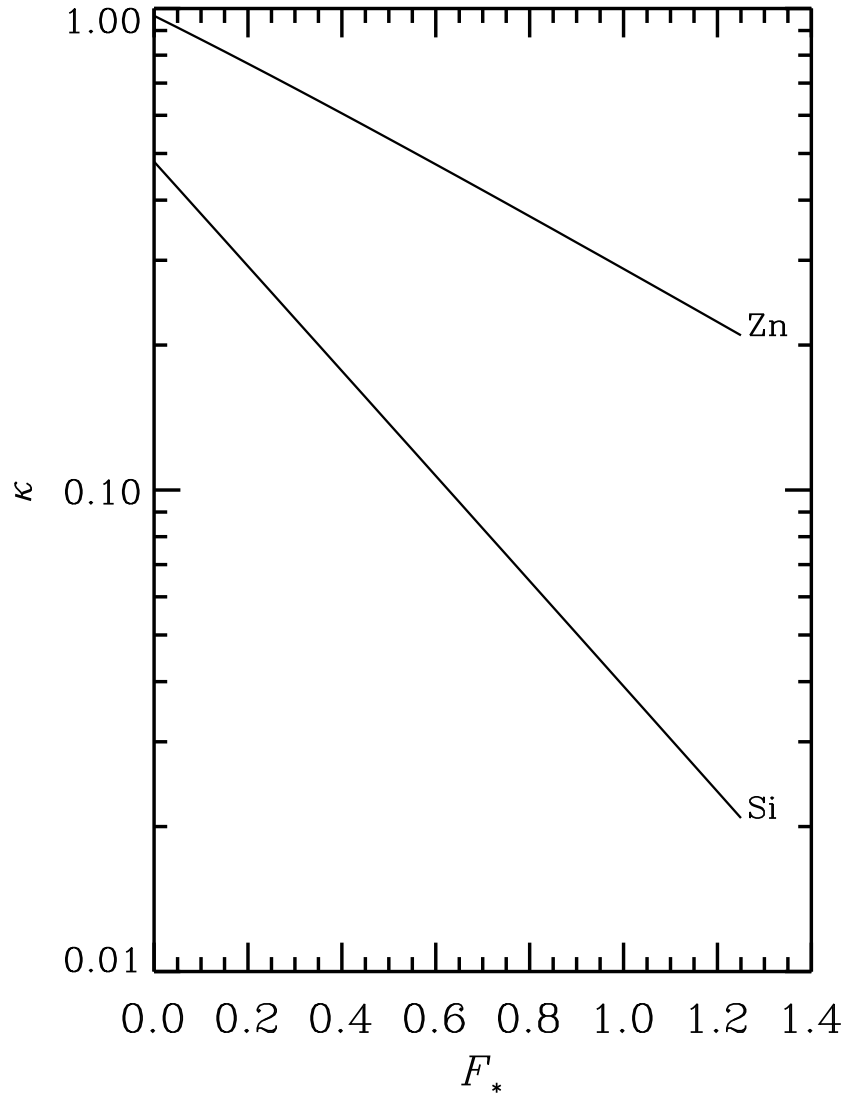


Fig. 21.— Trends with respect to F_* for the parameters κ^{Zn} (upper line) and κ^{Si} (lower line) used by Prochaska & Wolfe (2002) to exemplify the dust-to-gas ratios of different DLAs included in their investigation.

REFERENCES

- Abt, H. A. 1981, *ApJS*, 45, 437
- Adams, W. S. 1949, *ApJ*, 109, 354
- Afflerbach, A., Churchwell, E., & Werner, M. W. 1997, *ApJ*, 478, 190
- Albert, C. E., Blades, J. C., Morton, D. C., Lockman, F. J., Proulx, M., & Ferrarese, L. 1993, *ApJS*, 88, 81
- Allen, M. M., Jenkins, E. B., & Snow, T. P. 1992, *ApJS*, 83, 261
- Allende Prieto, C. 2008, in 14th Cambridge Workshop on Cool Stars, Stellar Systems, and the Sun, ed. G. T. van Belle (San Francisco: Astr. Soc. Pacific), p. 39
- Allende Prieto, C., Lambert, D. L., & Asplund, M. 2002, *ApJ*, 573, L137
- Aloisi, A., Savaglio, S., Heckman, T. M., Hoopes, C. G., Leitherer, C., & Sembach, K. R. 2003, *ApJ*, 595, 760
- Andersen, J., Clausen, J. V., Nordstrom, B., & Popper, D. M. 1985, *A&A*, 151, 329
- André, M., Oliveira, C., Howk, J. C., Ferlet, R., Désert, J. M., Hébrard, G., Lacour, S., Lecavelier des Étangs, A., Vidal-Madjar, A., & Moos, H. W. 2003, *ApJ*, 591, 1000
- Antia, H. M., & Basu, S. 2005, *ApJ*, 620, L129
- . 2006, *ApJ*, 644, 1292
- Asplund, M., Grevesse, N., Sauval, A. J., Allende Prieto, C., & Blomme, R. 2005, *A&A*, 431, 693
- Asplund, M., Grevesse, N., Sauval, A. J., Allende Prieto, C., & Kiselman, D. 2004b, *A&A*, 417, 751
- Badnell, N. R., Bautista, M. A., Butler, K., Delahaye, F., Mendoza, C., Palmeri, P., Zeippen, C. J., & Seaton, M. J. 2005, *MNRAS*, 360, 458
- Bahcall, J. N., Basu, S., Pinsonneault, M., & Serenelli, A. M. 2005a, *ApJ*, 618, 1049
- Bahcall, J. N., Serenelli, A. M., & Basu, S. 2005b, *ApJ*, 621, L85
- Barker, E. S., Lugger, P. M., Weiler, E. J., & York, D. G. 1984, *ApJ*, 280, 600
- Berghöfer, T. W., & Breitschwerdt, D. 2002, *A&A*, 390, 299
- Bertiau, F. C. 1958, *ApJ*, 128, 533
- Bidelman, W. P. 1954, *PASP*, 66, 249
- Boesgaard, A. M. 1985, *PASP*, 97, 37
- Bohlin, R. C., Savage, B. D., & Drake, J. F. 1978, *ApJ*, 224, 132
- Bohlin, R. C., Hill, J. K., Jenkins, E. B., Savage, B. D., Snow, T. P., Spitzer, L., & York, D. G. 1983, *ApJS*, 51, 277
- Bowen, D. V., Jenkins, E. B., Pettini, M., & Tripp, T. M. 2005, *ApJ*, 635, 880

- Bowen, D. V., Jenkins, E. B., Tripp, T. M., Sembach, K. R., Savage, B. D., Moos, H. W., Oegerle, W. R., Friedman, S. D., Gry, C., Kruk, J. W., Murphy, E., Sankrit, R., Shull, J. M., Sonneborn, G., & York, D. G. 2008, *ApJS*, 176, 59
- Breitschwerdt, D., & de Avillez, M. A. 2006, *A&A*, 452, L1
- Breitschwerdt, D., Egger, R., Freyberg, M. J., Frisch, P. C., & Vallergera, J. V. 1996, *Space Sci. Rev.*, 78, 183
- Burgh, E. B., France, K., & McCandliss, S. R. 2007, *ApJ*, 658, 446
- Caffau, E., Maiorca, E., Bonifacio, P., Faraggiana, R., Steffen, M., Ludwig, H.-G., Kamp, I., & Busso, M. 2009, 0903.3406,
- Calura, F., Matteucci, F., & Vladilo, G. 2003, *MNRAS*, 340, 59
- Calura, F., Pipino, A., & Matteucci, F. 2008, *A&A*, 479, 669
- Calura, F., Dessauges-Zavadsky, M., Prochaska, J. X., & Matteucci, F. 2009, *ApJ*, 693, 1236
- Cannon, J. M., Skillman, E. D., Sembach, K. R., & Bomans, D. J. 2005, *ApJ*, 618, 247
- Cardelli, J. A. 1994, *Sci*, 265, 209
- Cardelli, J. A., & Meyer, D. M. 1997, *ApJ*, 477, L57
- Cardelli, J. A., Sembach, K. R., & Savage, B. D. 1995, *ApJ*, 440, 241
- Cardelli, J. A., Savage, B. D., Bruhweiler, F. C., Smith, A. M., Ebbets, D. C., Sembach, K. R., & Sofia, U. J. 1991, *ApJ*, 377, L57
- Cardelli, J. A., Mathis, J. S., Ebbets, D. C., & Savage, B. D. 1993, *ApJ*, 402, L17
- Cardelli, J. A., Sofia, U. J., Savage, B. D., Keenan, F. P., & Dufton, P. L. 1994, *ApJ*, 420, L29
- Cardelli, J. A., Meyer, D. M., Jura, M., & Savage, B. D. 1996, *ApJ*, 467, 334
- Cartledge, S. I. B., Meyer, D. M., & Lauroesch, J. T. 2003, *ApJ*, 597, 408
- Cartledge, S. I. B., Meyer, D. M., Lauroesch, J. T., & Sofia, U. J. 2001, *ApJ*, 562, 394
- Cartledge, S. I. B., Lauroesch, J. T., Meyer, D. M., & Sofia, U. J. 2004, *ApJ*, 613, 1037
- 2006, *ApJ*, 641, 327
- Cartledge, S. I. B., Lauroesch, J. T., Meyer, D. M., Sofia, U. J., & Clayton, G. C. 2008, *ApJ*, 687, 1043
- Cassinelli, J. P., Cohen, D. H., MacFarlane, J. J., Drew, J. E., Lynas-Gray, A. E., Hoare, M. G., Vallergera, J. V., Welsh, B. Y., Vedder, P. W., Hubeny, I., & Lanz, T. 1995, *ApJ*, 438, 932
- Cassinelli, J. P., Cohen, D. H., MacFarlane, J. J., Drew, J. E., Lynas-Gray, A. E., Hubeny, I., Vallergera, J. V., Welsh, B. Y., & Hoare, M. G. 1996, *ApJ*, 460, 949
- Centeno, R., & Socas-Navarro, H. 2008, *ApJ*, 682, L61
- Centurión, M., Molaro, P., Vladilo, G., Péroux, C., Levshakov, S. A., & D’Odorico, V. 2003, *A&A*, 403, 55

- Chamblaud, G., Launay, J. M., Levy, B., Millie, P., Roueff, E., & Tran Minh, F. 1980, *J. Phys. B*, 13, 4205
- Collins, J. A., Shull, J. M., & Giroux, M. L. 2003, *ApJ*, 585, 336
- Costantini, E., Freyberg, M. J., & Predehl, P. 2005, *A&A*, 444, 187
- Cox, D. P., & Reynolds, R. J. 1987, *ARA&A*, 25, 303
- Crinklaw, G., Federman, S. R., & Joseph, C. L. 1994, *ApJ*, 424, 748
- Cunningham, N. J., McCray, R., & Snow, T. P. 2004, *ApJ*, 611, 353
- Dafon, S., Cunha, K., Smith, V. V., & Butler, K. 2003, *A&A*, 399, 525
- de Boer, K. S., Lenhart, H., Van Der Hucht, K. A., Kamperman, T. M., Kondo, Y., & Bruhweiler, F. C. 1986, *A&A*, 157, 119
- Deharveng, L., Peña, M., Caplan, J., & Costero, R. 2000, *MNRAS*, 311, 329
- Dessauges-Zavadsky, M., Prochaska, J. X., & D’Odorico, S. 2002, *A&A*, 391, 801
- Dessauges-Zavadsky, M., Calura, F., Prochaska, J. X., D’Odorico, S., & Matteucci, F. 2004, *A&A*, 416, 79
- Dessauges-Zavadsky, M., Prochaska, J. X., D’Odorico, S., Calura, F., & Matteucci, F. 2006, *A&A*, 445, 93
- Dessauges-Zavadsky, M., Calura, F., Prochaska, J. X., D’Odorico, S., & Matteucci, F. 2007, *A&A*, 470, 431
- Diplas, A., & Savage, B. D. 1994, *ApJS*, 93, 211
- Draine, B. T. 2003a, *ARA&A*, 41, 241
- 2003b, *ApJ*, 598, 1017
- 2003c, *ApJ*, 598, 1026
- 2004, in *Origin and Evolution of the Elements*, ed. A. Mc William & M. Rauch (Cambridge: Cambridge Univ. Press), p. 317
- 2009, in *Cosmic Dust, Near and Far*, ed. T. Henning, E. Grün & J. Steinacker (San Francisco: Ast. Soc. Pacific), in press (also arXiv 0903.1658)
- Draine, B. T., & Tan, J. C. 2003, *ApJ*, 594, 347
- Dufton, P. L., Smartt, S. J., Lee, J. K., Ryans, R. S. I., Hunter, L., Evans, C. J., Herrero, A., Trundle, C., Lennon, D. J., Irwin, M. J., & Dauber, A. 2006, *A&A*, 457, 265
- Dunham, T. 1939, *proc am phil soc*, 81, 277
- Dupin, O., & Gry, C. 1998, *A&A*, 335, 661
- Dwek, E. 1997, *ApJ*, 484, 779
- 1998, *ApJ*, 501, 643

- Dwek, E., & Scalo, J. M. 1980, *ApJ*, 239, 193
- Dwek, E., Zubko, V., Arendt, R. G., & Smith, R. K. 2004, in *Astrophysics of Dust*, ed. A. N. Witt, G. C. Clayton & B. T. Draine (San Francisco: Astr. Soc. Pacific), p. 499
- Eiroa, C., & Hodapp, K.-W. 1989, *A&A*, 210, 345
- Ellison, S. L., Prochaska, J. X., & Lopez, S. 2007, *MNRAS*, 380, 1245
- Feast, M. W. 1958, *MNRAS*, 118, 618
- Feast, M. W., Thackeray, A. D., & Wesselink, A. J. 1955, *MmRAS*, 67, 51
- Federman, S. R., Brown, M., Torok, S., Cheng, S., Irving, R. E., Schectman, R. M., & Curtis, L. J. 2007, *ApJ*, 660, 919
- Ferlet, R. 1999, *A&A Rev.*, 9, 153
- Field, G. B. 1974, *ApJ*, 187, 453
- Field, G. B., & Steigman, G. 1971, *ApJ*, 166, 59
- Fitzpatrick, E. L. 1996, *ApJ*, 473, L55
- Fitzpatrick, E. L., & Massa, D. 1990, *ApJS*, 72, 163
- Fitzpatrick, E. L., & Spitzer, L. 1994, *ApJ*, 427, 232
- 1997, *ApJ*, 475, 623
- Friedman, S. D., Howk, J. C., Chayer, P., Tripp, T. M., Hébrard, G., André, M., Oliveira, C., Jenkins, E. B., Moos, H. W., Oegerle, W. R., Sonneborn, G., Lamontagne, R., Sembach, K. R., & Vidal- Madjar, A. 2002, *ApJS*, 140, 37
- Frisch, P. C. 2007, *Space Sci. Rev.*, 130, 355
- Frisch, P. C., Dorschner, J. M., Geiss, J., Greenberg, J. M., Grün, E., Landgraf, M., Hoppe, P., Jones, A. P., Krätschmer, W., Linde, T. J., Morfill, G. E., Reach, W., Slavin, J. D., Svestka, J., Witt, A. N., & Zank, G. P. 1999, *ApJ*, 525, 492
- Fuchs, B., Breitschwerdt, D., de Avillez, M. A., Dettbarn, C., & Flynn, C. 2006, *MNRAS*, 373, 993
- Gail, H.-P., & Sedlmayr, E. 1986, *A&A*, 166, 225
- Garrison, R. F., & Gray, R. O. 1994, *AJ*, 107, 1556
- Garrison, R. F., & Kormendy, J. 1976, *PASP*, 88, 865
- Geary, R. C. 1930, *J. Royal Stat. Soc.*, 93, 442
- Gibson, B. K., Giroux, M. L., Penton, S. V., Stocke, J. T., Shull, J. M., & Tumlinson, J. 2001, *AJ*, 122, 3280
- Gillett, F. C., Jones, T. W., Merrill, K. M., & Stein, W. A. 1975, *A&A*, 45, 77
- Gilmore, G., & Wyse, R. F. G. 1991, *ApJ*, 367, L55
- Giveon, U., Sternberg, A., Lutz, D., Feuchtgruber, H., & Pauldrach, A. W. A. 2002, *ApJ*, 566, 880

- Golay, M., Mandwewala, N., & Bartholdi, P. 1977, *A&A*, 60, 181
- Greenberg, J. M. 1982, in *Comets*, ed. L. L. Wilkening (Tucson: Univ. Arizona Press), p. 131
— 1989, in *Interstellar Dust*, ed. L. J. Allamandola & A. G. G. M. Tielens (Dordrecht: Kluwer),
p. 345
- Grevesse, N., & Sauval, A. J. 1998, *Space Sci. Rev.*, 85, 161
- Gummershach, C. A., Kaufer, A., Schäfer, D. R., Szeifert, T., & Wolf, B. 1998, *A&A*, 338, 881
- Habing, H. 1969, *Bull. Astron. Inst. Netherlands*, 20, 177
- Harris, A. W., Gry, C., & Bromage, G. E. 1984, *ApJ*, 284, 157
- Hauck, B., & Mermilliod, M. 1998, *A&AS*, 129, 431
- Hébrard, G., Lemoine, M., Ferlet, R., & Vidal-Madjar, A. 1997, *A&A*, 324, 1145
- Hébrard, G., Mallouris, C., Ferlet, R., Koester, D., Lemoine, M., Vidal-Madjar, A., & York, D. 1999, *A&A*, 350, 643
- Herbig, G. H. 1968, *ZAp*, 68, 243
- Hill, P. W. 1970, *MNRAS*, 150, 23
- Hiltner, W. A. 1956, *ApJS*, 2, 389
- Hiltner, W. A., Garrison, R. F., & Schild, R. E. 1969, *ApJ*, 157, 313
- Hobbs, L. M., York, D. G., & Oegerle, W. 1982, *ApJ*, 252, L21
- Hobbs, L. M., Welty, D. E., Morton, D. C., Spitzer, L., & York, D. G. 1993, *ApJ*, 411, 750
- Hoffleit, D. 1956, *ApJ*, 124, 61
- Holweger, H. 2001, in *Solar and Galactic Composition, A Joint SOHO/ACE Workshop*, ed. R. F. Wimmer-Schweingruber (New York: AIP), p. 23
- Hoopes, C. G., Sembach, K. R., Hébrard, G., Moos, H. W., & Knauth, D. C. 2003, *ApJ*, 586, 1094
- Howk, J. C., & Savage, B. D. 1999, *ApJ*, 517, 746
- Howk, J. C., Savage, B. D., & Fabian, D. 1999, *ApJ*, 525, 253
- Howk, J. C., & Sembach, K. R. 1999, *ApJ*, 523, L141
- Howk, J. C., Sembach, K. R., & Savage, B. D. 2003, *ApJ*, 586, 249
— 2006, *ApJ*, 637, 333
- Ioppolo, S., Cuppen, H. M., Romanzin, C., van Dishoeck, E. F., & Linnartz, H. 2008, *ApJ*, 686, 1474
- Jaschek, C., & Jaschek, M. 1992, *A&AS*, 95, 535
- Jenkins, E. B. 1970, in *Ultraviolet Stellar Spectra and Related Ground-Based Observations*, ed. L. Houziaux & H. Butler (Dordrecht: Reidel), p. 281
— 1971, *ApJ*, 169, 25

- 1986, *ApJ*, 304, 739
- 1987, in *Interstellar Processes*, ed. D. J. Hollenbach & H. A. Thronson Jr. (Dordrecht: Reidel), p. 533
- 1996, *ApJ*, 471, 292
- 2004, in *Origin and Evolution of the Elements*, ed. A. Mc William & W. Rauch (Cambridge: Cambridge Univ. Press), p. 336
- 2009, *Physica Scripta*, in press.
- Jenkins, E. B., Gry, C., & Dupin, O. 2000, *A&A*, 354, 253
- Jenkins, E. B., & Savage, B. D. 1974, *ApJ*, 187, 243
- Jenkins, E. B., Savage, B. D., & Spitzer, L. 1986, *ApJ*, 301, 355
- Jenkins, E. B., Silk, J., & Wallerstein, G. 1976, *ApJS*, 32, 681
- Jenkins, E. B., & Tripp, T. M. 2006, *ApJ*, 637, 548
- Jenkins, E. B., & Wallerstein, G. 1996, *ApJ*, 462, 758
- Jenkins, E. B., Drake, J. F., Morton, D. C., Rogerson, J. B., Spitzer, L., & York, D. G. 1973, *ApJ*, 181, L122
- Jenkins, E. B., Tripp, T. M., Fitzpatrick, E. L., Lindler, D., Danks, A. C., Beck, T. L., Bowers, C. W., Joseph, C. L., Kaiser, M. E., Kimble, R. A., Kraemer, S. B., Robinson, R. D., Timothy, J. G., Valenti, J. A., & Woodgate, B. E. 1998, *ApJ*, 492, L147
- Jenkins, E. B., Tripp, T. M., Wozniak, P. R., Sofia, U. J., & Sonneborn, G. 1999, *ApJ*, 520, 182
- Jensen, A. G., Rachford, B. L., & Snow, T. P. 2005, *ApJ*, 619, 891
- 2007, *ApJ*, 654, 955
- Jensen, A. G., & Snow, T. P. 2007a, *ApJ*, 669, 378
- 2007b, *ApJ*, 669, 401
- Jensen, K. S. 1981, *A&AS*, 45, 455
- Johnson, H. L., & Morgan, W. W. 1953, *ApJ*, 117, 313
- Johnson, H. L., Mitchell, R. I., Iriarte, B., & Wisniewski, W. Z. 1966, *Comm. Lunar and Planetary Lab.*, 4, 99
- Jones, A. P., Duley, W. W., & Williams, D. A. 1990, *QJRAS*, 31, 567
- Joseph, C. L. 1988, *ApJ*, 335, 157
- Joseph, C. L., & Jenkins, E. B. 1991, *ApJ*, 368, 201
- Juett, A. M., Schulz, N. S., & Chakrabarty, D. 2004, *ApJ*, 612, 308
- Jura, M. 1974, *ApJ*, 190, L33
- Jura, M., & York, D. G. 1978, *ApJ*, 219, 861

- Kaltcheva, N., & Knude, J. 2002, *A&A*, 385, 1107
- Khare, P., Kulkarni, V. P., Lauroesch, J. T., York, D. G., Crotts, A. P. S., & Nakamura, O. 2004, *ApJ*, 616, 86
- Kilkenny, D., & Muller, S. 1989, *South African. Astr. Obs. Circ*, 13, 69
- Kim, S. H., & Martin, P. G. 1996, *ApJ*, 462, 296
- Kimura, H., Mann, I., & Jessberger, E. K. 2003, *ApJ*, 582, 846
- Knauth, D. C., Meyer, D. M., & Lauroesch, J. T. 2006, *ApJ*, 647, L115
- Knauth, D., Andersson, B.-G., McCandliss, S., & Moos, H. W. 2003, *ApJ*, 596, L51
- Knauth, D. C., Andersson, B.-G., McCandliss, S. R., & Moos, H. W. 2004, *Nature*, 429, 636
- 2006, in *Astrophysics in the Far Ultraviolet, Five Years of Discovery with FUSE*, ed. G. Sonneborn, H. W. Moos & B.-G. Andersson (San Francisco: *Ast. Soc. Pacific*), p. 421
- Kohoutek, L., & Wehmeyer, R. 1999, *A&AS*, 134, 255
- Kozasa, T., Nozawa, T., Tominaga, N., Umeda, H., Maeda, K., & Nomoto, K. 2009, arXiv 0903.0217
- Krüger, H. et al. 2006, *Planet. Space Sci.*, 54, 932
- Kruk, J. W., Howk, J. C., André, M., Moos, H. W., Oegerle, W. R., Oliveira, C., Sembach, K. R., Chayer, P., Linsky, J. L., Wood, B. E., Ferlet, R., Hébrard, G., Lemoine, M., Vidal-Madjar, A., & Sonneborn, G. 2002, *ApJS*, 140, 19
- Kulkarni, V. P., Fall, S. M., Lauroesch, J. T., York, D. G., Welty, D. E., Khare, P., & Truran, J. W. 2005, *ApJ*, 618, 68
- Lallement, R., Hébrard, G., & Welsh, B. Y. 2008, *A&A*, 481, 381
- Lallement, R., Welsh, B. Y., Vergely, J. L., Crifo, F., & Sfeir, D. 2003, *A&A*, 411, 447
- Landgraf, M., Baggaley, W. J., Grün, E., Krüger, H., & Linkert, G. 2000, *J. Geophys. Res.*, 105, 10343
- Laurent, C., Vidal-Madjar, A., & York, D. G. 1979, *ApJ*, 229, 923
- Lebouteiller, V., Kuassivi, & Ferlet, R. 2005, *A&A*, 443, 509
- Ledoux, C., Bergeron, J., & Petitjean, P. 2002, *A&A*, 385, 802
- Lehner, N., Jenkins, E. B., Gry, C., Moos, H. W., Chayer, P., & Lacour, S. 2003, *ApJ*, 595, 858
- Lesh, J. R. 1968, *ApJS*, 17, 371
- Levato, H. 1972, *PASP*, 84, 584
- Levato, H., & Abt, H. A. 1976, *PASP*, 88, 712
- Li, A. 2005, *ApJ*, 622, 965
- Ling, Z., Zhang, S. N., Xiang, J., & Tang, S. 2009, *ApJ*, 690, 224

- Linsky, J. L., Diplas, A., Wood, B. E., Brown, A., Ayres, T. R., & Savage, B. D. 1995, *ApJ*, 451, 335
- Lipman, K., & Pettini, M. 1995, *ApJ*, 442, 628
- Lodders, K. 2003, *ApJ*, 591, 1220
- Lu, L., Sargent, W. L. W., Barlow, T. A., Churchill, C. W., & Vogt, S. S. 1996, *ApJS*, 107, 475
- Luck, R. E., Kovtyukh, V. V., & Andrievsky, S. M. 2006, *AJ*, 132, 902
- Lugger, P. M., York, D. G., Blanchard, T., & Morton, D. C. 1978, *ApJ*, 224, 1059
- Maíz-Apellániz, J. 2001, *ApJ*, 560, L83
- Mallouris, C. 2003, *ApJS*, 147, 265
- Martin, E. R., & York, D. G. 1982, *ApJ*, 257, 135
- Martín-Hernández, N. L., Peeters, E., Morisset, C., Tielens, A. G. G. M., Cox, P., Roelfsema, P. R., Baluteau, J.-P., Schaerer, D., Mathis, J. S., Damour, F., Churchwell, E., & Kessler, M. F. 2002, *A&A*, 381, 606
- Martins, L. P., & Viegas, S. M. M. 2000, *A&A*, 361, 1121
- Massa, D., Van Steenberg, M. E., Oliverson, N., & Lawton, P. 1998, in *Ultraviolet Astrophysics Beyond the IUE Final Archive*, ed. W. Wamsteker & R. Gonzalez Riestra (Noordwijk: ESA), p. 723
- Mathis, J. S. 1990, *ARA&A*, 28, 37
- 1996, *ApJ*, 472, 643
- Meléndez, J., & Asplund, M. 2008, *A&A*, 490, 817
- Merrill, P. W., Sanford, R. F., Wilson, O. C., & Burwell, C. G. 1937, *ApJ*, 86, 274
- Meyer, D. M., Cardelli, J. A., & Sofia, U. J. 1997, *ApJ*, 490, L103
- Meyer, D. M., Jura, M., & Cardelli, J. A. 1998, *ApJ*, 493, 222
- Meyer, D. M., & Roth, K. C. 1990, *ApJ*, 363, 57
- Meyer, D. M., Jura, M., Hawkins, I., & Cardelli, J. A. 1994, *ApJ*, 437, L59
- Miller, A., Lauroesch, J. T., Sofia, U. J., Cartledge, S. I. B., & Meyer, D. M. 2007, *ApJ*, 659, 441
- Morgan, W. W., Code, A. D., & Whitford, A. E. 1955, *ApJS*, 2, 41
- Morgan, W. W., Hiltner, W. A., & Garrison, R. F. 1971, *AJ*, 76, 242
- Morgan, W. W., & Roman, N. G. 1950, *ApJ*, 112, 362
- Morris, P. M. 1961, *MNRAS*, 122, 325
- Morton, D. C. 1978, *ApJ*, 222, 863
- 1991, *ApJS*, 77, 119
- 2003, *ApJS*, 149, 205

- Morton, D. C., & Dinerstein, H. L. 1976, *ApJ*, 204, 1
- Morton, D. C., Jenkins, E. B., & Bohlin, R. C. 1968, *ApJ*, 154, 661
- Morton, D. C., & Spitzer, L. 1966, *ApJ*, 144, 1
- Morton, D. C., Drake, J. F., Jenkins, E. B., Rogerson, J. B., Spitzer, L., & York, D. G. 1973, *ApJ*, 181, L103
- Münch, G. 1957, *ApJ*, 125, 42
- Münch, G., & Zirin, H. 1961, *ApJ*, 133, 11
- Murphy, E. M., Sembach, K. R., Gibson, B. K., Shull, J. M., Savage, B. D., Roth, K. C., Moos, H. W., Green, J. C., York, D. G., & Wakker, B. P. 2000, *ApJ*, 538, L35
- Nieva, M. F., & Przybilla, N. 2008a, *A&A*, 481, 199
- 2008b, *Rev. Mexicana Astron. Astrofis.*, 33, 35
- Oegerle, W. R., & Polidan, R. S. 1984, *ApJ*, 285, 648
- Oliveira, C. M., & Hébrard, G. 2006, *ApJ*, 653, 345
- Oliveira, C. M., Hébrard, G., Howk, J. C., Kruk, J. W., Chayer, P., & Moos, H. W. 2003, *ApJ*, 587, 235
- Paerels, F., Brinkman, A. C., van der Meer, R. L. J., Kaastra, J. S., Kuulkers, E., den Boggende, A. J. F., Predehl, P., Drake, J. J., Kahn, S. M., Savin, D. W., & McLaughlin, B. M. 2001, *ApJ*, 546, 338
- Palumbo, M. E. 2006, *A&A*, 453, 903
- Péroux, C., Kulkarni, V. P., Meiring, J., Ferlet, R., Khare, P., Lauroesch, J. T., Vladilo, G., & York, D. G. 2006a, *A&A*, 450, 53
- Péroux, C., Meirling, J. D., Kulkarni, V. P., Ferlet, R., Khare, P., Lauroesch, J. T., Vladilo, G., & York, D. G. 2006b, *MNRAS*, 372, 369
- Péroux, C., Meiring, J. D., Kulkarni, V. P., Khare, P., Lauroesch, J. T., Vladilo, G., & York, D. G. 2008, *MNRAS*, 386, 2209
- Pettini, M. 2003, in *Cosmochemistry: The Melting Pot of the Elements*, ed. C. Esteban, R. J. Garci, A. H. López & F. Sánchez (Cambridge: Cambridge Univ.), p. 257
- Pettini, M., Boksenberg, A., & Hunstead, R. W. 1990, *ApJ*, 348, 48
- Pettini, M., Smith, L. J., Hunstead, R. W., & King, D. L. 1994, *ApJ*, 426, 79
- Pettini, M., King, D. L., Smith, L. J., & Hunstead, R. W. 1997, *ApJ*, 478, 536
- Pettini, M., Ellison, S. L., Steidel, C. C., & Bowen, D. V. 1999, *ApJ*, 510, 576
- Pettini, M., Ellison, S. L., Bergeron, J., & Petitjean, P. 2002, *A&A*, 391, 21
- Popper, D. M. 1943, *ApJ*, 97, 394

- Press, W. H., Teukolsky, S. A., Vetterling, W. T., & Flannery, B. P. 2007, *Numerical Recipes, The Art of Scientific Computing*, 3rd ed., (Cambridge: Cambridge Univ. Press)
- Prochaska, J. X. 2003, *ApJ*, 582, 49
- 2004, in *Origin and Evolution of the Elements*, ed. A. McWilliam & M. Rauch (Cambridge: Cambridge Univ. Press), p. 455
- Prochaska, J. X., Howk, J. C., & Wolfe, A. M. 2003, *Nature*, 423, 57
- Prochaska, J. X., Tripp, T. M., & Howk, J. C. 2005, *ApJ*, 620, L39
- Prochaska, J. X., & Wolfe, A. M. 2002, *ApJ*, 566, 68
- Prochaska, J. X., Howk, J. C., O’Meara, J. M., Tytler, D., Wolfe, A. M., Kirkman, D., Lubin, D., & Suzuki, N. 2002, *ApJ*, 571, 693
- Prochaska, J. X., Chen, H.-W., Desauges-Zavadsky, M., & Bloom, J. S. 2007, *ApJ*, 666, 267
- Przybilla, N., Nieva, M.-F., & Butler, K. 2008, *ApJ*, 688, L103
- Quast, R., Reimers, D., & Baade, R. 2008, *A&A*, 477, 443
- Rachford, B., Snow, T. P., Tumlinson, J., Shull, J. M., Blair, W. P., Ferlet, R., Friedman, S. D., Gry, C., Jenkins, E. B., Morton, D. C., Savage, B. D., Sonnentrucker, P., Vidal-Madjar, A., Welty, D. E., & York, D. G. 2002, *ApJ*, 577, 221
- Rachford, B. L., Snow, T. P., Tumlinson, J., Shull, J. M., Roueff, E., Andre, M., Desert, J.-M., Ferlet, R., Vidal-Madjar, A., & York, D. G. 2001, *ApJ*, 555, 839
- Rachford, B. L., Snow, T. P., Destree, J. D., Ross, T. L., Ferlet, R., Friedman, S. D., Gry, C., Jenkins, E. B., Morton, D. C., Savage, B. D., Shull, J. M., Sonnentrucker, P., Tumlinson, J., Vidal-Madjar, A., Welty, D. E., & York, D. G. 2009, *ApJS*, 180, 125
- Redfield, S., & Linsky, J. L. 2004a, *ApJ*, 602, 776
- 2004b, *ApJ*, 613, 1004
- Richter, P., Sembach, K. R., Wakker, B. P., Savage, B. D., Tripp, T. M., Murphy, E. M., Kalberla, P. M. W., & Jenkins, E. B. 2001, *ApJ*, 559, 318
- Rogerson, J. B., Spitzer, L., Drake, J. F., Dressler, K., Jenkins, E. B., Morton, D. C., & York, D. G. 1973a, *ApJ*, 181, L97
- Rogerson, J. B., York, D. G., Drake, J. F., Jenkins, E. B., Morton, D. C., & Spitzer, L. 1973b, *ApJ*, 181, L110
- Rolleston, W. R. J., Smartt, S. J., Dufton, P. L., & Ryans, R. S. I. 2000, *A&A*, 363, 537
- Roth, K. C., & Blades, J. C. 1995, *ApJ*, 445, L95
- 1997, *ApJ*, 474, L95
- Routly, P. M., & Spitzer, L. 1952, *ApJ*, 115, 227
- Ryu, K. S., Dixon, W. V., Hurwitz, M., Seon, K. I., Min, K. W., & Edelstein, J. 2000, *ApJ*, 529, 251

- Sahu, M. S., & Blades, J. C. 1997, *ApJ*, 484, L125
- Sarlin, S. P. 1998, Ph.D. Thesis, University of Colorado, Boulder.
- Savage, B. D., & Bohlin, R. C. 1979, *ApJ*, 229, 136
- Savage, B. D., Cardelli, J. A., & Sofia, U. J. 1992, *ApJ*, 401, 706
- Savage, B. D., & Jenkins, E. B. 1972, *ApJ*, 172, 491
- Savage, B. D., & Lehner, N. 2006, *ApJS*, 162, 134
- Savage, B. D., Massa, D., & Meade, M. 1985, *ApJS*, 59, 397
- Savage, B. D., Meade, M. R., & Sembach, K. R. 2001, *ApJS*, 136, 631
- Savage, B. D., & Panek, R. J. 1974, *ApJ*, 191, 659
- Savage, B. D., & Sembach, K. R. 1991, *ApJ*, 379, 245
- 1996a, *ARA&A*, 34, 279
- 1996b, *ApJ*, 470, 893
- Savage, B. D., Bohlin, R. C., Drake, J. F., & Budich, W. 1977, *ApJ*, 216, 291
- Schrijver, H. 1997, *The Hipparcos and Tycho Catalogues*, (ESA Publications, SP-1200), (Noordwijk: European Space Agency)
- Schulz, N. S., Cui, W., Canizares, C. R., Marshall, H. L., Lee, J. C., Miller, J. M., & Lewin, W. H. G. 2002, *ApJ*, 565, 1141
- Sembach, K. R., & Savage, B. D. 1996, *ApJ*, 457, 211
- Sembach, K. R., Savage, B. D., & Tripp, T. M. 1997, *ApJ*, 480, 216
- Shaver, P. A., McGee, R. X., Newton, L. M., Danks, A. C., & Pottasch, S. R. 1983, *MNRAS*, 204, 53
- Sheffer, Y., Rogers, M., Federman, S. R., Lambert, D. L., & Gredel, R. 2007, *ApJ*, 667, 1002
- Sheffer, Y., Rogers, M., Federman, S. R., Abel, N. P., Gredel, R., Lambert, D. L., & Shaw, G. 2008, *ApJ*, 687, 1075
- Shull, J. M., & McKee, C. F. 1979, *ApJ*, 227, 131
- Shull, J. M., & Van Steenberg, M. E. 1985, *ApJ*, 294, 599
- Shull, J. M., & York, D. G. 1977, *ApJ*, 211, 803
- Simonson, S. C. 1968, *ApJ*, 154, 923
- Slettebak, A. 1982, *ApJS*, 50, 55
- Smith, R. G., Sellgren, K., & Brooke, T. Y. 1993, *MNRAS*, 263, 749
- Smith, R. K. 2008, *ApJ*, 681, 343
- Smith, R. K., & Dwek, E. 1998, *ApJ*, 503, 831

- Smith, R. K., Dame, T. M., Costantini, E., & Predehl, P. 2006, *ApJ*, 648, 452
- Snow, T. P. 1976, *ApJ*, 204, 759
- 1977, *ApJ*, 216, 724
- Snow, T. P., Peters, G. J., & Mathieu, R. D. 1979, *ApJS*, 39, 359
- Snow, T. P., Rachford, B. L., & Figoski, L. 2002, *ApJ*, 573, 662
- Snow, T. P., & Witt, A. N. 1996, *ApJ*, 468, L65
- Snow, T. P., Black, J. H., van Dishoeck, E. F., Burks, G., Crutcher, R. M., Lutz, B. L., Hanson, M. M., & Shuping, R. Y. 1996, *ApJ*, 465, 245
- Snow, T. P., Rachford, B. L., Tumlinson, J., Shull, J. M., Welty, D. E., Blair, W. P., Ferlet, R., Friedman, S. D., Gry, C., Jenkins, E. B., Lecavelier, A., Lemoine, M., Morton, D. C., Savage, B. D., Sembach, K. R., Vidal-Madjar, A., York, D. G., Andersson, B.-G., Feldman, P. D., & Moos, H. W. 2000, *ApJ*, 538, L65
- Socas-Navarro, H., & Norton, A. A. 2007, *ApJ*, 660, L153
- Socrates, A., & Draine, B. T. 2008, arXiv, 0812.3913,
- Sofia, U. J., Cardelli, J. A., & Savage, B. D. 1994, *ApJ*, 430, 650
- Sofia, U. J., Fitzpatrick, E. L., & Meyer, D. M. 1998, *ApJ*, 504, L47
- Sofia, U. J., & Jenkins, E. B. 1998, *ApJ*, 499, 951
- Sofia, U. J., & Meyer, D. M. 2001, *ApJ*, 554, L221
- Sofia, U. J., & Parvathi, V. S. 2009, in *Cosmic Dust - Near and Far*, ed. T. Henning, E. Grün & J. Steinacker (San Francisco: Ast. Soc. Pacific), in press.
- Sofia, U. J., Cardelli, J. A., Guerin, K. P., & Meyer, D. M. 1997, *ApJ*, 482, L105
- Sofia, U. J., Lauroesch, J. T., Meyer, D. M., & Cartledge, S. I. B. 2004, *ApJ*, 605, 272
- Sofia, U. J., Gordon, K. D., Clayton, G. C., Misselt, K., Wolff, M. J., Cox, N. L. J., & Ehrenfreund, P. 2006, *ApJ*, 636, 753
- Sonneborn, G., Tripp, T. M., Ferlet, R., Jenkins, E. B., Sofia, U. J., Vidal-Madjar, A., & Wozniak, P. R. 2000, *ApJ*, 545, 277
- Sonnentrucker, P., Friedman, S. D., Welty, D. E., York, D. G., & Snow, T. P. 2003, *ApJ*, 596, 350
- Spitzer, L. 1985, *ApJ*, 290, L21
- Spitzer, L., Cochran, W. D., & Hirshfeld, A. 1974, *ApJS*, 28, 373
- Spitzer, L., & Field, G. B. 1955, *ApJ*, 121, 300
- Spitzer, L., & Fitzpatrick, E. L. 1993, *ApJ*, 409, 299
- 1995, *ApJ*, 445, 196
- Spitzer, L., & Jenkins, E. B. 1975, *ARA&A*, 13, 133

- Spitzer, L., Drake, J. F., Jenkins, E. B., Morton, D. C., Rogerson, J. B., & York, D. G. 1973, *ApJ*, 181, L116
- Stancil, P. C., Schultz, D. R., Kimura, M., Gu, J.-P., Hirsch, G., & Buenker, R. J. 1999, *A&AS*, 140, 225
- Stokes, G. M. 1978, *ApJS*, 36, 115
- Strassmeier, K. G., & Fekel, F. C. 1990, *A&A*, 230, 389
- Strömgren, B. 1948, *ApJ*, 108, 242
- Sudzius, J., & Bobinas, V. 1992, *Bull. Vilnius Astr. Obs.*, 86, 59
- Takei, Y., Fujimoto, R., Mitsuda, K., & Onaka, T. 2002, *ApJ*, 581, 307
- Thackeray, A. D. 1971, *MNRAS*, 154, 103
- Tielens, A. G. G. M. 1998, *ApJ*, 499, 267
- Tobin, W. 1985, *A&A*, 142, 189
- Tobin, W., & Kaufmann, J. P. 1984, *MNRAS*, 207, 369
- Tobin, W., Viton, M., & Sivan, J.-P. 1994, *A&AS*, 107, 385
- Tripp, T. M., Wakker, B. P., Jenkins, E. B., Bowers, C. W., Danks, A. C., Green, R. F., Heap, S. R., Joseph, C. L., Kaiser, M. E., Linsky, J. L., & Woodgate, B. E. 2003, *AJ*, 125, 3122
- Ueda, Y., Mitsuda, K., Murakami, H., & Matsushita, K. 2005, *ApJ*, 620, 274
- Vallerga, J. 1996, *Space Sci. Rev.*, 78, 277
- van Dishoeck, E. F. 1998, *Faraday Disc.*, 109, 31
- 2004, *ARA&A*, 42, 119
- van Leeuwen, F. 2007, *A&A*, 474, 653
- Van Steenberg, M. E., & Shull, J. M. 1988, *ApJS*, 67, 225
- Venn, K. A., Krwin, M., Shetrone, M. D., Tout, C. A., Hill, V., & Tolstoy, E. 2004, *AJ*, 128, 1177
- Vidal-Madjar, A., & Ferlet, R. 2002, *ApJ*, 571, L169
- Vidal-Madjar, A., Ferlet, R., Laurent, C., & York, D. G. 1982, *ApJ*, 260, 128
- Vladilo, G. 2002a, *A&A*, 391, 407
- 2002b, *ApJ*, 569, 295
- 2004, *A&A*, 421, 479
- Vladilo, G., Centurión, M., Levshakov, S. A., Péroux, C., Khare, P., Kulkarni, V. P., & York, D. G. 2006, *A&A*, 454, 151
- Vladilo, J. 2008, in *Pathways through an Exlectic Universe*, ed. J. H. Knapen, T. J. Mahoney, and A. Vazdakis, (San Francisco: Ast. Soc. Pacific), p. 562
- Wakker, B. P. 2001, *ApJS*, 136, 463

- Wakker, B. P., & Mathis, J. S. 2000, *ApJ*, 544, L107
- Wakker, B. P., Howk, J. C., Savage, B. D., van Woerden, H., Tufte, S. L., Schwarz, U. J., Benjamin, R., Reynolds, R. J., Peletier, R. F., & Kalberla, P. M. W. 1999, *Nature*, 402, 388
- Walborn, N. R. 1971, *ApJS*, 23, 257
- 1972, *AJ*, 77, 312
- Wallerstein, G., & Gilroy, K. K. 1992, *AJ*, 103, 1346
- Wallerstein, G., & Goldsmith, D. 1974, *ApJ*, 187, 237
- Wegner, W. 1994, *MNRAS*, 270, 229
- Welsh, B. Y., Sasseen, T., Craig, N., Jelinsky, S., & Albert, C. E. 1997, *ApJS*, 112, 507
- Welty, D. E., Lauroesch, J. T., Blades, J. C., Hobbs, L. M., & York, D. G. 1997, *ApJ*, 489, 672
- Welty, D. E., Hobbs, L. M., Lauroesch, J. T., Morton, D. C., Spitzer, L., & York, D. G. 1999, *ApJS*, 124, 465
- Welty, D. E., Lauroesch, J. T., Blades, J. C., Hobbs, L. M., & York, D. G. 2001, *ApJ*, 554, L75
- Whittet, D. C. B., Bode, M. F., Longmore, A. J., Adamson, A. J., McFadzean, A. D., Aitken, D. K., & Roche, P. F. 1988, *MNRAS*, 233, 321
- Whittet, D. C. B., Boogert, A. C. A., Gerakines, P. A., Schutte, W., Tielens, A. G. G. M., de Graauw, T., Prusti, T., van Dishoeck, E. F., Wesselius, P. R., & Wright, C. M. 1997, *ApJ*, 490, 729
- Witt, A. N., Smith, R. K., & Dwek, E. 2001, *ApJ*, 550, L201
- Wolfe, A. M., Gawiser, E., & Prochaska, J. X. 2005, *ARA&A*, 43, 861
- Wolff, B., Koester, D., & Lallement, R. 1999, *A&A*, 346, 969
- Wood, B. E., & Linsky, J. L. 1997, *ApJ*, 474, L39
- Wood, B. E., Redfield, S., Linsky, J. L., & Sahu, M. S. 2002, *ApJ*, 581, 1169
- Xiang, J., Zhang, S. N., & Yao, Y. 2005, *ApJ*, 628, 769
- Yao, Y., & Wang, Q. D. 2006, *ApJ*, 641, 930
- Yao, Y., Schulz, N. S., Gu, M. F., Nowak, M. A., & Canizares, C. R. 2009, arXiv 0902.2778
- York, D. G. 1976, *ApJ*, 204, 750
- 1983, *ApJ*, 264, 172
- York, D. G., & Kinahan, B. F. 1979, *ApJ*, 228, 127
- York, D. G., & Rogerson, J. B. 1976, *ApJ*, 203, 378
- York, D. G., Spitzer, L., Bohlin, R. C., Hill, J., Jenkins, E. B., Savage, B. D., & Snow, T. P. 1983, *ApJ*, 266, L55

Table 7. Observations and Fits for Carbon

HD Number ^a	Name	Observed $\log N(\text{C II})$				F_*	$[\text{C}_{\text{gas}}/\text{H}]_{\text{fit}}^{\text{c}}$	Residual ^d	Deviation ^e (in σ)
		l.l.	best	u.l.	Source ^b				
(1)	(2)	(3)	(4)	(5)	(6)	(7)	(8)	(9)	(10)
24398	ζ Per	17.26	17.34	17.41	CMJS96	0.88 ± 0.05	-0.201 ± 0.049	-0.111	-0.79
24534	X Per	17.35	17.51	17.62	SFM98	0.90 ± 0.06	-0.203 ± 0.050	-0.085	-0.58
24912	ξ Per	17.64	17.78	17.89	C++91	0.83 ± 0.02	-0.196 ± 0.046	0.225	1.47
27778	62 Tau	17.34	SLMC04
34029	α Aur	14.65	14.80	14.95	WRLS02	0.44 ± 0.05	-0.157 ± 0.095	0.257	1.27
35149	23 Ori	16.90	16.98	17.04	W++99	0.54 ± 0.04	-0.167 ± 0.076	0.055	0.32
36861	λ Ori A	16.79	17.00	17.14	CMJS96	0.57 ± 0.04	-0.169 ± 0.071	-0.085	-0.39
37021	θ^1 Ori	17.64	17.82	17.94	SLMC04
37061	ν Ori	18.07	18.13	18.17	SLMC04
38771	κ Ori	16.89	CMJS96	0.67 ± 0.03	-0.180 ± 0.055
57061	τ CMa	16.78	16.96	17.08	SCGM97	0.39 ± 0.04	-0.151 ± 0.106	-0.045	-0.24
143275	δ Sco	17.14	17.42	17.62	HYO82	0.90 ± 0.03	-0.203 ± 0.050	-0.006	-0.02
144217	β^1 Sco	17.27	17.37	17.45	CMJS96	0.81 ± 0.02	-0.194 ± 0.045	-0.027	-0.25
147888	ρ Oph D	17.91	18.00	18.07	SLMC04	0.88 ± 0.06	-0.201 ± 0.049	0.003	0.02
149757 (-15)	ζ Oph	17.24	17.36	17.45	CMES93	1.05 ± 0.02	-0.218 ± 0.071	-0.033	-0.24
152590	HD 152590	18.11	18.21	18.29	SLMC04	0.69 ± 0.03	-0.182 ± 0.052	0.464	4.03
154368	V1074 Sco	17.30	17.68	17.88	S++96	0.52 ± 0.07	-0.164 ± 0.080	-0.202	-0.66
207198	HD 207198	17.84	17.98	18.09	SLMC04	0.90 ± 0.03	-0.203 ± 0.050	0.047	0.33

^aTerms in parentheses indicate separate velocity components, if they are explicitly identified and not grouped together; see §4.3

^bCodes in this column are linked to references listed in Table 1

^cThe expected depletion $[\text{C}_{\text{gas}}/\text{H}]$ computed using Eq. 10. The listed errors do not include an overall systematic uncertainty of 0.04 in the solar abundance $\sigma(\text{C}/\text{H})_{\odot}$ in order to show just the formal error that arises from the uncertainties in location of line of best fit and the value of F_* .

^dThe observed $[\text{C}_{\text{gas}}/\text{H}]$ minus that computed using Eq. 10.

^eThe difference shown in the previous column divided by the expected difference due to the uncertainties in both the measured column density and the coefficients that appear in Eq. 10.

Note. — Tables 8 through 23 are published in the electronic edition of the *Astrophysical Journal*. This table illustrates the content and format of these tables.

Table 8. Observations and Fits for Nitrogen

HD Number ^a (1)	Name (2)	Observed $\log N(\text{N I})$				F_* (7)	$[\text{N}_{\text{gas}}/\text{H}]_{\text{fit}}^c$ (8)	Residual ^d (9)	Deviation ^e (in σ) (10)
		l.l. (3)	best (4)	u.l. (5)	Source ^b (6)				
5394	γ Cas	15.96	16.00	16.04	MCS97	0.52 ± 0.04	-0.109 ± 0.017	0.046	0.46
22928	δ Per	15.18	15.30	15.39	MY82
23180	\circ Per	16.87	17.02	17.17	Y++83	0.84 ± 0.06	-0.109 ± 0.029	0.039	0.21
24534	X Per	17.14	17.22	17.30	JRS07	0.90 ± 0.06	-0.109 ± 0.032	0.087	0.94
24760	ϵ Per	16.22	16.28	16.35	MY82	0.68 ± 0.04	-0.109 ± 0.020	-0.007	-0.06
27778	62 Tau	16.95	17.11	17.27	JRS07
34029	α Aur	13.78	13.87	13.96	WRLS02	0.44 ± 0.05	-0.109 ± 0.019	-0.164	-1.24
35149	23 Ori	16.47	16.57	16.65	W++99	0.54 ± 0.04	-0.109 ± 0.017	0.150	0.92
36486	δ Ori A	15.81	15.85	15.89	J++99	0.54 ± 0.02	-0.109 ± 0.017	-0.127	-2.15
36861	λ Ori A	16.63	16.65	16.68	MCS97	0.57 ± 0.04	-0.109 ± 0.017	0.058	0.51
37043	ι Ori	15.86	15.93	15.99	MCS97	0.41 ± 0.03	-0.109 ± 0.020	-0.014	-0.15
37903	HD 37903	16.54	16.89	17.27	JRS07	1.15 ± 0.03	-0.109 ± 0.050	-0.337	-0.90
38771	κ Ori	16.32	16.34	16.37	MCS97	0.67 ± 0.03	-0.109 ± 0.019	0.026	0.48
41161	HD 41161	16.94	17.00	17.06	OH06	0.44 ± 0.04	-0.109 ± 0.019	0.133	1.27
44743	β CMa	14.04	14.06	14.08	JGD00	-0.43 ± 0.03	-0.109 ± 0.080	-0.028	-0.27
48915 (+12)	α CMa	12.92	12.97	13.06	H++99	0.42 ± 0.11	-0.109 ± 0.020	-0.224	-1.05
(+18)		13.05	13.12	13.09	H++99	0.42 ± 0.08	-0.109 ± 0.020	-0.274	-1.79
53975	HD 53975	16.72	16.80	16.88	OH06	0.45 ± 0.03	-0.109 ± 0.019	-0.130	-1.29
66811	ζ Pup	15.80	15.85	15.90	ST++00	0.32 ± 0.02	-0.109 ± 0.025	0.100	1.46
68273	γ^2 Vel	15.55	15.58	15.62	ST++00	0.25 ± 0.02	-0.109 ± 0.029	0.080	1.33
73882	HD 73882	17.25	17.36	17.47	JRS07	0.68 ± 0.07	-0.109 ± 0.020	0.002	0.02
75309	HD 75309	16.74	16.86	16.96	KAMM03	0.63 ± 0.04	-0.109 ± 0.018	-0.111	-0.82
88115	HD 88115	16.50	16.67	16.79	KAMM03	0.35 ± 0.45	-0.109 ± 0.023	-0.118	-0.67
94493	HD 94493	16.69	16.82	16.92	KAMM03	0.29 ± 0.03	-0.109 ± 0.027	-0.143	-1.15
99857	HD 99857	17.13	17.19	17.25	KAMM03	0.54 ± 0.04	-0.109 ± 0.017	0.039	0.46
108248	α^1 Cru	15.39	15.49	15.59	Y++83	0.15 ± 0.05	-0.109 ± 0.036	0.095	0.65
110432	BZ Cru	17.02	17.09	17.15	KAMM03	1.17 ± 0.11	-0.109 ± 0.052	0.098	0.89
116658	α Vir	14.57	14.63	14.67	YK79	0.16 ± 0.05	-0.109 ± 0.035	-0.158	-1.35
118716	ϵ Cen	15.34	15.42	15.59	Y++83	0.15 ± 0.16	-0.109 ± 0.036	0.023	0.06
121263	ζ Cen	15.49	15.64	15.79	Y++83
122451	β Cen	15.04	15.19	15.34	LYBM78	0.23 ± 0.03	-0.109 ± 0.030	-0.145	-0.90
124314	HD 124314	17.23	17.28	17.33	KAMM03	0.59 ± 0.05	-0.109 ± 0.017	-0.023	-0.26
127972	η Cen	16.01	16.08	16.16	Y++83
143275	δ Sco	16.99	17.01	17.03	MCS97	0.90 ± 0.03	-0.109 ± 0.032	0.051	0.54
144217	β^1 Sco	16.97	17.10	17.22	Y++83	0.81 ± 0.02	-0.109 ± 0.027	0.176	1.32
147888	ρ Oph D	16.91	17.38	17.72	JRS07	0.88 ± 0.06	-0.109 ± 0.031	-0.148	-0.34
149757 (-15)	ζ Oph	16.90	16.96	17.01	SCS92	1.05 ± 0.02	-0.109 ± 0.043	0.015	0.17
158926	λ Sco	14.83	14.85	14.87	Y83	0.31 ± 0.02	-0.109 ± 0.025	-0.167	-3.79
160578	κ Sco	15.92	15.99	16.04	MCS97	0.50 ± 0.07	-0.109 ± 0.017	-0.026	-0.16

Table 8—Continued

HD Number ^a	Name	Observed $\log N(\text{N I})$				F_*	$[\text{N}_{\text{gas}}/\text{H}]_{\text{fit}}^{\text{c}}$	Residual ^d	Deviation ^e (in σ)
		l.l.	best	u.l.	Source ^b				
(1)	(2)	(3)	(4)	(5)	(6)	(7)	(8)	(9)	(10)
179406	20 Aql	16.91	17.04	17.13	KAMM03
185418	HD 185418	17.15	17.24	17.33	S++03	0.79 ± 0.03	-0.109 ± 0.025	0.036	0.30
191877	HD 191877	16.70	16.80	16.88	H++03	0.39 ± 0.04	-0.109 ± 0.021	-0.110	-0.88
192639	HD 192639	16.78	17.18	17.66	JRS07	0.64 ± 0.04	-0.109 ± 0.018	-0.091	-0.20
195965	HD 195965	16.73	16.79	16.86	H++03	0.52 ± 0.02	-0.109 ± 0.017	-0.137	-1.94
199579	HD 199579	17.06	17.16	17.26	JRS07	0.76 ± 0.27	-0.109 ± 0.024	0.120	0.97
206267	HD 206267	16.87	17.16	17.43	JRS07	0.87 ± 0.07	-0.109 ± 0.030	-0.168	-0.57
207198	HD 207198	17.22	17.41	17.59	JRS07	0.90 ± 0.03	-0.109 ± 0.032	-0.056	-0.29
210839	λ Cep	17.07	17.19	17.32	JRS07	0.66 ± 0.03	-0.109 ± 0.019	-0.047	-0.33
218915	HD 218915	16.86	16.97	17.05	KAMM03	0.70 ± 0.08	-0.109 ± 0.020	-0.078	-0.76
219188	HD 219188	16.74	16.88	16.99	KAMM03	1.24 ± 0.57	-0.109 ± 0.057	0.210	0.95
220057	HD 220057	17.00	17.04	17.07	KML06	0.75 ± 0.05	-0.109 ± 0.023	0.093	0.75
224151	V373 Cas	17.16	17.19	17.22	KML06	0.46 ± 0.04	-0.109 ± 0.018	-0.064	-0.95

^aTerms in parentheses indicate separate velocity components, if they are explicitly identified and not grouped together; see §4.3

^bCodes in this column are linked to references listed in Table 1

^cThe expected depletion $[\text{N}_{\text{gas}}/\text{H}]$ computed using Eq. 10. The listed errors do not include an overall systematic uncertainty of 0.11 in the solar abundance $\sigma(\text{N}/\text{H})_{\odot}$ in order to show just the formal error that arises from the uncertainties in location of line of best fit and the value of F_* .

^dThe observed $[\text{N}_{\text{gas}}/\text{H}]$ minus that computed using Eq. 10.

^eThe difference shown in the previous column divided by the expected difference due to the uncertainties in both the measured column density and the coefficients that appear in Eq. 10.

Table 9. Observations and Fits for Oxygen

HD Number ^a	Name	Observed $\log N(\text{O I})$				F_*	$[\text{O}_{\text{gas}}/\text{H}]_{\text{fit}}^{\text{c}}$	Residual ^d	Deviation ^e (in σ)
		l.l.	best	u.l.	Source ^b				
(1)	(2)	(3)	(4)	(5)	(6)	(7)	(8)	(9)	(10)
1383	HD 1383	18.09	18.15	18.21	CLMS04	0.61 ± 0.04	-0.148 ± 0.014	0.034	0.35
5394	γ Cas	16.72	16.76	16.80	MJC98	0.52 ± 0.04	-0.127 ± 0.015	-0.032	-0.32
12323	HD 12323	17.96	18.02	18.08	CLMS04	0.52 ± 0.04	-0.128 ± 0.014	0.103	1.08
13268	HD 13268	18.07	18.13	18.19	CLMS04	0.51 ± 0.04	-0.126 ± 0.015	0.079	0.82
14434	HD 14434	18.10	18.18	18.26	CLMS04	0.52 ± 0.04	-0.127 ± 0.015	0.080	0.73
22586	HD 22586	15.45	∞	∞	JW96	0.34 ± 0.07	-0.087 ± 0.023
23180	\circ Per	17.82	17.93	18.02	MJC98	0.84 ± 0.06	-0.200 ± 0.022	0.180	1.24
23478	HD 23478	17.70	17.79	17.88	C++08	-0.00 ± 0.50	-0.010 ± 0.116	-0.006	-0.03
24190	HD 24190	17.86	17.91	17.96	C++08	0.63 ± 0.24	-0.152 ± 0.056	0.003	0.03
24398	ζ Per	17.65	17.71	17.76	MJC98	0.88 ± 0.05	-0.210 ± 0.022	-0.035	-0.28
24534	X Per	17.85	17.87	17.89	KAMM03	0.90 ± 0.06	-0.213 ± 0.023	-0.019	-0.43
24760	ϵ Per	16.98	17.03	17.07	MJC98	0.68 ± 0.04	-0.163 ± 0.015	-0.066	-0.65
24912	ξ Per	17.75	17.81	17.86	C++91	0.83 ± 0.02	-0.198 ± 0.017	-0.043	-0.45
27778	62 Tau	17.79	17.83	17.87	CMLS01
30614	α Cam	17.86	17.98	18.07	MJC98	0.46 ± 0.04	-0.113 ± 0.016	0.245	1.87
34029	α Aur	14.85	15.01	15.37	WRLS02	0.44 ± 0.05	-0.109 ± 0.018	0.116	0.42
35149	23 Ori	17.22	17.32	17.42	CLMS04	0.54 ± 0.04	-0.132 ± 0.014	0.060	0.36
36486	δ Ori A	16.62	16.67	16.72	MJC98	0.54 ± 0.02	-0.132 ± 0.012	-0.146	-2.24
36861	λ Ori A	17.26	17.33	17.39	MJC98	0.57 ± 0.04	-0.138 ± 0.014	-0.089	-0.69
37021	θ^1 Ori	18.06	18.09	18.12	CMLS01
37043	ι Ori	16.67	16.76	16.84	MJHC94	0.41 ± 0.03	-0.103 ± 0.016	-0.044	-0.41
37061	ν Ori	18.21	18.23	18.25	CMLS01
37128	ϵ Ori	16.93	16.98	17.03	MJC98	0.54 ± 0.03	-0.132 ± 0.013	-0.096	-0.93
37367	HD 37367	17.98	18.06	18.14	CLMS04	0.65 ± 0.07	-0.158 ± 0.019	0.125	0.99
37903	HD 37903	17.86	17.88	17.90	CMLS01	1.15 ± 0.03	-0.269 ± 0.032	-0.048	-0.67
38666	μ Col	17.01	HSF99	0.11 ± 0.01	-0.036 ± 0.028
38771	κ Ori	16.98	17.03	17.07	MJHC94	0.67 ± 0.03	-0.161 ± 0.013	-0.086	-1.33
40893	HD 40893	18.04	18.07	18.10	C++08	0.61 ± 0.05	-0.147 ± 0.016	-0.079	-0.96
41161	HD 41161	17.99	18.04	18.09	OH06	0.44 ± 0.04	-0.109 ± 0.016	0.314	3.17
43818	LU Gem	18.19	18.22	18.25	CLMS04
44743	β CMa	14.98	15.00	15.02	JGD00	-0.43 ± 0.03	0.087 ± 0.056	-0.151	-1.79
47839	15 Mon	16.72	16.84	16.93	MJC98	0.25 ± 0.05	-0.066 ± 0.024	-0.162	-1.10
48915 (+12)	α CMa	13.61	13.71	13.82	H++99	0.42 ± 0.11	-0.105 ± 0.028	-0.347	-1.52
(+18)		14.39	14.54	14.70	H++99	0.42 ± 0.08	-0.104 ± 0.023	0.282	1.30
49798	HD 49798	15.70	∞	∞	JW96
53975	HD 53975	17.79	17.87	17.95	OH06	0.45 ± 0.03	-0.112 ± 0.015	0.082	0.82
57061	τ CMa	17.29	17.33	17.37	MJC98	0.39 ± 0.04	-0.097 ± 0.018	-0.031	-0.49
63005	HD 63005	17.91	17.95	17.99	CLMS04	0.64 ± 0.03	-0.155 ± 0.013	0.027	0.40
69106	HD 69106	17.64	17.69	17.74	C++08	0.64 ± 0.06	-0.155 ± 0.017	-0.007	-0.09

Table 9—Continued

HD Number ^a	Name	Observed $\log N(\text{O I})$				Source ^b	F_*	$[\text{O}_{\text{gas}}/\text{H}]_{\text{fit}}^{\text{c}}$	Residual ^d	Deviation ^e (in σ)
		l.l.	best	u.l.						
(1)	(2)	(3)	(4)	(5)	(6)	(7)	(8)	(9)	(10)	
72089 (+5)	HD 72089	16.30	∞	∞	JW96	
72754	FY Vel	17.68	17.74	17.80	CLMS04	0.76 ± 0.10	-0.182 ± 0.026	-0.123	-1.04	
75309	HD 75309	17.68	17.73	17.78	CMLS01	0.63 ± 0.04	-0.151 ± 0.014	-0.056	-0.61	
79186	GX Vel	18.00	18.04	18.08	CLMS04	0.69 ± 0.03	-0.166 ± 0.014	0.038	0.47	
88115	HD 88115	17.61	17.67	17.72	A++03	0.35 ± 0.45	-0.088 ± 0.103	0.004	0.03	
91824	HD 91824	17.95	18.00	18.05	CLMS04	0.45 ± 0.03	-0.111 ± 0.015	0.187	2.47	
91983	HD 91983	17.92	17.96	18.00	CLMS04	0.48 ± 0.04	-0.118 ± 0.015	0.078	0.88	
93030	θ Car	16.18	16.39	16.59	AJS92	0.45 ± 0.03	-0.111 ± 0.015	-0.524	-2.43	
93205	V560 Car	17.92	17.95	17.98	A++03	0.40 ± 0.03	-0.100 ± 0.016	-0.111	-2.17	
93222	HD 93222	18.11	18.13	18.15	A++03	0.39 ± 0.04	-0.098 ± 0.018	0.048	0.71	
94493	HD 94493	17.81	17.85	17.88	A++03	0.29 ± 0.03	-0.075 ± 0.021	-0.004	-0.08	
94454	HD 94454	17.79	17.83	17.87	C++08	
99857	HD 99857	17.86	17.89	17.92	A++03	0.54 ± 0.04	-0.132 ± 0.015	-0.095	-1.40	
99872	HD 99872	17.73	17.78	17.83	C++08	
102065	HD 102065	17.63	17.70	17.77	C++08	
104705	DF Cru	17.79	17.81	17.83	A++03	0.33 ± 0.05	-0.084 ± 0.021	-0.042	-0.52	
108639	HD 108639	18.03	18.09	18.15	C++08	0.37 ± 0.37	-0.094 ± 0.085	0.040	0.30	
112999	V946 Cen	17.68	17.75	17.82	C++08	
114886	HD 114886	17.89	17.95	18.01	C++08	0.87 ± 0.31	-0.206 ± 0.072	-0.006	-0.06	
115071	V961 Cen	18.17	18.20	18.23	C++08	0.22 ± 0.21	-0.061 ± 0.052	0.004	0.05	
116658	α Vir	15.44	15.54	15.64	YK79	0.16 ± 0.05	-0.047 ± 0.028	-0.169	-1.17	
116852	HD 116852	17.52	17.56	17.60	C++08	0.36 ± 0.04	-0.091 ± 0.018	-0.124	-1.36	
120086	HD 120086	16.20	∞	∞	JW96	
121968	HD 121968	16.99	17.10	17.21	LKF05	0.26 ± 0.06	-0.069 ± 0.025	-0.187	-1.09	
122879	HD 122879	18.08	18.14	18.20	CLMS04	0.55 ± 0.04	-0.133 ± 0.015	0.177	1.49	
124314	HD 124314	18.16	18.18	18.20	A++03	0.59 ± 0.05	-0.142 ± 0.016	0.053	0.69	
137595	HD 137595	17.72	17.76	17.80	C++08	0.77 ± 0.22	-0.185 ± 0.053	-0.036	-0.45	
141637	1 Sco	17.85	17.95	18.03	MJC98	0.69 ± 0.05	-0.166 ± 0.016	0.224	1.57	
143275	δ Sco	17.67	17.74	17.79	MJC98	0.90 ± 0.03	-0.212 ± 0.021	0.029	0.27	
144217	β^1 Sco	17.60	17.67	17.74	MJC98	0.81 ± 0.02	-0.193 ± 0.016	-0.030	-0.37	
144470	α^1 Sco	17.82	17.88	17.95	MJC98	0.81 ± 0.04	-0.192 ± 0.018	0.084	0.79	
144965	HD 144965	17.74	17.80	17.86	C++08	1.15 ± 0.35	-0.268 ± 0.084	-0.015	-0.12	
147165	σ Sco	17.93	18.07	18.18	MJC98	0.76 ± 0.06	-0.183 ± 0.020	0.132	0.61	
147683	V760 Sco	17.95	18.00	18.05	C++08	0.56 ± 0.47	-0.136 ± 0.107	-0.029	-0.17	
147888	ρ Oph D	18.16	18.18	18.20	CMLS01	0.88 ± 0.06	-0.209 ± 0.023	-0.109	-0.73	
147933	ρ Oph A	17.98	18.18	18.31	MJC98	1.09 ± 0.08	-0.256 ± 0.034	-0.023	-0.12	
148184	χ Oph	18.07	18.26	18.39	MJC98	0.96 ± 0.09	-0.226 ± 0.030	0.423	2.10	
148594	HD 148594	17.83	17.86	17.89	CLMS04	
149757 (-27)	ζ Oph	16.39	16.70	16.88	SCS92	

Table 9—Continued

HD Number ^a	Name	Observed $\log N(\text{O I})$				F_*	$[\text{O}_{\text{gas}}/\text{H}]_{\text{fit}}^{\text{c}}$	Residual ^d	Deviation ^e (in σ)
		l.l.	best	u.l.	Source ^b				
(1)	(2)	(3)	(4)	(5)	(6)	(7)	(8)	(9)	(10)
(–15)		17.59	17.63	17.67	SCS92	1.05 ± 0.02	-0.246 ± 0.026	–0.033	–0.47
151805	HD 151805	17.85	17.98	18.05	C++08	0.83 ± 0.36	-0.196 ± 0.083	0.011	0.08
152590	HD 152590	17.98	18.01	18.04	C++08	0.69 ± 0.03	-0.166 ± 0.014	–0.052	–0.86
154368	V1074 Sco	17.88	18.11	18.21	S++96	0.52 ± 0.07	-0.127 ± 0.019	–0.111	–0.64
157246	γ Ara	17.29	17.33	17.37	MJC98	0.46 ± 0.03	-0.114 ± 0.015	–0.020	–0.21
157857	HD 157857	18.07	18.11	18.15	CLMS04	0.62 ± 0.04	-0.151 ± 0.014	0.057	0.71
158926	λ Sco	15.87	15.88	15.90	Y83	0.31 ± 0.02	-0.081 ± 0.019	–0.034	–0.89
165246	HD 165246	17.96	18.00	18.04	C++08	0.77 ± 1.39	-0.183 ± 0.312	–0.032	–0.06
165955	HD 165955	17.70	17.79	17.88	CLMS04	0.42 ± 0.04	-0.105 ± 0.017	0.036	0.33
167264	15 Sgr	17.98	18.14	18.26	MJC98	0.68 ± 0.16	-0.164 ± 0.037	0.292	1.62
175360	HD 175360	17.53	17.59	17.65	CMLS01
177989	HD 177989	17.76	17.79	17.81	A++03	0.55 ± 0.05	-0.135 ± 0.015	0.081	1.08
185418	HD 185418	18.01	18.06	18.11	CMLS01	0.79 ± 0.03	-0.189 ± 0.017	0.078	0.87
190918	V1676 Cyg	18.04	18.12	18.20	CLMS04	0.46 ± 0.03	-0.114 ± 0.015	0.070	0.71
192035	RX Cyg	17.97	18.01	18.05	CLMS04	0.76 ± 0.04	-0.181 ± 0.016	0.048	0.62
192639	HD 192639	18.10	18.14	18.18	CLMS04	0.64 ± 0.04	-0.155 ± 0.014	0.054	0.67
195965	HD 195965	17.71	17.77	17.81	H++03	0.52 ± 0.02	-0.127 ± 0.012	0.005	0.10
198478	55 Cyg	17.97	18.02	18.07	CLMS04	0.81 ± 0.05	-0.192 ± 0.019	–0.094	–0.78
198781	HD 198781	17.71	17.77	17.83	CLMS04	0.59 ± 0.03	-0.143 ± 0.013	0.002	0.02
201345	HD 201345	17.60	17.66	17.72	CLMS04	0.34 ± 0.04	-0.086 ± 0.020	–0.015	–0.15
202347	HD 202347	17.51	17.58	17.64	A++03	0.56 ± 0.06	-0.136 ± 0.018	0.020	0.16
203374	HD 203374	17.98	18.02	18.06	C++08	0.56 ± 0.06	-0.136 ± 0.017	0.066	0.67
203532	HD 203532	17.83	17.85	17.87	CMLS01
206267	HD 206267	18.07	18.14	18.21	JRS05	0.87 ± 0.07	-0.206 ± 0.024	0.048	0.42
206773	HD 206773	17.85	17.90	17.95	CLMS04	0.53 ± 0.02	-0.131 ± 0.012	0.020	0.28
207198	HD 207198	18.09	18.13	18.17	CMLS01	0.90 ± 0.03	-0.213 ± 0.020	–0.093	–1.36
207538	HD 207538	18.29	18.32	18.35	JRS05	0.84 ± 0.07	-0.200 ± 0.023	0.179	2.16
208440	HD 208440	17.89	17.96	18.03	CLMS04	0.61 ± 0.04	-0.148 ± 0.014	0.041	0.39
208947	HD 208947	17.65	17.68	17.71	C++08
209339	HD 209339	17.92	17.96	18.00	C++08	0.58 ± 0.04	-0.140 ± 0.014	0.079	1.09
210809	HD 210809	17.92	17.99	18.06	CLMS04	0.41 ± 0.04	-0.103 ± 0.018	0.001	0.01
210839	λ Cep	18.09	18.11	18.13	A++03	0.66 ± 0.03	-0.158 ± 0.013	0.062	0.91
212791	V408 Lac	17.77	17.83	17.89	CLMS04	0.57 ± 0.08	-0.139 ± 0.022	0.086	0.44
218915	HD 218915	17.79	17.82	17.85	A++03	0.70 ± 0.08	-0.168 ± 0.022	–0.027	–0.53
219188	HD 219188	17.19	17.28	17.34	KAMM03	1.24 ± 0.57	-0.289 ± 0.134	–0.067	–0.29
220057	HD 220057	17.73	17.79	17.85	CLMS04	0.75 ± 0.05	-0.180 ± 0.018	0.053	0.40
224151	V373 Cas	18.03	18.06	18.09	A++03	0.46 ± 0.04	-0.115 ± 0.016	–0.048	–0.72
232522	HDE 232522	17.70	17.78	17.86	CLMS04	0.44 ± 0.03	-0.109 ± 0.016	–0.057	–0.59
303308	HDE 303308	18.06	18.09	18.11	A++03	0.38 ± 0.04	-0.097 ± 0.018	–0.052	–0.72

Table 9—Continued

HD Number ^a	Name	Observed $\log N(\text{O I})$				F_*	$[\text{O}_{\text{gas}}/\text{H}]_{\text{fit}}^{\text{c}}$	Residual ^d	Deviation ^e (in σ)
		l.l.	best	u.l.	Source ^b				
(1)	(2)	(3)	(4)	(5)	(6)	(7)	(8)	(9)	(10)
308813	HDE 308813	17.82	17.90	17.98	CLMS04	0.49 ± 0.04	-0.121 ± 0.015	-0.027	-0.24
	BD +53 2820	17.93	18.05	18.17	CLMS04	0.43 ± 0.05	-0.107 ± 0.018	0.009	0.06
	CPD -69 1743	17.68	17.80	17.92	CLMS04	0.42 ± 0.05	-0.105 ± 0.018	-0.015	-0.10

^aTerms in parentheses indicate separate velocity components, if they are explicitly identified and not grouped together; see §4.3

^bCodes in this column are linked to references listed in Table 1

^cThe expected depletion $[\text{O}_{\text{gas}}/\text{H}]$ computed using Eq. 10. The listed errors do not include an overall systematic uncertainty of 0.05 in the solar abundance $\sigma(\text{O}/\text{H})_{\odot}$ in order to show just the formal error that arises from the uncertainties in location of line of best fit and the value of F_* .

^dThe observed $[\text{O}_{\text{gas}}/\text{H}]$ minus that computed using Eq. 10.

^eThe difference shown in the previous column divided by the expected difference due to the uncertainties in both the measured column density and the coefficients that appear in Eq. 10.

Table 10. Observations and Fits for Magnesium

HD Number ^a	Name	Observed $\log N(\text{Mg II})$				F_*	$[\text{Mg}_{\text{gas}}/\text{H}]_{\text{fit}}^{\text{c}}$	Residual ^d	Deviation ^e (in σ)
		l.l.	best	u.l.	Source ^b				
(1)	(2)	(3)	(4)	(5)	(6)	(7)	(8)	(9)	(10)
1383	HD 1383	16.27	16.36	16.45	CLMS06	0.61 ± 0.04	-0.880 ± 0.044	0.115	0.92
2905	κ Cas	15.93	16.00	16.42	JSS86	0.58 ± 0.06	-0.849 ± 0.059	-0.060	-0.21
5394	γ Cas	14.86	14.91	14.96	JSS86	0.52 ± 0.04	-0.784 ± 0.043	-0.085	-0.76
12323	HD 12323	15.99	16.04	16.09	CLMS06	0.52 ± 0.04	-0.792 ± 0.037	-0.074	-0.77
13268	HD 13268	16.19	16.24	16.29	CLMS06	0.51 ± 0.04	-0.783 ± 0.041	-0.015	-0.15
13745	HD 13745	16.11	16.18	16.24	JS07b	0.43 ± 0.07	-0.694 ± 0.069	-0.120	-0.99
14434	HD 14434	16.22	16.27	16.32	CLMS06	0.52 ± 0.04	-0.787 ± 0.043	-0.031	-0.31
15137	HD 15137	16.13	16.15	16.17	JS07b	0.37 ± 0.09	-0.636 ± 0.089	-0.055	-0.36
18100	HD 18100	15.15	15.18	15.21	SS96b	0.14 ± 0.04	-0.406 ± 0.048	-0.187	-1.29
21278	HD 21278	15.39	15.66	∞	JSS86
21856	HD 21856	15.48	15.78	16.30	JSS86	0.67 ± 0.39	-0.941 ± 0.388	-0.002	-0.00
22586	HD 22586	14.82	JW96	0.34 ± 0.07	-0.609 ± 0.067
22928	δ Per	14.64	14.86	15.02	JSS86
22951	40 Per	15.31	15.44	15.54	JSS86	0.73 ± 0.05	-0.999 ± 0.052	-0.401	-2.42
23180	\circ Per	15.42	15.51	15.63	JSS86	0.84 ± 0.06	-1.111 ± 0.067	-0.189	-1.17
23480	23 Tau	14.42	14.89	15.46	JSS86
24398	ζ Per	15.67	15.71	15.75	S77	0.88 ± 0.05	-1.152 ± 0.053	0.044	0.35
24760	ϵ Per	15.09	15.13	15.16	JSS86	0.68 ± 0.04	-0.948 ± 0.040	-0.043	-0.41
24912	ξ Per	15.88	15.92	15.96	C++91	0.83 ± 0.02	-1.099 ± 0.029	0.106	1.17
27778	62 Tau	15.46	15.48	15.50	CLMS06
29248	ν Eri	14.96	15.07	14.37	JSS86
30614	α Cam	15.86	15.92	15.99	JSS86	0.46 ± 0.04	-0.725 ± 0.042	-0.062	-0.58
31237	π^5 Ori	15.10	15.19	15.31	JSS86	0.52 ± 0.21	-0.788 ± 0.207	0.200	0.46
34029	α Aur	12.80	12.81	12.82	L++95	0.44 ± 0.05	-0.708 ± 0.051	-0.342	-3.15
34816	λ Lep	14.97	15.04	15.15	JSS86	0.45 ± 0.05	-0.723 ± 0.053	-0.036	-0.26
35149	23 Ori	15.60	15.64	15.68	W++99	0.54 ± 0.04	-0.807 ± 0.039	0.196	1.34
35439	25 Ori	15.27	15.39	15.79	JSS86	0.72 ± 0.18	-0.989 ± 0.177	0.405	1.07
35715	ψ Ori	15.52	15.60	15.95	JSS86	0.66 ± 0.11	-0.931 ± 0.113	0.421	1.36
36166	HD 36166	15.22	15.55	∞	JSS86
36486	δ Ori A	15.06	15.09	15.13	JSS86	0.54 ± 0.02	-0.809 ± 0.022	0.090	1.52
36822	ϕ^1 Ori	15.56	15.59	15.76	JSS86	0.74 ± 0.08	-1.009 ± 0.081	0.143	0.93
36841	HD 36841	15.38	15.45	15.52	CLMS06
36861	λ Ori A	15.67	15.69	15.75	JSS86	0.57 ± 0.04	-0.834 ± 0.041	0.107	0.86
37021	θ^1 Ori	15.87	15.90	15.93	CLMS06
37043	ι Ori	15.01	15.04	15.07	JSS86	0.41 ± 0.03	-0.679 ± 0.029	-0.050	-0.64
37061	ν Ori	15.75	15.80	15.85	CLMS06
37128	ϵ Ori	15.25	15.27	15.29	JSS86	0.54 ± 0.03	-0.809 ± 0.031	0.010	0.10
37367	HD 37367	15.96	16.00	16.04	CLMS06	0.65 ± 0.07	-0.922 ± 0.068	-0.030	-0.24
37468	σ Ori	15.50	15.53	15.57	JSS86	0.58 ± 0.04	-0.851 ± 0.043	0.242	2.29

Table 10—Continued

HD Number ^a	Name	Observed $\log N(\text{Mg II})$				F_*	$[\text{Mg}_{\text{gas}}/\text{H}]_{\text{fit}}^{\text{c}}$	Residual ^d	Deviation ^e (in σ)
		l.l.	best	u.l.	Source ^b				
(1)	(2)	(3)	(4)	(5)	(6)	(7)	(8)	(9)	(10)
37903	HD 37903	15.56	15.62	15.68	CLMS06	1.15 ± 0.03	-1.414 ± 0.040	-0.023	-0.24
38666	μ Col	15.10	15.12	15.14	HFS99	0.11 ± 0.01	-0.381 ± 0.020	0.021	0.60
38771	κ Ori	15.35	15.35	15.41	JSS86	0.67 ± 0.03	-0.935 ± 0.029	0.146	2.33
40111	139 Tau	15.78	15.84	15.92	JSS86	0.49 ± 0.04	-0.758 ± 0.038	0.027	0.24
40893	HD 40893	16.30	16.33	16.36	JS07b	0.61 ± 0.05	-0.876 ± 0.055	0.050	0.51
43818	LU Gem	16.44	16.48	16.52	CLMS06
44506	HD 44506	15.11	15.32	15.45	JSS86	-0.03 ± 0.23	-0.239 ± 0.227	-0.146	-0.29
48915 (+12)	α CMa	11.95	12.00	12.04	H++99	0.42 ± 0.11	-0.688 ± 0.108	-0.333	-1.44
(+18)		12.20	12.23	12.26	H++99	0.42 ± 0.08	-0.686 ± 0.082	-0.305	-1.76
52266	HD 52266	16.07	16.09	16.11	CLMS06
52918	19 Mon	15.11	15.25	15.39	JSS86	0.44 ± 0.24	-0.712 ± 0.242	0.147	0.36
53975	HD 53975	16.05	16.10	16.15	OH06	0.45 ± 0.03	-0.718 ± 0.031	0.058	0.70
54662	HD 54662	15.71	15.90	16.06	JSS86	0.89 ± 0.09	-1.153 ± 0.093	0.021	0.09
55879	HD 55879	15.40	15.73	∞	JSS86
57060	29 CMa	15.57	15.70	15.79	JSS86	0.50 ± 0.05	-0.769 ± 0.048	0.152	1.02
57061	τ CMa	15.79	15.86	15.97	JSS86	0.39 ± 0.04	-0.655 ± 0.044	0.198	1.80
63005	HD 63005	16.00	16.03	16.06	CLMS06	0.64 ± 0.03	-0.908 ± 0.031	0.001	0.01
64740	HD 64740	...	14.46	14.77	JSS86	0.27 ± 0.30	-0.541 ± 0.301
64760	HD 64760	15.19	15.24	15.29	JSS86	0.35 ± 0.06	-0.624 ± 0.059	-0.015	-0.11
65575	χ Car	14.29	JSS86
65818	V Pup	15.32	15.43	15.54	JSS86	0.36 ± 0.09	-0.631 ± 0.090	-0.078	-0.39
66788	HD 66788	16.01	16.11	16.19	JS07b	0.53 ± 0.08	-0.799 ± 0.079	0.033	0.22
66811	ζ Pup	15.03	15.07	15.11	M78	0.32 ± 0.02	-0.592 ± 0.023	0.081	1.32
68273	γ^2 Vel	14.55	14.67	14.85	FS94	0.25 ± 0.02	-0.520 ± 0.024	-0.139	-0.88
69106	HD 69106	15.78	15.81	15.83	JS07b	0.64 ± 0.06	-0.909 ± 0.061	0.008	0.09
71634	HD 71634	15.75	15.79	15.83	CLMS06
72089 (+5)	HD 72089	15.07	15.12	15.22	JW96
75309	HD 75309	15.90	15.95	16.00	CLMS06	0.63 ± 0.04	-0.894 ± 0.040	0.047	0.47
79186	GX Vel	16.07	16.11	16.15	CLMS06	0.69 ± 0.03	-0.957 ± 0.036	0.039	0.46
79351	a Car	15.20	JSS86
81188	κ Vel	14.99	15.04	15.10	JSS86
91597	HD 91597	16.20	16.25	16.30	JS07b	0.44 ± 0.05	-0.713 ± 0.056	-0.072	-0.76
91651	HD 91651	16.22	16.26	16.29	JS07b	0.27 ± 0.04	-0.540 ± 0.044	0.023	0.28
91824	HD 91824	16.11	16.14	16.17	CLMS06	0.45 ± 0.03	-0.715 ± 0.032	0.070	1.00
91983	HD 91983	16.13	16.19	16.25	CLMS06	0.48 ± 0.04	-0.745 ± 0.041	0.075	0.71
92554	HD 92554	16.32	16.37	16.41	JS07b	0.27 ± 0.07	-0.538 ± 0.071	0.004	0.03
93030	θ Car	15.09	15.19	15.25	AJS92	0.45 ± 0.03	-0.714 ± 0.034	0.028	0.24
93205	V560 Car	16.29	16.32	16.34	JS07b	0.40 ± 0.03	-0.668 ± 0.030	-0.034	-0.62
93222	HD 93222	16.39	16.41	16.42	JS07b	0.39 ± 0.04	-0.658 ± 0.042	0.028	0.37

Table 10—Continued

HD Number ^a	Name	Observed $\log N(\text{Mg II})$				F_*	$[\text{Mg}_{\text{gas}}/\text{H}]_{\text{fit}}^c$	Residual ^d	Deviation ^e (in σ)
		l.l.	best	u.l.	Source ^b				
(1)	(2)	(3)	(4)	(5)	(6)	(7)	(8)	(9)	(10)
93521 (–66)	HD 93521	14.06	14.24	14.42	SF93	-0.31 ± 0.11	0.040 ± 0.113	0.071	0.18
(–58)		14.27	14.43	14.59	SF93	-0.01 ± 0.03	-0.264 ± 0.039	–0.265	–1.44
(–51)		14.38	14.50	14.65	SF93	-0.04 ± 0.04	-0.234 ± 0.050	–0.085	–0.47
(–39)		14.06	14.32	14.58	SF93	0.01 ± 0.08	-0.276 ± 0.085	0.097	0.29
(–18)		14.21	14.40	14.59	SF93	0.00 ± 0.03	-0.273 ± 0.037	–0.226	–1.10
(–10)		14.31	14.53	14.65	SF93	0.02 ± 0.04	-0.291 ± 0.045	–0.158	–0.83
(+3)		14.13	14.32	14.51	SF93	0.25 ± 0.04	-0.521 ± 0.040	–0.078	–0.37
(total)		15.06	15.25	15.42	SF93	0.06 ± 0.04	-0.328 ± 0.041	–0.143	–0.73
93843	HD 93843	16.23	16.25	16.27	JS07b	0.39 ± 0.05	-0.655 ± 0.052	–0.061	–0.64
94493	HD 94493	16.14	16.16	16.18	JS07b	0.29 ± 0.03	-0.557 ± 0.037	–0.073	–1.28
99857	HD 99857	16.08	16.21	16.24	JS07b	0.54 ± 0.04	-0.807 ± 0.044	0.040	0.37
99890	HD 99890	16.15	16.18	16.21	JS07b	0.17 ± 0.08	-0.439 ± 0.082	0.040	0.26
100340	HD 100340	15.41	15.48	15.55	SS96b	0.10 ± 0.06	-0.368 ± 0.061	–0.236	–1.74
103779	HD 103779	16.15	16.17	16.19	JS07b	0.43 ± 0.06	-0.703 ± 0.065	0.055	0.48
104705	DF Cru	16.17	16.19	16.21	JS07b	0.33 ± 0.05	-0.596 ± 0.047	–0.010	–0.11
106490	δ Cru	14.54	14.60	14.67	JSS86
108248	α^1 Cru	14.83	14.85	14.88	JSS86	0.15 ± 0.05	-0.421 ± 0.051	0.052	0.45
109399	HD 109399	15.90	15.95	16.00	JS07b	0.48 ± 0.05	-0.754 ± 0.051	–0.095	–1.02
111934	BU Cru	16.26	16.28	16.30	CLMS06
113904	θ Mus	15.67	15.80	15.96	JSS86
116781	V967 Cen	16.11	16.14	16.17	JS07b	0.44 ± 0.07	-0.713 ± 0.067	–0.011	–0.10
116852	HD 116852	15.87	15.91	15.95	CLMS06	0.36 ± 0.04	-0.625 ± 0.037	–0.100	–1.03
118716	ϵ Cen	14.79	14.84	14.89	JSS86	0.15 ± 0.16	-0.419 ± 0.165	0.038	0.10
119608	HD 119608	15.83	15.88	15.93	SST97
120086	HD 120086	15.32	15.37	15.47	JW96
120324	μ Cen	14.69	14.91	15.03	JSS86	-0.81 ± 3.74	0.536 ± 3.725	–0.002	–0.00
121263	ζ Cen	14.61	14.67	14.73	JSS86
122879	HD 122879	16.21	16.23	16.25	CLMS06	0.55 ± 0.04	-0.813 ± 0.044	0.088	0.78
124314	HD 124314	16.30	16.32	16.34	JS07b	0.59 ± 0.05	-0.854 ± 0.053	0.045	0.49
127972	η Cen	14.62	14.67	14.73	JSS86
135591	HD 135591	15.65	15.82	16.35	JSS86	0.56 ± 0.22	-0.833 ± 0.220	–0.085	–0.20
136298	δ Lup	14.88	14.93	14.99	JSS86
138690	γ Lup	14.70	14.83	14.90	JSS86
141637	1 Sco	15.78	15.84	15.91	JSS86	0.69 ± 0.05	-0.957 ± 0.052	0.046	0.34
143018	π Sco	14.94	15.14	15.34	JJ91	0.71 ± 0.03	-0.973 ± 0.035	–0.195	–0.92
143118	η Lup A	14.42	14.54	14.63	JSS86
143275	δ Sco	15.72	15.74	15.76	JSS86	0.90 ± 0.03	-1.163 ± 0.038	0.121	1.23
144217	β^1 Sco	15.70	15.72	15.75	JSS86	0.81 ± 0.02	-1.079 ± 0.025	0.047	0.93
144470	\omicron^1 Sco	15.78	15.82	15.87	JSS86	0.81 ± 0.04	-1.074 ± 0.041	0.047	0.45

Table 10—Continued

HD Number ^a	Name	Observed $\log N(\text{Mg II})$				Source ^b	F_*	$[\text{Mg}_{\text{gas}}/\text{H}]_{\text{fit}}^c$	Residual ^d	Deviation ^e (in σ)
		l.l.	best	u.l.						
(1)	(2)	(3)	(4)	(5)	(6)	(7)	(8)	(9)	(10)	
145502	ν Sco	15.68	15.94	16.60	JSS86	0.80 ± 0.11	-1.066 ± 0.114	0.262	0.51	
147165	σ Sco	15.87	15.93	16.10	JSS86	0.76 ± 0.06	-1.033 ± 0.062	-0.017	-0.08	
147888	ρ Oph D	15.99	16.03	16.07	CLMS06	0.88 ± 0.06	-1.148 ± 0.066	-0.180	-1.09	
147933	ρ Oph A	15.63	15.74	16.08	JSS86	1.09 ± 0.08	-1.359 ± 0.086	-0.220	-0.86	
148184	χ Oph	15.51	15.62	15.72	JSS86	0.96 ± 0.09	-1.224 ± 0.096	-0.078	-0.42	
148594	HD 148594	15.57	15.61	15.65	CLMS06	
148605	22 Sco	...	15.13	16.12	JSS86	0.53 ± 0.39	-0.798 ± 0.393	
149038	μ Nor	15.94	16.20	∞	JSS86	0.56 ± 0.05	-0.825 ± 0.048	
149757 (-27)	ζ Oph	14.65	14.70	14.75	SCS92	
(-15)		15.39	15.42	15.44	SCS92	1.05 ± 0.02	-1.312 ± 0.029	-0.039	-0.60	
151804	V973 Sco	15.90	16.00	16.11	JSS86	0.57 ± 0.08	-0.843 ± 0.076	0.031	0.18	
151890	μ^1 Sco	14.99	15.03	15.08	JSS86	-0.03 ± 3.47	-0.242 ± 3.462	0.067	0.01	
152590	HD 152590	16.11	16.20	16.29	CLMS06	0.69 ± 0.03	-0.958 ± 0.032	0.071	0.66	
154368	V1074 Sco	15.91	16.21	16.51	S++96	0.52 ± 0.07	-0.785 ± 0.066	-0.215	-0.69	
155806	V1075 Sco	15.92	15.97	16.03	JSS86	0.62 ± 0.07	-0.892 ± 0.067	0.108	0.74	
156110	HD 156110	15.10	15.14	15.18	CLMS06	
157246	γ Ara	15.51	15.55	15.60	JSS86	0.46 ± 0.03	-0.728 ± 0.035	-0.047	-0.46	
157857	HD 157857	16.13	16.19	16.25	CLMS06	0.62 ± 0.04	-0.890 ± 0.038	0.017	0.17	
160578	κ Sco	15.08	15.13	15.17	JSS86	0.50 ± 0.07	-0.764 ± 0.074	0.053	0.30	
164284	66 Oph	15.24	15.34	15.44	JSS86	0.89 ± 0.18	-1.157 ± 0.179	0.134	0.34	
165024	θ Ara	15.58	15.61	15.67	JSS86	0.56 ± 0.03	-0.832 ± 0.036	-0.017	-0.16	
165955	HD 165955	15.97	16.02	16.07	CLMS06	0.42 ± 0.04	-0.688 ± 0.042	-0.010	-0.12	
167264	15 Sgr	15.62	15.82	15.93	JSS86	0.68 ± 0.16	-0.948 ± 0.156	-0.102	-0.42	
167756	HD 167756	15.70	15.72	15.74	CSS95	
168941	HD 168941	15.77	15.87	15.95	JS07b	0.42 ± 0.17	-0.685 ± 0.165	-0.253	-0.81	
175360	HD 175360	15.55	15.60	15.65	CLMS06	
177989	HD 177989	15.80	15.83	15.86	JS07b	0.55 ± 0.05	-0.822 ± 0.046	-0.053	-0.60	
184915	κ Aql	15.38	15.57	15.71	JSS86	0.88 ± 0.05	-1.144 ± 0.052	0.049	0.26	
185418	HD 185418	15.94	15.96	15.98	CLMS06	0.79 ± 0.03	-1.059 ± 0.037	-0.012	-0.14	
188209	HD 188209	15.18	15.55	15.70	JSS86	0.66 ± 0.12	-0.932 ± 0.122	-0.135	-0.44	
190918	V1676 Cyg	16.30	16.34	16.38	CLMS06	0.46 ± 0.03	-0.731 ± 0.035	0.046	0.59	
192035	RX Cyg	15.89	15.93	15.97	CLMS06	0.76 ± 0.04	-1.026 ± 0.042	-0.047	-0.55	
192639	HD 192639	16.18	16.21	16.24	CLMS06	0.64 ± 0.04	-0.908 ± 0.039	0.018	0.21	
193322	HD 193322	...	15.76	∞	JSS86	
195965	HD 195965	15.84	15.89	15.93	JS07b	0.52 ± 0.02	-0.786 ± 0.018	-0.078	-1.46	
198478	55 Cyg	15.91	15.95	15.99	CLMS06	0.81 ± 0.05	-1.075 ± 0.055	-0.142	-1.11	
198781	HD 198781	15.72	15.76	15.80	CLMS06	0.59 ± 0.03	-0.856 ± 0.032	-0.155	-1.97	
200120	59 Cyg	14.61	14.98	15.17	JSS86	
201345	HD 201345	15.93	15.96	15.99	CLMS06	0.34 ± 0.04	-0.607 ± 0.042	-0.055	-0.56	

Table 10—Continued

HD Number ^a	Name	Observed $\log N(\text{Mg II})$				Source ^b	F_*	$[\text{Mg}_{\text{gas}}/\text{H}]_{\text{fit}}^c$	Residual ^d	Deviation ^e (in σ)
		l.l.	best	u.l.						
(1)	(2)	(3)	(4)	(5)	(6)	(7)	(8)	(9)	(10)	
202347	HD 202347	15.57	15.62	15.66	JS07b	0.56 ± 0.06	-0.826 ± 0.064	-0.110	-0.84	
202904	ν Cyg	15.22	15.29	15.37	JSS86	
203064	68 Cyg	15.70	15.87	16.27	JSS86	0.68 ± 0.20	-0.949 ± 0.204	0.056	0.15	
203374	HD 203374	16.05	16.07	16.09	JS07b	0.56 ± 0.06	-0.825 ± 0.060	-0.054	-0.50	
203532	HD 203532	15.56	15.58	15.60	CLMS06	
206267	HD 206267	16.01	16.05	16.09	JS07b	0.87 ± 0.07	-1.134 ± 0.072	0.027	0.22	
206773	HD 206773	15.97	15.99	16.01	CLMS06	0.53 ± 0.02	-0.803 ± 0.023	-0.078	-1.30	
207198	HD 207198	16.06	16.08	16.10	CLMS06	0.90 ± 0.03	-1.166 ± 0.035	-0.049	-0.76	
207308	HD 207308	15.88	15.93	15.98	JS07b	0.80 ± 0.06	-1.065 ± 0.061	-0.062	-0.62	
207538	HD 207538	16.03	16.07	16.10	JS07b	0.84 ± 0.07	-1.109 ± 0.073	-0.022	-0.20	
208440	HD 208440	16.00	16.05	16.10	CLMS06	0.61 ± 0.04	-0.878 ± 0.042	0.001	0.01	
209339	HD 209339	16.02	16.04	16.06	JS07b	0.58 ± 0.04	-0.845 ± 0.043	0.003	0.04	
209975	19 Cep	16.10	16.33	16.69	JSS86	0.57 ± 0.26	-0.841 ± 0.262	0.370	0.90	
210809	HD 210809	16.17	16.23	16.29	CLMS06	0.41 ± 0.04	-0.682 ± 0.044	-0.041	-0.37	
210839	λ Cep	16.02	16.05	16.08	JS07b	0.66 ± 0.03	-0.925 ± 0.035	-0.091	-1.16	
212791	V408 Lac	15.80	15.87	15.94	CLMS06	0.57 ± 0.08	-0.840 ± 0.083	-0.034	-0.16	
214080	HD 214080	14.91	15.27	15.78	JSS86	0.27 ± 0.10	-0.539 ± 0.102	-0.425	-0.86	
214680	10 Lac	15.66	15.69	15.73	JSS86	0.50 ± 0.06	-0.765 ± 0.064	0.108	0.74	
214993	12 Lac	15.43	15.50	15.58	JSS86	0.68 ± 0.10	-0.948 ± 0.096	0.006	0.04	
215733 (-59)	HD 215733	14.34	14.43	14.52	FS97	-0.11 ± 0.10	-0.160 ± 0.101	0.017	0.06	
(-54)		13.55	13.86	14.17	FS97	0.54 ± 0.15	-0.812 ± 0.150	-0.581	-1.08	
(-47)		14.10	14.32	14.54	FS97	
(-45)		13.66	13.97	14.28	FS97	-0.40 ± 0.28	0.133 ± 0.279	0.154	0.23	
(-42)		13.22	13.67	14.12	FS97	-0.16 ± 0.31	-0.107 ± 0.313	-0.376	-0.37	
(-32)		14.41	14.63	14.85	FS97	0.25 ± 0.09	-0.516 ± 0.090	-0.117	-0.42	
(-31)		13.07	13.68	14.29	FS97	
(-28)		14.13	14.32	14.51	FS97	-0.18 ± 0.07	-0.087 ± 0.072	-0.126	-0.55	
(-26)		14.31	14.48	14.65	FS97	-0.12 ± 0.07	-0.148 ± 0.071	-0.105	-0.48	
(-23)		13.18	13.72	14.26	FS97	0.24 ± 0.08	-0.512 ± 0.082	-0.641	-1.17	
(-21)		14.38	14.49	14.60	FS97	0.24 ± 0.05	-0.507 ± 0.053	0.004	0.03	
(-16)		14.60	14.68	14.76	FS97	0.93 ± 0.05	-1.195 ± 0.054	0.142	1.30	
(-11)		14.79	14.91	15.03	FS97	-0.01 ± 0.07	-0.263 ± 0.075	-0.050	-0.33	
(-9)		15.00	15.12	15.24	FS97	0.08 ± 0.04	-0.349 ± 0.040	-0.224	-1.49	
(-5)		14.07	14.31	14.55	FS97	0.77 ± 0.18	-1.040 ± 0.179	0.147	0.46	
(+1)		13.97	14.16	14.35	FS97	0.90 ± 0.05	-1.172 ± 0.055	-0.001	-0.01	
(total)		15.55	15.70	15.86	FS97	
217675	o And	15.10	15.27	15.81	JSS86	
218376	1 Cas	15.66	15.77	16.02	JSS86	0.60 ± 0.06	-0.869 ± 0.061	-0.047	-0.21	
219188	HD 219188	15.53	15.69	∞	JSS86	1.24 ± 0.57	-1.505 ± 0.571	

Table 10—Continued

HD Number ^a	Name	Observed $\log N(\text{Mg II})$				F_*	$[\text{Mg}_{\text{gas}}/\text{H}]_{\text{fit}}^c$	Residual ^d	Deviation ^e (in σ)
		l.l.	best	u.l.	Source ^b				
(1)	(2)	(3)	(4)	(5)	(6)	(7)	(8)	(9)	(10)
220057	HD 220057	15.63	15.66	15.69	CLMS06	0.75 ± 0.05	-1.020 ± 0.055	-0.096	-0.72
224151	V373 Cas	16.27	16.30	16.33	JS07b	0.46 ± 0.04	-0.734 ± 0.044	-0.049	-0.64
224572	σ Cas	15.48	15.56	15.63	JSS86	0.76 ± 0.07	-1.027 ± 0.072	-0.010	-0.07
232522	HDE 232522	16.08	16.11	16.14	CLMS06	0.44 ± 0.03	-0.706 ± 0.034	0.010	0.15
303308	HDE 303308	16.29	16.34	16.38	JS07b	0.38 ± 0.04	-0.652 ± 0.040	-0.107	-1.20
308813	HDE 308813	16.12	16.15	16.18	CLMS06	0.49 ± 0.04	-0.760 ± 0.041	0.003	0.03
	BD +35 4258	16.07	16.15	16.21	JS07b	0.40 ± 0.08	-0.674 ± 0.079	-0.092	-0.65
	CPD -59 2603	16.32	16.35	16.38	JS07b	0.17 ± 0.06	-0.438 ± 0.065	-0.037	-0.31

^aTerms in parentheses indicate separate velocity components, if they are explicitly identified and not grouped together; see §4.3

^bCodes in this column are linked to references listed in Table 1

^cThe expected depletion $[\text{Mg}_{\text{gas}}/\text{H}]$ computed using Eq. 10. The listed errors do not include an overall systematic uncertainty of 0.02 in the solar abundance $\sigma(\text{Mg}/\text{H})_{\odot}$ in order to show just the formal error that arises from the uncertainties in location of line of best fit and the value of F_* .

^dThe observed $[\text{Mg}_{\text{gas}}/\text{H}]$ minus that computed using Eq. 10.

^eThe difference shown in the previous column divided by the expected difference due to the uncertainties in both the measured column density and the coefficients that appear in Eq. 10.

Table 11. Observations and Fits for Silicon

HD Number ^a	Name	Observed $\log N(\text{Si II})$				Source ^b	F_*	$[\text{Si}_{\text{gas}}/\text{H}]_{\text{fit}}^c$	Residual ^d	Deviation ^e (in σ)
		l.l.	best	u.l.						
(1)	(2)	(3)	(4)	(5)	(6)	(7)	(8)	(9)	(10)	
18100	HD 18100	15.31	15.34	15.37	SS96b	0.14 ± 0.04	-0.378 ± 0.056	-0.046	-0.31	
22586	HD 22586	15.26	15.31	15.51	JW96	0.34 ± 0.07	-0.610 ± 0.078	-0.053	-0.24	
27778	62 Tau	15.94	M++07	
34029	α Aur	13.16	13.20	13.24	WRLS02	0.44 ± 0.05	-0.722 ± 0.062	0.076	0.64	
35149	23 Ori	15.36	15.44	15.51	W++99	0.54 ± 0.04	-0.835 ± 0.050	0.034	0.21	
37021	θ^1 Ori	16.04	16.16	16.24	M++07	
37061	ν Ori	16.10	16.16	16.21	M++07	
38666	μ Col	15.14	15.16	15.18	HSF99	0.11 ± 0.01	-0.349 ± 0.026	0.040	1.05	
44743	β CMa	14.08	14.10	14.12	DG98	-0.43 ± 0.03	0.270 ± 0.063	-0.077	-0.86	
48915 (+12)	α CMa	12.27	12.36	12.50	H++99	0.42 ± 0.11	-0.700 ± 0.125	0.053	0.20	
(+18)		12.33	12.41	12.53	H++99	0.42 ± 0.08	-0.697 ± 0.096	-0.100	-0.49	
49798	HD 49798	15.15	15.20	15.40	JW96	
66811	ζ Pup	15.13	15.23	15.43	M78	0.32 ± 0.02	-0.589 ± 0.030	0.250	1.58	
68273	γ^2 Vel	14.67	14.75	14.84	FS94	0.25 ± 0.02	-0.508 ± 0.031	-0.059	-0.60	
93521 (-66)	HD 93521	13.94	14.01	14.08	SF93	-0.31 ± 0.11	0.130 ± 0.130	-0.237	-0.66	
(-58)		14.59	14.62	14.65	SF93	-0.01 ± 0.03	-0.216 ± 0.046	-0.111	-1.14	
(-51)		14.52	14.57	14.62	SF93	-0.04 ± 0.04	-0.181 ± 0.058	-0.056	-0.42	
(-39)		14.07	14.10	14.13	SF93	0.01 ± 0.08	-0.230 ± 0.098	-0.157	-0.70	
(-29)		13.16	13.23	13.30	SF93	0.34 ± 0.17	-0.610 ± 0.192	-0.147	-0.37	
(-18)		14.48	14.52	14.56	SF93	0.00 ± 0.03	-0.226 ± 0.044	-0.141	-1.54	
(-10)		14.51	14.65	14.69	SF93	0.02 ± 0.04	-0.247 ± 0.052	-0.070	-0.56	
(+3)		14.28	14.34	14.40	SF93	0.25 ± 0.04	-0.509 ± 0.047	-0.058	-0.52	
(+7)		13.75	13.86	13.97	SF93	0.23 ± 0.12	-0.489 ± 0.138	-0.048	-0.16	
(total)		15.26	15.33	15.37	SF93	0.06 ± 0.04	-0.289 ± 0.048	-0.095	-0.94	
100340	HD 100340	15.13	∞	∞	SS96b	0.10 ± 0.06	-0.334 ± 0.071	
116658	α Vir	13.96	14.11	14.26	YK79	0.16 ± 0.05	-0.407 ± 0.060	-0.097	-0.51	
120086	HD 120086	15.26	15.31	15.51	JW96	
122451	β Cen	14.47	14.51	14.55	BLWY84	0.23 ± 0.03	-0.488 ± 0.038	-0.151	-2.03	
147933	ρ Oph A	16.03	16.12	16.19	M++07	1.09 ± 0.08	-1.464 ± 0.108	0.272	1.74	
149757 (-27)	ζ Oph	14.73	14.74	14.75	SCS94	
(-15)		15.31	15.34	15.37	C++94	1.05 ± 0.02	-1.410 ± 0.055	-0.010	-0.13	
149881	V600 Her	15.70	15.80	15.90	SF95	0.07 ± 0.06	-0.298 ± 0.076	-0.159	-0.71	
152590	HD 152590	15.75	15.92	16.04	M++07	0.69 ± 0.03	-1.007 ± 0.047	-0.150	-0.94	
154368	V1074 Sco	16.04	16.34	16.64	S++96	0.52 ± 0.07	-0.809 ± 0.079	-0.051	-0.16	
158926	λ Sco	14.06	14.09	14.11	Y83	0.31 ± 0.02	-0.577 ± 0.029	-0.175	-3.58	
167756	HD 167756	15.83	15.88	15.95	CSS95	
207198	HD 207198	15.55	15.84	16.01	M++07	0.90 ± 0.03	-1.244 ± 0.055	-0.201	-0.83	
215733 (-93)	HD 215733	12.92	12.95	12.98	FS97	-0.27 ± 0.19	0.081 ± 0.221	-0.128	-0.29	
(-83)		12.12	12.24	12.36	FS97	0.99 ± 0.30	-1.345 ± 0.341	-0.422	-0.69	

Table 11—Continued

HD Number ^a	Name	Observed $\log N(\text{Si II})$				F_*	$[\text{Si}_{\text{gas}}/\text{H}]_{\text{fit}}^c$	Residual ^d	Deviation ^e (in σ)
		l.l.	best	u.l.	Source ^b				
(1)	(2)	(3)	(4)	(5)	(6)	(7)	(8)	(9)	(10)
(−61)		13.34	13.61	13.88	FS97	1.06 ± 0.21	-1.431 ± 0.243	−0.006	−0.01
(−59)		14.31	14.37	14.43	FS97	-0.11 ± 0.10	-0.098 ± 0.116	−0.089	−0.30
(−54)		14.22	14.28	14.34	FS97	0.54 ± 0.15	-0.841 ± 0.173	−0.116	−0.26
(−47)		14.47	14.55	14.63	FS97
(−45)		13.00	13.41	13.82	FS97	-0.40 ± 0.28	0.237 ± 0.319	−0.494	−0.67
(−42)		13.60	13.86	14.12	FS97	-0.16 ± 0.31	-0.037 ± 0.357	−0.240	−0.25
(−40)		13.57	13.77	13.97	FS97	0.18 ± 0.24	-0.429 ± 0.278	−0.218	−0.31
(−32)		14.58	14.76	14.94	FS97	0.25 ± 0.09	-0.504 ± 0.104	0.017	0.07
(−31)		13.74	14.00	14.26	FS97
(−28)		14.25	14.39	14.53	FS97	-0.18 ± 0.07	-0.014 ± 0.083	−0.113	−0.58
(−26)		14.19	14.38	14.57	FS97	-0.12 ± 0.07	-0.084 ± 0.082	−0.253	−1.06
(−23)		14.10	14.30	14.50	FS97	0.24 ± 0.08	-0.499 ± 0.095	−0.058	−0.25
(−21)		13.98	14.15	14.32	FS97	0.24 ± 0.05	-0.493 ± 0.062	−0.334	−1.72
(−19)		14.20	14.31	14.42	FS97
(−16)		14.45	14.55	14.65	FS97	0.93 ± 0.05	-1.277 ± 0.073	0.110	0.82
(−11)		14.86	14.99	15.12	FS97	-0.01 ± 0.07	-0.215 ± 0.086	−0.002	−0.01
(−9)		15.18	15.24	15.30	FS97	0.08 ± 0.04	-0.313 ± 0.047	−0.124	−1.12
(−5)		13.19	13.73	14.27	FS97	0.77 ± 0.18	-1.100 ± 0.207	−0.357	−0.61
(+1)		13.68	13.82	13.96	FS97	0.90 ± 0.05	-1.250 ± 0.074	−0.247	−1.49
(+9)		12.69	12.77	12.85	FS97
(+15)		12.47	12.58	12.69	FS97	0.96 ± 0.08	-1.312 ± 0.103	−0.135	−0.77
(total)		15.66	15.77	15.90	FS97

^aTerms in parentheses indicate separate velocity components, if they are explicitly identified and not grouped together; see §4.3

^bCodes in this column are linked to references listed in Table 1

^cThe expected depletion $[\text{Si}_{\text{gas}}/\text{H}]$ computed using Eq. 10. The listed errors do not include an overall systematic uncertainty of 0.02 in the solar abundance $\sigma(\text{Si}/\text{H})_{\odot}$ in order to show just the formal error that arises from the uncertainties in location of line of best fit and the value of F_* .

^dThe observed $[\text{Si}_{\text{gas}}/\text{H}]$ minus that computed using Eq. 10.

^eThe difference shown in the previous column divided by the expected difference due to the uncertainties in both the measured column density and the coefficients that appear in Eq. 10.

Table 12. Observations and Fits for Phosphorus

HD Number ^a	Name	Observed $\log N(\text{P II})$				F_*	$[\text{P}_{\text{gas}}/\text{H}]_{\text{fit}}^{\text{c}}$	Residual ^d	Deviation ^e (in σ)
		l.l.	best	u.l.	Source ^b				
(1)	(2)	(3)	(4)	(5)	(6)	(7)	(8)	(9)	(10)
2905	κ Cas	14.43	14.78	∞	JSS86	0.58 ± 0.06	-0.253 ± 0.057
5394	γ Cas	13.33	13.41	13.51	JSS86	0.52 ± 0.04	-0.192 ± 0.042	-0.100	-0.75
18100	HD 18100	13.65	13.72	13.79	SS96b	0.14 ± 0.04	0.167 ± 0.047	-0.138	-0.88
21278	HD 21278	13.29	13.54	∞	JSS86
21856	HD 21856	14.08	14.38	∞	JSS86	0.67 ± 0.39	-0.340 ± 0.368
22928	δ Per	13.31	13.61	13.78	JSS86
22951	40 Per	13.85	14.03	14.15	JSS86	0.73 ± 0.05	-0.396 ± 0.051	-0.341	-1.78
23180	o Per	14.22	14.43	14.64	S76	0.84 ± 0.06	-0.501 ± 0.065	0.199	0.82
23408	20 Tau	14.08	14.33	∞	JSS86
23480	23 Tau	13.09	13.24	13.64	JSS86
23630	η Tau	12.88	13.26	∞	JSS86
24398	ζ Per	14.44	14.58	14.72	S77	0.88 ± 0.05	-0.540 ± 0.053	0.383	2.07
24534	X Per	14.37	14.42	14.47	LKF05	0.90 ± 0.06	-0.554 ± 0.058	0.092	1.10
24760	ϵ Per	13.43	13.56	13.63	JSS86	0.68 ± 0.04	-0.346 ± 0.040	-0.136	-0.97
24912	ξ Per	14.50	14.53	14.55	C++91	0.83 ± 0.02	-0.490 ± 0.032	0.182	2.12
27778	62 Tau	14.19	14.21	14.23	CLMS06
28497	228 Eri	13.60	13.91	14.20	SY77
29248	ν Eri	13.73	14.06	∞	JSS86
30614	α Cam	14.00	14.20	14.40	JY78	0.46 ± 0.04	-0.136 ± 0.041	-0.299	-1.37
31237	π^5 Ori	13.14	13.24	13.42	JSS86	0.52 ± 0.21	-0.195 ± 0.197	-0.263	-0.60
34816	λ Lep	13.22	13.39	13.54	JSS86	0.45 ± 0.05	-0.134 ± 0.051	-0.195	-1.01
35149	23 Ori	14.27	14.31	14.35	W++99	0.54 ± 0.04	-0.214 ± 0.038	0.348	2.39
35439	25 Ori	13.07	13.14	13.29	JSS86	0.72 ± 0.18	-0.386 ± 0.168	-0.369	-1.25
35715	ψ Ori	13.27	13.34	13.62	JSS86	0.66 ± 0.11	-0.331 ± 0.108	-0.359	-1.28
36166	HD 36166	13.19	13.59	∞	JSS86
36486	δ Ori A	13.13	13.33	13.53	JY78	0.54 ± 0.02	-0.215 ± 0.023	-0.184	-0.90
36822	ϕ^1 Ori	14.00	14.08	14.18	JSS86	0.74 ± 0.08	-0.405 ± 0.078	0.105	0.74
36841	HD 36841	13.87	13.93	13.99	CLMS06
36861	λ Ori A	13.98	14.03	14.08	JSS86	0.57 ± 0.04	-0.239 ± 0.040	-0.072	-0.57
37021	θ^1 Ori	14.44	14.47	14.50	CLMS06
37043	ι Ori	13.43	13.48	13.55	JSS86	0.41 ± 0.03	-0.092 ± 0.029	-0.121	-1.28
37128	ϵ Ori	13.70	13.78	13.85	JSS86	0.54 ± 0.03	-0.215 ± 0.031	0.002	0.01
37468	σ Ori	13.65	13.73	13.78	JSS86	0.58 ± 0.04	-0.255 ± 0.042	-0.078	-0.66
37903	HD 37903	14.05	14.09	14.13	CLMS06	1.15 ± 0.03	-0.789 ± 0.047	-0.095	-1.10
38666	μ Col	13.59	13.61	13.63	HSF99	0.11 ± 0.01	0.191 ± 0.024	0.021	0.57
38771	κ Ori	13.80	13.88	13.93	JSS86	0.67 ± 0.03	-0.334 ± 0.030	0.151	1.83
40111	139 Tau	14.13	14.23	14.30	JSS86	0.49 ± 0.04	-0.167 ± 0.037	-0.101	-0.81
41161	HD 41161	13.63	∞	∞	OH06	0.44 ± 0.04	-0.120 ± 0.041
44506	HD 44506	12.94	13.19	∞	JSS86	-0.03 ± 0.23	0.325 ± 0.216

Table 12—Continued

HD Number ^a	Name	Observed $\log N(\text{P II})$				F_*	$[\text{P}_{\text{gas}}/\text{H}]_{\text{fit}}^{\text{c}}$	Residual ^d	Deviation ^e (in σ)
		l.l.	best	u.l.	Source ^b				
(1)	(2)	(3)	(4)	(5)	(6)	(7)	(8)	(9)	(10)
47839	15 Mon	13.33	13.63	13.83	JY78	0.25 ± 0.05	0.061 ± 0.048	-0.285	-1.04
52918	19 Mon	13.37	13.49	13.72	JSS86	0.44 ± 0.24	-0.123 ± 0.230	-0.122	-0.29
53975	HD 53975	13.62	∞	∞	OH06	0.45 ± 0.03	-0.129 ± 0.030
54662	HD 54662	14.15	14.43	∞	JSS86	0.89 ± 0.09	-0.541 ± 0.090
55879	HD 55879	13.75	14.28	∞	JSS86
57060	29 CMa	13.85	13.93	14.00	JSS86	0.50 ± 0.05	-0.178 ± 0.047	-0.135	-1.07
64740	HD 64740	12.94	13.19	∞	JSS86	0.27 ± 0.30	0.039 ± 0.286
64760	HD 64760	13.70	13.78	13.85	JSS86	0.35 ± 0.06	-0.040 ± 0.057	0.017	0.12
65575	χ Car	12.82	12.89	13.04	JSS86
65818	V Pup	14.00	14.13	14.25	JSS86	0.36 ± 0.09	-0.047 ± 0.086	0.113	0.54
66811	ζ Pup	13.46	13.51	13.56	M78	0.32 ± 0.02	-0.009 ± 0.024	0.023	0.34
68273	γ^2 Vel	12.97	13.13	13.38	FS94	0.25 ± 0.02	0.059 ± 0.026	-0.182	-0.86
71634	HD 71634	14.29	14.32	14.35	CLMS06
72754	FY Vel	14.41	14.45	14.49	CLMS06	0.76 ± 0.10	-0.426 ± 0.096	0.054	0.38
75309	HD 75309	14.52	14.55	14.58	CLMS06	0.63 ± 0.04	-0.296 ± 0.039	0.131	1.44
79186	GX Vel	14.67	14.73	14.79	CLMS06	0.69 ± 0.03	-0.356 ± 0.036	0.141	1.45
79351	a Car	12.34	12.69	13.02	JSS86
81188	κ Vel	13.48	13.71	13.88	JSS86
91824	HD 91824	14.53	14.56	14.59	CLMS06	0.45 ± 0.03	-0.126 ± 0.032	-0.016	-0.22
91983	HD 91983	14.58	14.62	14.66	CLMS06	0.48 ± 0.04	-0.154 ± 0.040	-0.002	-0.02
93030	θ Car	13.47	13.64	13.70	AJS92	0.45 ± 0.03	-0.125 ± 0.033	-0.031	-0.22
93222	HD 93222	14.81	14.81	14.83	LKF05	0.39 ± 0.04	-0.072 ± 0.041	-0.078	-1.04
99857	HD 99857	14.62	14.64	14.66	LKF05	0.54 ± 0.04	-0.213 ± 0.043	-0.044	-0.58
104705	DF Cru	14.62	14.65	14.68	LKF05	0.33 ± 0.05	-0.013 ± 0.046	-0.053	-0.57
106490	δ Cru	12.87	12.94	13.09	JSS86
108248	α^1 Cru	13.17	13.24	13.32	JSS86	0.15 ± 0.05	0.153 ± 0.051	-0.052	-0.39
111934	BU Cru	14.68	14.73	14.78	CLMS06
116658	α Vir	12.19	12.39	12.49	YK79	0.16 ± 0.05	0.142 ± 0.051	-0.291	-1.56
118716	ϵ Cen	13.24	13.34	13.44	JSS86	0.15 ± 0.16	0.154 ± 0.157	0.044	0.11
120324	μ Cen	13.17	13.39	13.62	JSS86	-0.81 ± 3.74	1.060 ± 3.532	0.034	0.00
121263	ζ Cen	12.87	12.99	13.17	JSS86
121968	HD 121968	13.97	14.03	14.09	LKF05	0.26 ± 0.06	0.052 ± 0.060	-0.158	-1.02
124314	HD 124314	13.77	14.81	14.85	LKF05	0.59 ± 0.05	-0.258 ± 0.051	0.018	0.03
127972	η Cen	12.89	12.94	13.04	JSS86
135591	HD 135591	14.28	14.43	∞	JSS86	0.56 ± 0.22	-0.238 ± 0.209
136298	δ Lup	13.07	13.19	13.34	JSS86
138690	γ Lup	12.84	13.19	∞	JSS86
141637	1 Sco	14.10	14.23	14.35	JSS86	0.69 ± 0.05	-0.356 ± 0.051	-0.091	-0.52
143018	π Sco	13.70	13.90	14.10	JJ91	0.71 ± 0.03	-0.371 ± 0.036	0.036	0.17

Table 12—Continued

HD Number ^a	Name	Observed log $N(\text{P II})$				Source ^b	F_*	$[\text{P}_{\text{gas}}/\text{H}]_{\text{fit}}^c$	Residual ^d	Deviation ^e (in σ)
		l.l.	best	u.l.						
(1)	(2)	(3)	(4)	(5)	(6)	(7)	(8)	(9)	(10)	
143118	η Lup A	12.79	12.84	12.99	JSS86	
143275	δ Sco	14.18	14.23	14.30	JSS86	0.90 ± 0.03	-0.551 ± 0.041	0.072	0.63	
144217	β^1 Sco	14.15	14.23	14.30	JSS86	0.81 ± 0.02	-0.471 ± 0.029	0.023	0.26	
144470	α^1 Sco	14.20	14.28	14.35	JSS86	0.81 ± 0.04	-0.466 ± 0.042	-0.027	-0.23	
145502	ν Sco	14.18	14.48	∞	JSS86	0.80 ± 0.11	-0.459 ± 0.109	
147165	σ Sco	14.20	14.28	14.35	JSS86	0.76 ± 0.06	-0.427 ± 0.061	-0.199	-1.00	
147933	ρ Oph A	13.48	13.63	13.93	JSS86	1.09 ± 0.08	-0.737 ± 0.085	-0.878	-3.46	
148184	χ Oph	14.03	14.18	14.30	JSS86	0.96 ± 0.09	-0.609 ± 0.093	-0.060	-0.29	
148594	HD 148594	14.23	14.26	14.29	CLMS06	
148605	22 Sco	14.05	14.38	∞	JSS86	0.53 ± 0.39	-0.205 ± 0.373	
149038	μ Nor	14.15	14.48	∞	JSS86	0.56 ± 0.05	-0.230 ± 0.047	
149757 (-27)	ζ Oph	13.04	13.06	13.08	SCS92	
(-15)		13.67	∞	∞	SCS92	1.05 ± 0.02	-0.692 ± 0.036	
151804	V973 Sco	57.32	∞	∞	JSS86	0.57 ± 0.08	-0.247 ± 0.073	
151890	μ^1 Sco	13.31	13.41	13.51	JSS86	-0.03 ± 3.47	0.323 ± 3.282	-0.039	-0.00	
152590	HD 152590	14.62	14.64	14.66	CLMS06	0.69 ± 0.03	-0.357 ± 0.033	-0.008	-0.12	
154368	V1074 Sco	14.69	14.99	15.29	S++96	0.52 ± 0.07	-0.192 ± 0.064	0.048	0.15	
155806	V1075 Sco	57.35	∞	∞	JSS86	0.62 ± 0.07	-0.293 ± 0.064	
156110	HD 156110	13.68	13.72	13.76	CLMS06	
157246	γ Ara	13.98	14.08	14.18	JSS86	0.46 ± 0.03	-0.138 ± 0.035	-0.031	-0.23	
157857	HD 157857	14.57	14.61	14.65	CLMS06	0.62 ± 0.04	-0.292 ± 0.037	-0.078	-0.90	
158926	λ Sco	12.55	12.59	12.64	Y83	0.31 ± 0.02	0.001 ± 0.023	-0.177	-3.01	
160578	κ Sco	13.14	13.24	13.34	JSS86	0.50 ± 0.07	-0.173 ± 0.071	-0.349	-1.77	
164284	66 Oph	13.38	13.48	13.65	JSS86	0.89 ± 0.18	-0.545 ± 0.171	-0.264	-0.66	
165024	θ Ara	14.03	14.13	14.23	JSS86	0.56 ± 0.03	-0.237 ± 0.036	-0.016	-0.11	
167264	15 Sgr	14.73	14.83	∞	JSS86	0.68 ± 0.16	-0.347 ± 0.149	
175360	HD 175360	14.11	14.20	14.29	CLMS06	
177989	HD 177989	14.40	14.44	14.48	LKF05	0.55 ± 0.05	-0.227 ± 0.045	0.043	0.47	
184915	κ Aql	14.08	14.33	∞	JSS86	0.88 ± 0.05	-0.533 ± 0.053	
185418	HD 185418	14.60	14.63	14.66	CLMS06	0.79 ± 0.03	-0.452 ± 0.038	0.134	1.55	
188209	HD 188209	14.05	14.18	14.28	JSS86	0.66 ± 0.12	-0.332 ± 0.116	-0.031	-0.16	
193322	HD 193322	13.43	13.73	∞	JSS86	
198478	55 Cyg	14.65	14.68	14.71	CLMS06	0.81 ± 0.05	-0.467 ± 0.054	0.063	0.51	
198781	HD 198781	14.38	14.42	14.46	CLMS06	0.59 ± 0.03	-0.260 ± 0.032	-0.008	-0.11	
200120	59 Cyg	13.60	13.78	13.98	JSS86	
201345	HD 201345	14.35	14.41	14.47	CLMS06	0.34 ± 0.04	-0.023 ± 0.041	-0.106	-0.95	
202347	HD 202347	14.26	14.33	14.40	LKF05	0.56 ± 0.06	-0.231 ± 0.061	0.085	0.61	
202904	ν Cyg	13.39	13.49	13.67	JSS86	
203064	68 Cyg	14.00	14.23	∞	JSS86	0.68 ± 0.20	-0.348 ± 0.194	

Table 12—Continued

HD Number ^a	Name	Observed $\log N(\text{P II})$				F_*	$[\text{P}_{\text{gas}}/\text{H}]_{\text{fit}}^{\text{c}}$	Residual ^d	Deviation ^e (in σ)
		l.l.	best	u.l.	Source ^b				
(1)	(2)	(3)	(4)	(5)	(6)	(7)	(8)	(9)	(10)
203532	HD 203532	14.18	14.21	14.24	CLMS06
206773	HD 206773	14.56	14.60	14.64	CLMS06	0.53 ± 0.02	-0.209 ± 0.024	0.022	0.31
208440	HD 208440	14.54	14.61	14.68	CLMS06	0.61 ± 0.04	-0.281 ± 0.041	0.047	0.42
209975	19 Cep	14.23	14.43	∞	JSS86	0.57 ± 0.26	-0.246 ± 0.248
212791	V408 Lac	14.31	14.34	14.37	CLMS06	0.57 ± 0.08	-0.244 ± 0.079	-0.076	-0.38
214080	HD 214080	13.67	13.99	∞	JSS86	0.27 ± 0.10	0.041 ± 0.097
214680	10 Lac	13.83	13.88	13.93	JSS86	0.50 ± 0.06	-0.173 ± 0.062	-0.218	-1.46
214993	12 Lac	13.78	13.88	14.08	JSS86	0.68 ± 0.10	-0.347 ± 0.092	-0.139	-0.64
217675	o And	13.53	13.91	∞	JSS86
218376	1 Cas	14.30	14.48	∞	JSS86	0.60 ± 0.06	-0.272 ± 0.059
218915	HD 218915	14.39	14.46	14.53	LKF05	0.70 ± 0.08	-0.364 ± 0.078	0.029	0.27
219188	HD 219188	13.29	13.44	∞	JSS86	1.24 ± 0.57	-0.875 ± 0.543
220057	HD 220057	14.30	14.33	14.36	CLMS06	0.75 ± 0.05	-0.415 ± 0.054	0.052	0.39
224151	V373 Cas	14.78	14.87	14.96	LKF05	0.46 ± 0.04	-0.144 ± 0.043	0.010	0.09
224572	σ Cas	13.95	14.08	14.18	JSS86	0.76 ± 0.07	-0.422 ± 0.070	-0.021	-0.13

^aTerms in parentheses indicate separate velocity components, if they are explicitly identified and not grouped together; see §4.3

^bCodes in this column are linked to references listed in Table 1

^cThe expected depletion $[\text{P}_{\text{gas}}/\text{H}]$ computed using Eq. 10. The listed errors do not include an overall systematic uncertainty of 0.04 in the solar abundance $\sigma(\text{P}/\text{H})_{\odot}$ in order to show just the formal error that arises from the uncertainties in location of line of best fit and the value of F_* .

^dThe observed $[\text{P}_{\text{gas}}/\text{H}]$ minus that computed using Eq. 10.

^eThe difference shown in the previous column divided by the expected difference due to the uncertainties in both the measured column density and the coefficients that appear in Eq. 10.

Table 13. Observations and Fits for Sulfur

HD Number ^a	Name	Observed $\log N(\text{S II})$				F_*	$[\text{S}_{\text{gas}}/\text{H}]_{\text{fit}}^{\text{c}}$	Residual ^d	Deviation ^e (in σ)
		l.l.	best	u.l.	Source ^b				
(1)	(2)	(3)	(4)	(5)	(6)	(7)	(8)	(9)	(10)
22586	HD 22586	15.05	15.10	15.30	JW96	0.34 ± 0.07	-0.186 ± 0.091	-0.333	-1.47
22928	δ Per	14.75	14.82	14.88	MY82
34029	α Aur	13.59	WRLS02	0.44 ± 0.05	-0.312 ± 0.081
38666	μ Col	15.19	15.21	15.23	H9F99	0.11 ± 0.01	0.102 ± 0.028	-0.010	-0.26
44743	β CMa	14.50	14.54	14.58	DG98	-0.43 ± 0.03	0.790 ± 0.111	0.186	1.41
49798	HD 49798	15.25	15.30	15.50	JW96
66811	ζ Pup	15.17	15.21	15.25	M78	0.32 ± 0.02	-0.164 ± 0.042	0.158	2.24
68273	γ^2 Vel	14.95	15.02	15.11	FS94	0.25 ± 0.02	-0.074 ± 0.037	0.120	1.24
93521 (-66)	HD 93521	14.07	14.10	14.13	SF93	-0.31 ± 0.11	0.634 ± 0.159	-0.308	-0.85
(-58)		14.49	14.51	14.53	SF93	-0.01 ± 0.03	0.250 ± 0.055	-0.344	-3.47
(-51)		14.51	14.54	14.57	SF93	-0.04 ± 0.04	0.289 ± 0.069	-0.213	-1.60
(-39)		13.96	14.03	14.10	SF93	0.01 ± 0.08	0.235 ± 0.110	-0.349	-1.46
(-29)		12.97	13.17	13.37	SF93	0.34 ± 0.17	-0.187 ± 0.214	-0.287	-0.64
(-18)		14.50	14.52	14.54	SF93	0.00 ± 0.03	0.239 ± 0.052	-0.263	-2.94
(-10)		14.55	14.67	14.69	SF93	0.02 ± 0.04	0.216 ± 0.060	-0.170	-1.47
(+3)		14.51	14.53	14.55	SF93	0.25 ± 0.04	-0.075 ± 0.054	0.041	0.42
(+7)		13.92	13.98	14.04	SF93	0.23 ± 0.12	-0.053 ± 0.153	-0.021	-0.07
(total)		15.28	15.33	15.36	SF93	0.06 ± 0.04	0.169 ± 0.054	-0.200	-2.08
116658	α Vir	14.46	14.50	14.54	YK79	0.16 ± 0.05	0.038 ± 0.066	0.206	1.63
158926	λ Sco	14.51	14.54	14.57	Y83	0.31 ± 0.02	-0.150 ± 0.040	0.204	3.49
215733 (-93)	HD 215733	12.82	12.95	13.08	FS97	-0.27 ± 0.19	0.580 ± 0.253	-0.284	-0.60
(-61)		12.88	13.20	13.52	FS97	1.06 ± 0.21	-1.098 ± 0.303	-0.406	-0.72
(-59)		14.17	14.22	14.27	FS97	-0.11 ± 0.10	0.382 ± 0.134	-0.376	-1.23
(-54)		14.44	14.47	14.50	FS97	0.54 ± 0.15	-0.443 ± 0.201	0.019	0.04
(-47)		14.44	14.50	14.56	FS97
(-42)		13.57	13.82	14.07	FS97	-0.16 ± 0.31	0.448 ± 0.398	-0.422	-0.43
(-40)		13.65	13.78	13.91	FS97	0.18 ± 0.24	0.014 ± 0.308	-0.308	-0.45
(-32)		14.40	14.58	14.76	FS97	0.25 ± 0.09	-0.069 ± 0.116	-0.255	-1.00
(-31)		13.98	14.15	14.32	FS97
(-28)		14.37	14.49	14.61	FS97	-0.18 ± 0.07	0.474 ± 0.104	-0.158	-0.83
(-26)		14.50	14.62	14.74	FS97	-0.12 ± 0.07	0.397 ± 0.099	-0.151	-0.77
(-23)		12.92	13.52	14.12	FS97	0.24 ± 0.08	-0.064 ± 0.106	-0.930	-1.52
(-21)		14.53	14.63	14.73	FS97	0.24 ± 0.05	-0.057 ± 0.070	0.053	0.37
(-19)		13.35	13.69	14.03	FS97
(-16)		14.46	14.77	15.08	FS97	0.93 ± 0.05	-0.927 ± 0.143	0.323	0.94
(-9)		15.43	15.47	15.51	FS97	0.08 ± 0.04	0.142 ± 0.053	-0.006	-0.06
(+1)		13.56	13.71	13.86	FS97	0.90 ± 0.05	-0.898 ± 0.140	-0.366	-1.73
(total)		15.71	15.80	15.91	FS97

^aTerms in parentheses indicate separate velocity components, if they are explicitly identified and not grouped together; see §4.3

^bCodes in this column are linked to references listed in Table 1

^cThe expected depletion $[S_{\text{gas}}/H]$ computed using Eq. 10. The listed errors do not include an overall systematic uncertainty of 0.04 in the solar abundance $\sigma(S/H)_{\odot}$ in order to show just the formal error that arises from the uncertainties in location of line of best fit and the value of F_* .

^dThe observed $[S_{\text{gas}}/H]$ minus that computed using Eq. 10.

^eThe difference shown in the previous column divided by the expected difference due to the uncertainties in both the measured column density and the coefficients that appear in Eq. 10.

Table 14. Observations and Fits for Chlorine

HD Number ^a	Name	Observed $\log N(\text{Cl II})$				F_*	$[\text{Cl}_{\text{gas}}/\text{H}]_{\text{fit}}^c$	Residual ^d	Deviation ^e (in σ)
		l.l.	best	u.l.	Source ^b				
(1)	(2)	(3)	(4)	(5)	(6)	(7)	(8)	(9)	(10)
2905	κ Cas	13.85	14.21	15.11	JSS86	0.58 ± 0.06	-0.280 ± 0.076	-0.134	-0.21
5394	γ Cas	12.62	13.05	13.25	JSS86	0.52 ± 0.04	-0.199 ± 0.059	-0.243	-0.73
21278	HD 21278	14.25	14.55	∞	JSS86
21856	HD 21856	...	13.48	13.95	JSS86	0.67 ± 0.39	-0.394 ± 0.484
22928	δ Per	12.73	JSS86
22951	40 Per	14.24	14.33	14.54	JSS86	0.73 ± 0.05	-0.467 ± 0.070	0.241	1.23
23180	o Per	...	13.41	13.73	JSS86	0.84 ± 0.06	-0.606 ± 0.090
23408	20 Tau	12.76	14.06	15.14	JSS86
23480	23 Tau	13.23	13.68	14.55	JSS86
23630	η Tau	∞	JSS86
24398	ζ Per	13.15	S77	0.88 ± 0.05	-0.657 ± 0.076
24760	ϵ Per	13.00	13.19	13.30	JSS86	0.68 ± 0.04	-0.402 ± 0.055	-0.241	-1.33
24912	ξ Per	14.30	14.54	15.11	JSS86	0.83 ± 0.02	-0.591 ± 0.049	0.505	1.23
29248	ν Eri	13.50	13.64	13.79	JSS86
30614	α Cam	13.46	13.92	14.08	JSS86	0.46 ± 0.04	-0.125 ± 0.060	-0.377	-1.16
34816	λ Lep	12.03	12.90	13.16	JSS86	0.45 ± 0.05	-0.123 ± 0.072	-0.490	-0.85
35149	23 Ori	12.86	13.57	14.22	JSS86	0.54 ± 0.04	-0.228 ± 0.054	-0.166	-0.24
35439	25 Ori	13.22	13.67	14.22	JSS86	0.72 ± 0.18	-0.454 ± 0.222	0.437	0.75
35715	ψ Ori	13.22	13.62	13.79	JSS86	0.66 ± 0.11	-0.382 ± 0.142	0.179	0.48
36166	HD 36166	12.91	13.71	∞	JSS86
36486	δ Ori A	13.11	13.23	13.32	JSS86	0.54 ± 0.02	-0.230 ± 0.036	-0.062	-0.53
36822	ϕ^1 Ori	13.27	13.49	13.61	JSS86	0.74 ± 0.08	-0.479 ± 0.105	-0.200	-0.93
36861	λ Ori A	13.67	13.74	13.80	JSS86	0.57 ± 0.04	-0.261 ± 0.056	-0.129	-0.92
37043	ι Ori	12.96	13.10	13.19	JSS86	0.41 ± 0.03	-0.067 ± 0.049	-0.315	-2.20
37128	ϵ Ori	13.44	13.51	13.56	JSS86	0.54 ± 0.03	-0.229 ± 0.045	-0.043	-0.37
37468	σ Ori	13.64	13.72	13.78	JSS86	0.58 ± 0.04	-0.282 ± 0.058	0.150	1.19
38771	κ Ori	13.37	13.47	13.54	JSS86	0.67 ± 0.03	-0.386 ± 0.042	0.004	0.04
40111	139 Tau	13.86	13.97	14.06	JSS86	0.49 ± 0.04	-0.166 ± 0.054	-0.150	-1.09
41161	HD 41161	14.02	∞	∞	OH06	0.44 ± 0.04	-0.104 ± 0.060
44506	HD 44506	13.78	14.12	14.28	JSS86	-0.03 ± 0.23	0.480 ± 0.294	0.221	0.39
47839	15 Mon	13.38	13.57	13.77	JY78	0.25 ± 0.05	0.133 ± 0.078	-0.198	-0.84
52918	19 Mon	...	12.52	13.32	JSS86	0.44 ± 0.24	-0.109 ± 0.304
54662	HD 54662	13.71	14.03	14.23	JSS86	0.89 ± 0.09	-0.658 ± 0.122	-0.059	-0.19
55879	HD 55879	14.56	JSS86
57060	29 CMa	13.81	14.08	14.21	JSS86	0.50 ± 0.05	-0.180 ± 0.065	0.228	1.01
57061	τ CMa	13.88	14.03	14.14	JSS86	0.39 ± 0.04	-0.038 ± 0.066	0.036	0.24
64740	HD 64740	13.58	13.89	14.96	JSS86	0.27 ± 0.30	0.104 ± 0.378	0.402	0.48
64760	HD 64760	13.41	13.55	13.64	JSS86	0.35 ± 0.06	0.001 ± 0.083	-0.043	-0.24
65575	χ Car	12.55	13.05	13.27	JSS86

Table 14—Continued

HD Number ^a	Name	Observed $\log N(\text{Cl II})$				F_*	$[\text{Cl}_{\text{gas}}/\text{H}]_{\text{fit}}^c$	Residual ^d	Deviation ^e (in σ)
		l.l.	best	u.l.	Source ^b				
(1)	(2)	(3)	(4)	(5)	(6)	(7)	(8)	(9)	(10)
65818	V Pup	13.84	14.01	14.13	JSS86	0.36 ± 0.09	-0.008 ± 0.119	0.165	0.70
66811	ζ Pup	13.30	13.45	13.60	M78	0.32 ± 0.02	0.041 ± 0.050	0.124	0.76
68273	γ^2 Vel	...	12.86	13.24	JSS86	0.25 ± 0.02	0.130 ± 0.058
81188	κ Vel	12.41	13.00	13.16	JSS86
93030	θ Car	13.34	13.48	13.56	AJS92	0.45 ± 0.03	-0.111 ± 0.052	0.006	0.04
106490	δ Cru	12.89	13.07	13.19	JSS86
108248	α^1 Cru	12.96	13.02	13.08	JSS86	0.15 ± 0.05	0.254 ± 0.088	-0.166	-1.13
113904	θ Mus	...	13.31	13.70	JSS86
116658	α Vir	12.52	12.78	12.94	YK79	0.16 ± 0.05	0.240 ± 0.087	0.206	0.83
118716	ϵ Cen	12.92	13.07	13.17	JSS86	0.15 ± 0.16	0.256 ± 0.214	-0.120	-0.28
120324	μ Cen	13.22	13.57	13.80	JSS86	-0.81 ± 3.74	1.446 ± 4.645	0.034	0.00
121263	ζ Cen	...	12.42	12.76	JSS86
127972	η Cen	...	12.12	12.59	JSS86
135591	HD 135591	14.32	14.47	15.32	JSS86	0.56 ± 0.22	-0.259 ± 0.275	0.277	0.47
136298	δ Lup	13.15	13.29	13.39	JSS86
138690	γ Lup	12.85	13.23	13.41	JSS86
141637	1 Sco	13.85	14.13	14.30	JSS86	0.69 ± 0.05	-0.415 ± 0.068	0.079	0.30
143118	η Lup A	12.99	13.16	13.27	JSS86
143275	δ Sco	13.88	13.91	13.93	JSS86	0.90 ± 0.03	-0.671 ± 0.062	0.083	0.76
144217	β^1 Sco	13.81	13.85	13.89	JSS86	0.81 ± 0.02	-0.567 ± 0.044	-0.051	-0.72
144470	α^1 Sco	14.03	14.10	14.17	JSS86	0.81 ± 0.04	-0.560 ± 0.059	0.097	0.80
145502	ν Sco	12.94	13.79	14.46	JSS86	0.80 ± 0.11	-0.550 ± 0.145	-0.119	-0.15
147165	σ Sco	14.19	14.28	14.38	JSS86	0.76 ± 0.06	-0.508 ± 0.082	0.093	0.44
147933	ρ Oph A	13.86	14.08	14.51	JSS86	1.09 ± 0.08	-0.915 ± 0.123	-0.039	-0.11
148184	χ Oph	13.44	13.77	13.96	JSS86	0.96 ± 0.09	-0.747 ± 0.128	-0.120	-0.38
148605	22 Sco	13.45	13.79	14.32	JSS86	0.53 ± 0.39	-0.216 ± 0.491	-0.012	-0.02
149038	μ Nor	14.69	15.51	∞	JSS86	0.56 ± 0.05	-0.249 ± 0.064
151804	V973 Sco	13.81	14.29	14.49	JSS86	0.57 ± 0.08	-0.272 ± 0.097	0.035	0.10
151890	μ^1 Sco	12.95	13.18	13.30	JSS86	-0.03 ± 3.47	0.478 ± 4.315	-0.215	-0.02
155806	V1075 Sco	13.80	13.93	14.02	JSS86	0.62 ± 0.07	-0.332 ± 0.086	-0.206	-1.12
157246	γ Ara	14.23	14.29	14.34	JSS86	0.46 ± 0.03	-0.128 ± 0.053	0.380	3.34
158926	λ Sco	12.90	13.00	13.09	Y83	0.31 ± 0.02	0.055 ± 0.051	0.390	3.49
160578	κ Sco	13.40	13.48	13.53	JSS86	0.50 ± 0.07	-0.174 ± 0.096	0.099	0.51
164284	66 Oph	13.01	13.34	13.52	JSS86	0.89 ± 0.18	-0.663 ± 0.227	-0.074	-0.16
165024	θ Ara	13.88	13.93	13.99	JSS86	0.56 ± 0.03	-0.259 ± 0.050	0.017	0.15
167264	15 Sgr	13.98	JSS86	0.68 ± 0.16	-0.403 ± 0.196
184915	κ Aql	13.42	13.89	14.47	JSS86	0.88 ± 0.05	-0.647 ± 0.075	0.158	0.29
188209	HD 188209	13.83	JSS86	0.66 ± 0.12	-0.383 ± 0.154
193322	HD 193322	...	14.04	∞	JSS86

Table 14—Continued

HD Number ^a	Name	Observed $\log N(\text{Cl II})$				F_*	$[\text{Cl}_{\text{gas}}/\text{H}]_{\text{fit}}^{\text{c}}$	Residual ^d	Deviation ^e (in σ)
		l.l.	best	u.l.	Source ^b				
(1)	(2)	(3)	(4)	(5)	(6)	(7)	(8)	(9)	(10)
200120	59 Cyg	11.52	13.26	13.84	JSS86
202904	ν Cyg	13.14	13.49	13.67	JSS86
203064	68 Cyg	13.71	14.03	14.53	JSS86	0.68 ± 0.20	-0.404 ± 0.255	-0.044	-0.09
209975	19 Cep	13.93	14.29	15.13	JSS86	0.57 ± 0.26	-0.270 ± 0.327	0.043	0.06
214080	HD 214080	13.99	JSS86	0.27 ± 0.10	0.107 ± 0.135
214680	10 Lac	13.36	13.55	13.65	JSS86	0.50 ± 0.06	-0.174 ± 0.084	-0.336	-1.60
214993	12 Lac	13.33	13.71	13.91	JSS86	0.68 ± 0.10	-0.403 ± 0.122	-0.042	-0.12
217675	\omicron And	...	12.82	14.93	JSS86
218376	1 Cas	13.47	13.90	14.36	JSS86	0.60 ± 0.06	-0.305 ± 0.080	-0.197	-0.42
219188	HD 219188	15.01	JSS86	1.24 ± 0.57	-1.097 ± 0.716
224572	σ Cas	12.96	13.37	13.56	JSS86	0.76 ± 0.07	-0.501 ± 0.094	-0.441	-1.33

^aTerms in parentheses indicate separate velocity components, if they are explicitly identified and not grouped together; see §4.3

^bCodes in this column are linked to references listed in Table 1

^cThe expected depletion $[\text{Cl}_{\text{gas}}/\text{H}]$ computed using Eq. 10. The listed errors do not include an overall systematic uncertainty of 0.06 in the solar abundance $\sigma(\text{Cl}/\text{H})_{\odot}$ in order to show just the formal error that arises from the uncertainties in location of line of best fit and the value of F_* .

^dThe observed $[\text{Cl}_{\text{gas}}/\text{H}]$ minus that computed using Eq. 10.

^eThe difference shown in the previous column divided by the expected difference due to the uncertainties in both the measured column density and the coefficients that appear in Eq. 10.

Table 15. Observations and Fits for Titanium

HD Number ^a	Name	Observed $\log N(\text{Ti II})$				F_*	$[\text{Ti}_{\text{gas}}/\text{H}]_{\text{fit}}^c$	Residual ^d	Deviation ^e (in σ)
		l.l.	best	u.l.	Source ^b				
(1)	(2)	(3)	(4)	(5)	(6)	(7)	(8)	(9)	(10)
2905	κ Cas	12.03	12.09	12.15	S78	0.58 ± 0.06	-2.266 ± 0.120	0.069	0.39
5394	γ Cas	11.01	11.09	11.17	S78	0.52 ± 0.04	-2.133 ± 0.087	0.067	0.45
18100	HD 18100	10.93	A++93	0.14 ± 0.04	-1.356 ± 0.094
22586	HD 22586	11.38	11.58	11.78	JW96*	0.34 ± 0.07	-1.773 ± 0.136	-0.006	-0.02
22928	δ Per	10.45	10.62	10.89	S78
22951	40 Per	11.70	11.77	11.84	S78	0.73 ± 0.05	-2.575 ± 0.107	0.126	0.75
23180	o Per	11.30	11.43	11.56	S78	0.84 ± 0.06	-2.804 ± 0.136	0.045	0.21
23630	η Tau	10.69	10.84	10.99	S78
24398	ζ Per	11.15	11.24	11.33	S78	0.88 ± 0.05	-2.888 ± 0.108	-0.065	-0.36
24760	ϵ Per	11.04	11.11	11.18	S78	0.68 ± 0.04	-2.469 ± 0.082	0.081	0.57
24912	ξ Per	11.52	11.57	11.62	S78	0.83 ± 0.02	-2.780 ± 0.058	0.060	0.56
30614	α Cam	12.13	12.19	12.25	S78	0.46 ± 0.04	-2.012 ± 0.086	0.115	0.89
34816	λ Lep	11.13	11.18	11.23	W++97	0.45 ± 0.05	-2.007 ± 0.107	0.004	0.03
35149	23 Ori	11.18	11.21	11.24	W++99	0.54 ± 0.04	-2.181 ± 0.079	-0.244	-1.53
36486	δ Ori A	11.11	11.15	11.19	PTH05	0.54 ± 0.02	-2.184 ± 0.044	0.144	2.01
36861	λ Ori A	11.63	11.68	11.73	S78	0.57 ± 0.04	-2.236 ± 0.084	0.121	0.82
37043	ι Ori	11.28	11.31	11.34	PTH05	0.41 ± 0.03	-1.916 ± 0.057	0.076	0.83
37128	ϵ Ori	11.37	11.40	11.43	PTH05	0.54 ± 0.03	-2.183 ± 0.062	0.133	1.17
37468	σ Ori	11.01	11.10	11.19	S78	0.58 ± 0.04	-2.271 ± 0.087	-0.145	-0.94
37742	ζ Ori A	11.12	11.18	11.24	S78	0.57 ± 0.05	-2.235 ± 0.109	0.009	0.06
38666	μ Col	11.48	11.50	11.52	LHW08	0.11 ± 0.01	-1.304 ± 0.029	-0.056	-1.36
38771	κ Ori	10.96	11.06	11.16	S78	0.67 ± 0.03	-2.442 ± 0.059	-0.014	-0.11
40111	139 Tau	11.95	12.02	12.09	S78	0.49 ± 0.04	-2.079 ± 0.077	0.148	1.14
41161	HD 41161	12.09	12.13	12.17	EPL07	0.44 ± 0.04	-1.977 ± 0.084	0.031	0.25
42933	δ Pic	11.44	11.50	11.56	W++97	0.32 ± 0.06	-1.731 ± 0.121	-0.002	-0.01
44743	β CMa	10.50	W++97	-0.43 ± 0.03	-0.188 ± 0.088
47839	15 Mon	11.73	11.82	11.91	S78	0.25 ± 0.05	-1.586 ± 0.097	0.100	0.60
52089	ϵ CMa	10.36	W++97
53138	o ² Cma	11.44	11.50	11.56	W++97	0.10 ± 0.53	-1.277 ± 1.090	-0.011	-0.01
53975	HD 53975	12.24	12.28	12.32	EPL07	0.45 ± 0.03	-1.997 ± 0.061	0.137	1.46
57060	29 CMa	11.34	11.45	11.56	S78	0.50 ± 0.05	-2.103 ± 0.098	-0.143	-0.83
66811	ζ Pup	11.03	11.07	11.11	EPL07	0.32 ± 0.02	-1.737 ± 0.042	-0.153	-2.17
68273	γ^2 Vel	11.08	11.10	11.12	EPL07	0.25 ± 0.02	-1.591 ± 0.045	-0.019	-0.31
72089 (+5)	HD 72089	11.32	11.42	11.52	WG92
72127	HD 72127	11.43	11.53	11.63	WG92
74575	α Pyx	11.65	11.72	11.79	W++97	0.33 ± 0.09	-1.746 ± 0.178	-0.001	-0.01
91316	ρ Leo	11.84	11.88	11.92	S78	0.15 ± 0.04	-1.390 ± 0.083	0.026	0.20
93030	θ Car	11.30	11.31	11.32	EPL07	0.45 ± 0.03	-1.988 ± 0.067	0.038	0.37
93205	V560 Car	12.51	12.61	12.71	WG92	0.40 ± 0.03	-1.893 ± 0.058	0.106	0.87

Table 15—Continued

HD Number ^a	Name	Observed $\log N(\text{Ti II})$				F_*	$[\text{Ti}_{\text{gas}}/\text{H}]_{\text{fit}}^c$	Residual ^d	Deviation ^e (in σ)
		l.l.	best	u.l.	Source ^b				
(1)	(2)	(3)	(4)	(5)	(6)	(7)	(8)	(9)	(10)
93521 (–66)	HD 93521	10.98	11.08	11.18	SF93	-0.31 ± 0.11	-0.440 ± 0.226	0.008	0.02
(–58)		11.40	11.42	11.48	SF93	-0.01 ± 0.03	-1.065 ± 0.072	0.143	1.24
(–51)		11.04	11.17	11.30	SF93	-0.04 ± 0.04	-1.001 ± 0.095	–0.031	–0.16
(–39)		10.34	10.68	11.02	SF93	0.01 ± 0.08	-1.088 ± 0.172	–0.114	–0.26
(–18)		11.28	11.36	11.44	SF93	0.00 ± 0.03	-1.082 ± 0.067	0.160	1.28
(–10)		11.12	11.30	11.38	SF93	0.02 ± 0.04	-1.119 ± 0.086	0.057	0.34
(+3)		10.68	10.85	11.02	SF93	0.25 ± 0.04	-1.593 ± 0.078	0.141	0.69
(total)		11.93	12.03	12.14	SF93	0.06 ± 0.04	-1.196 ± 0.078	0.127	0.85
116658	α Vir	10.36	10.49	10.62	LHW08	0.16 ± 0.05	-1.409 ± 0.103	–0.101	–0.52
119608	HD 119608	12.30	12.34	12.38	A++93
120086	HD 120086	11.68	11.88	12.08	JW96
121968	HD 121968	12.03	12.06	12.09	LP95	0.26 ± 0.06	-1.605 ± 0.127	0.067	0.37
122451	β Cen	11.01	11.05	11.09	EPL07	0.23 ± 0.03	-1.554 ± 0.061	0.064	0.72
125924	HD 125924	12.08	12.13	12.18	LP95	0.20 ± 0.08	-1.493 ± 0.171	–0.007	–0.03
143018	π Sco	10.75	10.85	10.95	S78	0.71 ± 0.03	-2.522 ± 0.072	–0.316	–2.30
143275	δ Sco	10.90	10.97	11.04	S78	0.90 ± 0.03	-2.912 ± 0.078	–0.280	–2.06
144217	β^1 Sco	11.11	11.18	11.25	S78	0.81 ± 0.02	-2.739 ± 0.051	–0.212	–2.26
144470	σ^1 Sco	11.29	11.39	11.49	S78	0.81 ± 0.04	-2.728 ± 0.083	–0.108	–0.71
145502	ν Sco	11.29	11.41	11.53	S78	0.80 ± 0.11	-2.712 ± 0.234	–0.001	–0.00
147165	σ Sco	11.39	11.47	11.55	S78	0.76 ± 0.06	-2.643 ± 0.127	–0.245	–1.07
149038	μ Nor	11.94	11.99	12.04	W++97	0.56 ± 0.05	-2.216 ± 0.098	0.008	0.06
149757 (–27)	ζ Oph	11.23	11.28	11.33	W++97
(–15)		10.92	11.02	11.12	W++97	1.05 ± 0.02	-3.218 ± 0.057	0.083	0.66
149881	V600 Her	12.40	12.48	12.54	A++03	0.07 ± 0.06	-1.212 ± 0.131	0.040	0.17
152236	ζ^1 Sco	12.17	12.24	12.31	W++97	0.80 ± 0.06	-2.723 ± 0.120	0.117	0.66
154368	V1074 Sco	11.85	12.15	12.45	S++96	0.52 ± 0.07	-2.133 ± 0.136	–0.302	–0.90
157246	γ Ara	11.49	11.54	11.59	W++97	0.46 ± 0.03	-2.017 ± 0.071	–0.152	–1.24
158243	V861 Ara	12.45	12.47	12.49	LP95
158408	ν Sco	10.74	S78
158926	λ Sco	10.74	S78	0.31 ± 0.02	-1.715 ± 0.040
163522	HD 163522	12.74	12.76	12.78	LP95
164794	9 Sgr	11.76	11.83	11.90	W++97
165024	θ Ara	11.58	11.63	11.68	W++97	0.56 ± 0.03	-2.232 ± 0.073	0.019	0.15
179406	20 Aql	12.83	12.93	13.03	W++97
179407	HD 179407	12.39	12.41	12.44	LP95	0.35 ± 0.05	-1.799 ± 0.096	–0.000	–0.00
184915	κ Aql	11.11	11.18	11.25	W++97	0.88 ± 0.05	-2.873 ± 0.107	0.002	0.01
191877	HD 191877	12.22	12.24	12.26	PTH05	0.39 ± 0.04	-1.883 ± 0.091	0.001	0.01
195455	HD 195455	12.14	12.16	12.19	LP95
195965	HD 195965	12.00	12.02	12.04	PTH05	0.52 ± 0.02	-2.136 ± 0.036	0.022	0.47

Table 15—Continued

HD Number ^a	Name	Observed $\log N(\text{Ti II})$				F_*	$[\text{Ti}_{\text{gas}}/\text{H}]_{\text{fit}}^{\text{c}}$	Residual ^d	Deviation ^e (in σ)
		l.l.	best	u.l.	Source ^b				
(1)	(2)	(3)	(4)	(5)	(6)	(7)	(8)	(9)	(10)
200120	59 Cyg	11.41	11.52	11.63	S78
202904	<i>v</i> Cyg	11.26	11.35	11.44	S78
206144	HD 206144	12.16	12.20	12.23	LP95
206773	HD 206773	12.14	12.16	12.18	EPL07	0.53 ± 0.02	-2.172 ± 0.045	0.081	1.13
210839	λ Cep	12.08	12.14	12.20	S78	0.66 ± 0.03	-2.423 ± 0.071	0.120	1.07
214080	HD 214080	11.96	12.04	12.10	A++93	0.27 ± 0.10	-1.628 ± 0.208	0.052	0.17
214680	10 Lac	11.68	11.74	11.80	S78	0.50 ± 0.06	-2.092 ± 0.131	0.109	0.57
217675	o And	11.06	11.14	11.22	S78
218376	1 Cas	11.76	11.83	11.90	S78	0.60 ± 0.06	-2.308 ± 0.126	0.072	0.40
303308	HDE 303308	12.63	12.73	12.83	WG92	0.38 ± 0.04	-1.861 ± 0.080	0.116	0.81

^aTerms in parentheses indicate separate velocity components, if they are explicitly identified and not grouped together; see §4.3

^bCodes in this column are linked to references listed in Table 1

^cThe expected depletion $[\text{Ti}_{\text{gas}}/\text{H}]$ computed using Eq. 10. The listed errors do not include an overall systematic uncertainty of 0.03 in the solar abundance $\sigma(\text{Ti}/\text{H})_{\odot}$ in order to show just the formal error that arises from the uncertainties in location of line of best fit and the value of F_* .

^dThe observed $[\text{Ti}_{\text{gas}}/\text{H}]$ minus that computed using Eq. 10.

^eThe difference shown in the previous column divided by the expected difference due to the uncertainties in both the measured column density and the coefficients that appear in Eq. 10.

Table 16. Observations and Fits for Chromium

HD Number ^a	Name	Observed $\log N(\text{Cr II})$				F_*	$[\text{Cr}_{\text{gas}}/\text{H}]_{\text{fit}}^{\text{c}}$	Residual ^d	Deviation ^e (in σ)
		l.l.	best	u.l.	Source ^b				
(1)	(2)	(3)	(4)	(5)	(6)	(7)	(8)	(9)	(10)
18100	HD 18100	12.87	12.91	12.95	SS96b	0.14 ± 0.04	-1.024 ± 0.071	0.061	0.39
23630	η Tau	11.81	11.86	11.91	RB95
24912	ξ Per	12.88	12.90	12.91	C++91	0.83 ± 0.02	-2.030 ± 0.047	-0.080	-0.88
35149	23 Ori	12.73	12.74	12.75	W++99	0.54 ± 0.04	-1.607 ± 0.059	-0.004	-0.02
36486	δ Ori A	12.04	12.09	12.14	RB95	0.54 ± 0.02	-1.609 ± 0.036	-0.213	-2.89
37128	ϵ Ori	12.40	12.45	12.50	RB95	0.54 ± 0.03	-1.609 ± 0.048	-0.113	-1.00
38666	μ Col	12.60	12.63	12.66	HSF99	0.11 ± 0.01	-0.988 ± 0.034	0.036	0.73
47839	15 Mon	12.81	12.86	12.91	RB95	0.25 ± 0.05	-1.187 ± 0.072	0.015	0.11
57061	τ CMa	11.87	12.92	12.97	RB95	0.39 ± 0.04	-1.386 ± 0.066	-0.116	-0.21
66811	ζ Pup	12.04	12.24	12.44	M78	0.32 ± 0.02	-1.294 ± 0.036	-0.149	-0.72
72127	HD 72127	12.42	12.47	12.52	RB95
91316	ρ Leo	12.82	12.87	12.92	RB95	0.15 ± 0.04	-1.048 ± 0.064	-0.052	-0.43
116658	α Vir	12.32	YK79	0.16 ± 0.05	-1.062 ± 0.077
141637	1 Sco	13.00	13.05	13.10	RB95	0.69 ± 0.05	-1.825 ± 0.078	0.019	0.13
143018	π Sco	12.59	12.64	12.69	RB95	0.71 ± 0.03	-1.848 ± 0.055	0.074	0.77
144217	β^1 Sco	12.93	12.98	13.03	RB95	0.81 ± 0.02	-2.002 ± 0.043	0.125	1.65
147165	σ Sco	13.45	13.50	13.55	RB95	0.76 ± 0.06	-1.934 ± 0.093	0.349	1.71
149757 (-27)	ζ Oph	12.32	12.36	12.40	SCS92
(-15)		12.50	12.53	12.56	SCS92	1.05 ± 0.02	-2.340 ± 0.051	0.001	0.01
149881	V600 Her	13.39	13.44	13.49	RB95	0.07 ± 0.06	-0.922 ± 0.097	-0.010	-0.04
158926	λ Sco	11.71	11.76	11.81	RB95	0.31 ± 0.02	-1.278 ± 0.035	0.086	1.26
167756	HD 167756	13.26	13.29	13.32	CSS95
212571	π Aqr	12.74	12.79	12.84	RB95
215733 (-59)	HD 215733	12.11	12.18	12.25	FS97	-0.11 ± 0.10	-0.667 ± 0.148	0.177	0.56
(-54)		12.04	12.12	12.20	FS97	0.54 ± 0.15	-1.614 ± 0.219	0.384	0.81
(-47)		12.22	12.31	12.40	FS97
(-42)		11.71	11.93	12.15	FS97	-0.16 ± 0.31	-0.591 ± 0.454	0.271	0.27
(-40)		11.69	11.89	12.09	FS97	0.18 ± 0.24	-1.089 ± 0.354	0.449	0.62
(-32)		11.81	12.10	12.39	FS97	0.25 ± 0.09	-1.184 ± 0.132	-0.076	-0.22
(-31)		12.09	12.23	12.37	FS97
(-28)		11.84	12.05	12.26	FS97	-0.18 ± 0.07	-0.561 ± 0.106	-0.019	-0.07
(-26)		12.21	12.33	12.45	FS97	-0.12 ± 0.07	-0.650 ± 0.105	0.150	0.75
(-23)		11.76	11.99	12.22	FS97	0.24 ± 0.08	-1.179 ± 0.120	0.199	0.75
(-21)		11.62	11.87	12.12	FS97	0.24 ± 0.05	-1.170 ± 0.079	-0.050	-0.18
(-19)		11.39	11.69	11.99	FS97
(-16)		9.08	10.48	11.88	FS97	0.93 ± 0.05	-2.169 ± 0.083	-1.181	-0.84
(-11)		11.91	12.18	12.45	FS97	-0.01 ± 0.07	-0.817 ± 0.110	-0.323	-1.09
(-9)		12.67	12.79	12.91	FS97	0.08 ± 0.04	-0.942 ± 0.061	-0.058	-0.37
(-5)		11.03	11.55	12.07	FS97	0.77 ± 0.18	-1.944 ± 0.261	0.194	0.33

Table 16—Continued

HD Number ^a	Name	Observed $\log N(\text{Cr II})$			Source ^b	F_*	$[\text{Cr}_{\text{gas}}/\text{H}]_{\text{fit}}^c$	Residual ^d	Deviation ^e (in σ)
		l.l.	best	u.l.					
(1)	(2)	(3)	(4)	(5)	(6)	(7)	(8)	(9)	(10)
(+1)		11.35	11.67	11.99	FS97	0.90 ± 0.05	-2.136 ± 0.084	0.376	1.12
(total)		13.21	13.37	13.55	FS97

^aTerms in parentheses indicate separate velocity components, if they are explicitly identified and not grouped together; see §4.3

^bCodes in this column are linked to references listed in Table 1

^cThe expected depletion $[\text{Cr}_{\text{gas}}/\text{H}]$ computed using Eq. 10. The listed errors do not include an overall systematic uncertainty of 0.05 in the solar abundance $\sigma(\text{Cr}/\text{H})_{\odot}$ in order to show just the formal error that arises from the uncertainties in location of line of best fit and the value of F_* .

^dThe observed $[\text{Cr}_{\text{gas}}/\text{H}]$ minus that computed using Eq. 10.

^eThe difference shown in the previous column divided by the expected difference due to the uncertainties in both the measured column density and the coefficients that appear in Eq. 10.

Table 17. Observations and Fits for Manganese

HD Number ^a	Name	Observed $\log N(\text{Mn II})$				F_*	$[\text{Mn}_{\text{gas}}/\text{H}]_{\text{fit}}^{\text{c}}$	Residual ^d	Deviation ^e (in σ)
		l.l.	best	u.l.	Source ^b				
(1)	(2)	(3)	(4)	(5)	(6)	(7)	(8)	(9)	(10)
1383	HD 1383	13.54	13.60	13.66	CLMS06	0.61 ± 0.04	-1.432 ± 0.039	-0.054	-0.52
2905	κ Cas	13.36	13.41	13.85	JSS86	0.58 ± 0.06	-1.406 ± 0.051	-0.058	-0.21
5394	γ Cas	12.44	12.50	12.57	JSS86	0.52 ± 0.04	-1.350 ± 0.037	0.108	0.92
12323	HD 12323	13.45	13.53	13.61	CLMS06	0.52 ± 0.04	-1.357 ± 0.033	0.019	0.17
13268	HD 13268	13.55	13.59	13.63	CLMS06	0.51 ± 0.04	-1.349 ± 0.036	-0.060	-0.66
14434	HD 14434	13.53	13.60	13.67	CLMS06	0.52 ± 0.04	-1.352 ± 0.038	-0.097	-0.90
18100	HD 18100	12.71	12.74	12.77	SS96b	0.14 ± 0.04	-1.025 ± 0.043	0.036	0.25
21278	HD 21278	...	11.90	14.15	JSS86
21856	HD 21856	12.57	13.22	14.07	JSS86	0.67 ± 0.39	-1.485 ± 0.334	0.017	0.02
22928	δ Per	12.31	12.52	12.90	JSS86
22951	40 Per	13.23	13.33	13.63	JSS86	0.73 ± 0.05	-1.535 ± 0.046	0.060	0.26
23180	o Per	13.06	13.18	13.30	S76	0.84 ± 0.06	-1.631 ± 0.058	0.038	0.23
23408	20 Tau	...	13.08	∞	JSS86
23480	23 Tau	...	12.60	∞	JSS86
23630	η Tau	∞	JSS86
24398	ζ Per	13.12	13.26	13.40	S77	0.88 ± 0.05	-1.666 ± 0.047	0.149	0.81
24760	ϵ Per	12.62	12.67	12.72	JSS86	0.68 ± 0.04	-1.491 ± 0.036	0.077	0.71
24912	ξ Per	13.49	13.52	13.54	C++91	0.83 ± 0.02	-1.621 ± 0.027	0.268	3.17
27778	62 Tau	12.98	13.04	13.10	CLMS06
29248	ν Eri	...	11.17	11.56	JSS86
30614	α Cam	13.01	13.11	13.20	JSS86	0.46 ± 0.04	-1.300 ± 0.037	-0.263	-2.06
31237	π^5 Ori	12.07	12.40	12.65	JSS86	0.52 ± 0.21	-1.354 ± 0.178	0.012	0.02
35149	23 Ori	12.97	13.01	13.04	W++99	0.54 ± 0.04	-1.370 ± 0.034	0.169	1.18
35439	25 Ori	12.11	12.52	12.72	JSS86	0.72 ± 0.18	-1.526 ± 0.152	0.109	0.27
35715	ψ Ori	12.27	12.51	12.65	JSS86	0.66 ± 0.11	-1.477 ± 0.097	-0.086	-0.30
36166	HD 36166	...	12.46	∞	JSS86
36486	δ Ori A	12.22	12.27	12.33	JSS86	0.54 ± 0.02	-1.372 ± 0.020	-0.130	-1.79
36822	ϕ^1 Ori	12.49	12.60	12.69	JSS86	0.74 ± 0.08	-1.544 ± 0.071	-0.275	-1.86
36841	HD 36841	12.83	12.92	13.01	CLMS06
36861	λ Ori A	12.90	12.94	13.00	JSS86	0.57 ± 0.04	-1.393 ± 0.036	-0.047	-0.37
37043	ι Ori	12.52	12.58	12.62	JSS86	0.41 ± 0.03	-1.260 ± 0.026	0.108	1.25
37128	ϵ Ori	12.68	12.72	12.76	JSS86	0.54 ± 0.03	-1.371 ± 0.028	0.059	0.58
37367	HD 37367	13.38	13.42	13.46	CLMS06	0.65 ± 0.07	-1.469 ± 0.059	-0.026	-0.21
37468	σ Ori	12.43	12.50	12.55	JSS86	0.58 ± 0.04	-1.408 ± 0.038	-0.194	-1.67
37903	HD 37903	13.14	13.20	13.26	CLMS06	1.15 ± 0.03	-1.892 ± 0.039	0.073	0.78
38666	μ Col	12.39	12.41	12.43	HSF99	0.11 ± 0.01	-1.004 ± 0.021	-0.027	-0.77
38771	κ Ori	12.37	12.40	12.44	JSS86	0.67 ± 0.03	-1.480 ± 0.026	-0.222	-3.54
40111	139 Tau	13.13	13.16	13.22	JSS86	0.49 ± 0.04	-1.328 ± 0.034	-0.049	-0.50
43818	LU Gem	13.63	13.68	13.73	CLMS06

Table 17—Continued

HD Number ^a	Name	Observed $\log N(\text{Mn II})$				F_*	$[\text{Mn}_{\text{gas}}/\text{H}]_{\text{fit}}^{\text{c}}$	Residual ^d	Deviation ^e (in σ)
		l.l.	best	u.l.	Source ^b				
(1)	(2)	(3)	(4)	(5)	(6)	(7)	(8)	(9)	(10)
44506	HD 44506	12.45	JSS86	-0.03 ± 0.23	-0.882 ± 0.196
44743	β CMa	11.55	11.59	11.63	DG98	-0.43 ± 0.03	-0.537 ± 0.049	0.244	2.79
52266	HD 52266	13.38	13.42	13.46	CLMS06
52918	19 Mon	11.34	12.27	12.48	JSS86	0.44 ± 0.24	-1.288 ± 0.209	-0.220	-0.32
54662	HD 54662	12.91	13.18	13.55	JSS86	0.89 ± 0.09	-1.667 ± 0.081	-0.150	-0.43
55879	HD 55879	...	12.52	∞	JSS86
57060	29 CMa	12.74	12.92	13.00	JSS86	0.50 ± 0.05	-1.338 ± 0.042	-0.024	-0.15
57061	τ CMa	12.82	12.88	12.96	JSS86	0.39 ± 0.04	-1.239 ± 0.039	-0.163	-1.77
63005	HD 63005	13.25	13.31	13.37	CLMS06	0.64 ± 0.03	-1.457 ± 0.028	-0.133	-1.58
64740	HD 64740	...	12.09	12.88	JSS86	0.27 ± 0.30	-1.142 ± 0.259
64760	HD 64760	12.63	12.68	12.72	JSS86	0.35 ± 0.06	-1.213 ± 0.052	0.051	0.39
65575	χ Car	11.45	JSS86
65818	V Pup	12.58	12.75	12.87	JSS86	0.36 ± 0.09	-1.219 ± 0.078	-0.134	-0.62
66811	ζ Pup	12.40	12.44	12.48	M78	0.32 ± 0.02	-1.185 ± 0.021	0.086	1.42
68273	γ^2 Vel	12.31	12.39	12.47	FS94	0.25 ± 0.02	-1.123 ± 0.023	0.222	2.41
71634	HD 71634	13.28	13.34	13.40	CLMS06
75309	HD 75309	13.27	13.31	13.35	CLMS06	0.63 ± 0.04	-1.445 ± 0.035	-0.005	-0.05
79186	GX Vel	13.41	13.48	13.55	CLMS06	0.69 ± 0.03	-1.499 ± 0.032	-0.011	-0.11
79351	a Car	12.72	12.81	∞	JSS86
81188	κ Vel	12.19	12.29	12.37	JSS86
91824	HD 91824	13.36	13.42	13.48	CLMS06	0.45 ± 0.03	-1.290 ± 0.029	-0.036	-0.42
91983	HD 91983	13.41	13.47	13.53	CLMS06	0.48 ± 0.04	-1.316 ± 0.036	-0.035	-0.34
93030	θ Car	12.40	12.54	12.63	AJS92	0.45 ± 0.03	-1.290 ± 0.030	-0.007	-0.05
93521	HD 93521	11.68	11.74	11.80	SF93	-0.31 ± 0.11	-0.642 ± 0.099	0.291	0.84
(-58)		12.18	12.22	12.25	SF93	-0.01 ± 0.03	-0.904 ± 0.036	0.203	2.14
(-51)		12.10	12.14	12.18	SF93	-0.04 ± 0.04	-0.877 ± 0.045	0.236	1.88
(-39)		11.67	11.76	11.85	SF93	0.01 ± 0.08	-0.913 ± 0.075	0.212	0.92
(-29)		10.99	11.18	11.37	SF93	0.34 ± 0.17	-1.200 ± 0.144	0.419	1.01
(-18)		12.02	12.07	12.12	SF93	0.00 ± 0.03	-0.911 ± 0.035	0.120	1.29
(-10)		11.99	12.13	12.17	SF93	0.02 ± 0.04	-0.926 ± 0.041	0.115	0.95
(+3)		11.64	11.71	11.78	SF93	0.25 ± 0.04	-1.124 ± 0.036	-0.047	-0.42
(+7)		11.41	11.52	11.63	SF93	0.23 ± 0.12	-1.109 ± 0.104	0.258	0.88
(total)		12.81	12.88	12.94	SF93	0.06 ± 0.04	-0.958 ± 0.038	0.163	1.62
100340	HD 100340	12.81	12.89	12.97	SS96b	0.10 ± 0.06	-0.992 ± 0.054	-0.157	-1.14
106490	δ Cru	11.72	11.93	12.06	JSS86
108248	α^1 Cru	12.21	12.25	12.29	JSS86	0.15 ± 0.05	-1.038 ± 0.045	0.106	0.91
111934	BU Cru	13.58	13.63	13.68	CLMS06
113904	θ Mus	13.01	13.14	13.29	JSS86
116658	α Vir	11.36	11.55	11.68	YK79	0.16 ± 0.05	-1.048 ± 0.046	0.020	0.10

Table 17—Continued

HD Number ^a	Name	Observed $\log N(\text{Mn II})$				Source ^b	F_*	$[\text{Mn}_{\text{gas}}/\text{H}]_{\text{fit}}^c$	Residual ^d	Deviation ^e (in σ)
		l.l.	best	u.l.						
(1)	(2)	(3)	(4)	(5)	(6)	(7)	(8)	(9)	(10)	
116852	HD 116852	13.38	13.44	13.50	CLMS06	0.36 ± 0.04	-1.213 ± 0.033	0.056	0.53	
120324	μ Cen	...	11.98	12.28	JSS86	-0.81 ± 3.74	-0.216 ± 3.201	
121263	ζ Cen	12.10	12.20	12.29	JSS86	
122879	HD 122879	13.54	13.58	13.62	CLMS06	0.55 ± 0.04	-1.375 ± 0.039	0.038	0.32	
127972	η Cen	12.16	12.24	12.31	JSS86	
135591	HD 135591	13.12	13.25	13.65	JSS86	0.56 ± 0.22	-1.392 ± 0.189	-0.060	-0.17	
136298	δ Lup	12.03	12.15	12.24	JSS86	
138690	γ Lup	11.87	12.19	12.32	JSS86	
141637	1 Sco	13.12	13.20	13.27	JSS86	0.69 ± 0.05	-1.499 ± 0.045	-0.017	-0.12	
143018	π Sco	12.68	12.88	13.08	JJ91	0.71 ± 0.03	-1.513 ± 0.032	0.119	0.56	
143118	η Lup A	11.80	11.96	12.07	JSS86	
143275	δ Sco	13.20	13.22	13.24	JSS86	0.90 ± 0.03	-1.676 ± 0.035	0.148	1.55	
144217	β^1 Sco	13.12	13.15	13.18	JSS86	0.81 ± 0.02	-1.604 ± 0.024	0.037	0.71	
144470	α^1 Sco	13.23	13.29	13.35	JSS86	0.81 ± 0.04	-1.599 ± 0.037	0.077	0.72	
145502	ν Sco	12.87	12.98	13.36	JSS86	0.80 ± 0.11	-1.593 ± 0.098	-0.137	-0.41	
147165	σ Sco	13.41	13.50	13.75	JSS86	0.76 ± 0.06	-1.564 ± 0.054	0.119	0.48	
147888	ρ Oph D	13.37	13.44	13.51	CLMS06	0.88 ± 0.06	-1.663 ± 0.058	-0.217	-1.26	
147933	ρ Oph A	13.24	13.29	13.80	JSS86	1.09 ± 0.08	-1.844 ± 0.075	-0.149	-0.50	
148184	χ Oph	13.22	13.32	13.41	JSS86	0.96 ± 0.09	-1.728 ± 0.084	0.161	0.93	
148594	HD 148594	13.06	13.14	13.22	CLMS06	
148605	22 Sco	12.51	12.94	13.88	JSS86	0.53 ± 0.39	-1.362 ± 0.338	0.034	0.04	
149757 (-27)	ζ Oph	12.16	12.21	12.26	SCS92	
(-15)		13.01	13.04	13.07	SCS92	1.05 ± 0.02	-1.804 ± 0.029	0.111	1.68	
149881	V600 Her	13.30	13.36	13.42	SF95	0.07 ± 0.06	-0.965 ± 0.058	0.097	0.48	
151804	V973 Sco	13.08	13.28	13.64	JSS86	0.57 ± 0.08	-1.401 ± 0.066	-0.096	-0.32	
151890	μ^1 Sco	12.19	12.29	12.36	JSS86	-0.03 ± 3.47	-0.884 ± 2.975	0.006	0.00	
152590	HD 152590	13.47	13.56	13.65	CLMS06	0.69 ± 0.03	-1.500 ± 0.029	0.010	0.10	
154368	V1074 Sco	14.11	14.23	14.33	S++96	0.52 ± 0.07	-1.351 ± 0.057	0.412	3.06	
155806	V1075 Sco	13.26	13.30	13.35	JSS86	0.62 ± 0.07	-1.442 ± 0.058	0.024	0.17	
157246	γ Ara	12.93	12.96	12.99	JSS86	0.46 ± 0.03	-1.302 ± 0.031	-0.026	-0.27	
157857	HD 157857	13.50	13.57	13.64	CLMS06	0.62 ± 0.04	-1.441 ± 0.033	-0.014	-0.14	
160578	κ Sco	12.61	12.67	12.72	JSS86	0.50 ± 0.07	-1.333 ± 0.064	0.199	1.13	
164284	66 Oph	12.72	12.86	12.95	JSS86	0.89 ± 0.18	-1.671 ± 0.155	0.203	0.53	
165024	θ Ara	12.98	13.02	13.08	JSS86	0.56 ± 0.03	-1.392 ± 0.032	-0.010	-0.10	
165955	HD 165955	13.29	13.33	13.37	CLMS06	0.42 ± 0.04	-1.268 ± 0.037	-0.083	-1.01	
167264	15 Sgr	13.11	13.38	13.53	JSS86	0.68 ± 0.16	-1.491 ± 0.135	0.036	0.13	
175360	HD 175360	13.18	13.26	13.34	CLMS06	
184915	κ Aql	13.02	13.22	13.68	JSS86	0.88 ± 0.05	-1.660 ± 0.047	0.250	0.73	
185418	HD 185418	13.54	13.59	13.64	CLMS06	0.79 ± 0.03	-1.586 ± 0.033	0.184	1.96	

Table 17—Continued

HD Number ^a	Name	Observed $\log N(\text{Mn II})$				Source ^b	F_*	$[\text{Mn}_{\text{gas}}/\text{H}]_{\text{fit}}^c$	Residual ^d	Deviation ^e (in σ)
		l.l.	best	u.l.						
(1)	(2)	(3)	(4)	(5)	(6)	(7)	(8)	(9)	(10)	
188209	HD 188209	13.08	13.22	13.36	JSS86	0.66 ± 0.12	-1.477 ± 0.105	0.116	0.56	
190918	V1676 Cyg	13.56	13.62	13.68	CLMS06	0.46 ± 0.03	-1.304 ± 0.031	-0.062	-0.70	
192035	RX Cyg	13.17	13.24	13.31	CLMS06	0.76 ± 0.04	-1.558 ± 0.037	-0.167	-1.64	
192639	HD 192639	13.51	13.59	13.67	CLMS06	0.64 ± 0.04	-1.457 ± 0.035	-0.016	-0.14	
193322	HD 193322	13.35	13.58	∞	JSS86	
198478	55 Cyg	13.51	13.60	13.69	CLMS06	0.81 ± 0.05	-1.600 ± 0.048	0.071	0.48	
198781	HD 198781	13.23	13.28	13.33	CLMS06	0.59 ± 0.03	-1.412 ± 0.029	-0.041	-0.50	
200120	59 Cyg	12.52	12.71	12.87	JSS86	
201345	HD 201345	13.35	13.38	13.41	CLMS06	0.34 ± 0.04	-1.198 ± 0.037	-0.006	-0.06	
202904	ν Cyg	12.33	12.52	12.64	JSS86	
203064	68 Cyg	12.98	13.21	13.64	JSS86	0.68 ± 0.20	-1.492 ± 0.175	-0.026	-0.07	
203532	HD 203532	13.00	13.05	13.10	CLMS06	
206773	HD 206773	13.45	13.50	13.55	CLMS06	0.53 ± 0.02	-1.366 ± 0.021	0.034	0.45	
207198	HD 207198	13.50	13.57	13.64	CLMS06	0.90 ± 0.03	-1.679 ± 0.033	-0.009	-0.10	
208440	HD 208440	13.36	13.42	13.48	CLMS06	0.61 ± 0.04	-1.431 ± 0.037	-0.038	-0.36	
209975	19 Cep	13.15	13.36	13.62	JSS86	0.57 ± 0.26	-1.399 ± 0.225	-0.007	-0.02	
210809	HD 210809	13.55	13.59	13.63	CLMS06	0.41 ± 0.04	-1.262 ± 0.039	-0.062	-0.63	
212791	V408 Lac	13.24	13.28	13.32	CLMS06	0.57 ± 0.08	-1.398 ± 0.072	-0.027	-0.14	
214080	HD 214080	12.54	12.88	13.36	JSS86	0.27 ± 0.10	-1.139 ± 0.088	-0.177	-0.38	
214993	12 Lac	12.94	13.02	13.11	JSS86	0.68 ± 0.10	-1.491 ± 0.083	0.106	0.61	
215733 (-61)	HD 215733	10.89	11.25	11.61	FS97	1.06 ± 0.21	-1.820 ± 0.181	0.052	0.10	
(-59)		11.65	11.76	11.87	FS97	-0.11 ± 0.10	-0.814 ± 0.088	0.046	0.15	
(-54)		11.68	11.75	11.82	FS97	0.54 ± 0.15	-1.374 ± 0.130	-0.084	-0.19	
(-47)		11.90	11.99	12.08	FS97	
(-45)		11.01	11.24	11.47	FS97	-0.40 ± 0.28	-0.562 ± 0.241	0.164	0.26	
(-42)		11.23	11.45	11.67	FS97	-0.16 ± 0.31	-0.769 ± 0.269	0.111	0.12	
(-40)		11.15	11.35	11.55	FS97	0.18 ± 0.24	-1.064 ± 0.210	0.026	0.04	
(-32)		12.14	12.32	12.50	FS97	0.25 ± 0.09	-1.120 ± 0.078	0.222	0.92	
(-31)		11.43	11.64	11.85	FS97	
(-28)		11.61	11.79	11.97	FS97	-0.18 ± 0.07	-0.751 ± 0.064	0.053	0.24	
(-26)		11.89	12.04	12.19	FS97	-0.12 ± 0.07	-0.804 ± 0.063	0.156	0.77	
(-23)		11.64	11.76	11.88	FS97	0.24 ± 0.08	-1.117 ± 0.071	0.049	0.32	
(-21)		11.77	11.88	11.99	FS97	0.24 ± 0.05	-1.112 ± 0.047	0.044	0.32	
(-19)		11.54	11.66	11.78	FS97	
(-16)		11.49	11.61	11.73	FS97	0.93 ± 0.05	-1.703 ± 0.048	-0.375	-2.70	
(-9)		12.88	12.89	12.90	FS97	0.08 ± 0.04	-0.977 ± 0.037	0.219	2.47	
(+1)		11.34	11.48	11.62	FS97	0.90 ± 0.05	-1.683 ± 0.049	-0.125	-0.80	
(total)		13.16	13.24	13.34	FS97	
217675	o And	12.92	13.19	∞	JSS86	

Table 17—Continued

HD Number ^a	Name	Observed $\log N(\text{Mn II})$				F_*	$[\text{Mn}_{\text{gas}}/\text{H}]_{\text{fit}}^{\text{c}}$	Residual ^d	Deviation ^e (in σ)
		l.l.	best	u.l.	Source ^b				
(1)	(2)	(3)	(4)	(5)	(6)	(7)	(8)	(9)	(10)
218376	1 Cas	12.53	12.86	12.99	JSS86	0.60 ± 0.06	-1.423 ± 0.053	-0.368	-1.43
219188	HD 219188	12.05	12.76	13.47	JSS86	1.24 ± 0.57	-1.970 ± 0.491	0.272	0.31
220057	HD 220057	12.98	13.04	13.10	CLMS06	0.75 ± 0.05	-1.553 ± 0.049	-0.145	-1.03
224572	σ Cas	12.94	13.03	13.10	JSS86	0.76 ± 0.07	-1.559 ± 0.063	0.027	0.19
232522	HDE 232522	13.35	13.41	13.47	CLMS06	0.44 ± 0.03	-1.283 ± 0.030	-0.075	-0.89
308813	HDE 308813	13.42	13.46	13.50	CLMS06	0.49 ± 0.04	-1.330 ± 0.036	-0.080	-0.87
	BD +53 2820	13.65	13.71	13.77	CLMS06	0.43 ± 0.05	-1.274 ± 0.045	0.014	0.13
	CPD -69 1743	13.28	13.33	13.38	CLMS06	0.42 ± 0.05	-1.269 ± 0.043	-0.143	-1.37

^aTerms in parentheses indicate separate velocity components, if they are explicitly identified and not grouped together; see §4.3

^bCodes in this column are linked to references listed in Table 1

^cThe expected depletion $[\text{Mn}_{\text{gas}}/\text{H}]$ computed using Eq. 10. The listed errors do not include an overall systematic uncertainty of 0.03 in the solar abundance $\sigma(\text{Mn}/\text{H})_{\odot}$ in order to show just the formal error that arises from the uncertainties in location of line of best fit and the value of F_* .

^dThe observed $[\text{Mn}_{\text{gas}}/\text{H}]$ minus that computed using Eq. 10.

^eThe difference shown in the previous column divided by the expected difference due to the uncertainties in both the measured column density and the coefficients that appear in Eq. 10.

Table 18. Observations and Fits for Iron

HD Number ^a	Name	Observed $\log N(\text{Fe II})$				F_*	$[\text{Fe}_{\text{gas}}/\text{H}]_{\text{fit}}^{\text{c}}$	Residual ^d	Deviation ^e (in σ)
		l.l.	best	u.l.	Source ^b				
(1)	(2)	(3)	(4)	(5)	(6)	(7)	(8)	(9)	(10)
2905	κ Cas	14.93	15.01	15.46	JSS86	0.58 ± 0.06	-1.698 ± 0.076	-0.126	-0.43
5394	γ Cas	14.01	14.11	14.21	JSS86	0.52 ± 0.04	-1.614 ± 0.055	0.022	0.15
12323	HD 12323	15.09	15.16	15.23	JS07a	0.52 ± 0.04	-1.624 ± 0.048	-0.039	-0.35
13745	HD 13745	15.45	15.53	15.62	JS07a	0.43 ± 0.07	-1.498 ± 0.089	0.115	0.80
15137	HD 15137	15.31	15.39	15.49	JS07a	0.37 ± 0.09	-1.422 ± 0.115	0.054	0.28
18100	HD 18100	14.63	14.67	14.71	SS96b	0.14 ± 0.04	-1.126 ± 0.060	0.102	0.67
21278	HD 21278	14.36	15.01	∞	JSS86
21856	HD 21856	14.88	15.06	∞	JSS86	0.67 ± 0.39	-1.816 ± 0.501
22586	HD 22586	14.51	14.56	14.66	JW96	0.34 ± 0.07	-1.388 ± 0.086	0.054	0.27
22928	δ Per	13.93	14.11	14.28	JSS86
22951	40 Per	14.53	14.61	15.11	JSS86	0.73 ± 0.05	-1.892 ± 0.068	-0.264	-0.84
23180	o Per	14.61	14.76	∞	JSS86	0.84 ± 0.06	-2.035 ± 0.086
23408	20 Tau	15.46	15.71	∞	JSS86
23480	23 Tau	13.76	14.01	∞	JSS86
24398	ζ Per	14.28	14.43	14.58	S77	0.88 ± 0.05	-2.088 ± 0.069	-0.219	-1.11
24534	X Per	14.43	14.56	14.70	SRF02	0.90 ± 0.06	-2.108 ± 0.076	-0.212	-1.34
24760	ϵ Per	14.23	14.31	14.38	JSS86	0.68 ± 0.04	-1.825 ± 0.052	0.091	0.71
24912	ξ Per	14.69	14.72	14.75	C++91	0.83 ± 0.02	-2.020 ± 0.038	-0.093	-1.03
27778	62 Tau	14.41	14.42	14.43	M++07
28497	228 Eri	14.11	14.31	14.51	SY77
29248	ν Eri	13.86	14.06	∞	JSS86
30614	α Cam	14.98	15.11	∞	JSS86	0.46 ± 0.04	-1.538 ± 0.055
31237	π^5 Ori	13.98	14.11	14.51	JSS86	0.52 ± 0.21	-1.619 ± 0.267	0.028	0.05
34029	α Aur	12.45	12.46	12.47	L++95	0.44 ± 0.05	-1.516 ± 0.066	0.198	1.71
34816	λ Lep	14.44	14.74	∞	JSS86	0.45 ± 0.05	-1.535 ± 0.068
34989	HD 34989	14.57	14.77	14.97	SB79	0.72 ± 0.17	-1.872 ± 0.224	0.008	0.02
35149	23 Ori	14.36	14.38	14.41	W++99	0.54 ± 0.04	-1.644 ± 0.050	-0.148	-1.01
35439	25 Ori	13.53	13.81	∞	JSS86	0.72 ± 0.18	-1.878 ± 0.228
35715	ψ Ori	14.13	14.21	14.33	JSS86	0.66 ± 0.11	-1.804 ± 0.146	-0.019	-0.07
36166	HD 36166	14.06	14.46	∞	JSS86
36486	δ Ori A	14.01	14.06	14.13	JSS86	0.54 ± 0.02	-1.646 ± 0.029	-0.026	-0.33
36822	ϕ^1 Ori	14.36	14.46	14.61	JSS86	0.74 ± 0.08	-1.905 ± 0.105	-0.015	-0.08
36861	λ Ori A	14.56	14.61	14.68	JSS86	0.57 ± 0.04	-1.679 ± 0.053	-0.052	-0.38
37021	θ^1 Ori	15.42	15.44	15.46	M++07
37043	ι Ori	14.13	14.21	14.31	JSS86	0.41 ± 0.03	-1.478 ± 0.037	-0.004	-0.03
37061	ν Ori	15.42	15.44	15.46	M++07
37128	ϵ Ori	14.16	14.21	14.26	JSS86	0.54 ± 0.03	-1.646 ± 0.040	-0.137	-1.24
37468	σ Ori	14.41	14.56	∞	JSS86	0.58 ± 0.04	-1.701 ± 0.055
37903	HD 37903	14.77	14.87	14.99	JS07a	1.15 ± 0.03	-2.427 ± 0.053	0.322	2.36

Table 18—Continued

HD Number ^a	Name	Observed $\log N(\text{Fe II})$				F_*	$[\text{Fe}_{\text{gas}}/\text{H}]_{\text{fit}}^c$	Residual ^d	Deviation ^e (in σ)
		l.l.	best	u.l.	Source ^b				
(1)	(2)	(3)	(4)	(5)	(6)	(7)	(8)	(9)	(10)
38666	μ Col	14.30	14.31	14.32	HSF99	0.11 ± 0.01	-1.094 ± 0.022	0.004	0.13
38771	κ Ori	14.21	14.26	14.33	JSS86	0.67 ± 0.03	-1.808 ± 0.038	0.006	0.07
40111	139 Tau	14.81	14.86	15.16	JSS86	0.49 ± 0.04	-1.580 ± 0.049	-0.056	-0.28
40893	HD 40893	15.27	15.32	15.38	JS07a	0.61 ± 0.05	-1.732 ± 0.072	-0.022	-0.19
41161	HD 41161	14.92	14.98	15.04	OH06	0.44 ± 0.04	-1.516 ± 0.054	-0.119	-1.03
44506	HD 44506	14.53	14.61	14.66	JSS86	-0.03 ± 0.23	-0.911 ± 0.292	-0.107	-0.21
44743	β CMa	13.26	13.29	13.32	DG98	-0.43 ± 0.03	-0.394 ± 0.059	-0.154	-1.73
48915 (+12)	α CMa	11.68	11.71	11.74	H++99	0.42 ± 0.11	-1.490 ± 0.139	0.262	1.07
(+18)		11.89	11.91	11.92	H++99	0.42 ± 0.08	-1.487 ± 0.106	0.259	1.41
52918	19 Mon	13.98	14.11	∞	JSS86	0.44 ± 0.24	-1.521 ± 0.313
53975	HD 53975	14.79	14.84	14.89	OH06	0.45 ± 0.03	-1.528 ± 0.039	-0.311	-3.60
54662	HD 54662	14.81	14.91	14.98	JSS86	0.89 ± 0.09	-2.089 ± 0.120	0.042	0.22
55879	HD 55879	14.03	14.41	∞	JSS86
57060	29 CMa	14.71	14.81	14.91	JSS86	0.50 ± 0.05	-1.595 ± 0.062	0.163	1.10
57061	τ CMa	14.68	14.76	14.86	JSS86	0.39 ± 0.04	-1.448 ± 0.057	-0.034	-0.30
64740	HD 64740	13.98	14.16	14.61	JSS86	0.27 ± 0.30	-1.301 ± 0.388	-0.133	-0.23
64760	HD 64760	14.28	14.36	14.46	JSS86	0.35 ± 0.06	-1.407 ± 0.076	-0.035	-0.22
65575	χ Car	13.78	13.86	∞	JSS86
65818	V Pup	14.28	14.46	14.76	JSS86	0.36 ± 0.09	-1.417 ± 0.116	-0.186	-0.62
66788	HD 66788	15.07	15.14	15.22	JS07a	0.53 ± 0.08	-1.634 ± 0.101	-0.020	-0.13
66811	ζ Pup	14.06	14.08	14.16	M78	0.32 ± 0.02	-1.366 ± 0.028	-0.050	-0.72
68273	γ^2 Vel	13.86	13.95	14.04	FS94	0.25 ± 0.02	-1.274 ± 0.030	-0.024	-0.24
69106	HD 69106	14.49	14.74	15.03	JS07a	0.64 ± 0.06	-1.776 ± 0.079	-0.114	-0.40
73882	HD 73882	15.25	15.29	15.35	JS07a	0.68 ± 0.07	-1.822 ± 0.093	0.007	0.05
74375	HD 74375	14.39	14.59	14.79	SB79	0.61 ± 0.18	-1.738 ± 0.229	0.005	0.02
91597	HD 91597	15.44	15.51	15.59	JS07a	0.44 ± 0.05	-1.522 ± 0.072	0.080	0.67
91651	HD 91651	15.34	15.37	15.40	JS07a	0.27 ± 0.04	-1.299 ± 0.056	-0.027	-0.30
92554	HD 92554	15.46	15.51	15.57	JS07a	0.27 ± 0.07	-1.297 ± 0.092	-0.015	-0.10
93030	θ Car	14.13	14.20	14.26	AJS92	0.45 ± 0.03	-1.523 ± 0.043	-0.078	-0.69
93205	V560 Car	15.45	15.49	15.53	JS07a	0.40 ± 0.03	-1.464 ± 0.038	0.015	0.22
93222	HD 93222	15.48	15.55	15.63	JS07a	0.39 ± 0.04	-1.452 ± 0.054	0.043	0.39
93521 (-66)	HD 93521	13.55	13.59	13.63	SF93	-0.31 ± 0.11	-0.552 ± 0.143	0.094	0.26
(-58)		14.22	14.36	14.70	SF93	-0.01 ± 0.03	-0.944 ± 0.047	0.426	1.65
(-51)		13.88	13.91	13.94	SF93	-0.04 ± 0.04	-0.904 ± 0.061	0.076	0.59
(-39)		13.71	13.73	13.75	SF93	0.01 ± 0.08	-0.959 ± 0.109	0.271	1.18
(-29)		12.55	12.65	12.75	SF93	0.34 ± 0.17	-1.389 ± 0.216	0.121	0.29
(-18)		13.96	13.98	14.00	SF93	0.00 ± 0.03	-0.955 ± 0.044	0.117	1.37
(-10)		13.89	14.01	14.03	SF93	0.02 ± 0.04	-0.978 ± 0.055	0.090	0.79
(+3)		13.54	13.56	13.58	SF93	0.25 ± 0.04	-1.275 ± 0.050	-0.003	-0.03

Table 18—Continued

HD Number ^a	Name	Observed $\log N(\text{Fe II})$				F_*	$[\text{Fe}_{\text{gas}}/\text{H}]_{\text{fit}}^c$	Residual ^d	Deviation ^e (in σ)
		l.l.	best	u.l.	Source ^b				
(1)	(2)	(3)	(4)	(5)	(6)	(7)	(8)	(9)	(10)
(+7)		12.95	12.99	13.03	SF93	0.23 ± 0.12	-1.253 ± 0.155	-0.085	-0.29
(total)		14.74	14.82	14.98	SF93	0.06 ± 0.04	-1.026 ± 0.051	0.202	1.36
93843	HD 93843	15.45	15.48	15.50	JS07a	0.39 ± 0.05	-1.448 ± 0.067	0.043	0.41
94493	HD 94493	15.46	15.52	15.58	JS07a	0.29 ± 0.03	-1.320 ± 0.047	0.133	1.56
99171	HD 99171	14.44	14.64	14.84	SB79
99857	HD 99857	15.27	15.33	15.39	JS07a	0.54 ± 0.04	-1.644 ± 0.058	0.079	0.77
99890	HD 99890	15.24	15.28	15.33	JS07a	0.17 ± 0.08	-1.168 ± 0.105	-0.049	-0.29
100340	HD 100340	14.94	∞	∞	SS96b	0.10 ± 0.06	-1.077 ± 0.077
103779	HD 103779	15.12	15.17	15.22	JS07a	0.43 ± 0.06	-1.510 ± 0.084	-0.056	-0.42
104705	DF Cru	15.32	15.40	15.42	JS07a	0.33 ± 0.05	-1.371 ± 0.060	0.057	0.53
106490	δ Cru	13.79	13.84	13.92	JSS86
108248	α^1 Cru	13.94	13.99	14.04	JSS86	0.15 ± 0.05	-1.145 ± 0.065	-0.004	-0.03
109399	HD 109399	15.17	15.22	15.28	JS07a	0.48 ± 0.05	-1.575 ± 0.066	0.078	0.75
110432	BZ Cru	14.20	14.30	14.43	SRF02	1.17 ± 0.11	-2.457 ± 0.144	0.021	0.10
113904	θ Mus	14.93	15.06	15.46	JSS86
116658	α Vir	13.14	13.34	13.45	YK79	0.16 ± 0.05	-1.160 ± 0.065	-0.042	-0.22
116781	V967 Cen	15.20	15.27	15.36	JS07a	0.44 ± 0.07	-1.522 ± 0.087	0.010	0.07
116852	HD 116852	15.22	15.24	15.26	SS96a	0.36 ± 0.04	-1.409 ± 0.047	0.094	0.98
118716	ϵ Cen	13.94	13.99	14.07	JSS86	0.15 ± 0.16	-1.143 ± 0.212	-0.008	-0.02
120086	HD 120086	14.41	14.46	14.56	JW96
120324	μ Cen	13.94	14.14	14.59	JSS86	-0.81 ± 3.74	0.088 ± 4.803	-0.245	-0.03
121263	ζ Cen	13.79	13.84	13.94	JSS86
122879	HD 122879	15.20	15.25	15.31	JS07a	0.55 ± 0.04	-1.652 ± 0.057	0.028	0.22
124314	HD 124314	15.22	15.27	15.33	JS07a	0.59 ± 0.05	-1.704 ± 0.068	-0.073	-0.65
127972	η Cen	13.81	13.86	13.91	JSS86
135591	HD 135591	14.56	14.76	∞	JSS86	0.56 ± 0.22	-1.677 ± 0.284
136298	δ Lup	13.92	13.99	14.07	JSS86
138690	γ Lup	13.89	13.94	14.02	JSS86
141637	1 Sco	14.71	14.81	15.11	JSS86	0.69 ± 0.05	-1.837 ± 0.067	-0.029	-0.12
143018	π Sco	14.36	14.46	14.56	JJ91	0.71 ± 0.03	-1.858 ± 0.046	0.090	0.72
143118	η Lup A	14.13	14.21	14.28	JSS86
143275	δ Sco	14.66	14.76	14.86	JSS86	0.90 ± 0.03	-2.103 ± 0.050	0.155	1.09
144217	β^1 Sco	14.73	14.81	15.16	JSS86	0.81 ± 0.02	-1.995 ± 0.034	0.127	0.58
144470	σ^1 Sco	14.68	14.76	14.88	JSS86	0.81 ± 0.04	-1.987 ± 0.053	-0.025	-0.18
145502	ν Sco	14.46	14.86	∞	JSS86	0.80 ± 0.11	-1.977 ± 0.147
147165	σ Sco	14.96	15.11	∞	JSS86	0.76 ± 0.06	-1.934 ± 0.081
147888	ρ Oph D	15.48	15.50	15.53	JS07a	0.88 ± 0.06	-2.083 ± 0.086	0.307	1.79
147933	ρ Oph A	14.65	14.90	∞	M++07	1.09 ± 0.08	-2.355 ± 0.111
148184	χ Oph	14.71	14.81	∞	JSS86	0.96 ± 0.09	-2.181 ± 0.124

Table 18—Continued

HD Number ^a	Name	Observed $\log N(\text{Fe II})$				Source ^b	F_*	$[\text{Fe}_{\text{gas}}/\text{H}]_{\text{fit}}^c$	Residual ^d	Deviation ^e (in σ)
		l.l.	best	u.l.						
(1)	(2)	(3)	(4)	(5)	(6)	(7)	(8)	(9)	(10)	
148605	22 Sco	14.31	14.71	∞	JSS86	0.53 ± 0.39	-1.632 ± 0.507	
149038	μ Nor	14.68	15.01	∞	JSS86	0.56 ± 0.05	-1.666 ± 0.062	
149757 (–27)	ζ Oph	13.99	14.03	14.06	SCS92	
(–15)		14.36	14.39	14.41	SCS92	1.05 ± 0.02	-2.295 ± 0.039	–0.007	–0.10	
149881	V600 Her	15.14	15.20	15.26	SF95	0.07 ± 0.06	-1.036 ± 0.083	0.049	0.23	
151804	V973 Sco	15.06	15.11	15.23	JSS86	0.57 ± 0.08	-1.690 ± 0.098	0.063	0.37	
151890	μ^1 Sco	14.23	14.31	14.33	JSS86	-0.03 ± 3.47	-0.914 ± 4.464	0.097	0.01	
152236	ζ^1 Sco	15.15	15.23	15.32	JS07a	0.80 ± 0.06	-1.984 ± 0.076	–0.166	–1.04	
152590	HD 152590	15.17	15.19	15.20	M++07	0.69 ± 0.03	-1.839 ± 0.042	0.021	0.32	
154368	V1074 Sco	15.20	15.31	15.46	SRF02	0.52 ± 0.07	-1.614 ± 0.086	–0.203	–1.23	
155806	V1075 Sco	14.88	14.96	15.21	JSS86	0.62 ± 0.07	-1.752 ± 0.086	0.034	0.16	
157246	γ Ara	14.56	14.66	14.73	JSS86	0.46 ± 0.03	-1.541 ± 0.045	–0.047	–0.36	
158926	λ Sco	13.35	13.39	13.42	Y83	0.31 ± 0.02	-1.352 ± 0.027	–0.026	–0.49	
160578	κ Sco	13.99	14.09	14.17	JSS86	0.50 ± 0.07	-1.588 ± 0.095	–0.083	–0.41	
164284	66 Oph	14.38	14.51	14.61	JSS86	0.89 ± 0.18	-2.095 ± 0.231	0.317	0.76	
165024	θ Ara	14.63	14.71	14.81	JSS86	0.56 ± 0.03	-1.676 ± 0.047	0.004	0.03	
167264	15 Sgr	14.73	15.01	∞	JSS86	0.68 ± 0.16	-1.826 ± 0.202	
167756	HD 167756	14.90	∞	∞	CSS95	
167971	MY Ser	15.26	15.42	15.62	SRF02	0.70 ± 0.23	-1.857 ± 0.292	0.007	0.02	
168076	HD 168076	15.35	15.45	15.55	SRF02	0.68 ± 0.17	-1.828 ± 0.219	0.007	0.02	
168941	HD 168941	15.36	15.42	15.49	JS07a	0.42 ± 0.17	-1.486 ± 0.213	0.180	0.54	
170740	HD 170740	14.59	14.69	14.79	SRF02	1.02 ± 0.11	-2.263 ± 0.150	0.015	0.07	
177989	HD 177989	14.89	14.95	15.01	JS07a	0.55 ± 0.05	-1.662 ± 0.060	–0.010	–0.09	
179406	20 Aql	14.57	14.72	14.89	JS07a	
184915	κ Aql	14.61	14.86	∞	JSS86	0.88 ± 0.05	-2.078 ± 0.068	
185418	HD 185418	14.90	15.00	15.12	SRF02	0.79 ± 0.03	-1.968 ± 0.048	0.021	0.15	
188209	HD 188209	14.88	15.01	∞	JSS86	0.66 ± 0.12	-1.804 ± 0.157	
192639	HD 192639	15.06	15.14	15.24	SRF02	0.64 ± 0.04	-1.774 ± 0.051	–0.104	–0.84	
193322	HD 193322	14.61	14.86	∞	JSS86	
197512	HD 197512	14.94	15.06	15.21	SRF02	
199579	HD 199579	14.80	14.87	14.14	SRF02	0.76 ± 0.27	-1.933 ± 0.345	0.017	0.04	
200120	59 Cyg	13.98	14.11	14.36	JSS86	
202347	HD 202347	14.80	14.84	14.87	JS07a	0.56 ± 0.06	-1.668 ± 0.082	0.034	0.25	
202904	ν Cyg	14.26	14.31	14.36	JSS86	
203064	68 Cyg	14.68	14.96	∞	JSS86	0.68 ± 0.20	-1.826 ± 0.263	
203374	HD 203374	15.18	15.22	15.25	JS07a	0.56 ± 0.06	-1.667 ± 0.077	0.019	0.16	
203938	HD 203938	14.84	15.03	16.43	SRF02	0.99 ± 0.64	-2.222 ± 0.818	0.015	0.01	
206267	HD 206267	14.89	14.97	15.07	SRF02	0.87 ± 0.07	-2.065 ± 0.093	–0.039	–0.25	
207198	HD 207198	15.06	15.13	15.19	M++07	0.90 ± 0.03	-2.107 ± 0.047	0.021	0.22	

Table 18—Continued

HD Number ^a	Name	Observed $\log N(\text{Fe II})$				F_*	$[\text{Fe}_{\text{gas}}/\text{H}]_{\text{fit}}^c$	Residual ^d	Deviation ^e (in σ)
		l.l.	best	u.l.	Source ^b				
(1)	(2)	(3)	(4)	(5)	(6)	(7)	(8)	(9)	(10)
207308	HD 207308	15.02	15.10	15.19	JS07a	0.80 ± 0.06	-1.976 ± 0.079	0.101	0.77
207538	HD 207538	14.91	15.02	15.24	SRF02	0.84 ± 0.07	-2.033 ± 0.094	-0.065	-0.32
209339	HD 209339	15.05	15.09	15.13	JS07a	0.58 ± 0.04	-1.692 ± 0.056	-0.018	-0.19
209975	19 Cep	15.06	15.46	∞	JSS86	0.57 ± 0.26	-1.688 ± 0.337
210839	λ Cep	15.07	15.12	15.18	SRF02	0.66 ± 0.03	-1.796 ± 0.045	-0.068	-0.71
214080	HD 214080	14.73	15.21	∞	JSS86	0.27 ± 0.10	-1.297 ± 0.131
214680	10 Lac	14.18	14.31	14.51	JSS86	0.50 ± 0.06	-1.589 ± 0.083	-0.371	-1.67
214993	12 Lac	14.88	15.01	∞	JSS86	0.68 ± 0.10	-1.826 ± 0.124
215733 (-93)	HD 215733	12.58	12.59	12.60	FS97	-0.27 ± 0.19	-0.607 ± 0.248	0.270	0.59
(-83)		12.06	12.09	12.12	FS97	0.99 ± 0.30	-2.221 ± 0.384	0.374	0.60
(-61)		12.76	13.02	13.28	FS97	1.06 ± 0.21	-2.318 ± 0.270	0.361	0.71
(-59)		13.82	13.86	13.90	FS97	-0.11 ± 0.10	-0.810 ± 0.129	0.183	0.60
(-54)		13.73	13.77	13.81	FS97	0.54 ± 0.15	-1.650 ± 0.194	0.253	0.55
(-47)		13.91	13.97	14.03	FS97
(-45)		13.08	13.23	13.38	FS97	-0.40 ± 0.28	-0.431 ± 0.359	0.064	0.10
(-42)		13.57	13.68	13.79	FS97	-0.16 ± 0.31	-0.741 ± 0.403	0.354	0.37
(-40)		12.88	13.12	13.36	FS97	0.18 ± 0.24	-1.184 ± 0.314	-0.043	-0.06
(-32)		14.06	14.25	14.44	FS97	0.25 ± 0.09	-1.269 ± 0.116	0.342	1.30
(-31)		13.37	13.60	13.83	FS97
(-28)		13.74	13.88	14.02	FS97	-0.18 ± 0.07	-0.715 ± 0.090	0.148	0.75
(-26)		13.77	13.94	14.11	FS97	-0.12 ± 0.07	-0.794 ± 0.089	0.087	0.38
(-23)		13.33	13.52	13.71	FS97	0.24 ± 0.08	-1.264 ± 0.105	-0.003	-0.02
(-21)		13.65	13.76	13.87	FS97	0.24 ± 0.05	-1.256 ± 0.068	0.109	0.74
(-19)		13.36	13.47	13.58	FS97
(-16)		13.30	13.43	13.56	FS97	0.93 ± 0.05	-2.143 ± 0.071	-0.074	-0.47
(-9)		14.54	14.56	14.58	FS97	0.08 ± 0.04	-1.053 ± 0.050	0.006	0.07
(+1)		13.22	13.29	13.36	FS97	0.90 ± 0.05	-2.114 ± 0.072	0.157	1.40
(+9)		12.13	12.20	12.27	FS97
(+15)		11.79	11.88	11.97	FS97	0.96 ± 0.08	-2.184 ± 0.107	0.107	0.64
(total)		15.00	15.09	15.19	FS97
217675	o And	13.23	14.01	∞	JSS86
218376	1 Cas	14.81	15.01	∞	JSS86	0.60 ± 0.06	-1.724 ± 0.080
219188	HD 219188	14.21	14.46	∞	JSS86	1.24 ± 0.57	-2.544 ± 0.737
224151	V373 Cas	15.47	15.52	15.59	JS07a	0.46 ± 0.04	-1.549 ± 0.057	0.068	0.67
224572	σ Cas	14.66	14.76	15.01	JSS86	0.76 ± 0.07	-1.927 ± 0.094	0.165	0.74
303308	HDE 303308	15.55	15.60	15.65	JS07a	0.38 ± 0.04	-1.443 ± 0.051	0.027	0.28
	BD +35 4258	15.36	15.44	15.53	JS07a	0.40 ± 0.08	-1.472 ± 0.102	0.078	0.47
	CPD -59 2603	15.55	15.59	15.64	JS07a	0.17 ± 0.06	-1.167 ± 0.083	0.015	0.11

^aTerms in parentheses indicate separate velocity components, if they are explicitly identified and not grouped together; see §4.3

^bCodes in this column are linked to references listed in Table 1

^cThe expected depletion $[\text{Fe}_{\text{gas}}/\text{H}]$ computed using Eq. 10. The listed errors do not include an overall systematic uncertainty of 0.03 in the solar abundance $\sigma(\text{Fe}/\text{H})_{\odot}$ in order to show just the formal error that arises from the uncertainties in location of line of best fit and the value of F_* .

^dThe observed $[\text{Fe}_{\text{gas}}/\text{H}]$ minus that computed using Eq. 10.

^eThe difference shown in the previous column divided by the expected difference due to the uncertainties in both the measured column density and the coefficients that appear in Eq. 10.

Table 19. Observations and Fits for Nickel

HD Number ^a	Name	Observed $\log N(\text{Ni II})$				F_*	$[\text{Ni}_{\text{gas}}/\text{H}]_{\text{fit}}^c$	Residual ^d	Deviation ^e (in σ)
		l.l.	best	u.l.	Source ^b				
(1)	(2)	(3)	(4)	(5)	(6)	(7)	(8)	(9)	(10)
1383	HD 1383	13.95	13.98	14.01	CLMS06	0.61 ± 0.04	-1.848 ± 0.066	0.030	0.28
2905	κ Cas	13.27	13.51	14.21	JSS86	0.58 ± 0.06	-1.802 ± 0.088	-0.266	-0.54
12323	HD 12323	13.97	14.00	14.03	CLMS06	0.52 ± 0.04	-1.717 ± 0.056	0.137	1.42
13268	HD 13268	14.07	14.11	14.15	CLMS06	0.51 ± 0.04	-1.703 ± 0.062	0.102	0.98
14434	HD 14434	14.08	14.12	14.16	CLMS06	0.52 ± 0.04	-1.709 ± 0.066	0.067	0.63
18100	HD 18100	13.41	13.46	13.51	SS96b	0.14 ± 0.04	-1.140 ± 0.074	0.154	0.96
22586	HD 22586	13.35	13.40	13.50	JW96	0.34 ± 0.07	-1.444 ± 0.101	0.200	0.96
22951	40 Per	13.22	13.44	13.83	JSS86	0.73 ± 0.05	-2.027 ± 0.079	-0.043	-0.13
23180	o Per	12.63	S76	0.84 ± 0.06	-2.193 ± 0.100
24912	ξ Per	13.27	13.32	13.36	C++91	0.83 ± 0.02	-2.176 ± 0.043	-0.087	-0.88
27778	62 Tau	13.00	13.04	13.08	CLMS06
35149	23 Ori	12.85	12.98	13.08	W++99	0.54 ± 0.04	-1.740 ± 0.059	-0.205	-1.10
36841	HD 36841	12.98	13.05	13.12	CLMS06
37021	θ^1 Ori	13.78	13.80	13.82	CLMS06
37903	HD 37903	13.10	13.13	13.16	CLMS06	1.15 ± 0.03	-2.647 ± 0.061	0.046	0.51
38666	μ Col	12.92	12.96	13.02	HSF99	0.11 ± 0.01	-1.103 ± 0.038	-0.087	-1.33
40111	139 Tau	12.89	13.30	13.51	JSS86	0.49 ± 0.04	-1.666 ± 0.058	-0.275	-0.84
43818	LU Gem	13.92	13.95	13.98	CLMS06
52266	HD 52266	13.73	13.75	13.77	CLMS06
54662	HD 54662	13.10	13.53	14.37	JSS86	0.89 ± 0.09	-2.256 ± 0.139	0.085	0.13
63005	HD 63005	13.77	13.79	13.81	CLMS06	0.64 ± 0.03	-1.890 ± 0.047	0.069	0.94
66811	ζ Pup	12.30	12.70	13.10	M78	0.32 ± 0.02	-1.417 ± 0.038	-0.131	-0.32
71634	HD 71634	13.25	13.32	13.39	CLMS06
75309	HD 75309	13.44	13.49	13.54	CLMS06	0.63 ± 0.04	-1.869 ± 0.060	-0.112	-1.03
79186	GX Vel	13.68	13.70	13.72	CLMS06	0.69 ± 0.03	-1.964 ± 0.054	-0.038	-0.43
91824	HD 91824	13.77	13.82	13.87	CLMS06	0.45 ± 0.03	-1.601 ± 0.050	-0.037	-0.42
91983	HD 91983	13.81	13.86	13.91	CLMS06	0.48 ± 0.04	-1.646 ± 0.063	-0.027	-0.24
100340	HD 100340	13.85	13.90	13.95	SS96b	0.10 ± 0.06	-1.083 ± 0.094	0.226	1.55
111934	BU Cru	13.89	14.00	14.11	CLMS06
116658	α Vir	12.17	YK79	0.16 ± 0.05	-1.179 ± 0.080
116852	HD 116852	14.01 ^f	14.05 ^f	14.09 ^f	CLMS06	0.36 ± 0.04	-1.467 ± 0.057	0.208	1.95
120086	HD 120086	13.85	13.90	14.00	JW96
122879	HD 122879	13.74	13.75	13.76	CLMS06	0.55 ± 0.04	-1.749 ± 0.067	-0.131	-1.07
143275	δ Sco	13.01	13.09	13.15	JSS86	0.90 ± 0.03	-2.271 ± 0.058	-0.090	-0.72
147888	ρ Oph D	13.77	13.83	13.89	CLMS06	0.88 ± 0.06	-2.248 ± 0.099	0.047	0.25
147933	ρ Oph A	12.09	12.95	13.78	JSS86	1.09 ± 0.08	-2.564 ± 0.128	-0.473	-0.55
148184	χ Oph	...	12.68	13.07	JSS86	0.96 ± 0.09	-2.363 ± 0.144
148594	HD 148594	13.35	13.38	13.41	CLMS06
149757 (-27)	ζ Oph	12.76	12.79	12.82	SCS92

Table 19—Continued

HD Number ^a	Name	Observed $\log N(\text{Ni II})$				F_*	$[\text{Ni}_{\text{gas}}/\text{H}]_{\text{fit}}^c$	Residual ^d	Deviation ^e (in σ)
		l.l.	best	u.l.	Source ^b				
(1)	(2)	(3)	(4)	(5)	(6)	(7)	(8)	(9)	(10)
(–15)		12.92	12.94	12.96	SCS92	1.05 ± 0.02	-2.494 ± 0.044	–0.004	–0.05
151804	V973 Sco	13.14	13.45	13.69	JSS86	0.57 ± 0.08	-1.793 ± 0.114	–0.238	–0.75
154368	V1074 Sco	13.87	14.17	14.47	S++96	0.52 ± 0.07	-1.706 ± 0.100	–0.008	–0.02
155806	V1075 Sco	13.49	13.65	13.91	JSS86	0.62 ± 0.07	-1.865 ± 0.100	0.093	0.36
157857	HD 157857	13.89	13.93	13.97	CLMS06	0.62 ± 0.04	-1.864 ± 0.057	0.056	0.57
164284	66 Oph	10.53	12.57	12.91	JSS86	0.89 ± 0.18	-2.262 ± 0.268	–0.199	–0.16
165955	HD 165955	13.84	13.92	14.00	CLMS06	0.42 ± 0.04	-1.562 ± 0.064	0.089	0.75
175360	HD 175360	13.27	13.32	13.37	CLMS06
185418	HD 185418	13.27	13.32	13.37	CLMS06	0.79 ± 0.03	-2.116 ± 0.055	–0.269	–2.59
190918	V1676 Cyg	14.06	14.09	14.12	CLMS06	0.46 ± 0.03	-1.625 ± 0.054	0.016	0.20
192035	RX Cyg	13.66	13.72	13.78	CLMS06	0.76 ± 0.04	-2.067 ± 0.063	0.109	1.01
192639	HD 192639	13.85	13.91	13.97	CLMS06	0.64 ± 0.04	-1.890 ± 0.059	0.026	0.24
198478	55 Cyg	13.67	13.74	13.81	CLMS06	0.81 ± 0.05	-2.139 ± 0.082	0.039	0.25
198781	HD 198781	13.73	13.75	13.77	CLMS06	0.59 ± 0.03	-1.813 ± 0.050	0.117	1.47
201345	HD 201345	13.94	13.98	14.02	CLMS06	0.34 ± 0.04	-1.440 ± 0.065	0.124	1.09
203532	HD 203532	12.87	12.95	13.03	CLMS06
206773	HD 206773	13.66	13.71	13.76	CLMS06	0.53 ± 0.02	-1.733 ± 0.036	–0.102	–1.26
207198	HD 207198	13.78	13.84	13.90	CLMS06	0.90 ± 0.03	-2.276 ± 0.053	0.146	1.54
208440	HD 208440	13.67	13.72	13.77	CLMS06	0.61 ± 0.04	-1.846 ± 0.063	–0.035	–0.31
210809	HD 210809	14.11	14.14	14.17	CLMS06	0.41 ± 0.04	-1.552 ± 0.068	0.065	0.59
212791	V408 Lac	13.69	13.77	13.85	CLMS06	0.57 ± 0.08	-1.788 ± 0.125	0.141	0.60
220057	HD 220057	13.44	13.49	13.54	CLMS06	0.75 ± 0.05	-2.058 ± 0.083	0.097	0.64
224572	σ Cas	...	12.61	13.06	JSS86	0.76 ± 0.07	-2.068 ± 0.109
232522	HDE 232522	13.91	13.95	13.99	CLMS06	0.44 ± 0.03	-1.588 ± 0.053	0.058	0.70
308813	HDE 308813	13.91	13.96	14.01	CLMS06	0.49 ± 0.04	-1.670 ± 0.063	0.048	0.43
	BD +53 2820	14.16	14.20	14.24	CLMS06	0.43 ± 0.05	-1.573 ± 0.079	0.091	0.75
	CPD –69 1743	13.93	13.97	14.01	CLMS06	0.42 ± 0.05	-1.565 ± 0.075	0.080	0.68

^aTerms in parentheses indicate separate velocity components, if they are explicitly identified and not grouped together; see §4.3

^bCodes in this column are linked to references listed in Table 1

^cThe expected depletion $[\text{Ni}_{\text{gas}}/\text{H}]$ computed using Eq. 10. The listed errors do not include an overall systematic uncertainty of 0.03 in the solar abundance $\sigma(\text{Ni}/\text{H})_{\odot}$ in order to show just the formal error that arises from the uncertainties in location of line of best fit and the value of F_* .

^dThe observed $[\text{Ni}_{\text{gas}}/\text{H}]$ minus that computed using Eq. 10.

^eThe difference shown in the previous column divided by the expected difference due to the uncertainties in both the measured column density and the coefficients that appear in Eq. 10.

^fThe entry 13.44 for the adopted value of $N(\text{Ni II})$ stated by CLMS06 is incorrect; this number should be 13.94, as confirmed by Cartledge (private communication). The value listed here includes a correction for a change in the transition f -value by -0.106 dex – see Table 1.

Table 20. Observations and Fits for Copper

HD Number ^a	Name	Observed $\log N(\text{Cu II})$				F_*	$[\text{Cu}_{\text{gas}}/\text{H}]_{\text{fit}}^c$	Residual ^d	Deviation ^e (in σ)
		l.l.	best	u.l.	Source ^b				
(1)	(2)	(3)	(4)	(5)	(6)	(7)	(8)	(9)	(10)
1383	HD 1383	12.65	12.73	12.81	CLMS06	0.61 ± 0.04	-1.031 ± 0.037	-0.083	-0.72
2905	κ Cas	11.95	12.34	12.61	JSS86	0.58 ± 0.06	-1.009 ± 0.047	-0.279	-0.79
12323	HD 12323	12.50	12.55	12.60	CLMS06	0.52 ± 0.04	-0.969 ± 0.036	-0.107	-1.12
13268	HD 13268	12.62	12.67	12.72	CLMS06	0.51 ± 0.04	-0.962 ± 0.038	-0.125	-1.30
14434	HD 14434	12.76	12.83	12.90	CLMS06	0.52 ± 0.04	-0.965 ± 0.040	-0.013	-0.12
22951	40 Per	12.46	12.65	12.79	JSS86	0.73 ± 0.05	-1.117 ± 0.041	0.206	1.02
23180	o Per	12.12	12.42	12.72	S76	0.84 ± 0.06	-1.196 ± 0.051	0.085	0.27
24398	ζ Per	12.27	12.32	12.37	S77	0.88 ± 0.05	-1.225 ± 0.044	0.010	0.08
24912	ξ Per	12.13	12.20	12.26	C++91	0.83 ± 0.02	-1.187 ± 0.028	-0.248	-2.39
27778	62 Tau	12.21	12.26	12.31	CLMS06
35149	23 Ori	11.99	12.02	12.05	W++99	0.54 ± 0.04	-0.980 ± 0.036	0.028	0.20
36841	HD 36841	11.95	12.05	12.15	CLMS06
37021	θ^1 Ori	12.78	12.81	12.84	CLMS06
37061	ν Ori	12.93	12.95	12.97	CLMS06
37367	HD 37367	12.54	12.59	12.64	CLMS06	0.65 ± 0.07	-1.062 ± 0.052	-0.021	-0.18
37903	HD 37903	12.31	12.35	12.39	CLMS06	1.15 ± 0.03	-1.412 ± 0.048	-0.015	-0.17
38666	μ Col	11.66	HSF99	0.11 ± 0.01	-0.676 ± 0.056
40111	139 Tau	11.83	12.38	12.55	JSS86	0.49 ± 0.04	-0.944 ± 0.038	0.033	0.09
43818	LU Gem	12.87	12.89	12.91	CLMS06
47839	15 Mon	11.54	H++93	0.25 ± 0.05	-0.773 ± 0.056
52266	HD 52266	12.58	12.61	12.64	CLMS06
54662	HD 54662	...	12.37	12.82	JSS86	0.89 ± 0.09	-1.226 ± 0.070
63005	HD 63005	12.49	12.54	12.59	CLMS06	0.64 ± 0.03	-1.051 ± 0.029	-0.066	-0.85
66811	ζ Pup	11.39	M78	0.32 ± 0.02	-0.826 ± 0.042
71634	HD 71634	12.35	12.40	12.45	CLMS06
75309	HD 75309	12.43	12.48	12.53	CLMS06	0.63 ± 0.04	-1.041 ± 0.034	0.004	0.04
79186	GX Vel	12.59	12.63	12.67	CLMS06	0.69 ± 0.03	-1.086 ± 0.031	-0.032	-0.38
91824	HD 91824	12.42	12.49	12.56	CLMS06	0.45 ± 0.03	-0.914 ± 0.037	-0.101	-1.05
91983	HD 91983	12.50	12.59	12.68	CLMS06	0.48 ± 0.04	-0.935 ± 0.040	-0.054	-0.43
111934	BU Cru	12.77	12.82	12.87	CLMS06
116658	α Vir	12.41	YK79	0.16 ± 0.05	-0.712 ± 0.062
116852	HD 116852	12.18	12.26	12.34	CLMS06	0.36 ± 0.04	-0.850 ± 0.044	-0.245	-2.02
122879	HD 122879	12.65	12.70	12.75	CLMS06	0.55 ± 0.04	-0.984 ± 0.039	0.008	0.07
141637	1 Sco	12.28	12.33	12.38	H++93	0.69 ± 0.05	-1.087 ± 0.041	-0.057	-0.45
143018	π Sco	11.93	12.01	12.07	H++93	0.71 ± 0.03	-1.098 ± 0.031	0.076	0.78
143275	δ Sco	12.05	12.14	12.21	JSS86	0.90 ± 0.03	-1.233 ± 0.035	-0.129	-1.06
147933	ρ Oph A	12.50	12.75	13.24	JSS86	1.09 ± 0.08	-1.373 ± 0.070	0.084	0.22
148184	χ Oph	11.51	12.09	12.39	JSS86	0.96 ± 0.09	-1.277 ± 0.073	-0.276	-0.60
148594	HD 148594	12.39	12.42	12.45	CLMS06

Table 20—Continued

HD Number ^a	Name	Observed $\log N(\text{Cu II})$				F_*	$[\text{Cu}_{\text{gas}}/\text{H}]_{\text{fit}}^{\text{c}}$	Residual ^d	Deviation ^e (in σ)
		l.l.	best	u.l.	Source ^b				
(1)	(2)	(3)	(4)	(5)	(6)	(7)	(8)	(9)	(10)
149757 (–27)	ζ Oph	11.18	11.35	11.48	SCS92
(–15)		12.18	12.20	12.23	SCS92	1.05 ± 0.02	-1.339 ± 0.038	0.048	0.69
151804	V973 Sco	12.06	12.48	12.74	JSS86	0.57 ± 0.08	-1.005 ± 0.059	–0.047	–0.13
152590	HD 152590	12.63	12.71	12.79	CLMS06	0.69 ± 0.03	-1.087 ± 0.029	–0.010	–0.10
155806	V1075 Sco	11.34	12.06	12.38	JSS86	0.62 ± 0.07	-1.040 ± 0.051	–0.374	–0.69
157857	HD 157857	12.66	12.70	12.74	CLMS06	0.62 ± 0.04	-1.039 ± 0.033	–0.045	–0.52
164284	66 Oph	11.57	11.99	12.25	JSS86	0.89 ± 0.18	-1.229 ± 0.130	0.136	0.28
165955	HD 165955	12.52	12.58	12.64	CLMS06	0.42 ± 0.04	-0.895 ± 0.043	0.036	0.37
175360	HD 175360	12.12	12.21	12.30	CLMS06
185418	HD 185418	12.59	12.63	12.67	CLMS06	0.79 ± 0.03	-1.159 ± 0.032	0.038	0.43
190918	V1676 Cyg	12.70	12.79	12.88	CLMS06	0.46 ± 0.03	-0.925 ± 0.038	–0.029	–0.26
192035	RX Cyg	12.55	12.63	12.71	CLMS06	0.76 ± 0.04	-1.136 ± 0.035	0.042	0.39
192639	HD 192639	12.77	12.81	12.85	CLMS06	0.64 ± 0.04	-1.051 ± 0.034	0.041	0.48
198478	55 Cyg	12.72	12.75	12.78	CLMS06	0.81 ± 0.05	-1.170 ± 0.043	0.034	0.28
201345	HD 201345	12.44	12.51	12.58	CLMS06	0.34 ± 0.04	-0.837 ± 0.048	0.005	0.04
203532	HD 203532	12.22	12.29	12.36	CLMS06
208440	HD 208440	12.63	12.67	12.71	CLMS06	0.61 ± 0.04	-1.030 ± 0.036	0.053	0.56
210809	HD 210809	12.58	12.67	12.76	CLMS06	0.41 ± 0.04	-0.890 ± 0.045	–0.112	–0.87
212571	π Aqr	11.86	11.96	12.03	H++93
212791	V408 Lac	12.28	12.35	12.42	CLMS06	0.57 ± 0.08	-1.003 ± 0.063	–0.111	–0.54
220057	HD 220057	12.32	12.39	12.46	CLMS06	0.75 ± 0.05	-1.131 ± 0.043	0.025	0.17
224572	σ Cas	12.01	12.34	12.55	JSS86	0.76 ± 0.07	-1.136 ± 0.055	0.159	0.54
308813	HDE 308813	12.66	12.71	12.76	CLMS06	0.49 ± 0.04	-0.946 ± 0.040	0.028	0.29
	BD +53 2820	12.51	12.60	12.69	CLMS06	0.43 ± 0.05	-0.900 ± 0.048	–0.228	–1.73
	CPD -69 1743	12.60	12.66	12.72	CLMS06	0.42 ± 0.05	-0.896 ± 0.047	0.056	0.50

^aTerms in parentheses indicate separate velocity components, if they are explicitly identified and not grouped together; see §4.3

^bCodes in this column are linked to references listed in Table 1

^cThe expected depletion $[\text{Cu}_{\text{gas}}/\text{H}]$ computed using Eq. 10. The listed errors do not include an overall systematic uncertainty of 0.06 in the solar abundance $\sigma(\text{Cu}/\text{H})_{\odot}$ in order to show just the formal error that arises from the uncertainties in location of line of best fit and the value of F_* .

^dThe observed $[\text{Cu}_{\text{gas}}/\text{H}]$ minus that computed using Eq. 10.

^eThe difference shown in the previous column divided by the expected difference due to the uncertainties in both the measured column density and the coefficients that appear in Eq. 10.

Table 21. Observations and Fits for Zinc

HD Number ^a	Name	Observed $\log N(\text{Zn II})$				F_*	$[\text{Zn}_{\text{gas}}/\text{H}]_{\text{fit}}^c$	Residual ^d	Deviation ^e (in σ)
		l.l.	best	u.l.	Source ^b				
(1)	(2)	(3)	(4)	(5)	(6)	(7)	(8)	(9)	(10)
18100	HD 18100	12.57	12.62	12.67	SS96b	0.14 ± 0.04	-0.024 ± 0.044	-0.212	-1.42
23630	η Tau	12.62	12.66	12.72	RB95
24912	ξ Per	13.38	13.39	13.41	C++91	0.83 ± 0.02	-0.448 ± 0.032	-0.154	-1.84
35149	23 Ori	13.20	13.28	13.34	W++99	0.54 ± 0.04	-0.270 ± 0.031	0.219	1.41
36486	δ Ori A	12.57	12.62	12.66	RB95	0.54 ± 0.02	-0.271 ± 0.025	-0.004	-0.06
37128	ϵ Ori	12.91	12.97	13.02	RB95	0.54 ± 0.03	-0.271 ± 0.028	0.085	0.80
38666	μ Col	12.51	12.59	12.67	HSF99	0.11 ± 0.01	-0.009 ± 0.037	0.036	0.40
47839	15 Mon	12.81	12.86	12.91	RB95	0.25 ± 0.05	-0.093 ± 0.041	-0.062	-0.52
57061	τ CMa	13.20	13.24	13.30	RB95	0.39 ± 0.04	-0.177 ± 0.036	0.022	0.28
66811	ζ Pup	12.24	12.44	12.64	M78	0.32 ± 0.02	-0.138 ± 0.029	-0.078	-0.38
72127	HD 72127	12.77	12.82	12.87	RB95
91316	ρ Leo	12.83	12.88	12.93	RB95	0.15 ± 0.04	-0.034 ± 0.042	-0.039	-0.36
116658	α Vir	11.61	YK79	0.16 ± 0.05	-0.040 ± 0.045
116852	HD 116852	13.20	13.23	13.25	SS96a	0.36 ± 0.04	-0.158 ± 0.033	-0.325	-3.60
141637	1 Sco	13.44	13.49	13.54	RB95	0.69 ± 0.05	-0.362 ± 0.039	0.013	0.10
143018	π Sco	13.11	13.14	13.16	RB95	0.71 ± 0.03	-0.371 ± 0.031	0.115	1.53
144217	β^1 Sco	13.47	13.52	13.57	RB95	0.81 ± 0.02	-0.436 ± 0.030	0.116	1.69
147165	σ Sco	13.62	13.66	13.72	RB95	0.76 ± 0.06	-0.408 ± 0.045	0.010	0.05
149757 (-27)	ζ Oph	12.37	12.38	12.40	SCS92
(-15)		13.14	13.19	13.24	RB95	1.05 ± 0.02	-0.579 ± 0.041	-0.088	-1.07
149881	V600 Her	13.14	13.19	13.24	RB95	0.07 ± 0.06	0.019 ± 0.054	-0.184	-0.92
158926	λ Sco	11.70	11.76	11.81	RB95	0.31 ± 0.02	-0.131 ± 0.029	-0.044	-0.68
167756	HD 167756	13.26	13.27	13.28	CSS95
212571	π Aqr	13.14	13.19	13.24	RB95
215733 (-59)	HD 215733	11.48	11.56	11.64	FS97	-0.11 ± 0.10	0.126 ± 0.077	-0.219	-0.75
(-54)		11.58	11.66	11.74	FS97	0.54 ± 0.15	-0.273 ± 0.094	-0.400	-0.92
(-47)		11.74	11.82	11.90	FS97
(-42)		11.14	11.32	11.50	FS97	-0.16 ± 0.31	0.159 ± 0.198	-0.072	-0.08
(-32)		11.01	11.35	11.69	FS97	0.25 ± 0.09	-0.092 ± 0.062	-0.901	-2.42
(-31)		11.18	11.40	11.62	FS97
(-28)		11.77	11.86	11.95	FS97	-0.18 ± 0.07	0.171 ± 0.067	0.076	0.49
(-26)		11.69	11.80	11.91	FS97	-0.12 ± 0.07	0.134 ± 0.064	-0.147	-0.84
(-23)		9.22	10.31	11.40	FS97	0.24 ± 0.08	-0.089 ± 0.058	-1.554	-1.42
(-21)		11.87	11.93	11.99	FS97	0.24 ± 0.05	-0.086 ± 0.043	-0.057	-0.56
(-16)		12.23	12.29	12.35	FS97	0.93 ± 0.05	-0.507 ± 0.045	-0.016	-0.18
(-11)		12.36	12.43	12.50	FS97	-0.01 ± 0.07	0.063 ± 0.061	0.064	0.60
(-9)		12.64	12.69	12.74	FS97	0.08 ± 0.04	0.011 ± 0.044	-0.094	-0.90
(-5)		11.47	11.69	11.91	FS97	0.77 ± 0.18	-0.412 ± 0.113	-0.181	-0.68
(total)		13.08	13.16	13.25	FS97

Table 21—Continued

HD Number ^a	Name	Observed $\log N(\text{Zn II})$			Source ^p	F_*	$[\text{Zn}_{\text{gas}}/\text{H}]_{\text{fit}}^c$	Residual ^d	Deviation ^e (in σ)
		l.l.	best	u.l.					
(1)	(2)	(3)	(4)	(5)	(6)	(7)	(8)	(9)	(10)

^aTerms in parentheses indicate separate velocity components, if they are explicitly identified and not grouped together; see §4.3

^bCodes in this column are linked to references listed in Table 1

^cThe expected depletion $[\text{Zn}_{\text{gas}}/\text{H}]$ computed using Eq. 10. The listed errors do not include an overall systematic uncertainty of 0.04 in the solar abundance $\sigma(\text{Zn}/\text{H})_{\odot}$ in order to show just the formal error that arises from the uncertainties in location of line of best fit and the value of F_* .

^dThe observed $[\text{Zn}_{\text{gas}}/\text{H}]$ minus that computed using Eq. 10.

^eThe difference shown in the previous column divided by the expected difference due to the uncertainties in both the measured column density and the coefficients that appear in Eq. 10.

Table 22. Observations and Fits for Germanium

HD Number ^a	Name	Observed $\log N(\text{Ge II})$				Source ^b	F_*	$[\text{Ge}_{\text{gas}}/\text{H}]_{\text{fit}}^c$	Residual ^d	Deviation ^e (in σ)
		l.l.	best	u.l.						
(1)	(2)	(3)	(4)	(5)	(6)	(7)	(8)	(9)	(10)	
1383	HD 1383	12.36	12.45	12.54	CLMS06	0.61 ± 0.04	-0.677 ± 0.033	-0.077	-0.63	
12323	HD 12323	12.09	12.15	12.21	CLMS06	0.52 ± 0.04	-0.623 ± 0.032	-0.213	-2.14	
13268	HD 13268	12.37	12.44	12.51	CLMS06	0.51 ± 0.04	-0.617 ± 0.034	-0.060	-0.56	
27778	62 Tau	12.10	12.14	12.18	CLMS06	
35149	23 Ori	11.85	11.89	11.93	W++99	0.54 ± 0.04	-0.633 ± 0.033	0.191	1.32	
37021	θ^1 Ori	12.28	12.32	12.36	CLMS06	
37061	ν Ori	12.46	12.51	12.56	CLMS06	
37367	HD 37367	12.30	12.34	12.38	CLMS06	0.65 ± 0.07	-0.703 ± 0.046	0.011	0.09	
37903	HD 37903	11.99	12.02	12.05	CLMS06	1.15 ± 0.03	-1.007 ± 0.047	-0.110	-1.33	
43818	LU Gem	12.52	12.58	12.64	CLMS06	
47839	15 Mon	11.25	11.41	11.51	H++93	0.25 ± 0.05	-0.454 ± 0.050	-0.143	-0.83	
52266	HD 52266	12.39	12.43	12.47	CLMS06	
63005	HD 63005	12.27	12.31	12.35	CLMS06	0.64 ± 0.03	-0.695 ± 0.026	-0.013	-0.18	
71634	HD 71634	11.96	12.02	12.08	CLMS06	
72754	FY Vel	12.15	12.20	12.25	CLMS06	0.76 ± 0.10	-0.771 ± 0.064	-0.014	-0.11	
75309	HD 75309	12.16	12.22	12.28	CLMS06	0.63 ± 0.04	-0.686 ± 0.031	0.028	0.28	
79186	GX Vel	12.28	12.34	12.40	CLMS06	0.69 ± 0.03	-0.725 ± 0.028	-0.043	-0.46	
91824	HD 91824	12.25	12.33	12.41	CLMS06	0.45 ± 0.03	-0.575 ± 0.034	0.041	0.40	
91983	HD 91983	12.33	12.37	12.41	CLMS06	0.48 ± 0.04	-0.594 ± 0.036	0.024	0.26	
111934	BU Cru	12.52	12.56	12.60	CLMS06	
116852	HD 116852	11.93	12.00	12.07	CLMS06	0.36 ± 0.04	-0.520 ± 0.040	-0.195	-1.72	
122879	HD 122879	12.40	12.47	12.54	CLMS06	0.55 ± 0.04	-0.636 ± 0.035	0.070	0.55	
141637	1 Sco	12.01	12.04	12.06	H++93	0.69 ± 0.05	-0.725 ± 0.036	-0.066	-0.56	
143018	π Sco	11.64	11.72	11.78	H++93	0.71 ± 0.03	-0.735 ± 0.028	0.066	0.68	
147888	ρ Oph D	12.42	12.48	12.54	CLMS06	0.88 ± 0.06	-0.843 ± 0.047	-0.115	-0.70	
148594	HD 148594	12.09	12.15	12.21	CLMS06	
149757 (-15)	ζ Oph	11.94	11.98	12.02	SCS92	1.05 ± 0.02	-0.944 ± 0.037	0.074	0.99	
152590	HD 152590	12.39	12.44	12.49	CLMS06	0.69 ± 0.03	-0.726 ± 0.026	-0.002	-0.02	
156110	HD 156110	11.30	11.37	11.44	CLMS06	
157857	HD 157857	12.43	12.52	12.61	CLMS06	0.62 ± 0.04	-0.684 ± 0.030	0.060	0.51	
165955	HD 165955	12.15	12.19	12.23	CLMS06	0.42 ± 0.04	-0.559 ± 0.038	-0.050	-0.60	
175360	HD 175360	11.85	11.91	11.97	CLMS06	
185418	HD 185418	12.40	12.44	12.48	CLMS06	0.79 ± 0.03	-0.788 ± 0.030	0.117	1.34	
192035	RX Cyg	12.28	12.33	12.38	CLMS06	0.76 ± 0.04	-0.767 ± 0.032	0.014	0.16	
198478	55 Cyg	12.44	12.48	12.52	CLMS06	0.81 ± 0.05	-0.797 ± 0.039	0.031	0.25	
198781	HD 198781	12.14	12.20	12.26	CLMS06	0.59 ± 0.03	-0.663 ± 0.028	0.011	0.13	
201345	HD 201345	12.03	12.09	12.15	CLMS06	0.34 ± 0.04	-0.509 ± 0.043	-0.103	-0.92	
203532	HD 203532	12.02	12.07	12.12	CLMS06	
206773	HD 206773	12.29	12.34	12.39	CLMS06	0.53 ± 0.02	-0.630 ± 0.026	0.019	0.25	

Table 22—Continued

HD Number ^a	Name	Observed $\log N(\text{Ge II})$				F_*	$[\text{Ge}_{\text{gas}}/\text{H}]_{\text{fit}}^{\text{c}}$	Residual ^d	Deviation ^e (in σ)
		l.l.	best	u.l.	Source ^b				
(1)	(2)	(3)	(4)	(5)	(6)	(7)	(8)	(9)	(10)
207198	HD 207198	12.43	12.48	12.53	CLMS06	0.90 ± 0.03	-0.854 ± 0.032	-0.042	-0.53
208440	HD 208440	12.29	12.35	12.41	CLMS06	0.61 ± 0.04	-0.676 ± 0.032	0.019	0.19
210809	HD 210809	12.50	12.56	12.62	CLMS06	0.41 ± 0.04	-0.555 ± 0.040	0.083	0.76
212571	π Aqr	11.43	11.51	11.57	H++93
212791	V408 Lac	12.08	12.15	12.22	CLMS06	0.57 ± 0.08	-0.652 ± 0.055	-0.021	-0.10
220057	HD 220057	12.10	12.15	12.20	CLMS06	0.75 ± 0.05	-0.764 ± 0.039	0.057	0.43
232522	HDE 232522	12.17	12.25	12.33	CLMS06	0.44 ± 0.03	-0.570 ± 0.035	-0.066	-0.65
308813	HDE 308813	12.32	12.37	12.42	CLMS06	0.49 ± 0.04	-0.604 ± 0.035	-0.014	-0.15
	BD +53 2820	12.29	12.38	12.47	CLMS06	0.43 ± 0.05	-0.563 ± 0.043	-0.145	-1.12
	CPD -69 1743	12.18	12.24	12.30	CLMS06	0.42 ± 0.05	-0.560 ± 0.042	-0.060	-0.55

^aTerms in parentheses indicate separate velocity components, if they are explicitly identified and not grouped together; see §4.3

^bCodes in this column are linked to references listed in Table 1

^cThe expected depletion $[\text{Ge}_{\text{gas}}/\text{H}]$ computed using Eq. 10. The listed errors do not include an overall systematic uncertainty of 0.05 in the solar abundance $\sigma(\text{Ge}/\text{H})_{\odot}$ in order to show just the formal error that arises from the uncertainties in location of line of best fit and the value of F_* .

^dThe observed $[\text{Ge}_{\text{gas}}/\text{H}]$ minus that computed using Eq. 10.

^eThe difference shown in the previous column divided by the expected difference due to the uncertainties in both the measured column density and the coefficients that appear in Eq. 10.

Table 23. Observations and Fits for Krypton

HD Number ^a	Name	Observed $\log N(\text{Kr I})$				F_*	$[\text{Kr}_{\text{gas}}/\text{H}]_{\text{fit}}^c$	Residual ^d	Deviation ^e (in σ)
		l.l.	best	u.l.	Source ^b				
(1)	(2)	(3)	(4)	(5)	(6)	(7)	(8)	(9)	(10)
23478	HD 23478	12.18	12.23	12.28	C++08	-0.00 ± 0.50	-0.218 ± 0.110	0.042	0.24
24190	HD 24190	12.29	12.35	12.41	C++08	0.63 ± 0.24	-0.323 ± 0.046	0.013	0.15
24398	ζ Per	12.15	12.18	12.20	CM97	0.88 ± 0.05	-0.365 ± 0.031	-0.011	-0.09
24760	ϵ Per	11.38	11.46	11.53	CM97	0.68 ± 0.04	-0.331 ± 0.022	-0.070	-0.58
27778	62 Tau	12.31	12.37	12.41	CMLS01
35149	23 Ori	11.72	W++99	0.54 ± 0.04	-0.308 ± 0.027
36861	λ Ori A	11.74	11.80	11.85	CM97	0.57 ± 0.04	-0.312 ± 0.026	-0.045	-0.36
37021	θ^1 Ori	12.59	12.63	12.67	CMLS01
37061	ν Ori	12.68	12.72	12.74	CMLS01
37128	ϵ Ori	11.30	11.40	11.48	CM97	0.54 ± 0.03	-0.308 ± 0.026	-0.101	-0.78
37367	HD 37367	12.46	12.51	12.56	CML03	0.65 ± 0.07	-0.327 ± 0.024	0.144	1.30
37903	HD 37903	12.25	12.31	12.37	CMLS01	1.15 ± 0.03	-0.409 ± 0.053	-0.078	-0.78
38771	κ Ori	11.41	11.50	11.58	CM97	0.67 ± 0.03	-0.329 ± 0.022	-0.050	-0.51
40893	HD 40893	12.49	12.56	12.63	C++08	0.61 ± 0.05	-0.319 ± 0.025	-0.017	-0.16
57061	τ CMa	11.69	11.75	11.80	CM97	0.39 ± 0.04	-0.282 ± 0.038	-0.027	-0.33
69106	HD 69106	12.10	12.19	12.28	C++08	0.64 ± 0.06	-0.325 ± 0.024	0.063	0.58
72754	FY Vel	12.13	12.23	12.33	CML03	0.76 ± 0.10	-0.345 ± 0.028	-0.070	-0.49
75309	HD 75309	12.09	12.21	12.30	CMLS01	0.63 ± 0.04	-0.322 ± 0.023	-0.005	-0.04
94454	HD 94454	12.28	12.36	12.44	C++08
99857	HD 99857	12.19	12.29	12.37	A++03	0.54 ± 0.04	-0.308 ± 0.027	-0.120	-1.08
99872	HD 99872	12.18	12.25	12.32	C++08
102065	HD 102065	12.05	12.16	12.27	C++08
104705	DF Cru	11.92	12.12	12.26	A++03	0.33 ± 0.05	-0.272 ± 0.043	-0.143	-0.75
108639	HD 108639	12.30	12.40	12.50	C++08	0.37 ± 0.37	-0.279 ± 0.073	-0.064	-0.43
112999	V946 Cen	12.18	12.27	12.36	C++08
114886	HD 114886	12.29	12.43	12.57	C++08	0.87 ± 0.31	-0.363 ± 0.059	0.030	0.19
115071	V961 Cen	12.57	12.64	12.71	C++08	0.22 ± 0.21	-0.255 ± 0.063	0.038	0.36
116852	HD 116852	12.00	12.06	12.12	C++08	0.36 ± 0.04	-0.277 ± 0.040	-0.038	-0.35
122879	HD 122879	12.47	12.60	12.73	C++08	0.55 ± 0.04	-0.309 ± 0.027	0.213	1.27
124314	HD 124314	12.61	12.70	12.79	C++08	0.59 ± 0.05	-0.315 ± 0.025	0.146	1.24
137595	HD 137595	12.27	12.34	12.41	C++08	0.77 ± 0.22	-0.347 ± 0.044	0.106	1.12
141637	1 Sco	12.09	12.24	12.30	H++93	0.69 ± 0.05	-0.333 ± 0.023	0.080	0.52
143018	π Sco	11.44	H++93	0.71 ± 0.03	-0.335 ± 0.022
144965	HD 144965	12.22	12.30	12.38	C++08	1.15 ± 0.35	-0.408 ± 0.078	0.025	0.18
147165	σ Sco	12.40	12.45	12.50	C++08	0.76 ± 0.06	-0.345 ± 0.025	0.072	0.39
147683	V760 Sco	12.46	12.52	12.58	C++08	0.56 ± 0.47	-0.311 ± 0.082	0.065	0.40
147888	ρ Oph D	12.70	12.73	12.76	CMLS01	0.88 ± 0.06	-0.364 ± 0.031	-0.004	-0.02
148594	HD 148594	12.29	12.37	12.45	CML03
149757 (-15)	ζ Oph	11.95	12.04	12.11	CM97	1.05 ± 0.02	-0.392 ± 0.043	-0.079	-0.76

Table 23—Continued

HD Number ^a	Name	Observed $\log N(\text{Kr I})$				Source ^b	F_*	$[\text{Kr}_{\text{gas}}/\text{H}]_{\text{fit}}^c$	Residual ^d	Deviation ^e (in σ)
		l.l.	best	u.l.						
(1)	(2)	(3)	(4)	(5)	(6)	(7)	(8)	(9)	(10)	
151805	HD 151805	12.33	12.41	12.49	C++08	0.83 ± 0.36	-0.355 ± 0.065	-0.000	-0.00	
152590	HD 152590	12.49	12.54	12.59	C++08	0.69 ± 0.03	-0.333 ± 0.022	0.045	0.61	
165246	HD 165246	12.47	12.53	12.59	C++08	0.77 ± 1.39	-0.345 ± 0.231	0.060	0.13	
175360	HD 175360	11.91	12.01	12.09	CMLS01	
177989	HD 177989	12.18	12.25	12.32	C++08	0.55 ± 0.05	-0.310 ± 0.026	0.116	1.14	
185418	HD 185418	12.43	12.50	12.56	CMLS01	0.79 ± 0.03	-0.350 ± 0.025	0.079	0.79	
198478	55 Cyg	12.52	12.60	12.68	CML03	0.81 ± 0.05	-0.352 ± 0.026	0.046	0.33	
203374	HD 203374	12.50	12.56	12.62	C++08	0.56 ± 0.06	-0.311 ± 0.027	0.181	1.63	
203532	HD 203532	12.15	12.26	12.34	CMLS01	
206267	HD 206267	12.55	12.65	12.75	C++08	0.87 ± 0.07	-0.362 ± 0.031	0.115	0.84	
207198	HD 207198	12.58	12.68	12.77	CMLS01	0.90 ± 0.03	-0.367 ± 0.031	0.012	0.10	
208440	HD 208440	12.33	12.43	12.53	CML03	0.61 ± 0.04	-0.319 ± 0.024	0.083	0.64	
208947	HD 208947	11.91	11.99	12.07	C++08	
209339	HD 209339	12.29	12.35	12.41	C++08	0.58 ± 0.04	-0.314 ± 0.025	0.042	0.48	
212571	π Aqr	11.70	H++93	
220057	HD 220057	12.11	12.19	12.27	CML03	0.75 ± 0.05	-0.343 ± 0.024	0.017	0.12	
224151	V373 Cas	12.46	12.58	12.70	C++08	0.46 ± 0.04	-0.295 ± 0.032	0.052	0.38	
303308	HDE 303308	12.23	12.32	12.41	C++08	0.38 ± 0.04	-0.282 ± 0.038	-0.237	-2.02	

^aTerms in parentheses indicate separate velocity components, if they are explicitly identified and not grouped together; see §4.3

^bCodes in this column are linked to references listed in Table 1

^cThe expected depletion $[\text{Kr}_{\text{gas}}/\text{H}]$ computed using Eq. 10. The listed errors do not include an overall systematic uncertainty of 0.08 in the solar abundance $\sigma(\text{Kr}/\text{H})_{\odot}$ in order to show just the formal error that arises from the uncertainties in location of line of best fit and the value of F_* .

^dThe observed $[\text{Kr}_{\text{gas}}/\text{H}]$ minus that computed using Eq. 10.

^eThe difference shown in the previous column divided by the expected difference due to the uncertainties in both the measured column density and the coefficients that appear in Eq. 10.